Investigation of the Effect of Inlet Valve Timing on the Gas Exchange Process in High-Speed Engines

By

Dimitar Nouhov

A Doctoral Thesis

Submitted in partial fulfilment of the requirements for the award of Doctor of Philosophy of Loughborough University

June 2004

Abstract

The motivation for this investigation is the potential for the application of Variable Valve Actuation (VVA) technology in high-speed and high power to volume density, four stroke, spark ignition, internal combustion engines. The benefits of this technology have already been proven in medium-speed automotive engines. In the beginning of this thesis the differences between high-speed and medium-speed engines are outlined and a case is presented why this investigation is required.

During the preliminary study VVA technology was reviewed and classification was created based on system functionality. Valvetrain and camdrive dynamic considerations were used to identify VVA technologies, which will allow high-speed operation.

The main aspect of this investigation focuses on the effect of individual valve events on the gas exchange process of a high-speed engine. If the optimum valve events in terms of engine output for different engine speeds can be defined, this will allow assessment of the potential of selected VVA systems. To accomplish this, a parametric study exploring the sensitivity of charging efficiency to variation of the individual inlet valve events was performed. Results for five different Inlet Valve Opening (IVO) and Inlet Valve Closing (IVC) points are presented. The study employed engine simulation, which was fully validated experimentally. The use of simulation allows not only the study of the effects of valve events on engine performance but also allows explanation of the results by examining the cylinder filling mechanisms and the gas dynamic processes in the inlet and exhaust system.

A control strategy was created for each of the selected VVA systems so that it best satisfies the optimum valve events. An assessment and comparison of their potential for improving engine performance was possible.

Acknowledgments

I dedicate this work to my wife Eleanor, mother Stefka and grandmother Dora.

I also want to thank my parents-in-law Valerie and Steve and godmother Jane for their continuous support and faith in me.

I would like to express my gratitude to my supervisors Dr. Chen and Dr. Ibrahim for their academic guidance and understanding.

A great deal of appreciation is given to Triumph Motorcycles who provided motivation for this research and generously sponsored me throughout my university career. Special gratitude goes to the people working there who never spared advice or interest in my work.

Special thanks to Lotus Engineering for providing the engine simulation software used as a tool in this investigation and to Richard Pearson and Mike Bassett for their patience and advice.

This research would have not been possible without the help of the technical support staff at the Department of Aeronautical and Automotive Engineering and especially Adrian Broster and Graham Smith.

And finally thanks to all my friends that shared the postgraduate experience with me.

List of Contents

List of tables and figures

Nomenclature

Greek letters

η_v	Volumetric efficiency
η_t	Trapping efficiency
η_c	Charging efficiency
τ_w	Sheer stress
ρ_r	Reference density
θ	Crankshaft angle after the start of combustion
θ_b	Total combustion duration

Latin letters

A	Wiebe function coefficient
B	Wiebe function coefficient
C_{CFL}	Courant number
$c_{\max}^n$	Maximum wave speed
c_p	Specific heat capacity at constant pressure
D	Equivalent hydraulic diameter of the duct
d	Characteristic length
E_0	The total stagnation internal energy
$\dot{e}$	Fresh air mass flow rate through exhausts ports
e_0	Stagnation internal energy
e	Specific internal energy
F	Cross sectional area
f	Duct wall friction coefficient
H_0	The total stagnation enthalpy

h_0	Stagnation enthalpy
$\dot{i}$	Fresh air mass flow rate through ports
t_e	Time the exhaust valves are open
t_i	Time the inlet valves are open
k	Gas conductivity
L	Stroke
m_{frac}	mass fraction burnt
m_s	Supplied fresh air mass per cylinder per cycle
m_t	Trapped fresh air mass in cylinder after IVC
N	Crankshaft speed
p	Pressure
$\dot{Q}$	The heat transfer rate
q	Rate of heat transfer per unit mass
S_P	Piston speed
t	Time
t_i	Time from IVO to IVC
t_e	Time from EVO to EVC
u	Velocity of flow
V_c	Cylinder volume
v	Gas velocity
$\dot{W}_S$	The work done by or on the system
x	Distance

Abbreviations

ABDC	After Bottom Dead Centre
ATDC	After Top Dead Centre
BBDC	Before Bottom Dead Centre

BTDC	Before Top Dead Centre
CA	Crankshaft angle
CI	Compressions Ignition
EVC	Exhaust Valve Closing
EVO	Exhaust Valve Opening
IVC	Inlet Valve Closing
IVO	Inlet Valve Opening
MOP	Maximum Open Point
SI	Spark Ignition
VVA	Variable Valve Actuation

Chapter 1

Introduction

This thesis considers the effects of the individual inlet valve event timings on the Wide Open Throttle (WOT) performance of high-speed, high power to volume density, four stroke, Spark Ignition (SI) engines in relation to Variable Valve Actuation (VVA). Firstly, a classification of current VVA technology and assessment of high-speed compatibility based on camdrive and valvetrain considerations is reported. Secondly, the gas dynamic behaviour in the inlet and exhaust systems and the related cylinder filling mechanisms in such engines are examined. Using this knowledge, the investigation focuses on the effects of Inlet Valve Opening (IVO) and Inlet Valve Closing (IVC) timings on the gas exchange process. As a result, the optimum IVO and IVC in terms of breathing efficiency are established. They are compared with the abilities of VVA systems, which were identified during the preliminary study as dynamically suitable for high-speed operation. A strategy is suggested for best utilising these abilities and a comparison is made of the performance improvement potential of each VVA system.

This chapter begins with introduction of the current commercial climate in the automotive industry and comments on the merits of the high-speed engine. In this thesis, the term 'high-speed engine' is used for powerplants with maximum crankshaft speeds exceeding 10000 rpm. The challenges associated with the design of such engines and the reasons for the performance compromise related to the wide speed range are discussed. The potential of VVA systems to resolve some of these issues is identified and exploring it provides motivation for this investigation.

The advantages of VVA technology, which have been long proven for medium speed automotive engines by Grohn and Wolf (1989) and Inoue (1989) are then discussed. The differences between high-speed and medium-speed engines are outlined and a case is presented why this investigation is needed. The main objectives of the research are

formulated and the steps required to achieve them are defined. Finally, an overview of the thesis structure is presented.

1.1 Current commercial climate and trends in the automotive industry

In recent years, automotive manufacturers have been subjected to continuously increasing legislative and marketing pressures. There are growing environmental and health concerns linked to the production of harmful exhaust emissions created from the combustion of fossil fuels. This has brought the implementation of emissions and tax laws, which both compel and encourage manufacturers to develop cleaner vehicles. Due to the fast rate of global usage of fossil fuels, the increasing consumer expectations for reduced fuel consumption and because of the direct relation to exhaust emissions, manufacturers are also looking into the development of more fuel-efficient vehicles. Meanwhile marketing demands related to better longitudinal and lateral dynamic performance, safety and comfort of vehicles are growing.

Some of the chassis related solutions to these problems include the development of low aerodynamic drag vehicles, low rolling resistance tyres and reduction of vehicle mass by efficient design or the use of light materials.

As far as powertrains are concerned, the automotive industry has been looking at different methods to increase the operating efficiency of the internal combustion engine, as well as to include it in hybrid applications in order to improve the fuel efficiency of vehicles. A major trend has been the move towards reduction of engine capacity, also known as downsizing. Doing this without compromising the maximum power output requires increase of the specific output of the engine. This has been addressed by increase of the useful crankshaft speed range or by pressure charging. Soltic and Guzzella (2000) show that both of these engine concepts can offer substantial gains in terms of fuel economy compared with a larger capacity engine with the same power output. It is also desirable to develop these powerplants in such a way that they are able to provide high torque at low engine speeds allowing the use of tall gear ratios further improving fuel consumption and reducing noise.

1.1.1 Specifics of the motorcycle sector

Similar pressures are felt in the motorcycle sector. Due to the lack of motorcycle specific legislation in the past, the industry was abiding by the passenger car emission limits, which were relatively easy to satisfy. More recently, motorcycle specific legislation was put in place and there will be a steep reduction of the exhaust emissions limits over the next few years as shown in Table 1.1. The introduction of electronic fuel injection systems and emissions after treatment technology, such as catalytic converters combined with pulsed Secondary Air Injection (SAI), help to maintain exhaust emissions within limits.

Year	Engine capacity	CO_2	HC	NO_x
	[cm^3]	[g/km]	[g/km]	[g/km]
2003	<150	5.5	1.2	0.3
	>150	5.5	1.0	0.3
2006	<150	2.0	0.8	0.15
	>150	2.0	0.3	0.15

Table 1.1: Current and future emission limits for type approval for motorcycles (Directive 2002/51/EC of the European Parliament)

Noise legislation challenges engine manufacturers to find a compromise between low backpressure and noise suppression in the design of silencing systems. The use of valves in the exhaust system (Nakayasu et. al., 2001) and secondary throttles in the inlet allows reduction of exhaust and inlet noise.

The marketing demands are slightly different from the passenger car sector. While fuel consumption is desirable, the customer is focused on vehicle dynamic performance. Therefore, high-speed, high specific output powertrains with high specific torque at low engine speeds are required.

1.1.2 Engines for motorsport application

When developing engines for motorsport application the emphasis is on high specific power output rather than fuel efficiency. Emissions are not an issue in most series. The regulations defined by the Federation Internationale de L'automobile (FIA, 2004) usually determine the maximum engine capacity and maximum boost pressure if pressure charging is allowed. In order to increase the specific output, the maximum operating speeds of such powerplants are continuously increasing.

1.2 The need for high-speed engines

The useful crankshaft speed range of engines has been continuously increasing since the birth of the Internal Combustion (IC) engine. The above discussion relating to different sectors of the automotive industry shows that this is desirable for two reasons:

- It allows the development of small capacity engines with high specific output bringing improvements in fuel economy and exhaust emissions as well as reduction of weight and packaging constraints. This type of engines are best utilised in motorcycles, low weight passenger vehicles and hybrid applications.
- It allows increase of specific output for a fixed engine capacity – a major benefit for motorsport and high performance passenger car applications.

1.3 Challenges and solutions associated with the design of high-speed engines

Whether to compensate for engine capacity downsizing in passenger cars or purely to increase peak output for motorsport and high performance road applications, the development of high-speed engines has presented engineers with a variety of challenges. Complete engine component groups are being redesigned in order to cope with the increased dynamic and friction loads. The durability problems associated with reliable operation at elevated piston speeds are being overcome with the development of materials with higher strength to weight ratio and recent tribological advances in the area of surface coatings (Kodai A. *et al.*, 2001, Sulzer Metco, 2004). The speed increase has also required a solution of a variety of problems concerning the ignition and fuel system abilities. In addition, high-speed production engines are subject to emissions and noise regulations.

The solution of the above problems is best illustrated with the engineering achievements allowing the increase of engine speeds in Formula 1 (F1) engines. Engine speed, was and is, one of the major limiting factors on the specific power output in powerplants for motorsport applications. Since the 1950's and especially since the ban on pressure charging in 1991 in F1 Grand Prix racing there has been a gradual increase in engine speeds almost proportional to the increase in power output as demonstrated by Wright (2001) in Figure 1.1. Thorough understanding of spring dynamics and metallurgical advances have allowed the development of lightweight, conventional spring, valvetrain systems facilitating reliable operation at speeds up to 15000 rpm. It was the development of the pneumatic spring that facilitated engine speed increase above 15000 rpm. These valvetrain developments paralleled with research in piston materials permit current speeds to exceed 19000 rpm.

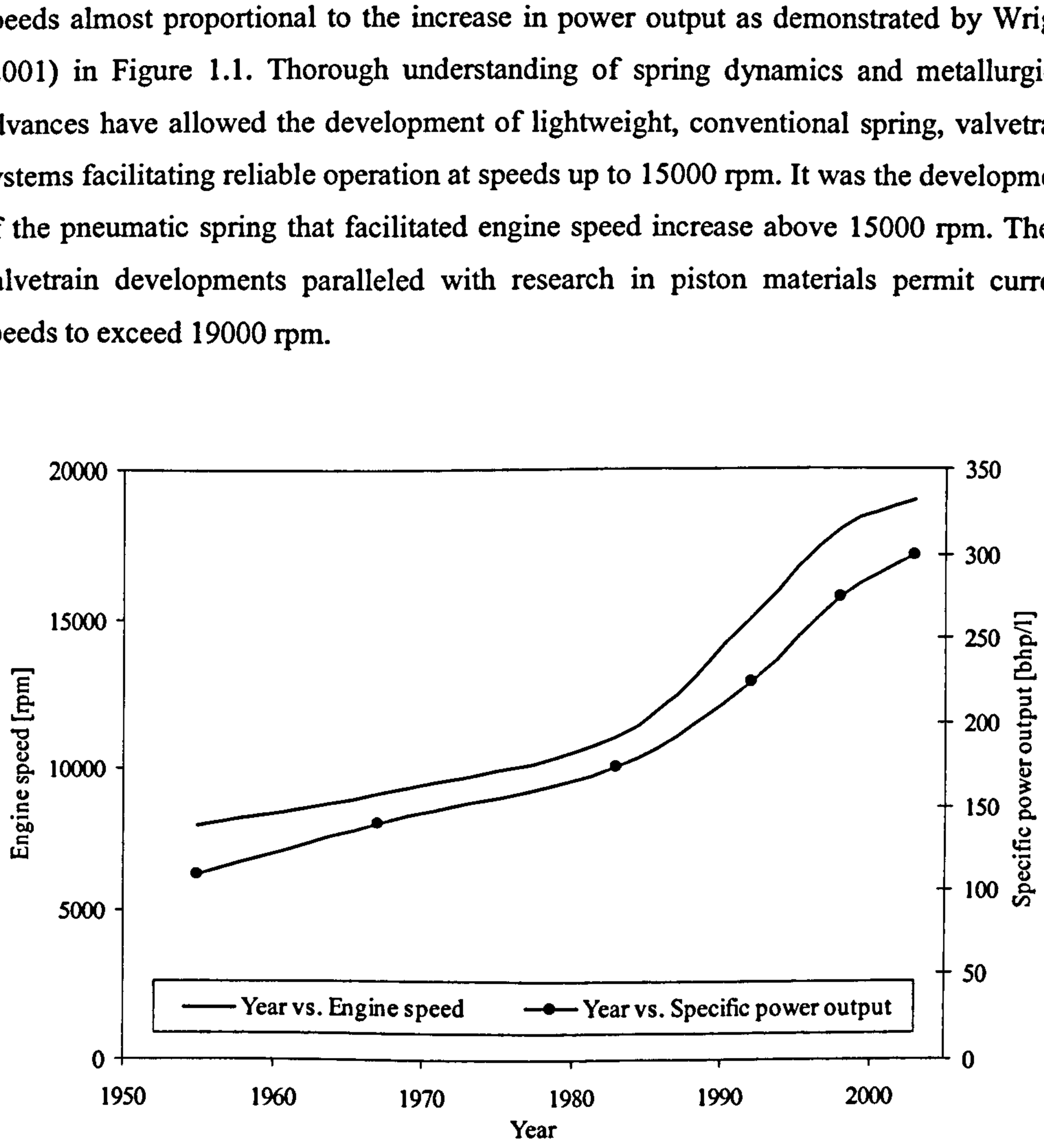

Figure 1.1: Engine speed and specific power output trends over the last 50 years in Formula 1 engines (Wright, 2001)

This research attempts to contribute towards another major challenge that is related to the output performance of high-speed engines. Due to the wide speed range, low speed torque is often traded off for peak power. Further, due to different gas dynamic effects taking place in the inlet and exhaust systems the shape of the torque curve consists of a number of dips and peaks. Figure 1.2 illustrates the output curves measured from a typical high-speed engine in Test Cell 6 of the Faculty of Engineering Powertrain Laboratory at Loughborough University. It can be seen that torque below 6000 rpm is below 60% of the maximum value and the shape of the curve would suggest poor drivability at WOT below this speed.

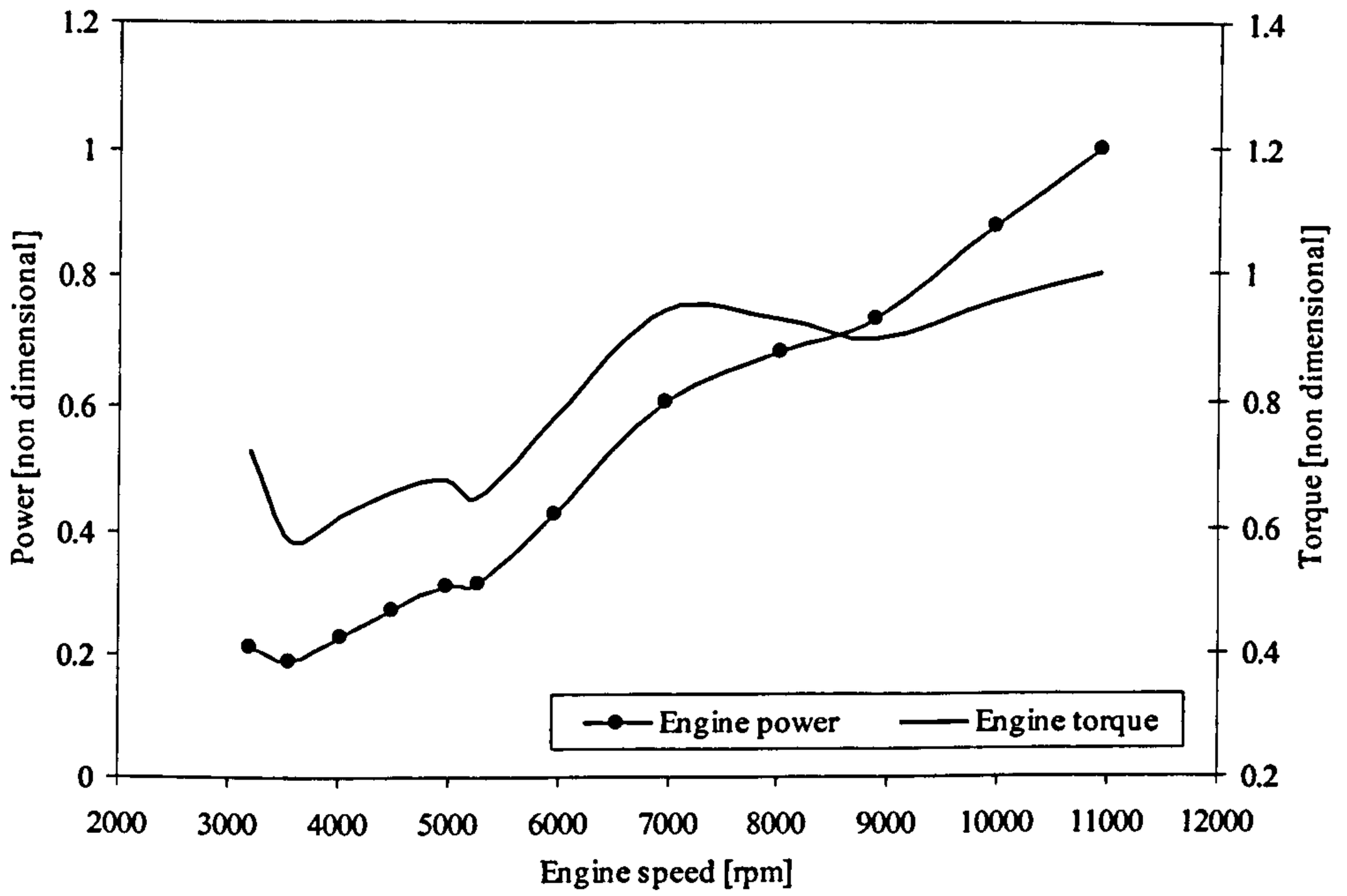

Figure 1.2: Engine power and torque vs. engine speed for a typical high-speed 4 cyl. engine with 68mm bore and 41.3mm stroke (both power and torque are normalised with their peak values)

It is very desirable to ensure high torque output throughout a broad speed range. Higher torque at low speeds will allow the use of taller gear ratios in passenger vehicles. This allows reduction of engine speed for the same vehicle speed reducing fuel consumption and noise without affecting acceleration rates and driveability.

While motorcycle users will also benefit from good low speed torque, allowing acceptable acceleration rates at high gear ratios, in this sector of the automotive industry emphasis is on the torque curve shape. When a high output engine is coupled to a low inertia vehicle, even torque spread and torque delivery without peaks or troughs is essential in order to achieve good WOT driveability in lower gears. Taller overall gearing will also reduce drive-by noise.

Engines for motorsport applications are designed to operate in a narrow speed range near the speed at which maximum power output occurs. Even with high driving skills and gearboxes with a number of closely spaced gear ratios it is impossible to operate the engine at maximum power speed continuously. In addition, due to the long straights on some circuits, taller overall gearing ratio is selected and broader part of the engine speed range is used for WOT operation. This is why widening the speed range where maximum power is achieved has the potential of increasing the vehicle acceleration rates in top gear, hence reducing lap times. A torque curve free of dips and peaks is also essential to ensure good drivability and lateral dynamic performance.

In order to achieve high torque at wide speed range it is essential to ensure high breathing and combustion efficiency. This is inhibited by the compromises imposed by the fixed geometry of conventional inlet and exhaust systems as well as the speed independent operation of the valvetrain mechanism. The emerging of variable inlet and exhaust geometry systems has resolved some of the tradeoffs. However, due to the nature of the gas exchange process their effect is somehow limited. It has been known from very early stages of the development of IC engines that VVA can greatly reduce the performance compromise associated with conventional valvetrains.

1.4 Previous research of the merits of VVA technology

VVA technology is currently widely used in piston engines due to the number of benefits that it offers. Numerous patents (Ingenieurbüro Bockhmann and Hannibal, 2004), surveys (Ahmad and Theobald, 1989), and reviews (Stone and Kwan, 1989), document the continuing efforts to develop and improve the VVA systems. Manufacturers have developed a great number of mechanisms, which allow different degrees of variability of

the valve events and also bringing a range of benefits. Factors such as production cost, emission regulations and marketing requirements have often dictated the type of system employed and its design targets. Many experimental and theoretical studies have been conducted in the past, where the effects from varying the valve events on different areas of engine performance has been examined over a speed range between 1000 rpm and 6000 rpm. The following sections provide details of some of the reported benefits.

1.4.1 Improvement of engine output

The most publicised benefit of VVA technology is the ability to improve the WOT torque of the engine over the entire speed range. This is achieved by increase of the fresh charge trapped in the cylinder and by minimising of the pumping loses. Gray (1988) presents results of measurements taken on a typical 2 litre SI engine at full load and shows how advancing Inlet Maximum Opening Point (IMOP) can improve low speed Brake Mean Effective Pressures (BMEP) and retarding IMOP increases high-speed BMEP compared with the standard camshaft timing. Maekawa *et al.* (1989) use simulation to predict possible improvements in maximum specific output as motivation for the development of VVA system for varying the inlet camshaft phasing.

In practice, increase of the fresh charge trapped is achieved by reduction of backflow at IVO and IVC and optimal expelling of gasses from the previous cycle. Grohn and Wolf (1989) found that retardation of inlet camshaft phasing at higher engine speeds allows reduction of backflow into the inlet during the reduced valve overlap period and take advantage from the aftercharge dynamic effect before IVC leading to increase in trapped mass. Retarding the inlet camshaft timing with increase of engine speed is also reported as beneficial by Otto *et al.* (2000).

1.4.2 Reduction of fuel consumption

Fuel consumption reduction can be achieved by combustion efficiency improvement allowing operation with lean Air Fuel Ratio (AFR) mixtures. Horie *et al.* (1992) report 12% reduction in Brake Specific Fuel Consumption (BSFC) while operating at part load conditions with AFR ratio of 22. This was made possible by the use of a VVA mechanism deactivating one the inlet valves at part load and creating asymmetrical entry

path resulting in local enrichment in the area of the spark plug. Combustion enhancement was also achieved due to the increased turbulence generated by the swirl. Tolerance to operating with lean AFR mixtures by the use of asymmetric valve strategies was also reported by Wilson *et al.* (1993).

Reduction of pumping losses during part load operation can bring significant improvement in fuel efficiency. Such reduction can be achieved by throttle free load control operation by utilising Early Inlet Valve Closing (EIVC) or Late Inlet Valve Closing (LIVC). Kreuter *et al.* (1992) demonstrate significant reduction in pumping loses using either EIVC or LIVC concepts however this is not proportional to fuel consumption reduction unless special measures are taken to improve mixture formation.

Variation of EVC timing can reduce the compromise between useful work and pumping losses at different engine speeds. Stein *et al.* (1995) report fuel consumption benefits of 3.2% on a 4.6l engine by variation of the exhaust camshaft timing.

VVA systems can be used to reduce the duration of the valve overlap period during idle conditions. This has the potential of lowering the contents of exhaust residuals and improving combustion stability allowing lower idle speed and fuel consumption.

1.4.3 Reduction of exhaust emissions

The effects of the individual valve event timings on exhaust emissions have been extensively explored by Siewert (1971). The ability to reduce the contents of harmful substances in the exhaust emissions by controlling the valve events is one of the main motivations for the development of VVA systems.

Nakayama *et al.* (1994) report 45% reduction in hydrocarbon emissions during cold start resulting from the use of leaner air fuel mixtures facilitated by reducing valve lift and the duration of valve overlap. Similar improvement was achieved by Kishi *et al.* (1998). This was possible due to combustion stability improvement caused by the charge swirling motion generated from partial deactivation of one of the inlet valves.

Reduction of 30% of out-of-engine NO_x emissions by controlling the duration of inlet valve open duration is reported by Parker (2000). A study conducted by Stone *et al.* (1993) found that reduction of NO_x is also possible by valve disablement.

Quick catalyst light-off can be achieved by early Exhaust Valve Opening (EVO) during cold start according to FEV Motorentechnik GmbH (2004). This allows exhaust gasses with high temperatures to exit the cylinder and warm up the catalyst.

1.4.4 Impact on noise and vibrations

An indirect benefit of the use of VVA technology is the reduction of noise and vibrations. Increasing the torque available at low speed allows the use of a taller overall gear ratio. This lowers the engine speed for the same vehicle speed.

Abthoff *et al.* (1991) report reduction of idle speed as well as improvement in idle stability achieved by shortening of the valve overlap period by advancing the inlet camshaft timing.

1.4.5 Controlled Auto-Ignition (CAI) combustion technology

CAI combustion process is a relatively new concept and is currently under extensive investigation. Milovanovic and Chen (2001) review the current experimental and theoretical studies and report on the merits this technology can offer. It is evident that amongst other factors flexible control of the valve events is essential to realise this concept. Wolters *et al.* (2003) report on the use of Electro-mechanical VVA system used in conjunction with CAI combustion technology.

1.5 Why this research is required and the specifics of high-speed engines?

While there are comprehensive studies of the effects of valve events on medium-speed engine performance, there is limited published data on these effects for a wider speed range. Boretti *et al.* (1996) performed numerical optimisation of a racing engine reporting improvements of IMEP in the mid speed range between 8000 and 12000 rpm. For a variety of reasons, active valvetrain systems have not been widely used in high-

speed applications so far. The only VVA mechanism featured in a high-speed production engine running at speeds above 10000 rpm is described by Tsukui *et al.* (1999). The device deactivates one inlet and exhaust valves in each cylinder.

A great number of design parameters are different between high and medium speed engines. Some are related to the gas exchange process and influence the way valve events affect engine performance. Others impose special requirements on the dynamic abilities of VVA systems. The following sections discuss some of these differences and illustrate why this research is required.

1.5.1 Valvetrain dynamic requirements

High speed valve – spring, spring and camdrive dynamics present limitations on the design of the valvetrain system. Minimum effective dynamic valve mass and high mechanism stiffness are the main design parameters that determine the type of valvetrain system used. This is why directly actuated tappets are generally favoured and special materials and efficient component design are utilised. These design requirements for a high-speed valvetrain system significantly limits the choice of VVA systems suitable for high-speed operation as it becomes evident in the next chapter.

1.5.2 Intake and exhaust systems

High-speed, high-performance engines used in motorcycle and motorsport applications are not subject to the same exhaust and noise emission, durability and packaging requirements as medium speed passenger car engines. Therefore, the use of emissions control and noise suppression systems has a small negative effect on the engine breathing efficiency. Typically, these engines have higher mean pressures upstream of the inlet valve and lower mean backpressures downstream of the exhaust valve at full load compared with medium speed engines. The significance of this becomes apparent in Chapter 5. The wide speed range makes the gas exchange process susceptible to the effects of a higher number of the acoustic event harmonics occurring in the exhaust and inlet system.

1.5.3 Valve events

The IVO timing in a high-speed engine occurs much earlier than in medium speed engines and is often limited by piston to valve or inlet valve to exhaust valve clearances. Typical values are in the region of 30-60° BTDC for high-speed engines (American Performance Engineering, 2004) and 10-25° for medium speed engines (Asmus, 1982).

According to Stone (1999) typical IVC occurs around 40° ABDC in a medium speed automotive engine. In a typical 600cc motorcycle engine, IVC occurs in the region of 70-80° ABDC (American Performance Engineering, 2004).

The maximum lift and valve areas are often higher than for medium speed engines with the same cylinder capacity.

1.5.4 Maximum mean piston speed and effect on engine design

Mean piston speed S_p is a function of engine speed and stroke, which can be expressed by the following equation:

$$S_P = \frac{LN}{30000} \tag{1.1}$$

where L [mm] is the stroke and N [rpm] is the crankshaft speed.

S_p is an important parameter relating to the inertia loading experienced by the crankshaft mechanism and the tribological phenomena occurring in the piston, piston ring and cylinder bore interaction. Mean piston speed is limited to a maximum value that can be tolerated by the engine structural design. From equation (1.1) can be seen that increase in engine speed must be accompanied by reduction of piston stroke in order to maintain constant maximum mean piston speed.

According to Heywood (1988) maximum mean piston speed for automotive engines is around 15m/s. Due to variety of technological developments recent powerplants are able to operate at higher maximum mean piston speeds. Some data for a variety of different

Engine	Application	Capacity [cc]	Cylinder number	L [mm]	N_{max} [rpm]	S_p [m/s]
BMW S65	passenger car	4999	10	75.2	8250	20.7
BMW M54	passenger car	2979	6	89.6	6000	17.9
Rover K16	passenger car	1795	4	89.3	7000	20.8
BMW P83	F1	3000*	10	39*	19200	25
Triumph 600cc	motorcycle	600	4	41.3	13500	18.6

Table 1.2: Stroke, maximum engine speed and maximum mean piston speed for several automotive engines (BMW AG Website, 2004; Stone 1999) (*Calculated values)

types of current SI engines used in series production passenger cars is included in Table 1.2. It becomes apparent that max S_p for some SI automotive engines exceeds 20m/s where for a Formula 1 engine it is in the region of 25m/s. The mean piston speed for the high-speed motorcycle engine with stroke L=41.3mm which is used in this research is 18.6m/s and maximum crankshaft speed N=13500rpm. Comparing this with the data in Table 1.2 shows that while this engine has higher maximum crankshaft speed than production car engines its highest mean piston speed is lower than the maximum values for some car engines.

In order to maintain acceptable maximum piston speeds high-speed engines use short stroke. Reducing the stroke for a cylinder with fixed swept volume results in an increase of cylinder bore. Large bore allows the accommodation of valves with larger head diameters, however if the same compression ratio is to be used a much lower combustion chamber roof is necessary. This arrangement compromises the shape of the combustion chamber and reduces the compound angle between the inlet and exhaust valves in a conventional pent-roof arrangement. More importantly it presents a limitation on how early and at what rate the inlet valve can be open. Similarly it restricts how late and with what rate the exhaust valve can be closed. In some engines designed for motorsport application piston to valve clearance is the main limitation on the inlet valve opening timing and rate.

1.5.5 Performance and other issues related to high-speed operation

Achieving high output at high engine speed calls for the use of extreme inlet valve events, which is detrimental to low speed performance. The design of the inlet and exhaust system is also aimed to benefit high-speed performance. In addition to this the torque curve exhibits dips and peaks caused by the exposure to acoustic events occurring in the exhaust and inlet systems. Some of these problems are partially present in medium speed engines but due to the narrower speed range they are not of such magnitude.

High-speed engines often experience very rapid changes in engine speed during transient operating conditions. This is mainly the case during acceleration in low gears or downshifts. While beyond the scope of this research it is important to note that this presents a significant challenge for the design and operation of VVA systems. Jacquelin (2003) reports on the improvement in fuel consumption and NO_x emissions from increasing the response time of VVA system.

1.6 The reasons for investigating the inlet valve events rather than exhaust valve events

This research is motivated by the potential of VVA systems to increase the output of high-speed engines throughout their speed range. This is why it is important to establish which of the valve events have larger significance on engine performance. While acknowledging that there are many factors responsible for engine output, considerations mainly based on the effect on breathing efficiency, thermal efficiency and pumping losses reported in previous research are used.

IVO is the beginning of the valve overlap and as such it has effect on the flow in and out of the cylinder during this period. According to Grohn and Wolf (1989) the effect from variation of IVO timing within certain range on engine performance can reduce backflow into the inlet and increase breathing efficiency. The potential improvements are likely to be higher for high speed engines due to the wider speed range and larger valve overlap.

IVC has a direct effect on the amount of fresh charge trapped in the cylinder. Grohn and Wolf (1989) found that by controlling IVC timing it is possible to reduce the amount of

backflow after BDC and increase the breathing efficiency. Asmus (1982) claims that the timing of this event is the single most significant determinant of the balance between low speed and high-speed breathing efficiency. Increasing breathing efficiency generally results in proportional increase of brake power.

Asmus (1982) acknowledges that EVC is important for the amount of exhaust residuals trapped in the cylinder. However, he also demonstrates that the effect of EVC on low speed volumetric efficiency is lower than that caused by IVC.

The timing of EVO has an effect on both thermal efficiency and pumping losses of the engine during the blowdown process. However according to Asmus' research, varying this timing for different engine speeds results only in small improvement of the power output. This is because advancing EVO at elevated speeds reduces pumping losses however it reduces the thermal efficiency of the engine minimising the net effect on break power. In addition to this the reduced time in which the combustion process takes place leads to increased exhaust temperature. This limits the potential range for EVO advancement because of the thermal properties of the valve materials. Similarly delaying EVO at medium speeds in order to increase thermal efficiency is accompanied by increase in pumping losses again reducing the overall effect.

In view of these findings from previous research the effect on engine output from varying the inlet valve events is considered more significant than that of varying the exhaust valve events. This is why the inlet valve events become the focus for this research.

1.7 Objectives of this research

The main objective of this research is to investigate the effect of the inlet valve event timing on the gas exchange process in high-speed IC engines and to use this knowledge to assess the feasibility of using selected VVA systems.

To achieve this, the research focuses in three areas:

1) The aim of the first part of the research is to establish the high-speed feasibility of VVA systems. It is appreciated that depending on the complexity, the design effort and cost involved most VVA systems can be adapted to very high-speed operation. However, without discarding completely any technology, a general guide is presented for the current VVA systems suitable for high-speed operation.

2) The second part of the research concentrates on the effect that inlet valve event timings have on breathing efficiency in high-speed IC engines. The objective is to explain the reason for these effects by looking at the gas exchange mechanisms involved. This allows the optimum valve events in terms of breathing efficiency to be determined.

3) This knowledge is used to assess the abilities of particular VVA systems and to suggest a strategy for best matching the optimum valve events. A recommendation is given regarding simpler systems that can also satisfy these events and inspire design effort for making it suitable for high-speed operation.

1.8 Overview of the thesis

Acknowledging the great variety of VVA systems, Chapter 2 attempts to classify them and present an example of each major group. The information presented for each system includes operating principle and valve event variation ability. An assessment is also made of their dynamic suitability for high-speed operation.

Chapter 3 describes the engine simulation software used in this investigation. It discusses the limitations and advantages of using such simulation and provides details

for the individual submodels used to represent the engine elements and processes. An assessment is made of the effect of the assumptions employed on the results. Details of the engine model used in this research are presented.

Chapter 4 introduces the experimental set up used to validate the engine simulations software. Correlation of predicted and experimental data is also presented. Good agreement exists between the inlet and exhaust instantaneous pressure demonstrating correct modelling of the gas dynamic behaviour, which is very important for this investigation.

Chapter 5 explores the effect of gas dynamic behaviour in the inlet and exhaust system on the gas exchange process and identifies the main cylinder filling mechanisms. This is essential in order to be able to later discuss the effects of the individual valve timings. The breathing process in a multicylinder engine like the one used in this research is a function of the complex gas dynamic behaviour in the inlet and exhaust system and the cylinders. Examining it is complex and unnecessary as it relates to a particular engine arrangement. It is more important to understand the fundamentals of this gas dynamic behaviour. This is done by investigating the gas exchange process in two single cylinder engine models, one with infinitely short exhaust and the other with an infinitely short inlet ducts.

Chapter 6 describes the findings from the parametric study of the effect of IVO timing on charging efficiency. The effect of five profiles with different IVO timings has been explored by using engine simulation. The results are explained by identifying the most sensitive part of the inlet process and examining the gas flow and pressure differential across the cylinder during this period.

Chapter 7 presents the results from the parametric study of the effect of IVC timing on charging efficiency. Again the effect of five profiles with different IVC timings has been explored by using engine simulation. The results are explained in a similar way to the previous chapter by identifying the most sensitive part of the inlet process and examining the gas flow and pressure differential across the cylinder during this period.

Chapter 8 comments on the ability of particular VVA systems to satisfy the optimum inlet valve timings. The independence of the results from the two parametric studies presented in Chapter 6 and 7 enables the combined use of the optimal IVO and IVC for different engine speeds. This is compared with the abilities of VVA systems identified as dynamically suitable for high-speed operation in Chapter 2. A possible control strategy to best utilise these abilities is suggested and the performance of the systems are compared. Another VVA system that is not immediately suitable for high-speed operation but is simple and can satisfy these requirements comparatively well is also identified as worthy for dynamic development.

Chapter 9 concludes this thesis and identifies possible areas for future research.

Chapter 2

Classification and Review of Variable Valve Actuation Systems

The IC engine has evolved a lot since its invention. Its progress has been in various areas and has been guided by different aims. Initially the design effort was purely devoted to increase of efficiency and durability and reduction of production costs. Modern IC engines are used to propel vehicles, where they are required to perform efficiently in a wide range of operating and environmental conditions or to power generators, where they normally operate at a fixed speed and load. It is the first application, which presents the bigger challenge and requires a degree of variability in parts of the engine hardware, as well as the appropriate control capabilities so that it performs optimally in different operating and environmental conditions.

The progress in the electronics field gave birth to digitally managed fuel injection and ignition for SI and more recently for Compression Ignition (CI) engines. It also allowed control of certain hardware parameters, such as variable turbocharger geometry (Jain, 2004), intake system geometry (Hatamura *et al.*, 1987; Larsson *et al.*, 1991; Nishimura *et al.*, 1987; Matsumoto and Ohata, 1986)) and exhaust system geometry (Yamabe and Ueda, 1988; Nakayasu *et al.*, 2001). One of the biggest compromises on engine performance is imposed by the limitations of the conventional valvetrain, which is unable to vary the valve events as a function of speed and load. This chapter discusses the range of VVA systems that are designed to provide a solution to this problem.

Considering the great variety of VVA devices in existence, an attempt is made to classify them and list few examples of each major group. The information presented for each mechanism includes the operating principle and valve event variation ability. An assessment, based on valvetrain and camdrive dynamic considerations, is made of the suitability of each type for high-speed operation.

2.1 Definition of valve event parameters

Before describing the different VVA systems it is necessary to define certain valve event parameters shown in Figure 2.1, which will be later used to discuss their abilities.

2.1.1 Valve event timing

The *valve event timing* is a term used to quantify the occurrence of the valve event in the engine cycle. It is defined as the angular position of the crankshaft when valve events occur and is expressed in Crankshaft Angle (CA) degrees relative to TDC or BDC. The valve event referred to is either the valve opening or closing point. Because the exact point when valve motion starts or ends is difficult to measure for practical reasons the crankshaft position at a particular lift used. The lift defined by the appropriate SAE standard is 1 mm, however, others are also used by different manufacturers. The timing of Maximum Opening Point (MOP) combined with valve event duration is commonly used if the lift profile is symmetrical relative to this point.

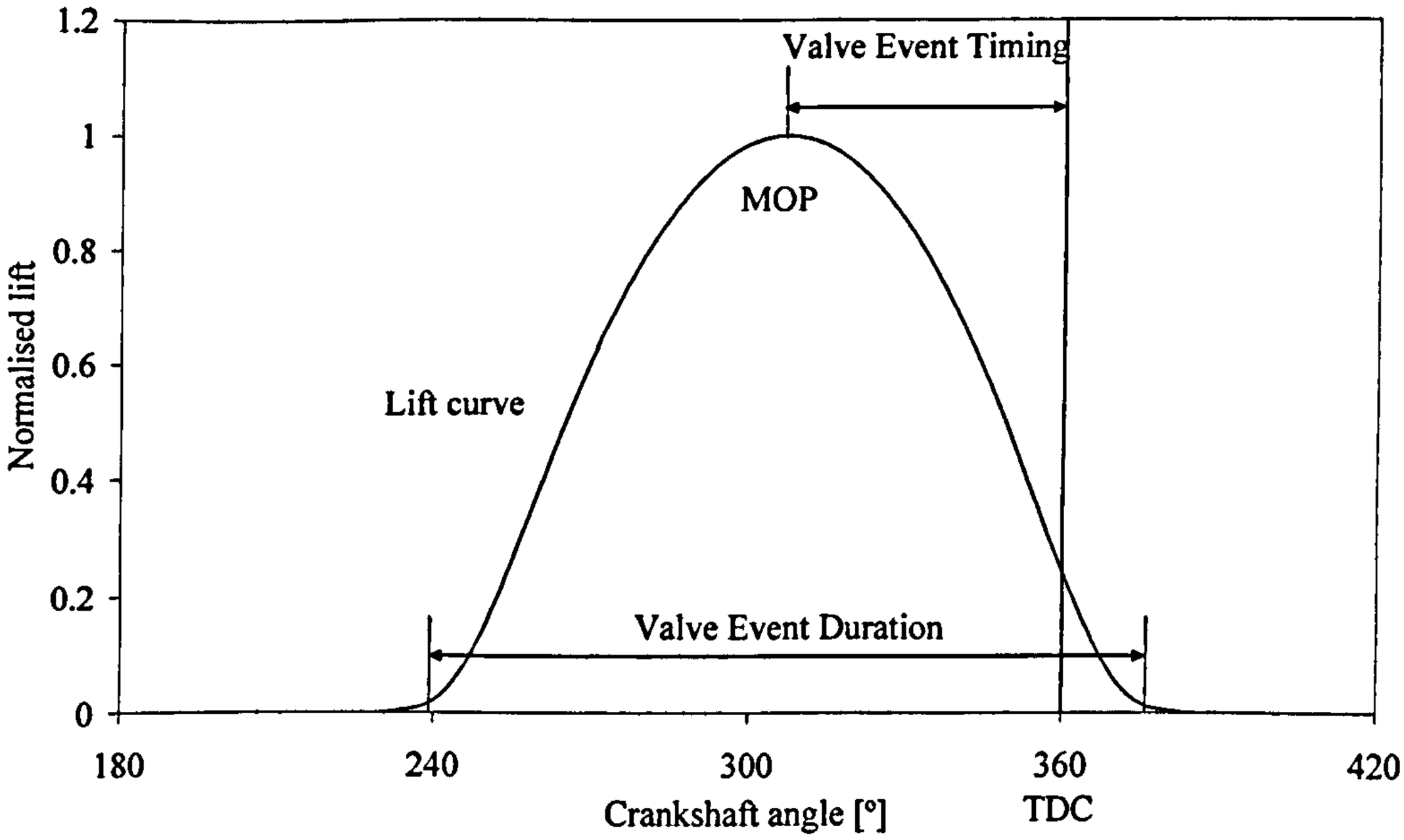

Figure 2.1: Valve event parameters
(the lift is normalised with maximum lift value)

2.1.2 Valve event duration

Valve event duration is the period in CA degrees during which the valve is not closed. For the reasons described in the previous section, reference lift is used rather than the actual start or end point of the lift motion.

2.1.3 Lift curve

The *lift curve* gives information of the valve motion during the valve event duration. It can provide information on valve velocity, acceleration and jerk. The area under the valve lift curve is an indication of the flow capabilities of the valve during valve event duration.

2.2 Current VVA technology

VVA technology has been a topic of various review publications (Gray, 1988) and comparison studies (Bozza *et al.*, 2001; Freudenstein, 1988). A number of different classifications have been suggested (Ahmad and Theobald, 1989; Dresner and Barkan, 1989). Figure 2.2 shows classification similar to that suggested by Stone and Kwan (1989) based on mechanism type and technology employed. According to Ingenieurbüro Bockhmann and Hannibal (2004) there are already around 4000 patents in existence. A large number of patent applications for new mechanisms are made every, year however few of them are conceptually different. This is why the VVA systems described below are by no means a comprehensive list of all existing mechanisms. An attempt is made to give a few examples of each type. The information for each individual system is presented in the following format:

- Manufacturer or research body developing the system
- System's abilities
- Description and operating principal of the system
- Suitability for high-speed operation considering the effect of the VVA system on valvetrain dynamics
- Additional comments

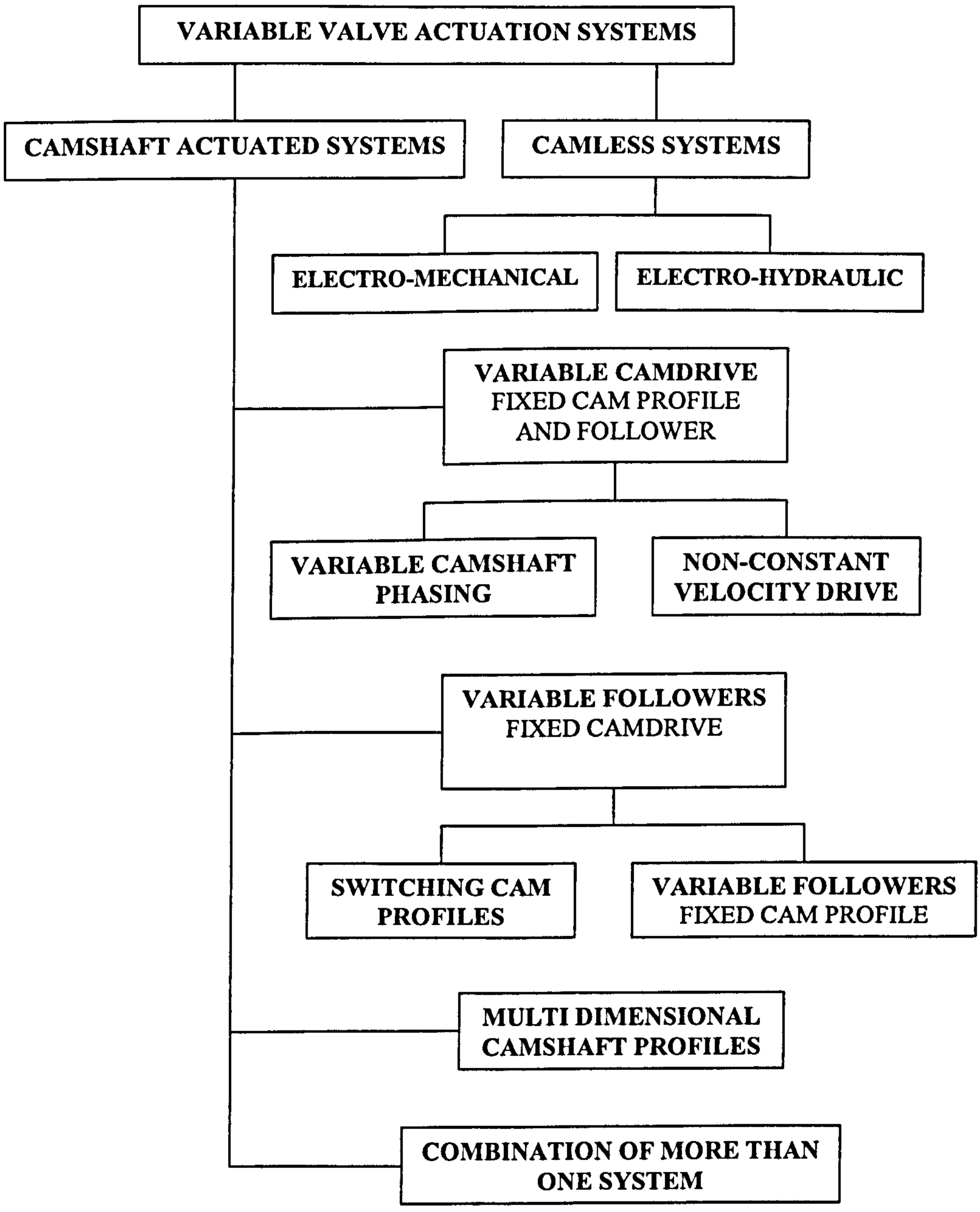

Figure 2.2: Classification of current VVA technology

2.2.1 Camshaft actuated systems

The mechanisms classified in this group use a camshaft profile to actuate the poppet valves. A great number of designs have been proposed, each of them enabling variation of the valve event parameters to a different degree.

2.2.1.1 Variable camdrive

2.2.1.1.1 Variable Camshaft Phasing (VCP)

Manufacturers or research bodies developing the system:

BMW AG (Otto *et al.*, 2000), Ford Motor Company and INA-Schaeffer KG (Steinberg *et al.*, 1998), Mercedes-Benz AG (Grohn, 1990), Nissan Motor Corporation (Maekawa *et al.*, 1989), Toyota Motor Corporation (Nakamura *et al.*, 1997), Dr. Ing. h.c. F. Porsche AG (Becker, 2000), Delphi Corporation (Delphi Corporation Website, 2004), AFT Atlas Fahrzeugtechnik GmbH (AFT Atlas Fahrzeugtechnik GmbH Website, 2004) and others.

Abilities:

Continuous or discrete variation of the phasing of the valve events in relation to the crankshaft (Figure 2.3).

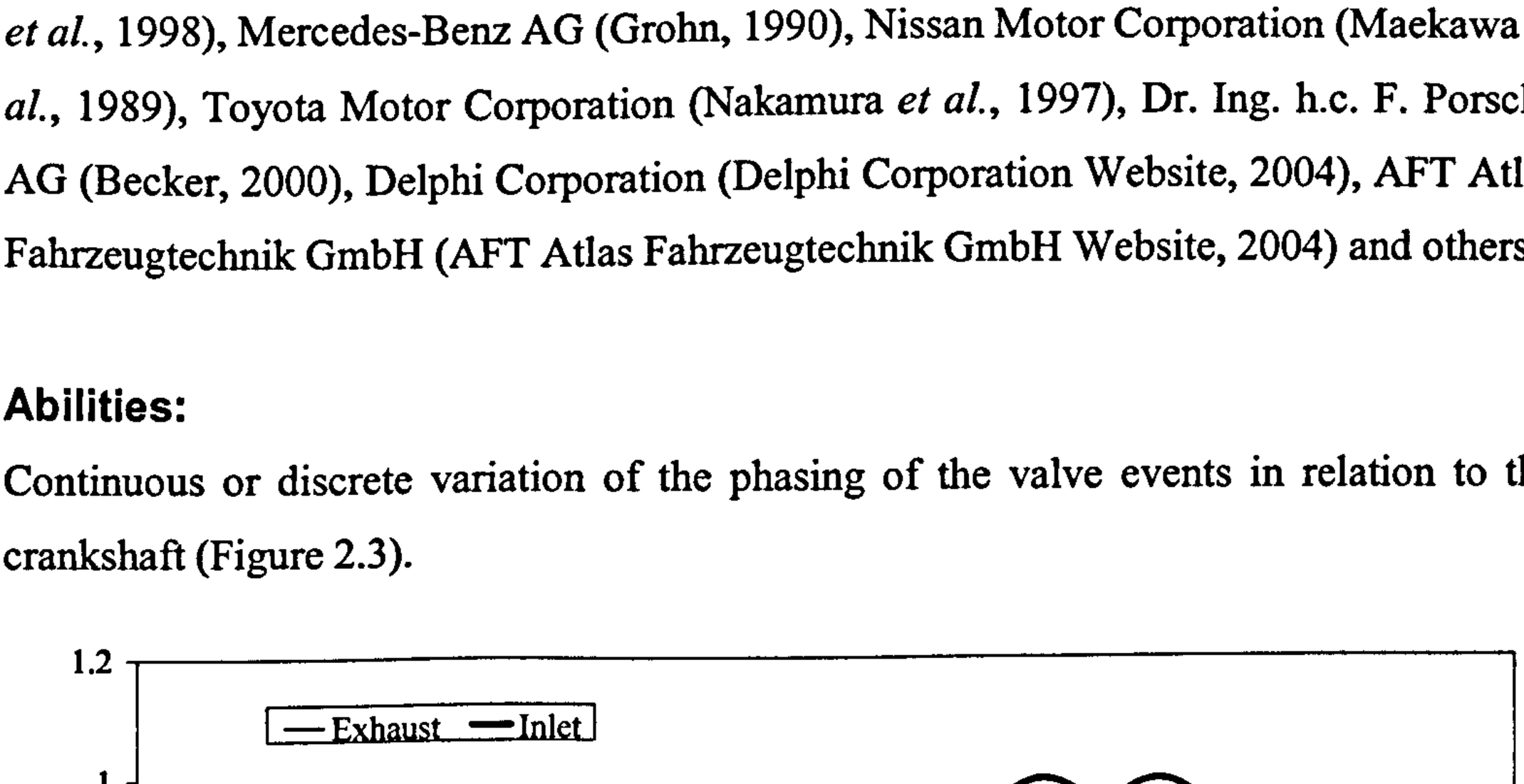

Figure 2.3: Variable Camshaft Phasing system abilities

(the lift is normalised with maximum lift value)

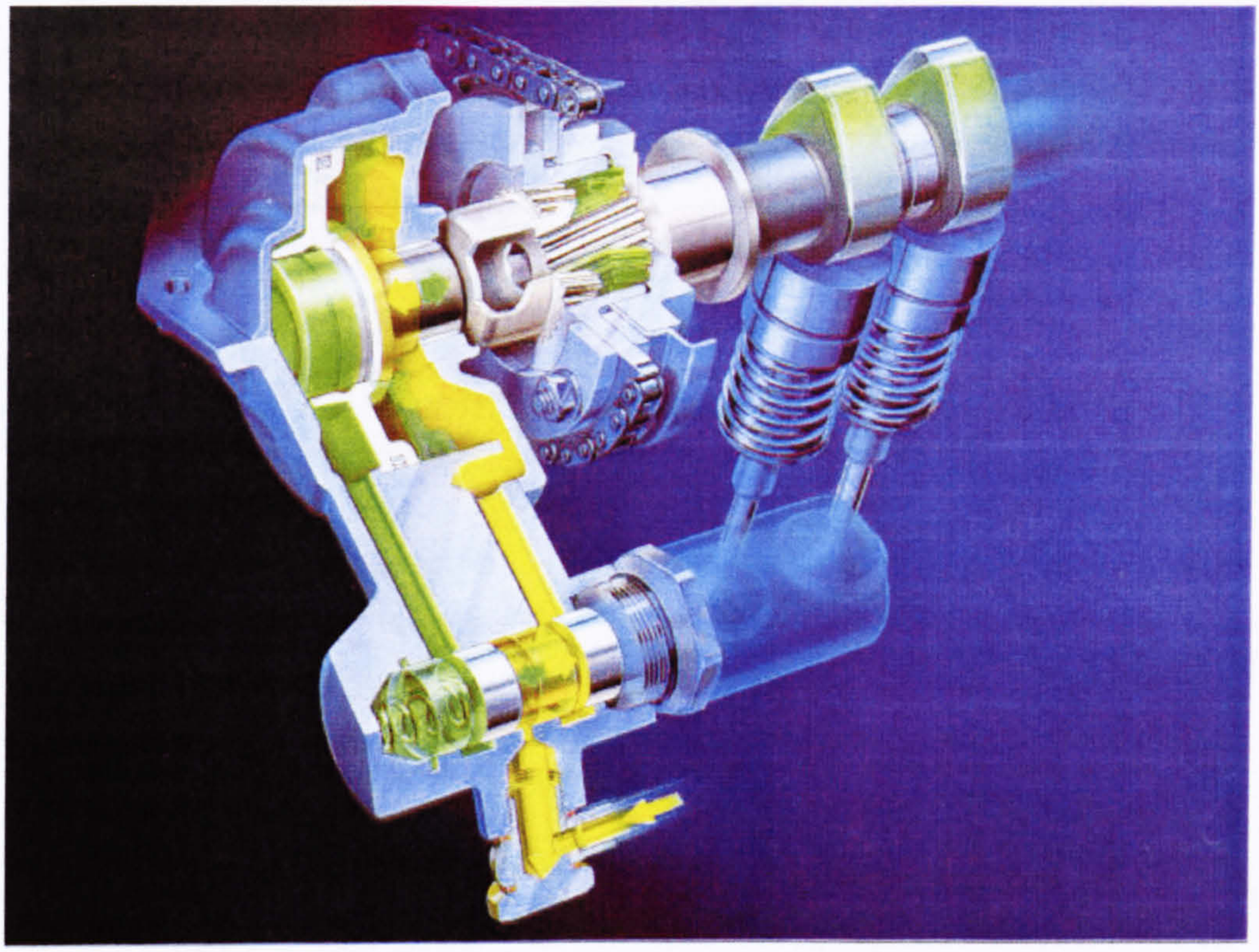

Figure 2.4: Typical helical spline type VCP system

(Auto Innovations Website, 2004)

Description:

There are two different methods of varying the camshaft phasing. In the most commonly used arrangement this is achieved by changing the angular position of the camshaft drive sprocket relative to the camshaft. There are currently at least three different types of mechanisms for achieving this. Figure 2.4 shows a typical system where drive sprocket meshes with an intermediate gear with helical splines. The intermediate gear is connected to the camshaft by straight or helical splines with the opposite angle. Moving the intermediate gear along the camshaft axis changes the angular position of the drive gear and camshaft. This movement is controlled by hydraulic pressure regulated by a solenoid valve.

Another similar arrangement is the vane type system. Change in the relative angular position of the camshaft and drive sprocket is achieved by controlling the pressure on both sides of the vanes inside the sprocket, as illustrated in Figure 2.5.

AFT Atlas Fahrzeugtechnik GmbH (2004) recently launched an electric variable phasing device. Angular position change is achieved with an electric motor. Improvement in response time and achieving of required position before engine start are claimed.

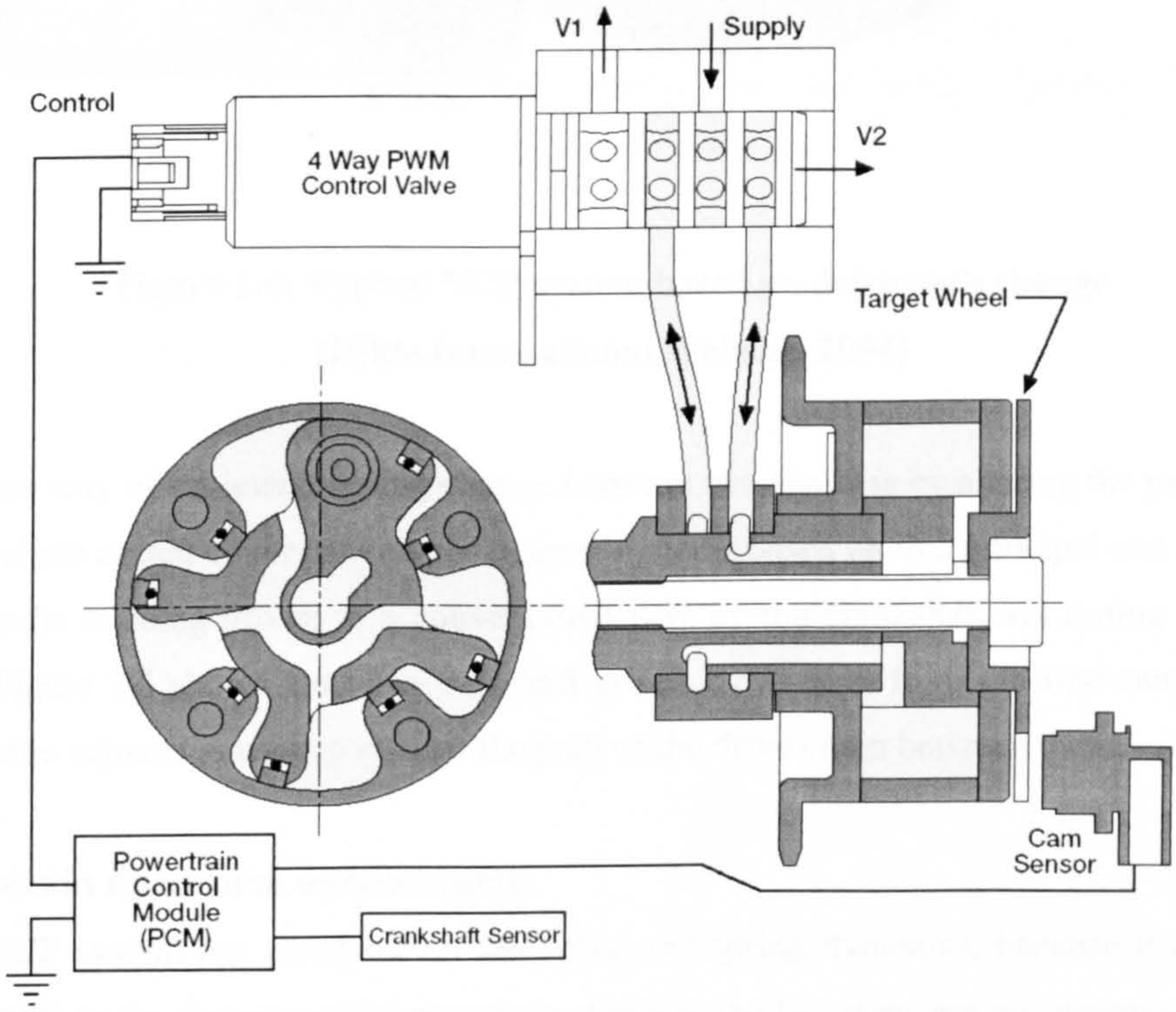

Figure 2.5: Typical vane type VCP system
(Delphi Corporation Website, 2004)

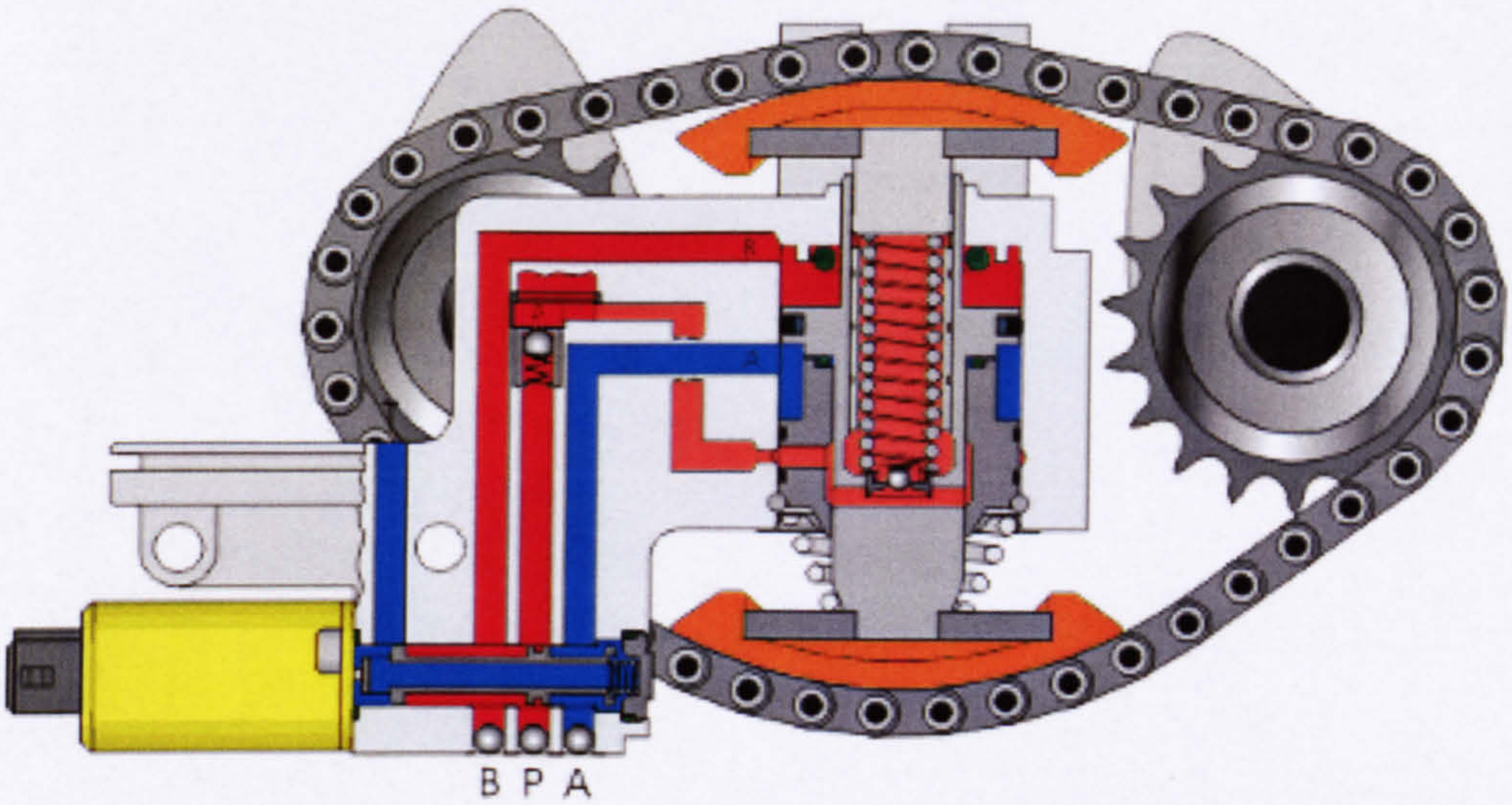

Figure 2.6: Typical VCP system based on drive path change
(Hilite International Website, 2004)

Another way of achieving timing change between two shafts is by altering the path of the drive chain or belt connecting them. In most systems based on this principal one of the camshafts is being driven in a conventional way by the crankshaft via timing chain or belt. Figure 2.6 shows the other camshaft driven by a chain from the first camshaft. A hydraulic adjuster is used to change the path of the drive chain between them.

Valvetrain dynamics assessment:

The VCP system has no effect on the valve and spring dynamics, because it does not contribute to the dynamic valvetrain mass. Despite the fact there are no current examples for use of this system on high-speed engines it is identified as one of the most suitable. The effect on cam drive dynamics at elevated speeds as well as the short response times required in high performance engine should be considered when designing the system.

Additional comments:

Along with the three-dimensional cam lobe system, the VCP arrangement was one of the first systems employed. It is by far the most popular system used by manufacturers because of the relatively low cost and suitability to be adapted to most engine configurations without significant modifications to the conventional valvetrain components. The systems offer independent and continuous control of the camshaft timing.

2.2.1.1.2 Non-constant velocity drive

Manufacturers or research bodies developing the system:

Rover Group Limited -Variable Valve Control (VVC), (Parker, 2000)

Märkische Fachhoschule Iserlohn and Ingenieurbüro KORO Neckarsulm - VAST, (Hannibal and Bertsch, 1998)

Abilities:

Continuous variation of valve event duration (Figure 2.7).

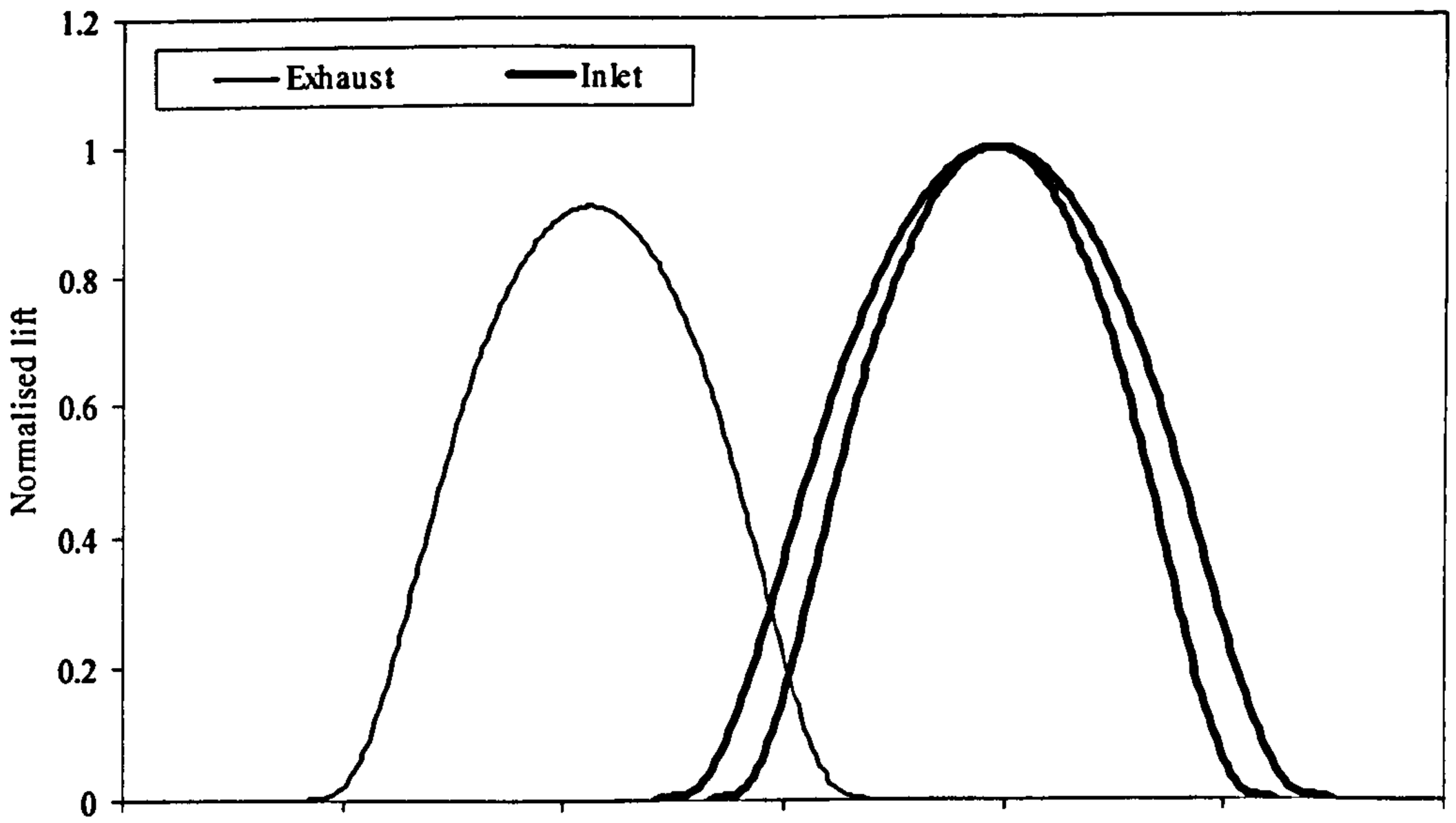

Figure 2.7: Non-constant velocity drive system abilities

(the lift is normalised with maximum lift value)

Description:

This system is based on the Non-constant velocity drive principle. The cam lobes are driven via a drive pin from a drive gear, which has an axis of rotation different from that of the cam lobes. The rotational velocity of the cam lobes is a function of the distance between the two axes. Both the Rover VVC and VAST systems shown on Figures 2.8 and 2.9 respectively are based on this principal.

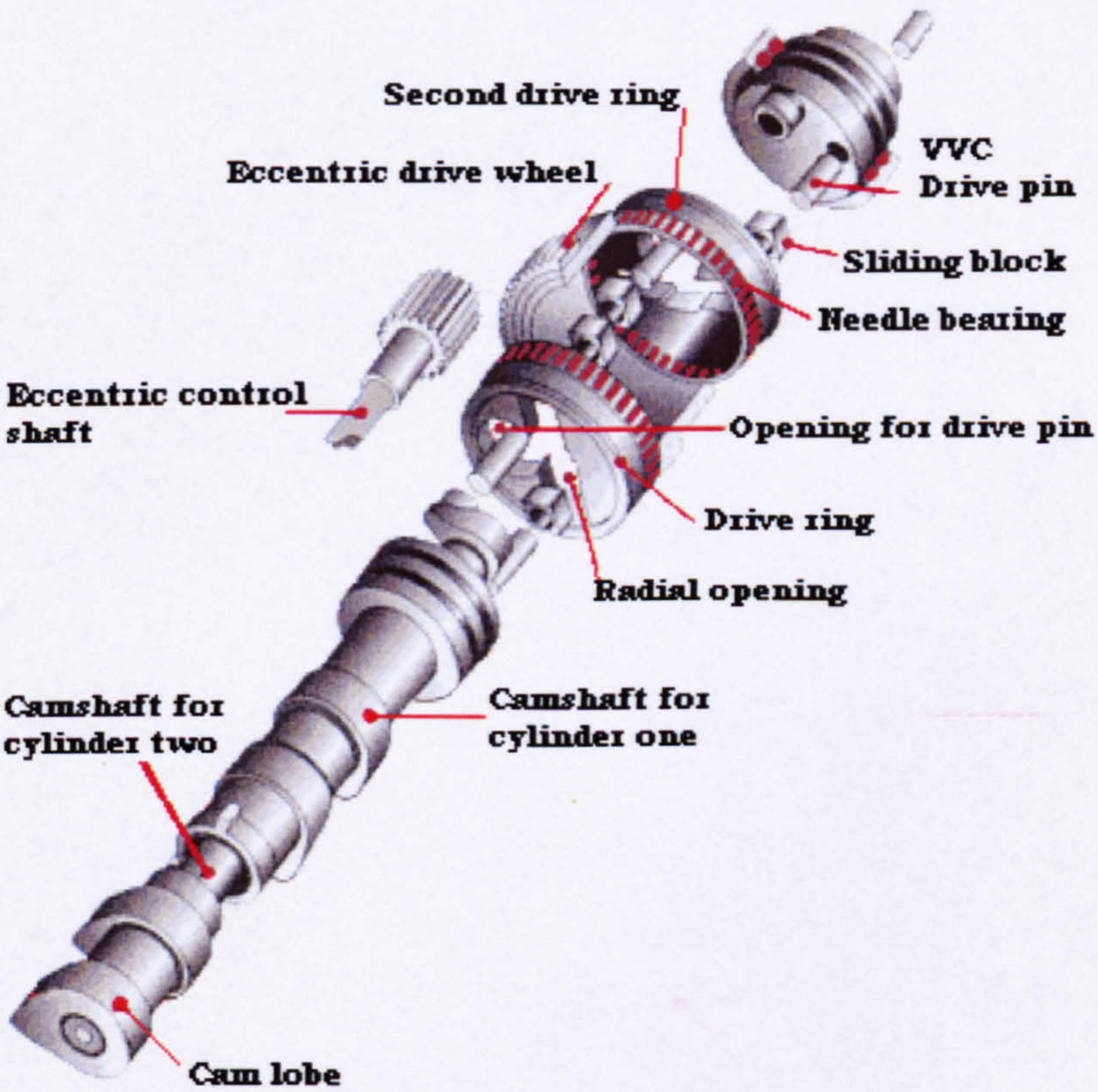

Figure 2.8: Rover VVC system

(MGFcar Website, 2004)

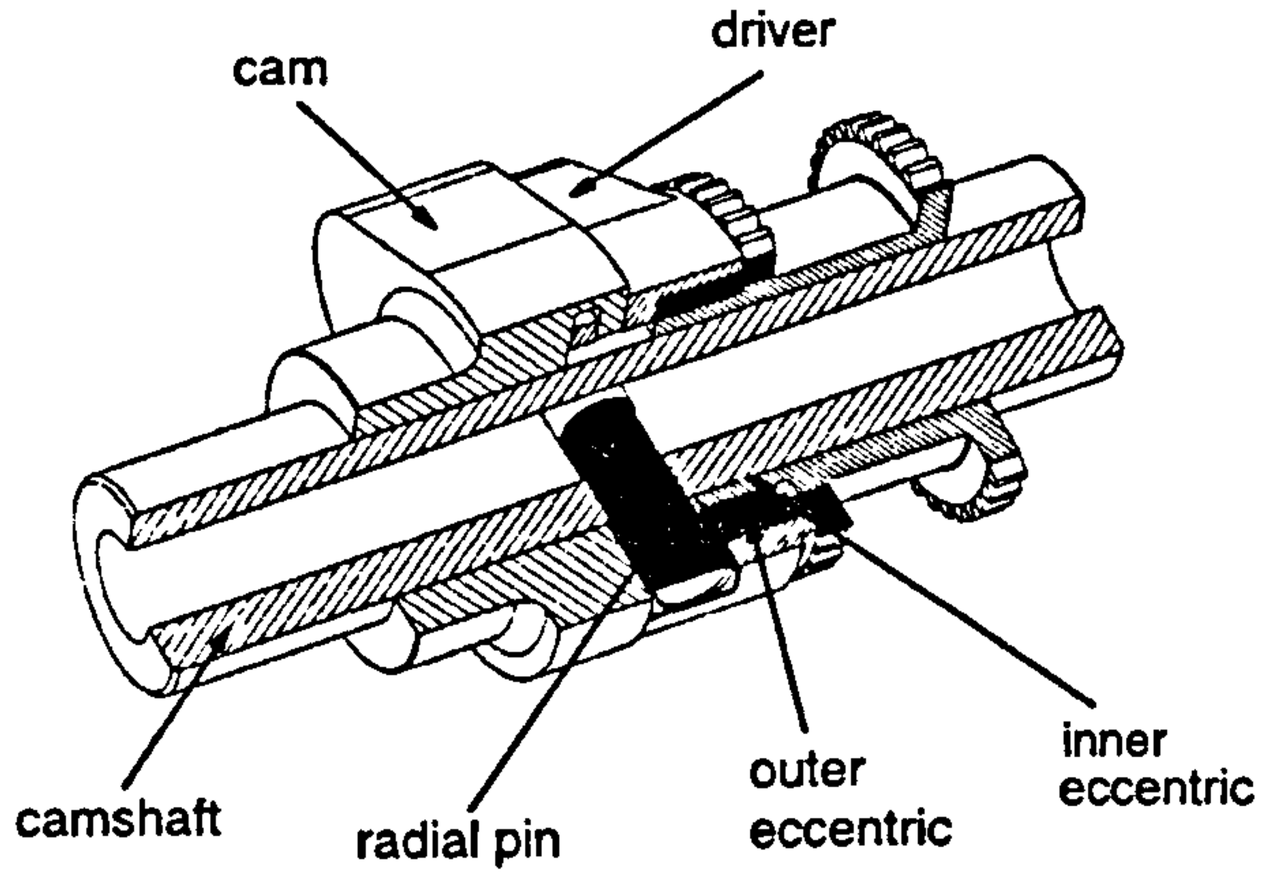

Figure 2.9: VAST system

(Hannibal and Bertsch, 1998)

Valvetrain dynamics assessment:

The system can be used with directly actuated tappets and does not contribute to the dynamic valvetrain mass. The main concern is the reliability of such a complex arrangement operating at high speeds.

Additional comments:

The system used by Rover allows for increase of the valve event duration from 220 to 295 CA° while the MOP remains approximately the same. The system is complex and requires separate drives to the camshafts for each two cylinders. The VAST system has a similar ability; however there is a slight shift of MOP. The latter is more compact and can easily be applied to double overhead camshaft engines. Large changes of angular velocity of the lobes leads to high friction in the system.

2.2.1.2 Variable cam followers

2.2.1.2.1 Switching profiles

Manufacturers or research bodies developing the system:

Honda Motor Company, Variable Valve Timing and Lift Electronic Control (VTEC), (Hosaka and Hamazaki, 1991)

Mitsubishi Motors Corporation, Mitsubishi Innovative Valve Timing and Lift Electronic Control (MIVEC), (Hatano *et al.*, 1993),

Toyota Motor Corporation, Variable Valve Timing with intelligence (VVTi) (Shikida *et al.*, 2000)

Dr. Ing. h.c. F. Porsche AG, Variable Valve System (VVS), (Brustle and Schwarzenthal, 1998)

Abilities:

Actuation of the valves by two or three different camshaft profiles as shown in Figure 2.10.

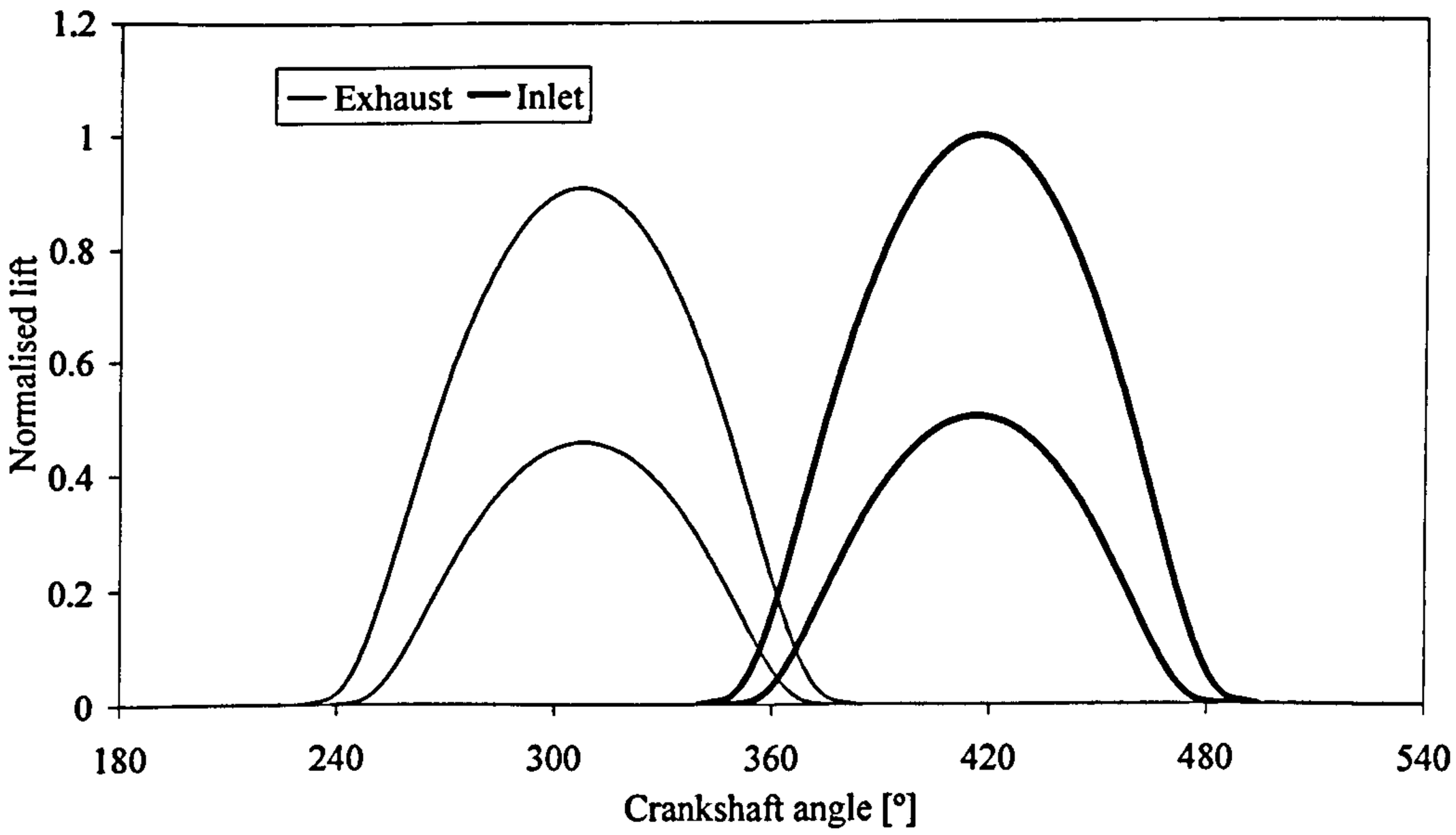

Figure 2.10: Variable cam follower – switching profiles system abilities (the lift is normalised with maximum lift value)

Description:

In the Honda VTEC (Figure 2.11), Mitsubishi MIVEC and the Toyota VVTi systems two or three camshaft lobes with different profiles act on individual rocker arm mechanisms. The rocker arms actuated by the low lift lobes act directly on the valves. The rocker arm in contact with the high lift lobe is not connected directly to the valves. When low valve lift is required the eccentricity of the high lift lobe is translated in lost motion of its rocker arm. When high lift operation is needed the appropriate high lift rocker arm is connected by a pin to the others and translates the lobe's eccentricity into valve lift. The pin is actuated by oil pressure and is controlled by a solenoid valve. The engagement and disengagement of the pin coincides with the angular position of the camshaft when the rocker arms are contacting the base circle of the lobes.

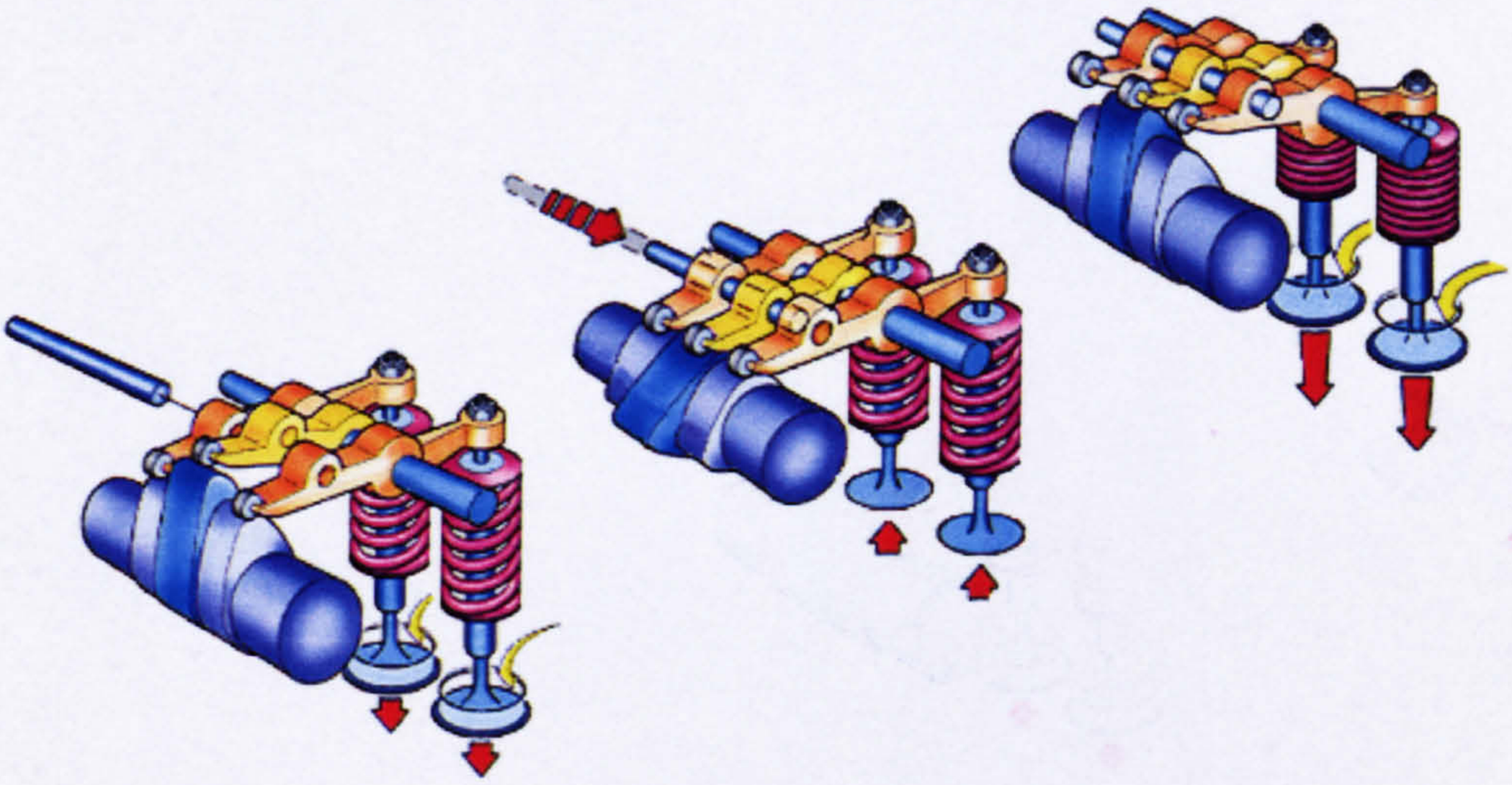

Figure 2.11: Honda VTEC system

(Honda Motor Company Website, 2004)

The Porsche VVS system employs two lobe profiles directly acting on a tappet constructed of two co-axial pieces. The tappet mechanism, originally designed by Lotus Engineering and produced by INA, is shown in Figure 2.12. The outer piece can be locked to the inner one by means of hydraulic pistons. When the low lift profile is required the outer piece is not engaged and the inner lobe actuates the valve. When the other profile is needed, the outer piece is locked and the outer lobe governs the motion.

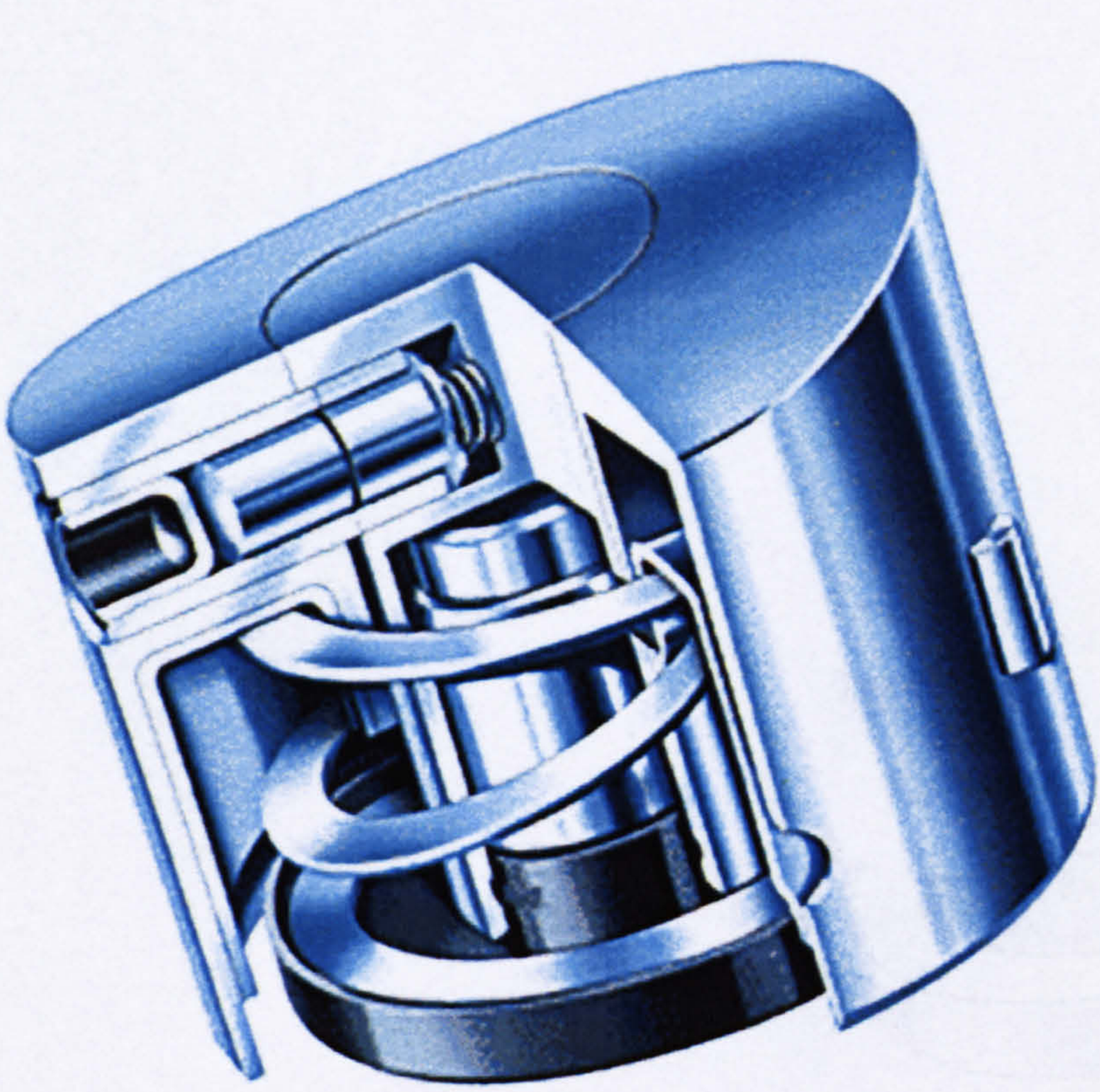

Figure 2.12: INA switchable tappet

(INA-Schaeffer KG Website, 2004)

Valvetrain dynamics assessment:

The Honda VTEC system is currently used in engines with maximum crankshaft speed of 9000 rpm. Due to the high dynamic valvetrain mass and low stiffness associated with the finger follower arrangement and the associated locking elements it requires further design effort to allow operation at significantly higher speeds.

The Porsche's VVS system is employed in engines operating at maximum speeds of 8500 rpm. Due to the increased mass of the tappet high-speed operation requires further development.

Additional comments:

Because of the step change between the two different profiles there is a sharp change in the airflow in the engine. Brustle and Schwarzenthal (1998) report a step change in torque of 60Nm in a Porsche engine, which can lead to driveability problems. This is compensated for by changing fuel quantity, ignition timing and even throttle angle.

2.2.1.2.2 Follower lost motion

Manufacturers or research bodies developing the system:

Honda Motor Company, Honda Hyper VTEC (Takaaki *et al.*, 1999)

Abilities:

Valve deactivation.

Description:

This system is similar to the switchable tappet arrangement described in the previous section, but differs in the fact that only deactivation can be achieved. The valves are actuated by a conventional camshaft lobe as shown in Figure 2.13. The camshaft follower has hydraulic and spring elements allowing it to achieve lost motion so that the camshaft eccentricity does not cause valve lift. The locking is controlled by a solenoid interrupting the oil supply to the tappet. Independent deactivation of one inlet and exhaust valve per cylinder is possible.

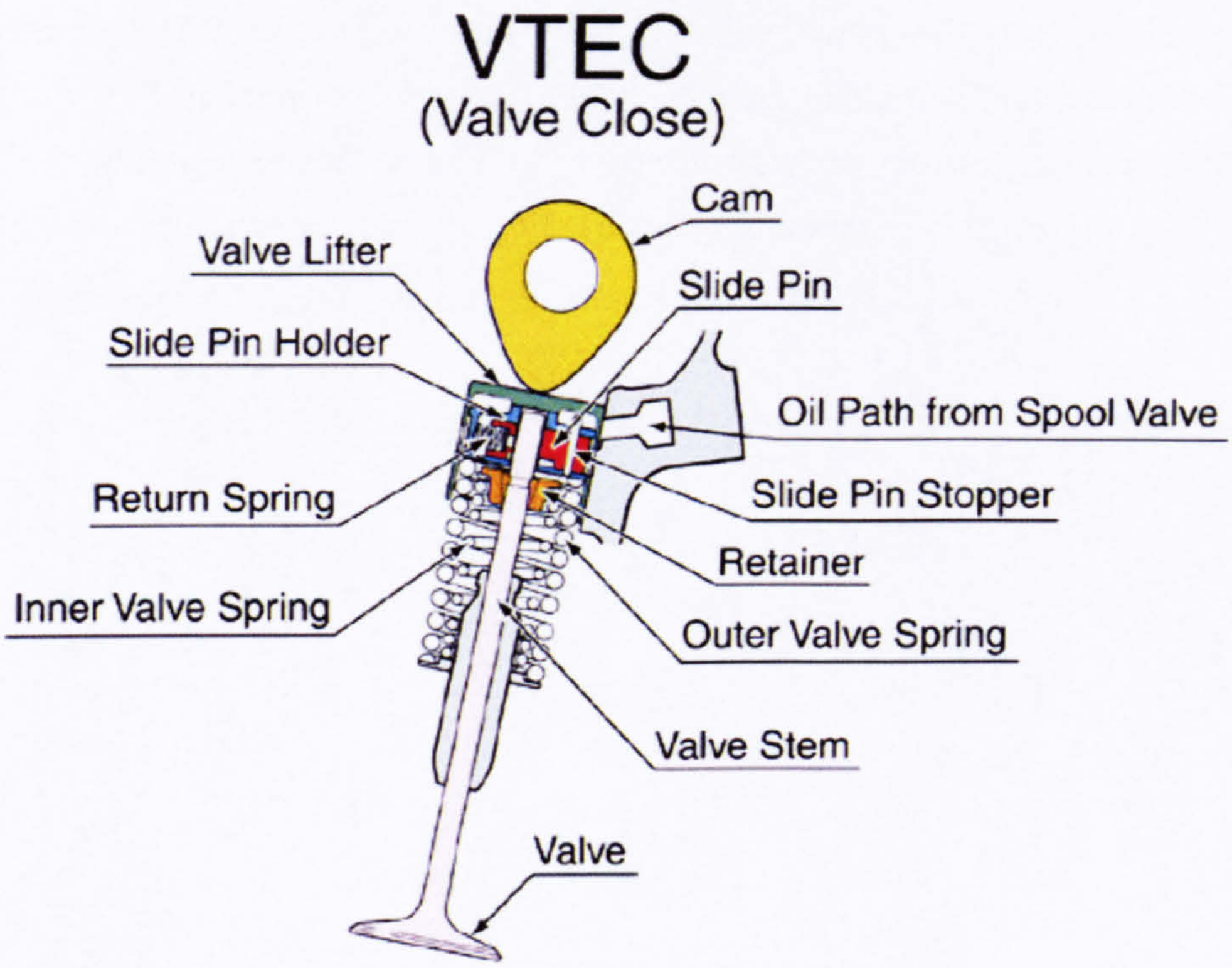

Figure 2.13: Honda Hyper VTEC system

(CMG Website, 2004)

Valvetrain dynamics assessment:

Adding mass to the cam follower is detrimental to valvetrain dynamics. Takaaki *et al.* (1999), show how by careful design it can be kept to a minimum allowing operation at speeds of 12000 rpm.

Additional comments:

The Hyper VTEC system deactivates only one of the inlet valves. This increases the gas velocity through the active valve. Deactivating one of the inlet valves completely can cause fuel to accumulate behind the inactive valve and cause AFR instabilities when the valve opens. To avoid this problem the VTEC system used on another Honda engine opens the valve with 0.65 mm as reported by Horie *et al.* (1992).

2.2.1.2.3 Multicam systems

Manufacturers or research bodies developing the system:

General Motors Corporation, (Pierik and Gecim, 1997), Helsinki University of Technology, (Jarvi, 1998; Jarvi, 2003), University of Karlsruhe (Berg and Kachel., 1997), BMW AG (BMW AG Website, 2004), Meta Motoren – und Energie –Technik GmbH (Kreuter and Heuser, 1998)

Abilities:

Independent and continuous variation of all valve event parameters is possible depending on the complexity of the system.

Description:

There is a big variety of systems of this type but they are all based on the same operating principal. The lift motion is a function of the geometry of one or more camshafts and the geometry of other elements as shown in Figure 2.14. Due to their complexity only the BMW Valvetronic system illustrated in Figure 2.15 is used in a production engine.

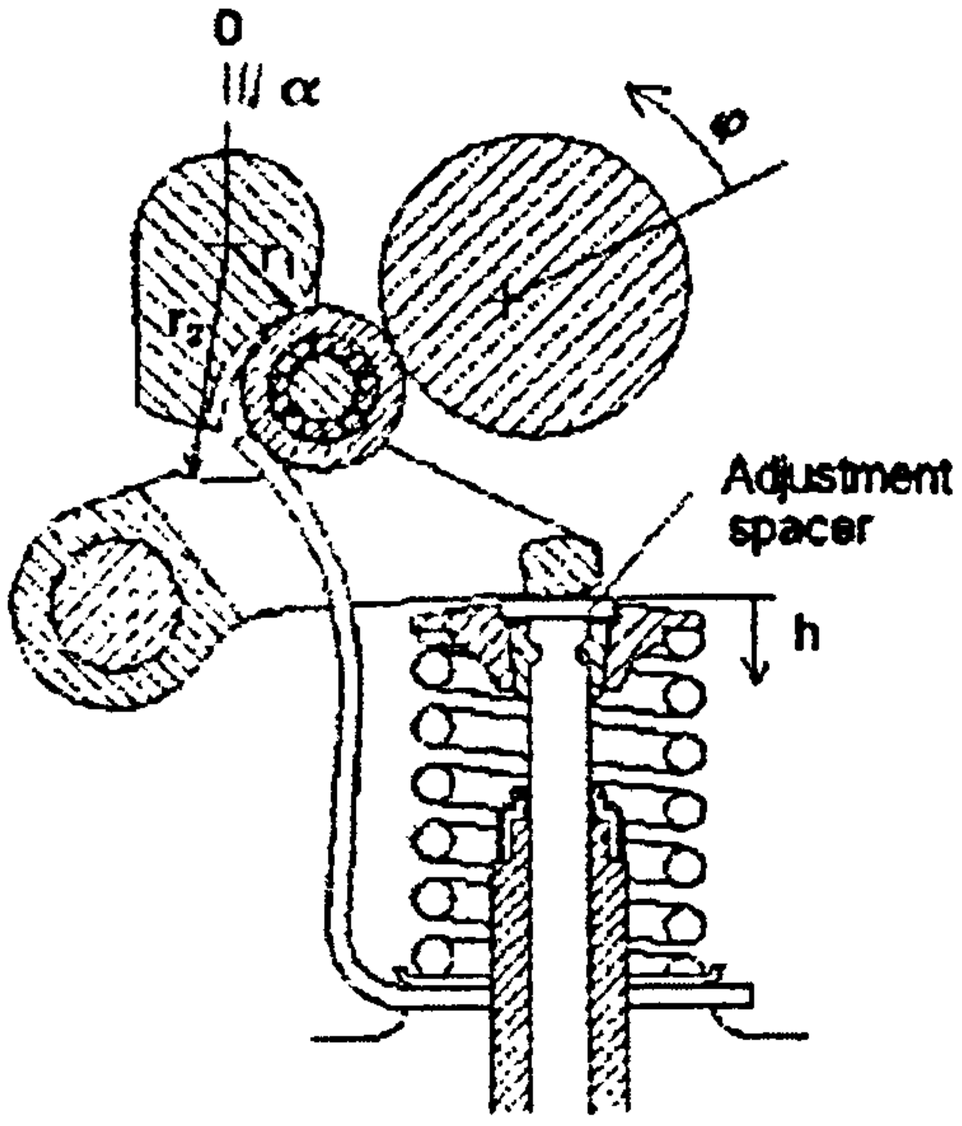

Figure 2.14: Typical multicam system

(Jarvi, 1998)

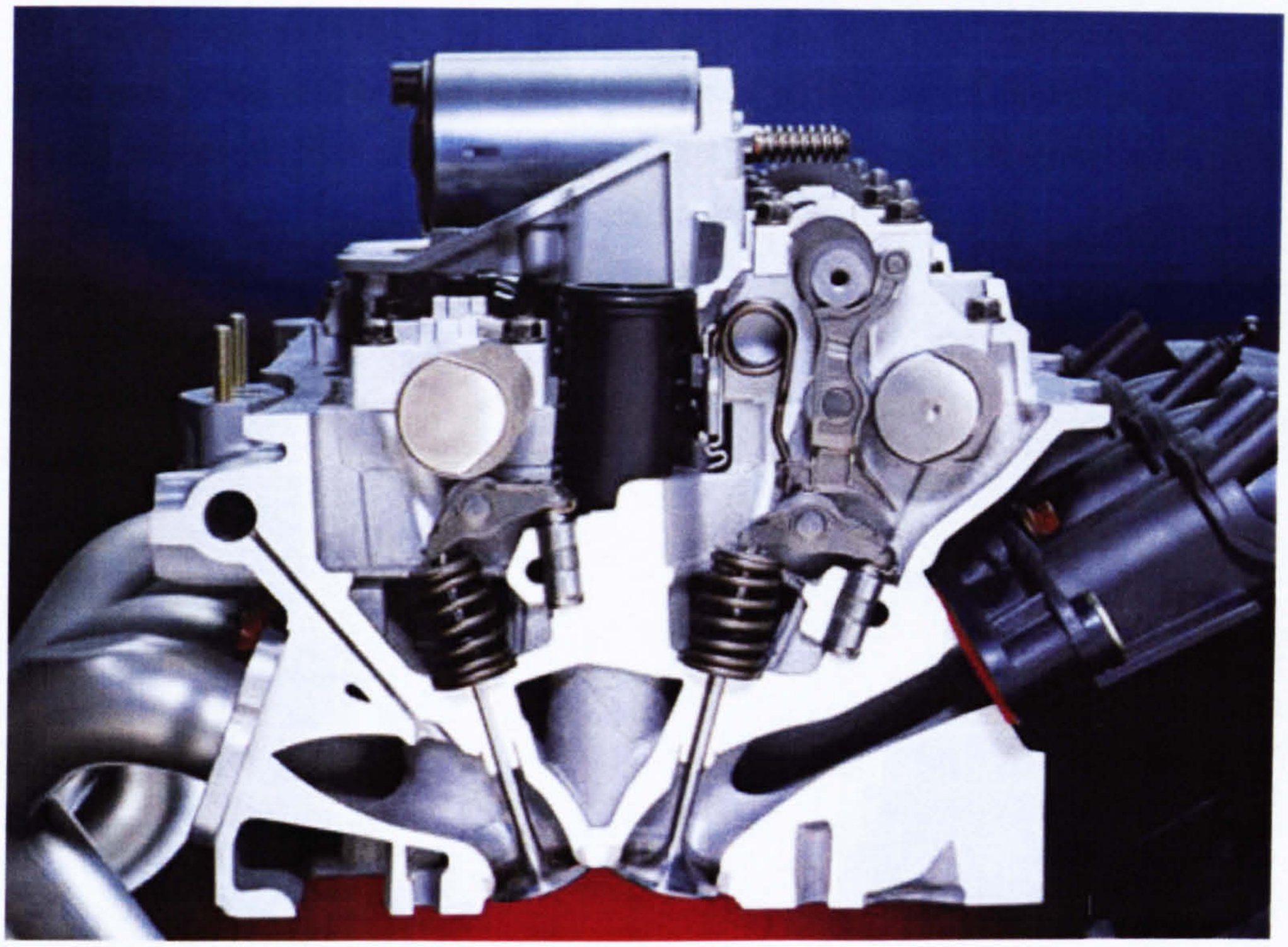

Figure 2.15: Valvetronic system

(BMW AG Website, 2004)

Valvetrain dynamics assessment:

Due to the number of mechanical elements involved in generating the valve motion these mechanisms have low stiffness and in most cases contribute to the dynamic valve mass. This together with reliability concerns associated with their complexity makes them unsuitable for high-speed operation.

Additional comments:

BMW AG (2004) claim that the Valvetronic system allows throttle-less load control.

2.2.1.2.4 Variable ratio rocker arms

Manufacturers or research bodies developing the system:

Atsugi Motor Parts Co and Nissan. (Hara *et al.*, 1989)

Ricardo and Motive Engineering (McElwee *et al.*, 1997)

The Entzminger Corp. (Entzminger W., 1988)

Bangkok University (Anontaphan T., 2003)

Abilities:

Variation of the effective event duration and proportional scaling of the lift curve (Figure 2.16).

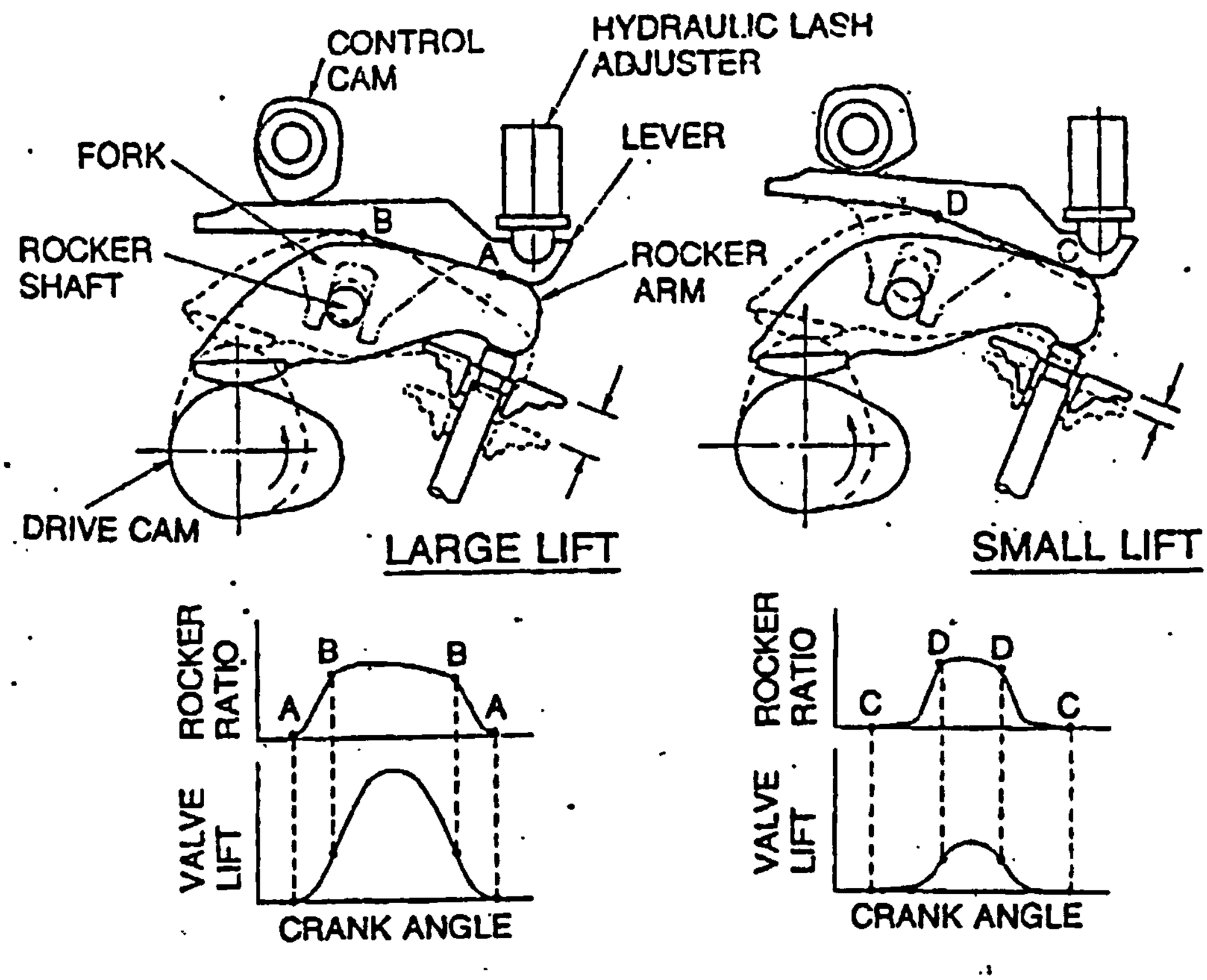

Figure 2.16: Nissan variable ratio rocker arms system diagram and abilities (Podnar and Kubesh, 1998)

Description:

Numerous mechanisms have been proposed which are capable of varying the valve events by moving of the pivot point of the rocker arm. This by itself does not change the point when the valve motion starts and ends but significantly alters the lift curve. The Nissan mechanism provides variation of the rocker ratio during different parts of the lift curve. This is done by a lever that supports and runs along the gently curved back of the rocker arm. The range of rocker ratios is controlled by the angular position of this lever. The latter is adjusted with the use of a cam connected to a DC motor. A hydraulic lash adjuster is used to compensate for the valve to rocker arm clearance.

The Ricardo system uses a toothed rocker arm on a toothed pivot, which runs in a toothed holder. Small valve event timing shift can be achieved due to the design of the toothed pairs.

Valvetrain dynamics assessment:

Similar to the mechanisms described in the previous section, the number of mechanical elements involved in generating the valve motion results in low stiffness and contributes to the dynamic valve mass. This and reliability concerns associated with their complexity makes them unsuitable for high-speed operation.

Additional comments:

These types of systems is mechanically complex and presents packaging constraints.

2.2.1.2.5 Variable follower height

Manufacturers or research bodies developing the system:

Institute of Internal Combustion Engines, Technical University of Vienna (Lenz *et al.*, 1989)

Hyundai Motor Company and Siemens VDO Automotive AG (Lee *et al.*, 1995)

Abilities:

Semi-independent variation of valve lift and duration as shown in Figure 2.17.

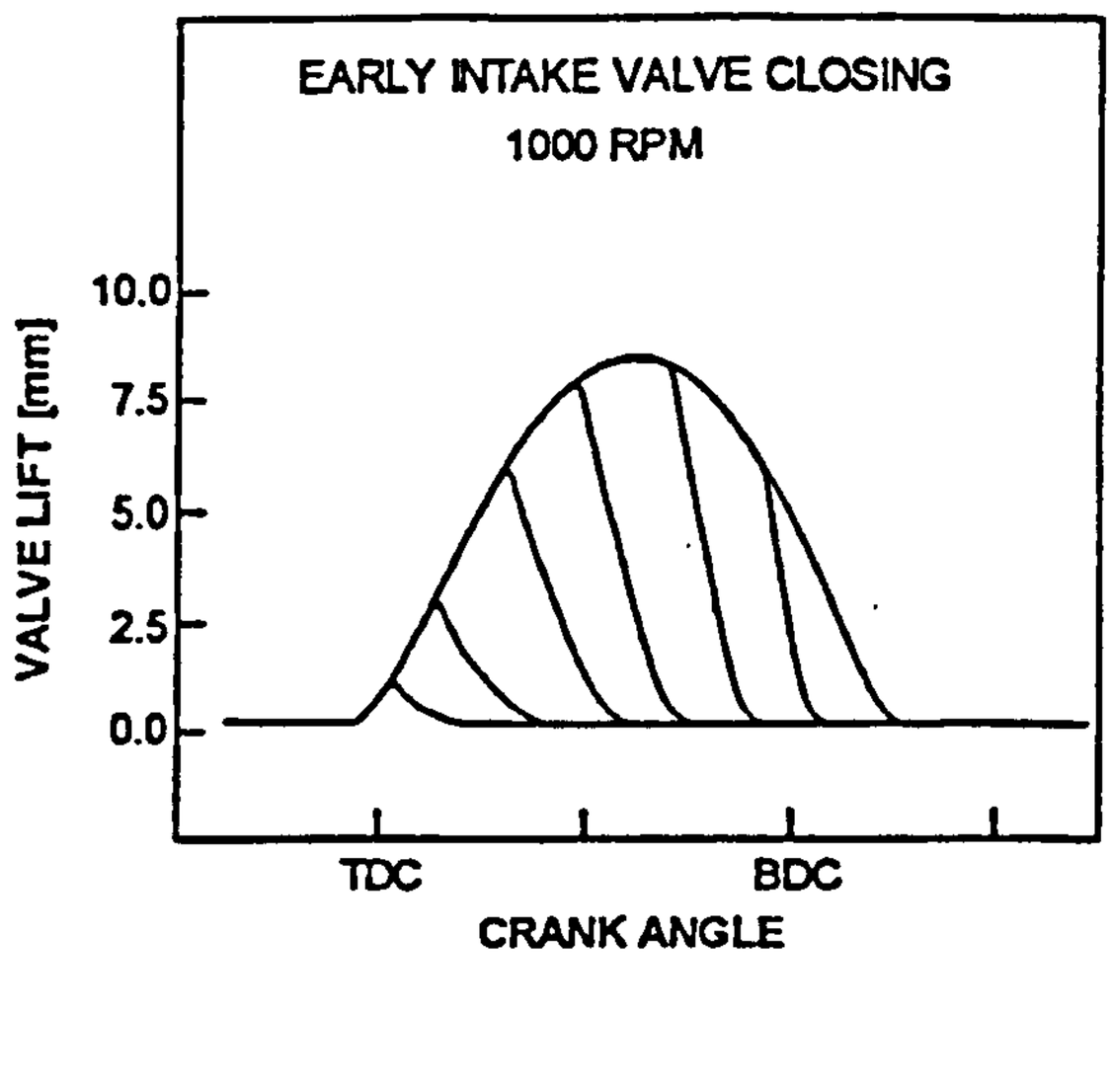

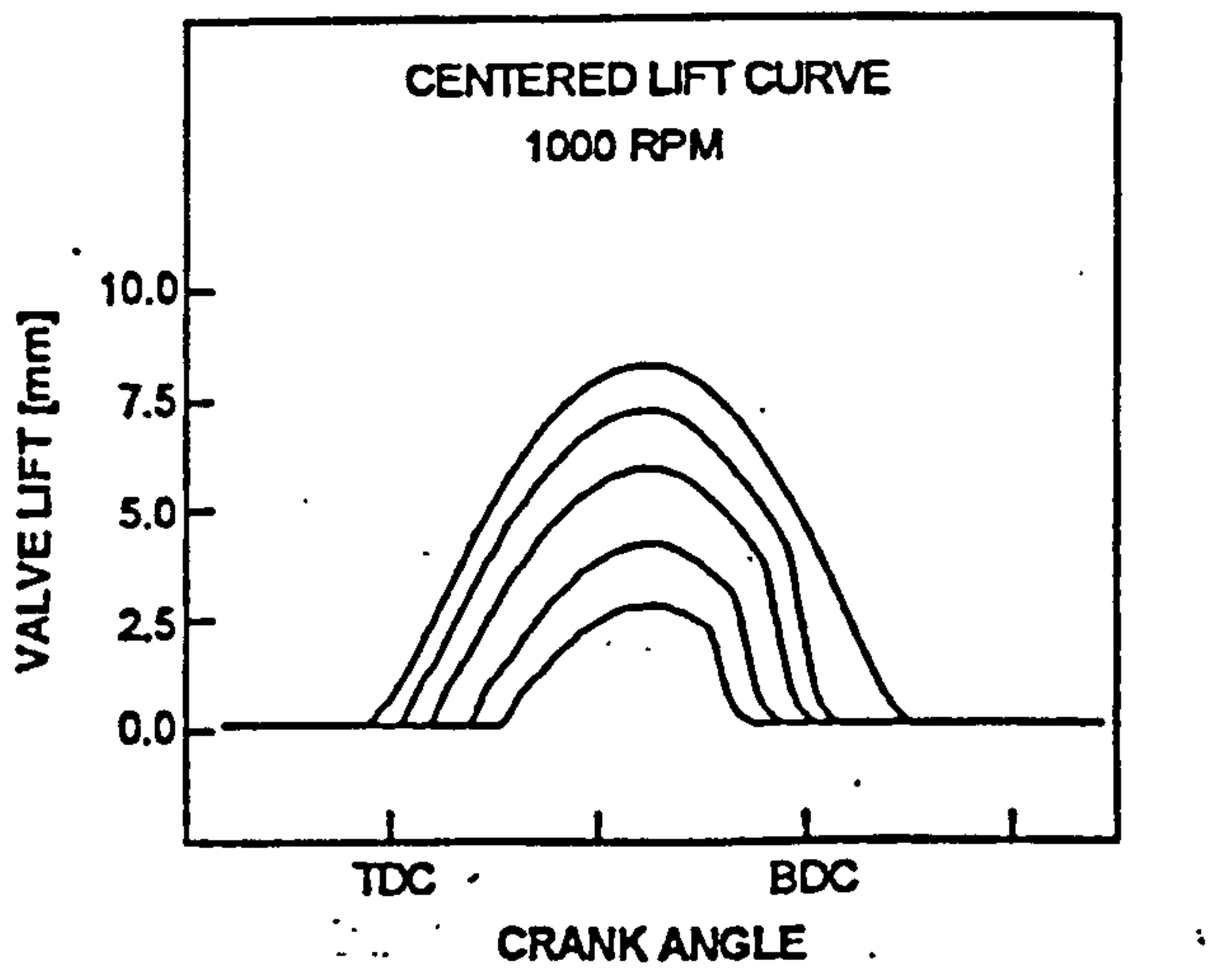

Figure 2.17: Variable follower height system abilities

(Lee *et al.*, 1995)

Description:

The system incorporates a hydraulic cam lobe follower, which is capable of transmitting only part of the cam motion into valve motion as shown in Figure 2.18. This normally involves a hydraulic chamber connected to the follower via a solenoid valve. The valve event duration is controlled by the solenoid valve allowing hydraulic fluid to escape. In this way camshaft eccentricity is transformed into lost motion. If the valve is open before maximum possible lift then duration and lift are related. However, if the valve opens after this then the duration is independent of maximum lift.

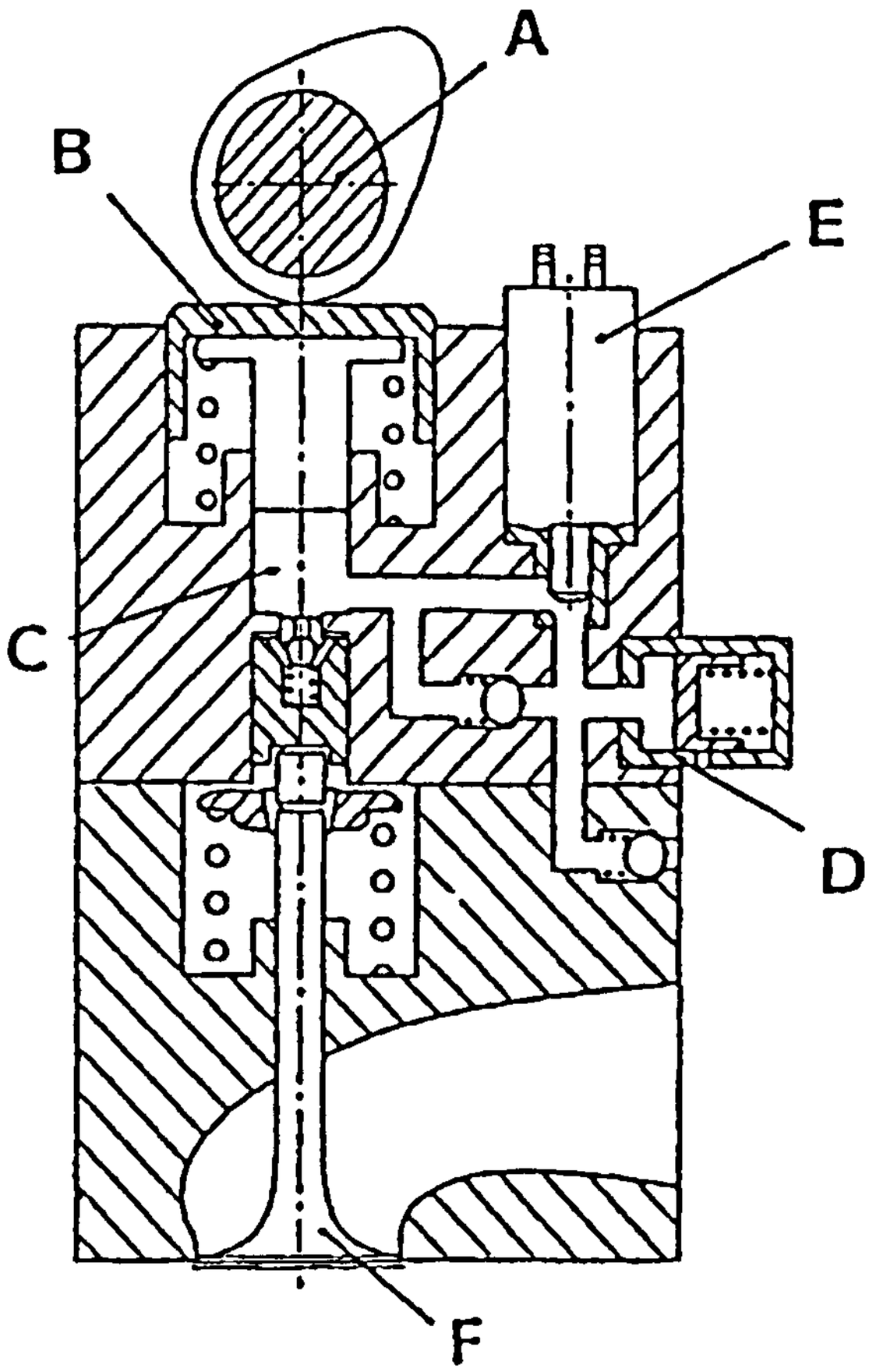

Figure 2.18: Variable follower height system

(Lenz *et al.*, 1989)

Valvetrain dynamics assessment:

This arrangement is characterised by low stiffness and increase in the dynamic valve train mass, which inhibits its high-speed operation. In addition, it will be impossible to use the systems variability due to the frequency response limitations of the solenoid valves.

Additional comments:

This is a complex system and the control of quantity of oil, which flows through the valve, is crucial for its ability and speed range.

2.2.1.3 Three-dimensional cam lobes

Manufacturers or research bodies developing the system:

Ferrari S.p.A. and Fiat S.p.A. (Titolo, 1991)

Abilities:

Continuous, but not independent variation of valve lift, valve event duration (Figure 2.19).

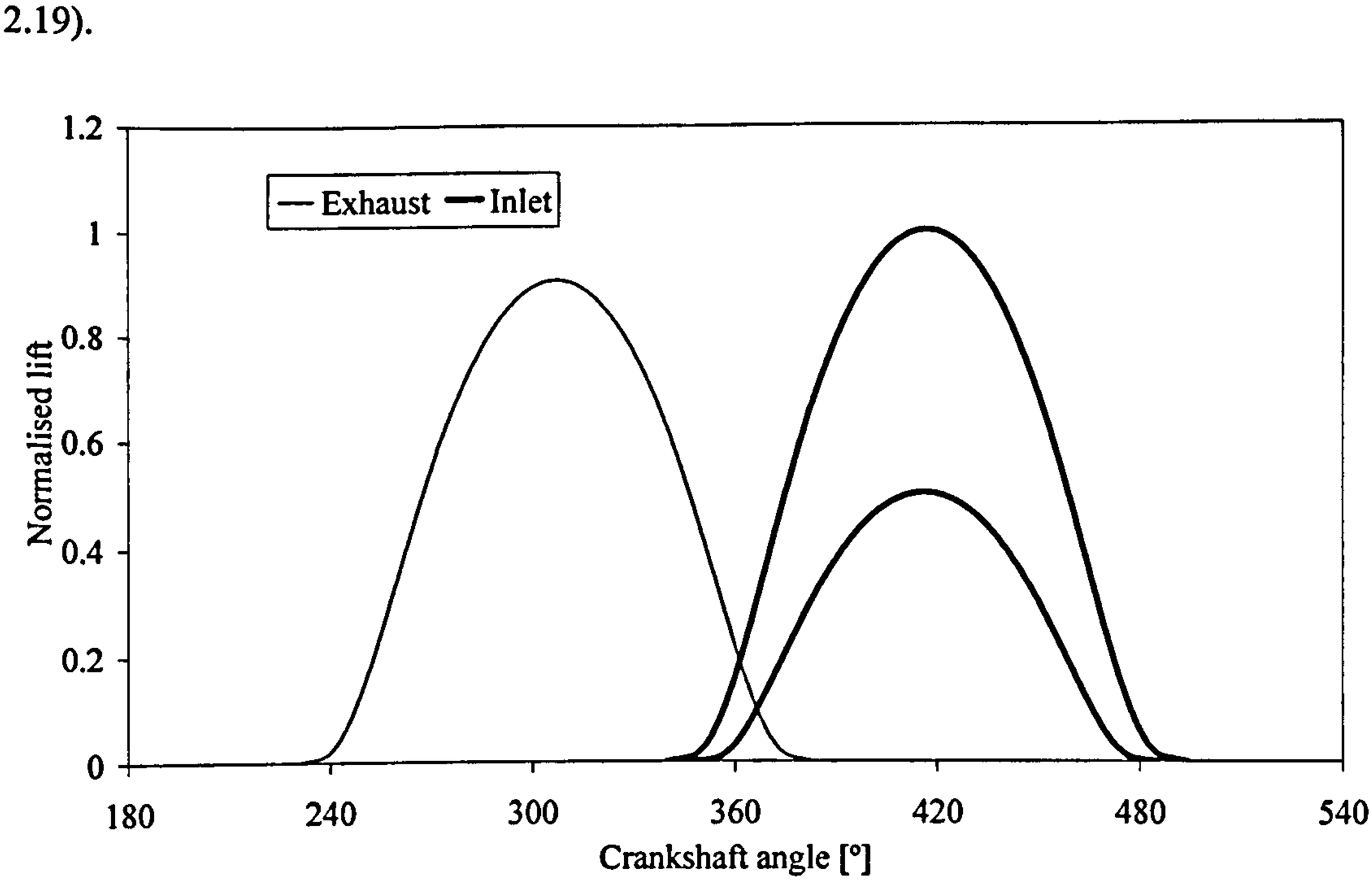

Figure 2.19: Three-dimensional cam lobes system abilities

(the lift is normalised with maximum inlet lift value)

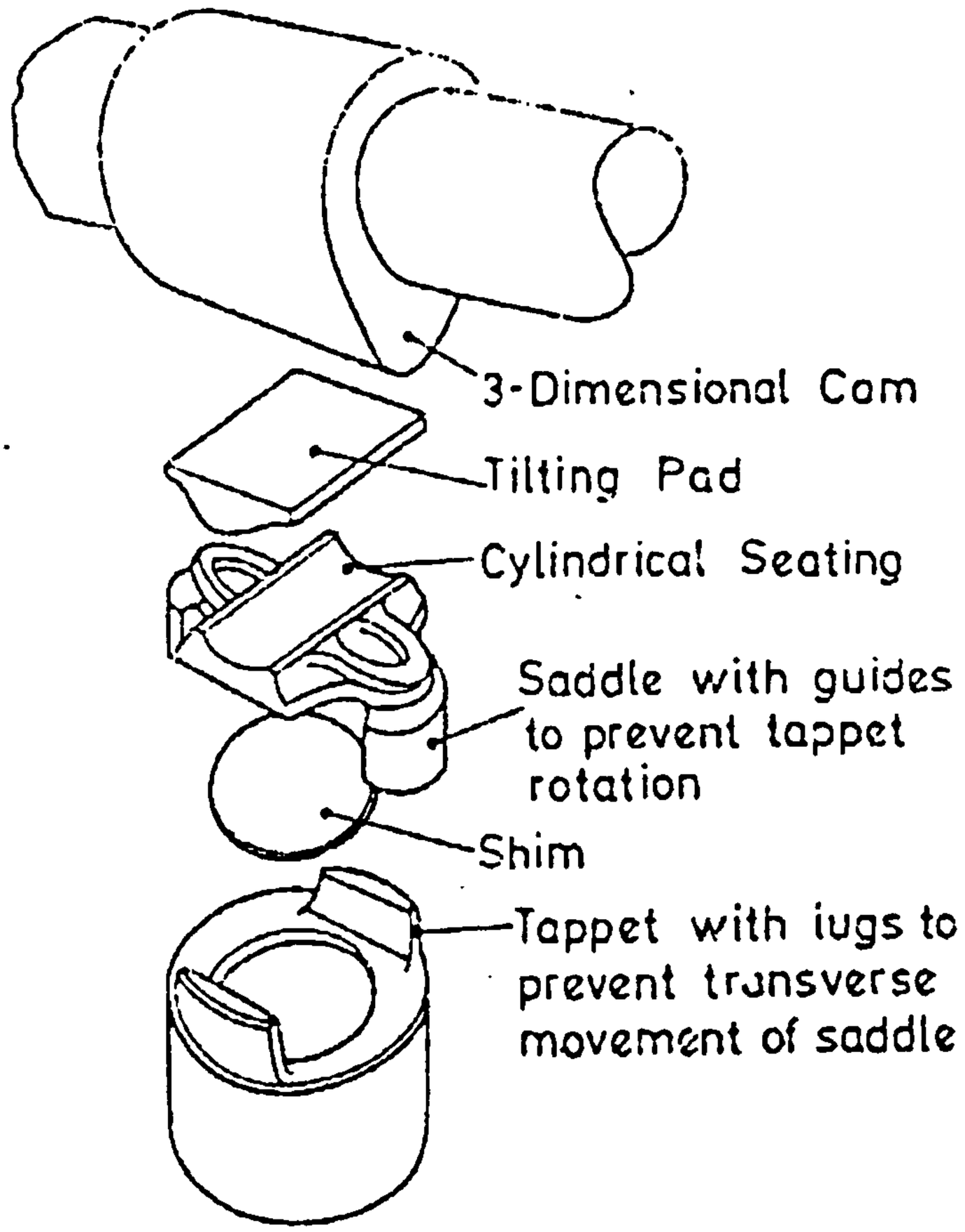

Figure 2.20: Three-dimensional cam lobes system

(Gray, 1988)

Description:

The camshaft lobes are three-dimensional (Figure 2.20). The camshaft is moved along its axis causing a change of the valve lift curve.

Valvetrain dynamics assessment:

Cam followers with pivoting contact plane matching the three-dimensional lobe are heavier than conventional ones and restrict high-speed operation.

Additional comments:

The system is easy to control and provides continuous variation of the lift profile. The main disadvantage is the cost of machining the three-dimensional lobe profile.

2.2.1.4 Combination of other systems

Manufacturers or research bodies developing the system:

Honda Motor Company, Intelligent Variable Valve Timing and Lift Electronic Control (i-VTEC) (Davis, 2004)

Toyota Motor Corporation, Intelligent Variable Valve Timing and Lift (VVTL - i) (Shikida *et al.*, 2000)

Dr. Ing. h.c. F. Porsche AG, Variocam and Variable Valve System (VVS) (Becker, 2000)

Abilities:

Switching between lift profiles and independently varying valve event timing (Figure 2.21).

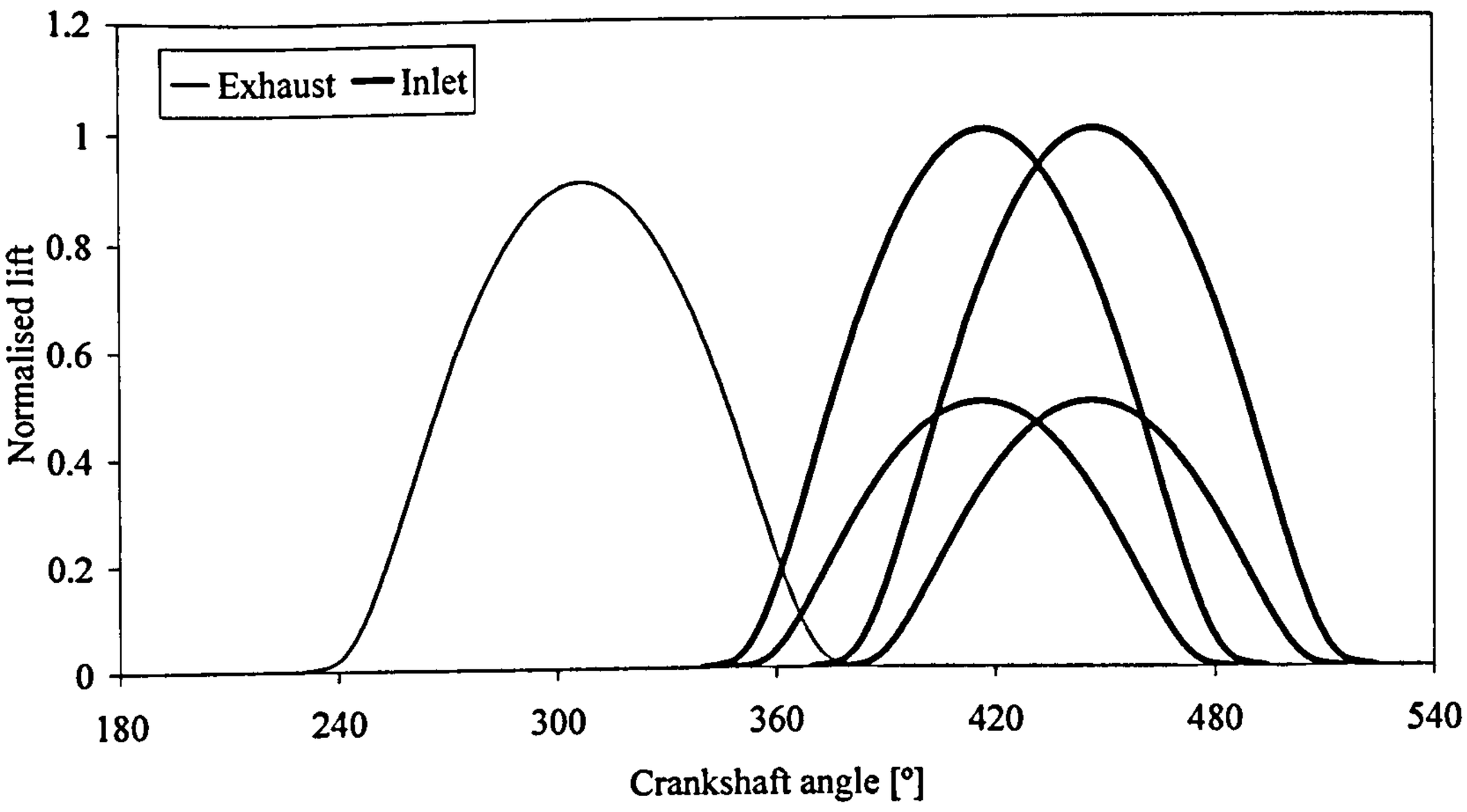

Figure 2.21: Profile switching and valve event timing change system abilities (the lift is normalised with maximum inlet lift value)

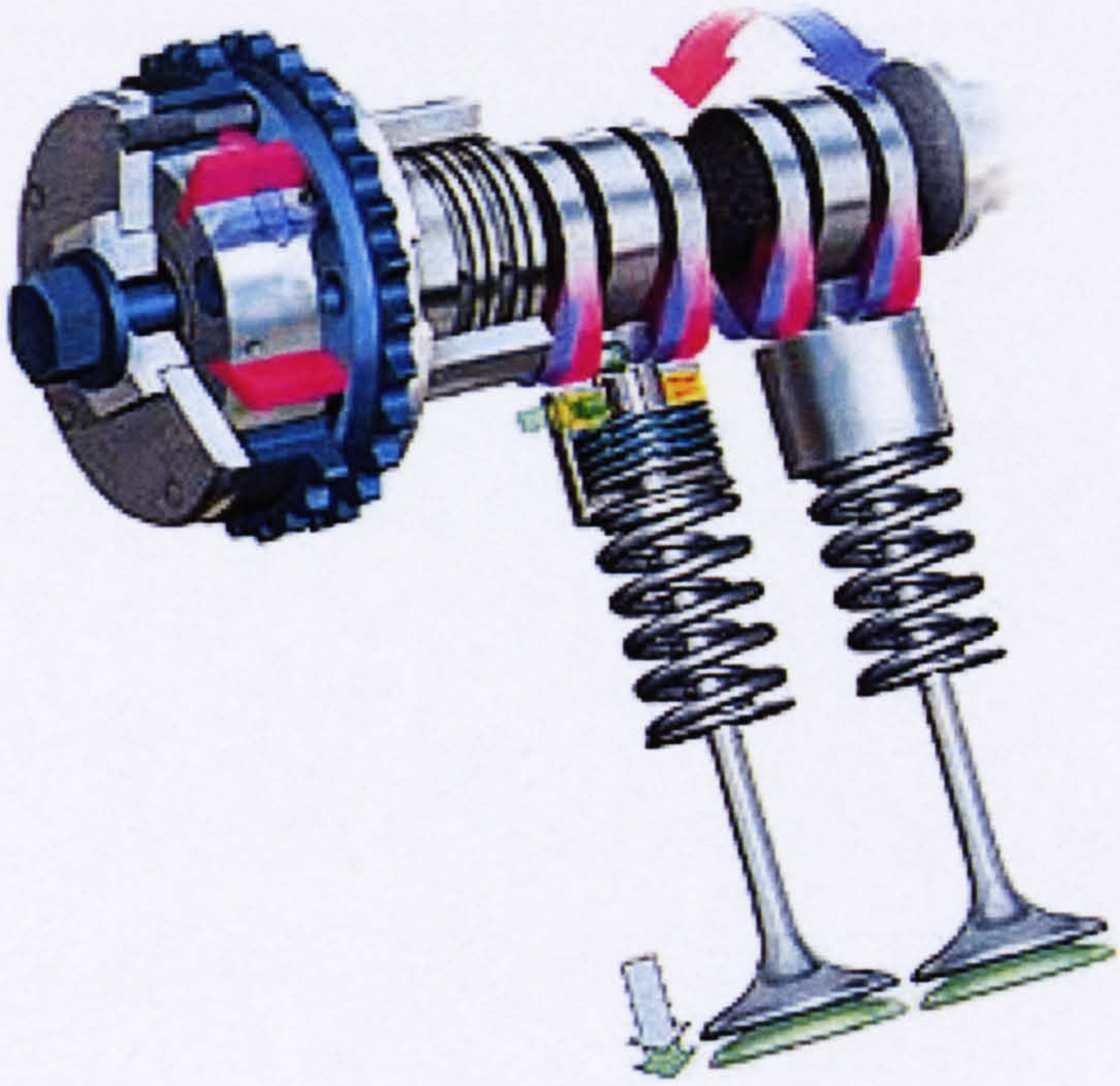

Figure 2.22: Combination of profile switching and VCP system

(Best Cars Website, 2004)

Description:

Some of the systems listed above, which do not involve the same component groups can be applied together. Honda, Toyota and Porsche (Figure 2.22) combine systems like VTEC, VVT-i and VVS to switch between two different lobe profiles and VCP system to vary the inlet camshaft timing.

Valvetrain dynamics assessment:

High-speed operation is limited by the abilities of the individual systems.

Additional comments:

The cost and weight of the valvetrain mechanism is increased. The existing systems can not vary lift and duration independently. They are an attempt to achieve some of the variation abilities offered by fully VVA technology described in the next sections.

2.2.2 Camless actuation systems

This group of systems do not use camshafts for actuating the valves. There are two basics operating principals. In the first instance, pressurised fluid actuates the valves. In the second type, electromagnets control the motion.

2.2.2.1 Electro-hydraulic actuation

Manufacturers or research bodies developing the system:

Ford Research Laboratory (Schechter and Levin, 1996), (Kim *et al.*, 1997)

Lotus Engineering (Wilson *et al.*, 1993)

Abilities:

The system allows independent and continuous variation of the valve events. Potentially any parameter of the valve event can be controlled independently for each valve.

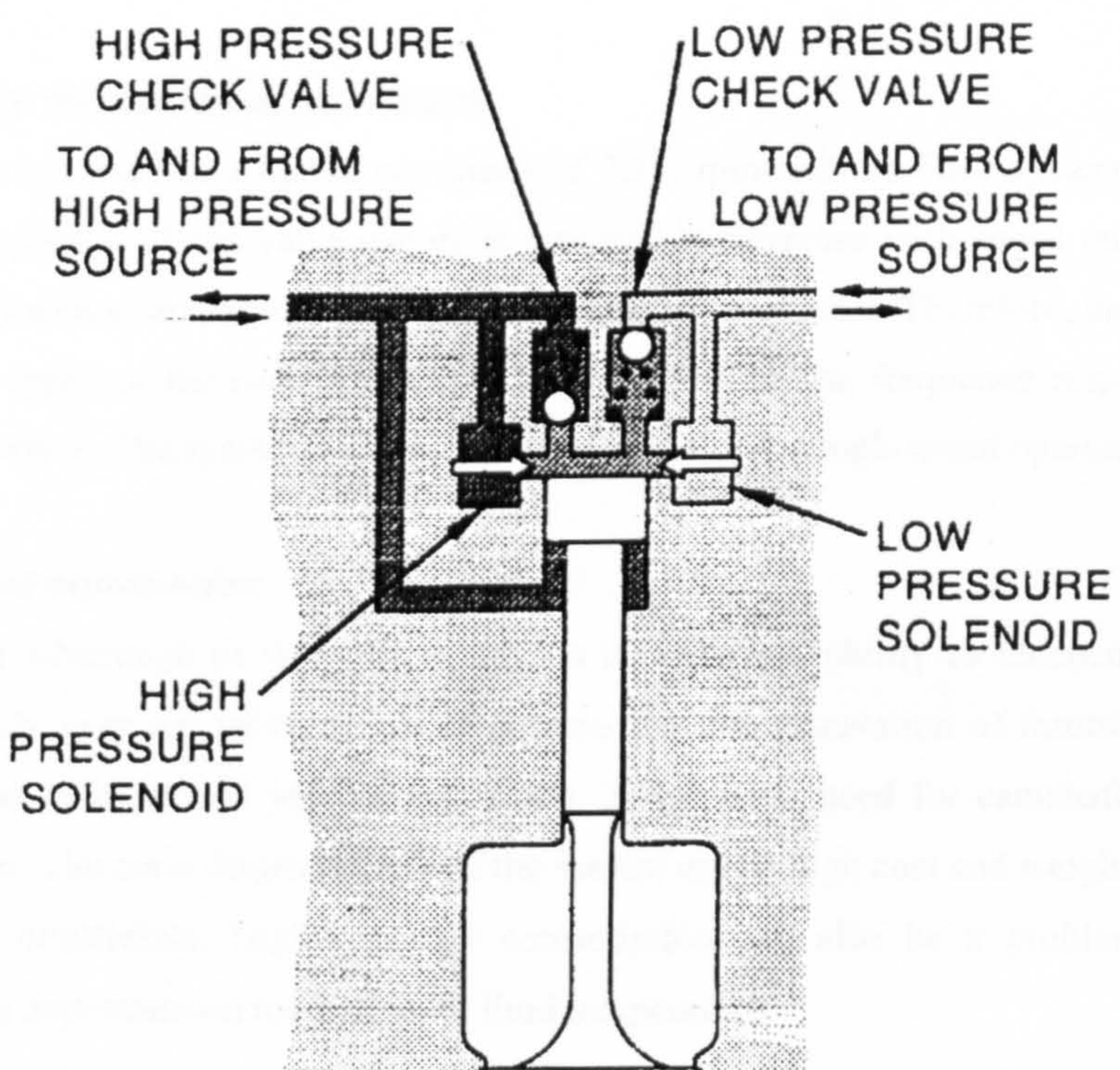

Figure 2.23: Electro-hydraulic system

(Schechter and Levin, 1996)

Description:

Typical arrangement consists of a high pressure pump, solenoid valves, a piston attached to the poppet valve stem, and a return spring as illustrated in Figure 2.23. The pump supplies high pressure fluid to one side of the piston via the solenoid valve, which is controlled by the ECU. This accelerates the piston and valve mass and compresses the return spring. To close the poppet valve the ECU opens an exit valve allowing the spring to force the fluid out.

The Ford system differs by the fact that high pressure fluid is also supplied to the bottom side of the piston instead of the return spring. During valve opening high pressure fluid is supplied to both sides of the piston and the force acting on the piston and poppet valve is due to the area difference between both sides of the piston. In order to decelerate the valve near the end of the closing stage and reduce seating velocities the Ford system closes and opens the hydraulic exit valve several times.

Valvetrain dynamics assessment:

The Lotus system has a maximum speed of 7200 rpm and the Ford system 8000 rpm. Control accuracy of the valve events is reported to decrease with speed and increased seating velocities can cause high noise and reliability problems. Therefore, the maximum operating speed of the system is likely to be limited by the frequency response of the solenoid valves. The system is identified as not suitable for high-speed operation.

Additional comments:

The major advantage of this system type is its excellent ability to independently and continuously vary the valve events. It permits the implementation of throttle free load control and cylinder and valve deactivation. There is no need for camshaft and drive mechanism. The main disadvantages of the system are its high cost and weight as well as packaging constraints. Higher energy consumption can also be a problem. Control accuracy is dependant on the hydraulic fluid temperature.

2.2.2.2 Electro-mechanical actuation

Manufacturers or research bodies developing the system:

General Motors Corporation (Theobald *et al.*, 1994)

Aura Systems Electro-magnetic Valve Actuator (EVA) and SwRi, (Podnar and Kubesh, 1998)

FEV Motorentechnic GmbH Electromechanical Variable Valve Timing System (EMV), (FEV Website, 2004)

Siemens VDO Automotive AG, (Siemens VDO Automotive AG Website, 2002)

Massachusetts Institute of Technology, (Chang *et al.*, 2003)

University of Shefield (University of Sheffield website, 2004), (Figure 2.24)

Abilities:

Continuous independent variation of all valve events.

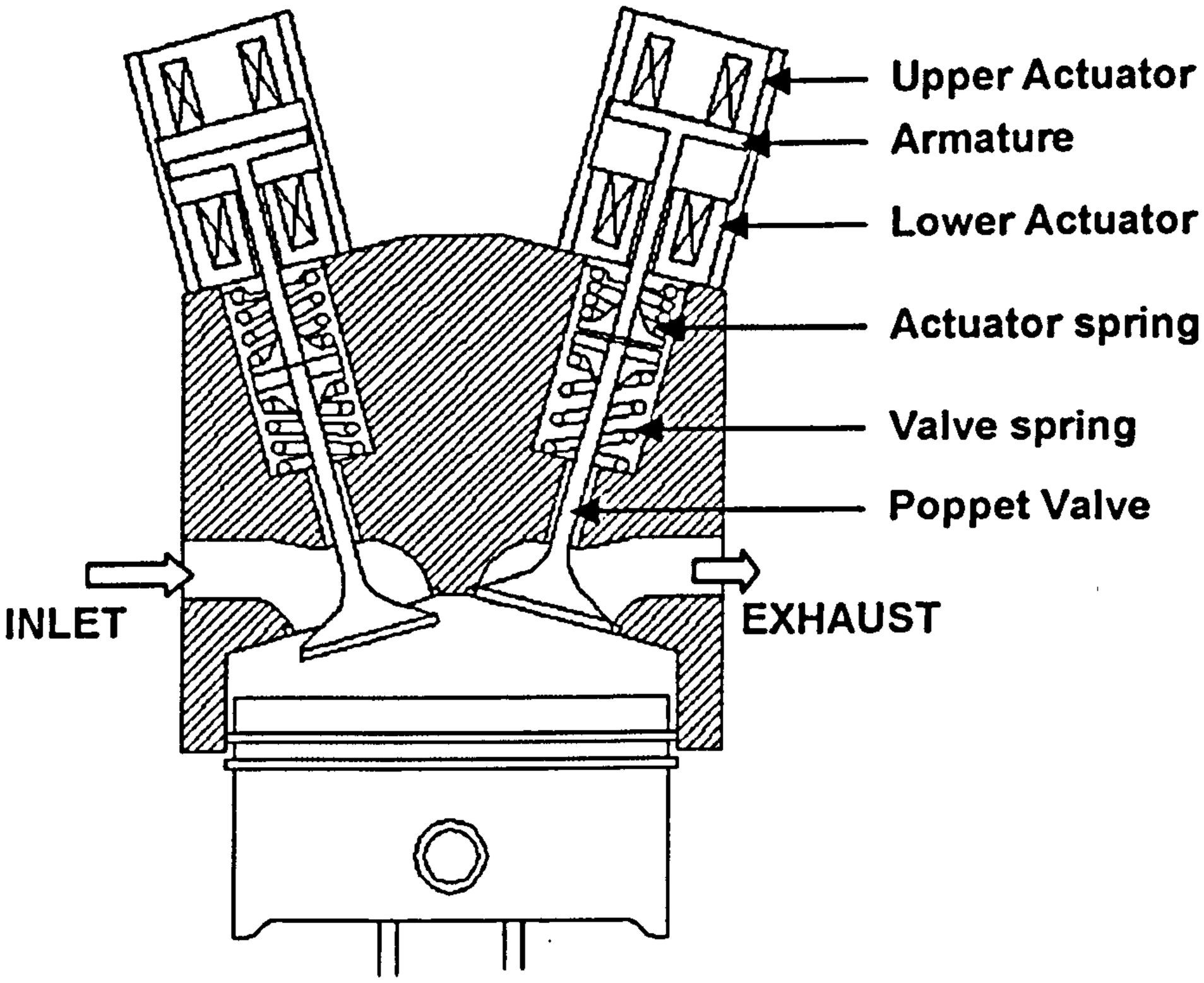

Figure 2.24: Typical Electro-mechanical system (University of Sheffield website, 2004)

Description:

The actuator operates as a free oscillating system. An armature disk is attached to the end of the valve stem and is suspended between two electro-magnets. This position corresponds to half the valve lift. When the engine is cranked during starting the ECU senses the crankshaft position and determines the appropriate valve position. A current of 3.5-4 A is applied across the electromagnet to hold the valve in the open or closed position. When the valve has to change position the holding electromagnet is de-energised and the force of the spring accelerates the valve towards the other position. The other electromagnet is switched on to pull and hold the valve. Energy saving is claimed as the spring force is used to accelerate the valve.

Valvetrain dynamics assessment:

Operating speeds of 10000 rpm for the Aura EVA and 6000rpm for the FEV system are claimed. Response times of 3ms for moving from open to close position is reported which accounts for 108° CA at 6000 rpm and is probably the limiting factor for the maximum speed. This combined with the high energy consumption are the reasons why this type of system is not considered suitable for high-speed operation.

Additional comments:

Potentially any lift curve can be achieved independently for each valve permitting throttle free load control as well as cylinder and valve deactivation. Disadvantages of the system are the high weight, packaging constraints, high energy consumption, high seating velocity and noise. The cost advantage from removing the camshaft and drive mechanism is offset by the requirement for high voltage supply to reduce the current level.

2.2.2.3 Electrically driven cams

Manufacturers or research bodies developing the system:

General Motors Corporation (Henry and Lequesne, 1997), (Henry, 2002)

Abilities:

Independent variation of valve event duration and timing as well as valve deactivation.

Description:

The system achieves variation of the valve event duration in a similar way to the variable velocity system. Each valve is actuated by individual electric motors, which rotate at half the crankshaft speed (Figure 2.25). The mechanism consists of an axial lobe attached to the motor rotor and two roller followers transmitting the eccentricity to the valve. Variation of the valve event duration is achieved by changes of the angular speed of the motor during each revolution. Valve event timing is altered by changing of the phasing of the electric motor relative to the crankshaft. Valve deactivation is possible by 'parking' the motor in the zero lift position.

Valvetrain dynamics assessment:

High-speed ability may be inhibited by the frequency response limitations of the electric motors. Increase of dynamic valvetrain mass is also a problem for high-speed operation.

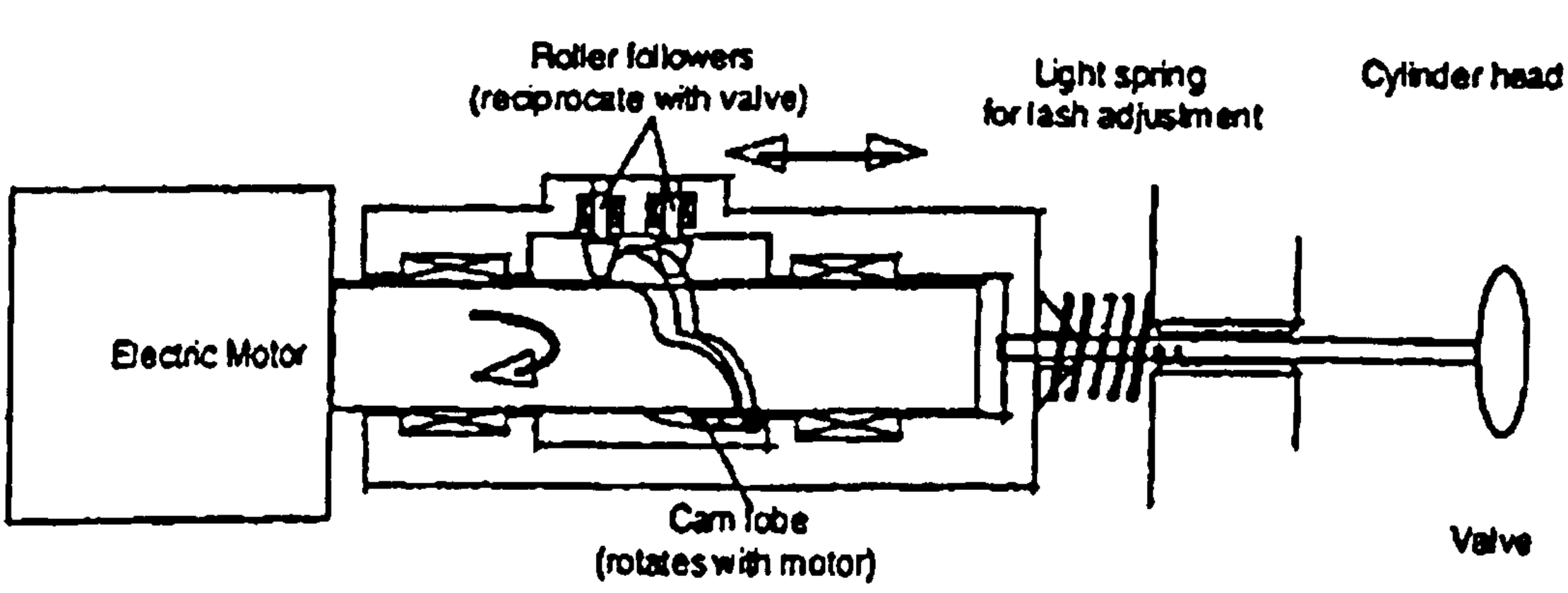

Figure 2.25: Electrically driven cams system

(Henry and Lequesne, 1997)

Additional comments:

There are significant packaging constraints associated with the installation of the electric motors. The mechanical independence of each valve and motor from the crankshaft demands good position control. Other problems include high cost and power consumption.

2.3 Alternative technology - Secondary inlet valves

This section describes alternative technology designed to have a similar effect to VVA but does not involve the valvetrain.

Manufacturers or research bodies developing the system:

Swiss Federal Institute of Technology and Ford Motor Co., (Vogel *et al.*, 1997)

Abilities:

The system has the effect of delayed IVO and advanced IVC on the flow to the cylinder.

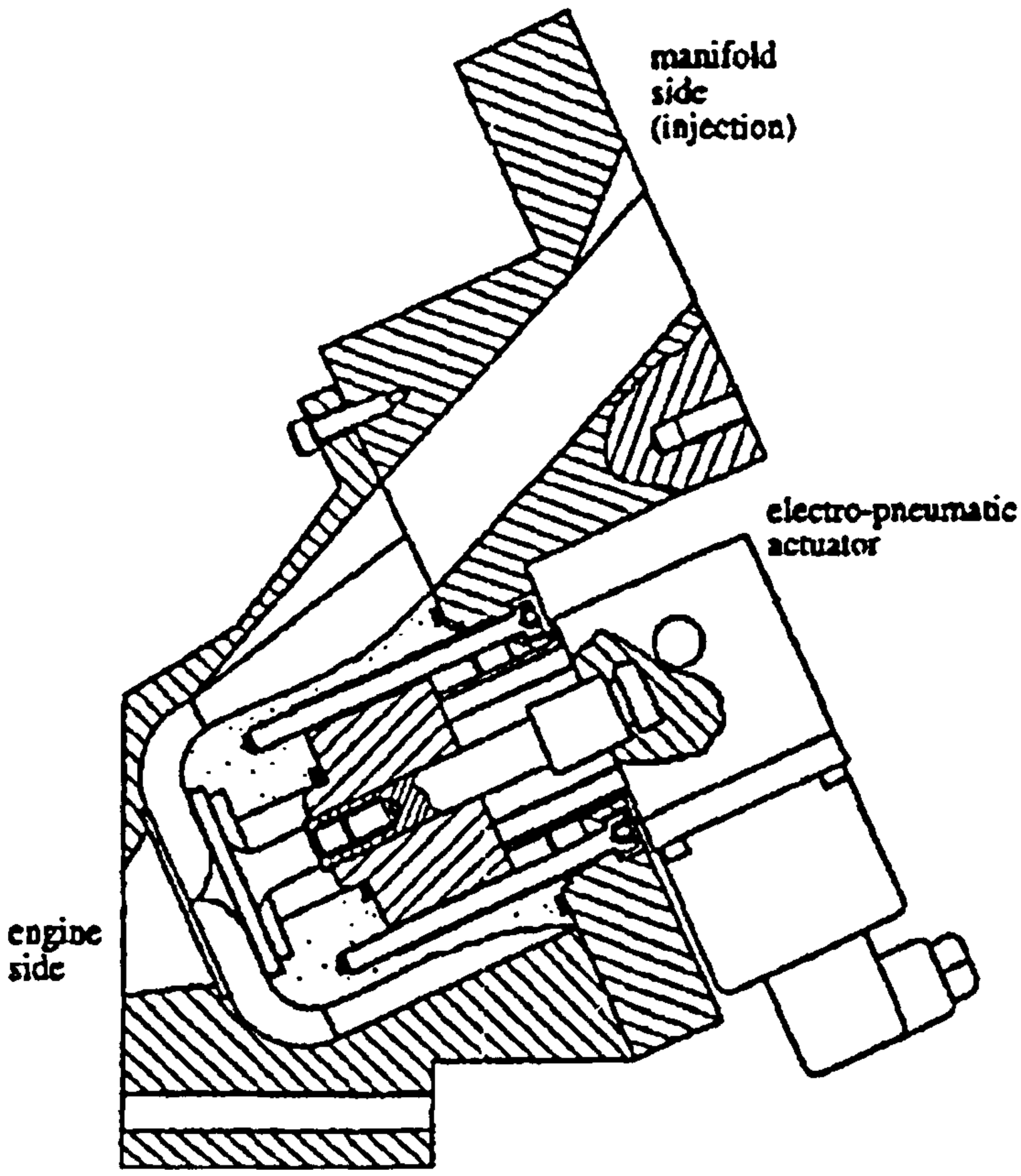

Figure 2.26: Secondary inlet valve system (Vogel *et al.*, 1997)

Description:

The secondary valve is positioned upstream of the poppet valve in the intake port as shown in Figure 2.26. They operate at the same frequency as the poppet valve but can open after and close before it.

Valvetrain dynamics assessment:

The electromagnetic valves have to operate at camshaft frequencies, which limits their high-speed ability.

Additional comments:

Late IVO and early EVO can improve breathing efficiency under certain conditions. The disadvantage of the system is that gasses can return back into the port section between the poppet and secondary valve. Because the secondary valve does not sustain combustion temperatures and pressures, the sealing arrangement and type of valve can be simple. Throttle valves or rotary valves can be used.

2.4 Discussion:

Due to the large variety of VVA systems in existence this chapter only attempt to provide general information and an example of each major type. VVA mechanisms vary greatly in their complexity and abilities. Table 2.1 presents a summary of these abilities and assessment of the suitability for high-speed operation. Continuous and independent variation of all valve events is the ultimate goal for VVA technology, however only Electro-mechanical and Electro-hydraulic systems are able to achieve that. Despite the long term developments and benefits offered by these systems, their complexity and high cost still prohibit their use in production engines. A more practical approach in achieving greater variability is to combine two or more mechanical VVA systems.

The main aim of this chapter is to identify systems, which are dynamically suitable for high-speed operation. Despite the large number of arrangements available it is only the Variable Camshaft Phasing and the Non-constant velocity drive mechanisms that do not have an impact on the valve and spring dynamics. This makes them suitable for high-speed operation.

There are examples of other systems, which are not considered dynamically optimum for high-speed operation, but are used in engines running at 9000 rpm and even 12000 rpm such as the Honda VTEC and Hyper VTEC. This is evidence that other mechanisms apart from the VCP systems can be adapted to high-speed operation. This is why establishing the ideal valve events in terms of engine performance is important, not only for assessment of the abilities of the VCP and Non-constant velocity drive systems but also to give direction for future VVA technology development. This motivates the investigation described is Chapter 6 and 7, which looks into the effect of IVO and IVC timing on breathing efficiency.

VVA System Type			Variable Valve Event Parameter			High-speed ability
			Timing	Duration	Max. Lift	
Camshaft actuated	Variable camdrive	Variable Camshaft Phasing	Yes/C	No	No	Yes
		Non-constant velocity drive	No	Yes/C	No	Yes
	Variable cam followers	Switching profiles	No	Yes	Yes	No/P
		Follower lost motion	Deactivation only			No/P
		Multicam systems	No	Yes/C	Yes/C	No
		Variable ratio rocker arms	No	Yes/C	Yes/C	No
		Variable follower height	No	Yes/C	Yes/C	No
	3-dimensional cam lobes		No	Yes/C	Yes/C	No
	Combination of systems		Depends on type of systems combined			
Camless	Electro-hydraulic		Yes/C/I	Yes/C/I	Yes/C/I	No
	Electro-mechanical		Yes/C/I	Yes/C/I	Yes/C/I	No
	Electrically driven cams		Yes/C/I	Yes/C/I	No	No

Table 2.1: Summary of VVA System abilities

(C – Continuous, I – Independent, P – Possible subject to development)

Chapter 3

The Simulation Tool

The focus of discussion in this chapter is the Lotus Engine Simulation (LES) software (Lotus Engineering, 2002). Explanation is provided why it is a suitable tool for the investigation of gas exchange phenomena in high-speed engines. The theory of each submodel is briefly described and the level of complexity used is justified. Finally the simulation model for the engine used in this research is presented.

3.1 Introduction to engine performance simulation

Engine performance simulation software models the physical processes taking place in internal combustion engines and aims to predict global parameters such as power output, thermodynamic, volumetric and fuel efficiency. The software is also able to calculate crankshaft angle resolved parameters for different locations in the engine such as instantaneous pressure, mass flow, temperature etc. This type of simulation is becoming increasingly popular in educational and research establishments as well as in industry. The rising popularity comes not only from the benefit of reduced development time and cost but also from the ability to study phenomena which are otherwise difficult or impossible to measure or investigate experimentally. Early criticisms related to long solution runtime have been resolved with increase in computing power allowing large algorithms to be executed in relatively short time. Some opponents of engine performance simulation are sceptical about the accuracy of the results. This is why, as with any simulation it is very important to fully understand the limitations arising from the level of complexity of the model and the data used to create it. This should be reflected in the interpretation of the results.

There are a large number of commercially available engine performance simulation codes promoted by some of the largest automotive consultancies. The four most publicised names are Lotus Engine Simulation (Lotus Engineering), Boost (AVL),

WAVE (Ricardo) and GT Power (Gamma Technologies). They differ in their user interface and complexity but generally use similar structure and algorithms. The simulation models generally consist of separate submodels representing the gas dynamics, combustion and heat release, heat transfer and friction in the internal combustion engines. Each of these submodels can vary in their complexity and engineering judgment must be made when using them. A large variety of interfacing software can be combined to provide the required sophistication (e.g. three dimensional simulation of flow in the combustion chamber) or measured data can be used instead of a theoretical model where appropriate (e.g. friction data from motoring test).

3.2 The Lotus Engine Simulation

The LES software was selected due to its availability at Loughborough University and working relationship with its creators. It is in-house code developed by Lotus Engineering since the late 1980's. The aim of the code is to predict gas flow, combustion and overall performance.

Global performance parameters such as power output, volumetric efficiency, and specific fuel consumption have been validated on a large range of production powerplants. Other parameters such as cylinder pressure, heat release and gas dynamics have also been correlated (Lotus Engineering, 2002).

3.3 Model structure

The program structure consists of three modules:

- The *Data module* requires the input of general engine data in order to model different engine elements and provide essential information for the submodel.
- The *Solver module* performs the required algorithms and iteration loops in order to achieve a converging solution of a number of equations reflecting the physical processes in the engine.
- The *Results module provi*des an interface where the calculated data can be displayed.

3.4 Engine components representation

All components constituting a part of the flow path through the engine are represented by a library of elements:

- Cylinders -zero-dimensional elements with combustion and heat transfer
- Plenums -zero-dimensional elements with heat transfer
- Ducts -one-dimensional elements with wall friction and heat transfer
- Inlet -infinite source of inlet gas at defined pressure and temperature
- Exhaust -exhaust boundary with specified pressure
- Valves -flow regulating elements with defined timing and flow area
- Ports -flow regulating elements with defined discharge coefficient

3.5 Submodel for ducts

3.5.1 Gas dynamics in ducts

The fundamental equations of fluid mechanics are mathematical statements that define the conservation of mass, momentum, and energy for a control volume. A conservation law implies that the rate of change of a conserved flow property in a fixed volume is the result of the net effect of the flux of the same property across the boundary of the volume and the change in that property caused by internal sources. Consider the flow of a compressible fluid through an infinitesimal section of duct in which the area of the cross-section perpendicular to the axis of the duct varies, as shown in Figure 3.1. If the area variation is gradual the fluid properties, pressure p, density ρ and velocity of flow u can

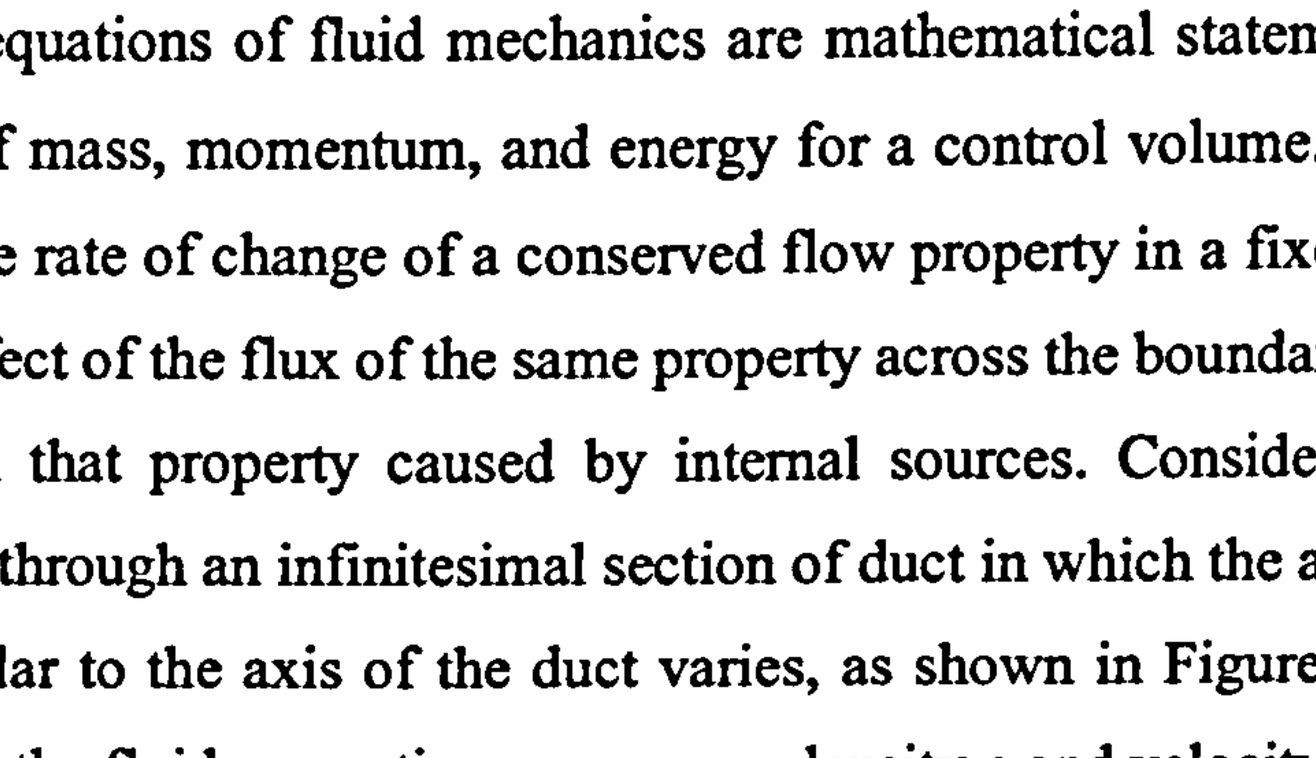

Figure 3.1: Control volume in a duct

be assumed uniform across any cross-section and can be taken as functions of distance x and time t only. This type of flow is defined as quasi-one-dimensional.

3.5.1.1 The continuity equation

Conservation of mass requires that its rate of change within the control volume shown in Figure 3.1 is equal to the net mass flow rate through the element. If the length of the duct element is dx and its cross-sectional area is F, then the rate of change of mass within the control volume is $\partial(\rho F dx)/\partial t$. The term $\partial(\rho u F)/\partial x$ represents the gradient of the mass flux and the product of this quantity with the length dx gives the net mass flow across the element. Thus the continuity equation can be expressed as

$$\frac{\partial(\rho F dx)}{\partial t} = \frac{\partial(\rho u F)}{\partial x} dx \tag{3.1}$$

3.5.1.2 The momentum equation

The momentum equation dictates that the sum of the pressure forces and the shear forces acting on the surface of the control volume is equal to the sum of the rate of change of momentum within the control volume and the net efflux of momentum out of the control volume. The resultant force on the control volume is caused by the pressure difference between the end faces and the component, in the x-direction, of the pressure on the sides of the volume. The difference in the pressure forces across the end faces of the control volume can be expressed with the product of the gradient of the force with the length of the element

$$-\frac{\partial(pF)}{\partial x} dx$$

The presence of the minus sign in this term arises from the convention that the forces are regarded as positive in the x-direction.

The pressure on the sides of the control volume produces a force in the x-direction equal to

$$p\frac{dF}{dx}dx$$

For flows in engine manifolds the duct walls can be assumed to be non-distensible, hence the duct area is a function of x alone.

The shear forces on the control volume arise due to the friction between the moving fluid and the stationary duct walls and can be modelled simply as a shear stress, τ_w, opposing the fluid motion. For an infinitely small control volume the surface force is given by

$$-\pi D\tau_w dx$$

where D is an equivalent, or hydraulic, diameter of the duct. The shear stress can be expressed in terms of the duct wall friction coefficient f:

$$\tau_w = \frac{1}{2}\rho u^2 f \qquad (3.2)$$

This allows the surface force on the control volume to be represented as

$$-\frac{1}{2}\rho u^2 f\pi D dx$$

The inclusion of this term is usually the only concession to recognizing the presence of fluid viscosity in one-dimensional models of the gas dynamic processes in engine manifolds. Hence the character of the governing equations remains essentially inviscid.

The rate of change of momentum within the control volume is given by

$$\frac{\partial(u\rho F dx)}{\partial t}$$

and the net efflux of momentum from the control surface is

$$\frac{\partial(\rho F u^2)}{\partial x} dx$$

Therefore the momentum equation is given by

$$-\frac{\partial(pF)}{\partial x}dx + p\frac{dF}{dx}dx - \frac{1}{2}\rho u^2 f \pi D dx = \frac{\partial(u\rho F dx)}{\partial t} + \frac{\partial(\rho F u^2)}{\partial x}dx \qquad (3.3)$$

3.5.1.3 The energy equation

By applying the first law of thermodynamics to the control volume shown in Figure 3.1. the energy equation can be derived in the form

$$\dot{Q} - \dot{W}_S = \frac{\partial E_0}{\partial t} + \frac{\partial H_0}{\partial x}dx \qquad (3.4)$$

where $\dot{Q}$ is the heat transfer rate, $\dot{W}_s$ is the work done by or on the system, E_0 is the total stagnation internal energy and H_0 is the total stagnation enthalpy of the control volume. The first term on the right-hand side of equation (3.4) can be expressed in terms of the specific stagnation internal energy as

$$\frac{\partial(e_0 \rho F dx)}{\partial t}$$

where the specific stagnation internal energy e_0 is related to specific internal energy e with the equation:

$$e_0 = e + \frac{1}{2}u^2 \qquad (3.5)$$

The second term on the right-hand side of equation (3.4) represents the net efflux of stagnation enthalpy across the control surface and is expressed by

$$\frac{\partial(h_0 \rho F u)}{\partial x} dx$$

where h_0 is the stagnation enthalpy of the gas, which is related to the stagnation internal energy via the equation:

$$h_0 = e_0 + \frac{p}{\rho} \tag{3.6}$$

Radial heat transfer from the gas to the manifold wall, or vice versa, is easily incorporated into the energy equation. If the heat transfer rate per unit mass of gas is denoted as q, then using the convention that heat transfer is positive into the control volume, the total heat transfer rate from and to the control volume is

$$q\rho F dx .$$

The work done by or on the system, $\dot{W}_s$, is zero for gas flow in a duct element of an engine manifold. Hence, the energy equation takes the form

$$q\rho F dx = \frac{\partial(e_o \rho F dx)}{\partial t} + \frac{\partial(h_o \rho F u)}{\partial x} dx \tag{3.7}$$

The governing equations for the one-dimensional flow of a compressible fluid in a duct with area variation, wall friction, and heat transfer are thus:

continuity $$\frac{\partial(\rho F)}{\partial t} + \frac{\partial(\rho u F)}{\partial x} = 0 \tag{3.8}$$

momentum $$\frac{\partial(\rho u F)}{\partial t} + \frac{\partial(\rho u^2 + p)}{\partial x} - p\frac{dF}{dx} + \frac{1}{2}\rho u^2 f \pi D = 0 \tag{3.9}$$

energy $$\frac{\partial(\rho e_o F)}{\partial t} + \frac{\partial(\rho u h_o F)}{\partial x} - q\rho F = 0 \tag{3.10}$$

These relationships are a set of non-linear hyperbolic partial differential equations.

3.5.1.4 Equations in conservation law form

Expanding and re-arranging equations (3.8) - (3.10) leads to

$$\frac{\partial \rho}{\partial t}+\frac{\partial(\rho u)}{\partial x}+\frac{\rho u}{F}\frac{dF}{dx}=0 \tag{3.11}$$

$$\frac{\partial(\rho u)}{\partial t}+\frac{\partial\left(\rho u^2+p\right)}{\partial x}+\frac{\rho u^2}{F}\frac{dF}{dx}+\rho G=0 \tag{3.12}$$

$$\frac{\partial(\rho e_0)}{\partial t}+\frac{\partial(\rho u h_0)}{\partial x}+\frac{\rho u h_0}{F}\frac{dF}{dx}-\rho q=0 \tag{3.13}$$

where

$$G=\frac{1}{2}u|u|f\frac{4}{D} \tag{3.14}$$

The term $u|u|$ is used to ensure that the duct wall friction always opposes the fluid motion.

Equations (3.11) - (3.13) can be written in symbolic vector form as

$$\frac{\partial W}{\partial t}+\frac{\partial F(W)}{\partial x}+C=0 \tag{3.15}$$

where

$$W=\begin{bmatrix}\rho\\ \rho u\\ \rho e_0\end{bmatrix}\ F(W)=\begin{bmatrix}\rho u\\ \rho u^2+p\\ \rho u h_0\end{bmatrix}\ C=\begin{bmatrix}\rho u\\ \rho u^2\\ \rho u h_0\end{bmatrix}\frac{d(\ln F)}{dx}+\begin{bmatrix}0\\ \rho G\\ -\rho q\end{bmatrix}$$

When there is no duct area variation, wall friction or heat transfer the equations reduce to

$$\frac{\partial W}{\partial t}+\frac{\partial F(W)}{\partial x}=0 \tag{3.16}$$

and are known as the one-dimensional Euler · equations. This presentation of the equations is referred to as the conservation law form since the equations can be obtained directly from the integral conservation equations of mass, momentum, and energy applied to the fixed control volume shown in Figure 3.1.

Equations (3.8) to (3.10) can be expressed in a manner which enforces more directly the conservation of the fluid properties when the flow in ducts with area variation is considered. By retaining the duct cross-sectional area in the differential terms the governing equations become

$$\frac{\partial W}{\partial t}+\frac{\partial F(W)}{\partial x}+C=0 \tag{3.17}$$

where

$$W=\begin{bmatrix}\rho F\\ \rho u F\\ \rho e_0 F\end{bmatrix}\ F(W)=\begin{bmatrix}\rho u F\\ \left(\rho u^2+p\right)F\\ \rho u h_0 F\end{bmatrix}\ C=\begin{bmatrix}0\\ p\dfrac{dF}{dx}\\ 0\end{bmatrix}+\begin{bmatrix}0\\ \rho G F\\ -\rho p F\end{bmatrix} \tag{3.18}$$

The continuity equation is now strictly homogeneous, since it contains no source terms. If there is no fluid friction or heat transfer the source vector contains only a term representing the extra pressure force arising from the change of area across the control volume. This form of the governing equations also gives advantages of mass conservation in ducts of varying cross-sectional area when numerical methods, which employ flux limiter functions, are used in order to achieve second-order accuracy. Equations (3.17) and (3.18) are those upon which the algorithms used in the engine simulation code are based.

3.5.2 Numerical Methods

The software uses shock-capturing finite volume scheme (Winterbone and Pearson, 2000) to solve the governing equations of gas flow in ducts. The numerical method is based on the two-step Lax-Wendroff scheme, used in conjunction with a symmetric non-

linear flux limiter, giving second-order spatial and temporal accuracy. This scheme is a member of the class of shock-capturing finite difference schemes, which are capable of handling shock waves, and super-sonic flows that can occur in the manifolds of high-performance engines. The flux limiter, which is based on the Total Variation Diminishing (TVD) criterion helps to prevent the occurrence of spurious oscillations in the solution when shock waves and contact discontinuities are encountered.

3.5.2.1 The Two-Step Lax-Wendroff (Richtmyer) method

The two-step Lax-Wendroff method is a space-centred scheme based on the computational stencil shown below in Figure 3.2.

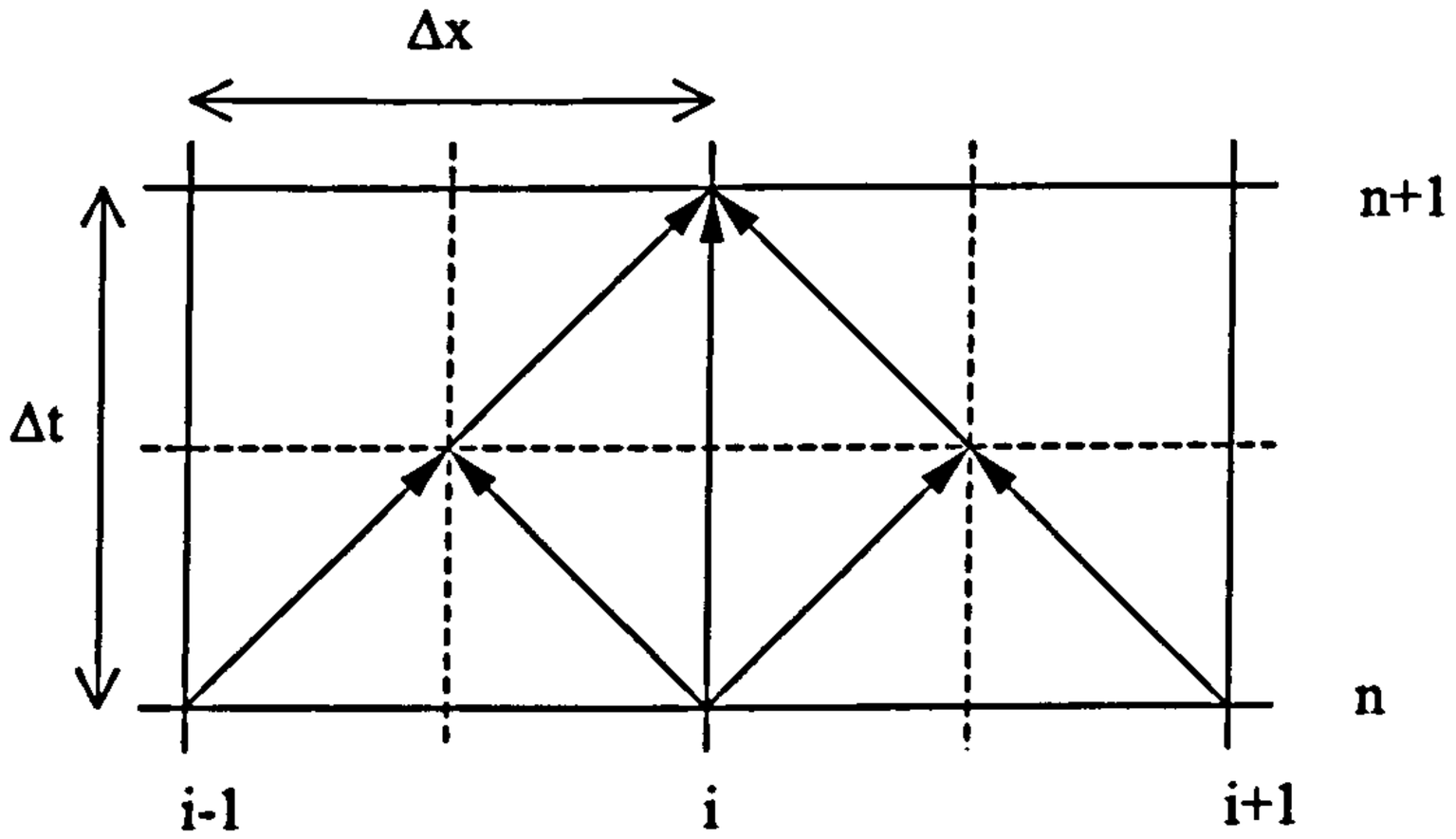

Figure 3.2: Computational stencil for two-step Lax-Wendroff scheme

The set of equations used to characterise the flow in engine manifolds can be expressed in symbolic vector notation as

$$\frac{\partial W}{\partial t}+\frac{\partial F(W)}{\partial x}+C=0 \qquad (3.19)$$

The first step of the scheme uses a space-centred differences about the points $[(i+1/2)\Delta x,n\Delta t]$ and $[(i-1/2)\Delta x,n\Delta t]$ whilst the second step is a calculation, which uses a time difference, centred about the point $(i\Delta x, (n+1/2)\Delta t)$. Thus the scheme can be expressed in the form

$$W_{i+1/2}^{n+1/2} = \frac{1}{2}\left(W_{i+1}^{n} + W_{i}^{n}\right) - \frac{\Delta t}{2\Delta x}\left(F_{i+1}^{n} - F_{i}^{n}\right) - \frac{\Delta t}{4}\left(C_{i+1}^{n} + C_{i}^{n}\right) \tag{3.20}$$

$$W_{i-1/2}^{n+1/2} = \frac{1}{2}\left(W_{i}^{n} + W_{i-1}^{n}\right) - \frac{\Delta t}{2\Delta x}\left(F_{i}^{n} - F_{i-1}^{n}\right) - \frac{\Delta t}{4}\left(C_{i-1}^{n} + C_{i}^{n}\right) \tag{3.21}$$

and

$$W_{i}^{n+1} = W_{i}^{n} - \frac{\Delta t}{\Delta x}\left(F_{i+1/2}^{n+1/2} - F_{i-1/2}^{n+1/2}\right) - \frac{\Delta t}{2}\left(C_{i+1/2}^{n+1/2} + C_{i-1/2}^{n+1/2}\right) \tag{3.22}$$

The Godunov Theorem states that all second-order schemes having constant coefficients will generate spurious oscillations at discontinuities such as shock waves and contact surfaces. This obstacle to the development of numerical methods for hyperbolic equations can be circumvented by the construction of non-linear difference schemes in which the coefficients of the scheme are functions of the solution itself. One approach to constructing non-linear difference schemes is based on the TVD criterion which is a measure of the variation of the solution at any given time step, given by

$$TV\left(W^{n}\right) = \sum_{i} \left| W_{i+1}^{n} - W_{i}^{n} \right| \tag{3.23}$$

In order to prevent the occurrence of spurious oscillations the total variation of the solution must satisfy the condition

$$TV\left(W^{n+1}\right) \leq TV\left(W^{n}\right) \tag{3.24}$$

This criterion can be utilised in a numerical scheme in the form of a 'smoothness monitor', which tests the sign of consecutive gradients of the solution between duct meshes.

The two-step Lax-Wendroff scheme can be modified to fulfil the TVD criterion by appending the term

$$\left[\overline{G^{+}_{i+1/2}\left(r^{+}_{i}\right)+G^{-}_{i+1/2}\left(r^{-}_{i+1}\right)}\right]\Delta W^{n}_{i+1/2}-\left[\overline{G^{+}_{i-1/2}\left(r^{+}_{i-1}\right)+G^{-}_{i-1/2}\left(r^{-}_{i-1}\right)}\right]\Delta W^{n}_{i-1/2}$$

after the second-step, where

$$\overline{G^{\pm}}\left(r^{\pm}_{i}\right)=\frac{1}{2}C(\nu)\left[1-\phi\left(r^{\pm}_{i}\right)\right] \tag{3.25}$$

and

$$\left.\begin{aligned} r^{=}_{i-1} &= \left[\frac{\Delta W^{n}_{i-3/2},\Delta W^{n}_{i-1/2}}{\Delta W^{n}_{i-1/2},\Delta W^{n}_{i-1/2}}\right], r^{-}_{i}\left[\frac{\Delta W^{n}_{i-1/2},\Delta W^{n}_{i+1/2}}{\Delta W^{n}_{i-1/2},\Delta W^{n}_{i-1/2}}\right] \\ r^{=}_{i-1} &= \left[\frac{\Delta W^{n}_{i-1/2},\Delta W^{n}_{i+1/2}}{\Delta W^{n}_{i+1/2},\Delta W^{n}_{i+1/2}}\right], r^{-}_{i}\left[\frac{\Delta W^{n}_{i+1/2},\Delta W^{n}_{i+3/2}}{\Delta W^{n}_{i+1/2},\Delta W^{n}_{i+1/2}}\right] \end{aligned}\right\} \tag{3.26}$$

This approach to producing a symmetric TVD scheme was proposed by Davis S., (1984). The local Courant number is defined as

$$\nu=\max_{k}\left|\lambda_{k}\right|\frac{\Delta t}{\Delta x} \tag{3.27}$$

where C(ν) is given by

$$C(\nu)=\begin{cases}\nu(1-\nu), & \nu\le 0.5\\ 0.25, & \nu>0.5\end{cases} \tag{3.28}$$

The flux limiter can be defined as

$$\Phi(r)=\begin{cases}\min(2r,1), & r>0\\ 0, & r\le 0\end{cases} \tag{3.29}$$

This limiter constrains the Courant number of the scheme to 0.7. The interface between the intra-duct gas dynamic calculations and the boundary conditions is dealt with by using the Mesh Method of Characteristics.

3.5.2.2 Mesh length and the Courant-Friedrichs-Lewy stability condition

In setting up the computational domain for any problem the value of the mesh size, x, is determined by the user, or the programmer (when 'automatic' mesh generation is requested) by establishing criteria, which fixes the compromise between accuracy and computational speed. The upper limit for the mesh length is dictated by the size of the smallest duct element in the system. This gives the model with the lowest possible spatial accuracy for a given numerical method for non-linear waves. The value of the time step, t, however is subject to constraints imposed through stability considerations which arise from the well known criterion of Courant, Friedrichs and Lewy (CFL) (Courant *et al.*, 1952). This criterion requires that information, in the form of disturbances, or waves cannot travel more than one mesh length in one calculation time increment, and this is expressed by the equation

$$\Delta t = C_{CFL} \frac{\Delta x}{c^n_{\max}} \tag{3.30}$$

where

$$0 < C_{CFL} \leq 1 \tag{3.31}$$

and represents the largest wave speed present is the entire solution domain at time level n. The parameter C_{CFL} is known as the Courant, or CFL, number. The time marching procedure will be most efficient when the value of this parameter is close to 1.

The method of characteristics is based on a transformation of the governing equations, which enables the paths of disturbances to be tracked explicitly as they propagate through the flow field. It is clear that the physical interpretation of the case $C_{CFL}=1$ corresponds to a situation where, in at least one computational cell, a wave starts from $[(i-1)\Delta x, n\Delta t]$ or $[(i+1)\Delta x, n\Delta t]$ and reaches $[i\Delta x,(n+1)\Delta t]$. It is only strictly safe to use a

Courant number of one if the maximum wave speed, c^n_{max}, does not increase as the wave travels across the cell. When the flow field is non-homentropic however, the wave speed will not be constant over the cell and a more cautious (i.e. lower) value of C_{CFL} should be used. The TVD scheme used in the code dictates a Courant number of 0.7.

For non-linear waves c^n_{max} can be estimated with the relationship

$$c^n_{max} = \max\left\{\left|u^n_i\right| + a^n_i\right\} \tag{3.32}$$

The number of meshes used in the ducts will determine the accuracy of the duct flow calculations. It is difficult however to generalise on the mesh requirements. The stability requirement imposed on the calculations is that a wave cannot traverse a mesh in one time step. Mesh lengths of between 15-20 mm for inlet ducts and 25-30 mm for exhaust ducts are usually sufficient. It should be noted that the speed of simulation will slow dramatically with increasing mesh density. In general simulation run times increase with mesh density to the power of 1.5.

Additional duct meshes may improve computational stability, especially in ducts containing severe tapers.

3.5.3 Heat transfer model in ducts

The heat transfer term, q, in the energy equation 3.37 is used to represent simple convective heat transfer in the radial direction from the gas to the duct.

An approximate treatment for convective heat transfer, due to (Benson, 1982), is adopted in the LES code. The approach is based on the assumption that the analogy between heat and momentum transfer in steady flow can be applied to non-steady flow. This assumption is not strictly true. In addition to the fact that the Reynolds analogy oversimplifies the mechanism of turbulent heat transfer, it also ignores the existence of any laminar sub-layer. The approach, however, is reasonable as a first approximation and is described below. The heat transfer rate per unit mass is

$$q = \frac{4h}{\rho D}\left(T_w - T_g\right) \tag{3.33}$$

where h is the convective heat transfer coefficient and T_w and T_g are the temperatures of the duct inner wall and gas. Reynolds' analogy defines this coefficient as

$$h = \frac{f}{2}\rho u c_p, \tag{3.34}$$

where f is the duct wall friction factor. Equation (3.33) then becomes

$$q = \frac{2fu}{D} c_p\left(T_W - T_g\right) \tag{3.35}$$

and for an ideal gas,

$$q = \frac{2fu}{D}\frac{kR}{k-1}\left(T_W - T_g\right) \tag{3.36}$$

At the end of each cycle the total heat transferred to the walls at all the meshes in the duct is summed and used to perform a simple one-dimensional heat transfer calculation to determine the duct inner wall temperature that should be used for the next cycle. Thus it is necessary to specify the duct wall thickness, material type and method of cooling.

Good representation of the heat transfer in ducts is critical for establishing the correct gas temperature and hence gas velocity in the model. In addition to the assumptions already mentioned there are other shortcomings of such simplistic representation that may have an effect on the accuracy of results. According to the model, there is no heat transfer when the flow is stationary. The convective heat transfer coefficient defined in equation 3.34 is valid only for fluids with Prandtl number of one and for engine applications this number is approximately 0.7 according to Douglas et al. (1991). Cheng et al. (1991) showed that the presence of liquid fuel significantly complicates the heat transfer model in the inlet system.

3.5.4 Wall friction model

The duct wall friction factor, f, is defined as

$$f = \frac{\tau_w}{(1/2)\rho u^2} \tag{3.37}$$

It is a common practice, in wave-action simulations, to use a constant value of f in the region of 0.004-0.01. For ducts containing bends higher values are often used. The curve on the Moody diagram for a smooth duct (surface roughness k 2.5 μm) gives values in the range 0.0035-0.008 for Reynolds numbers in the range $1x10^4$-$5x10^5$.

The software allows the user to specify the wall friction factor in three ways. The first method is by inputting directly the value of the wall friction factor. The second way is by specifying a surface roughness for the duct from which the friction factor is derived. In the third method the software uses the default value for the wall surface roughness based on the material type to calculate the friction factor. The second and third methods use the following equations to calculate the wall friction factor based on the surface roughness.

For Reynolds numbers in the range $3.5\times10^3 \leq Re \leq 10^8$, and relative roughness values in the range $10^{-6} \leq (k/D) \leq 10^{-2}$, equation proposed by Swamee and Jain (1976) is used:

$$f = \frac{0.25}{\left[\log_{10}\left(\frac{k}{3.7D} + \frac{5.47}{\mathrm{Re}^{0.9}}\right)\right]^2} \tag{3.38}$$

to evaluate the duct wall friction factor, where D is the duct diameter. Reynolds number in this equation is given by

$$\mathrm{Re} = \frac{\rho U D}{\mu} \tag{3.39}$$

The gas viscosity μ is a function of its temperature and is evaluated by the code. For Reynolds numbers less than 3500 the flow is assumed to be laminar and the duct wall friction factor is given by the expression

$$f = \frac{16}{\mathrm{Re}} \tag{3.40}$$

In the interests of maintaining reasonable computer run times equations (3.38) and (3.40) is applied to give an average value of f for each duct section comprising the manifold rather than each individual mesh point.

3.6 Modelling of cylinders and plenums

Cylinders and plenums are modelled as a zero dimensional elements and mass, pressure, temperature and volume are calculated at each crank angle by solving the energy equation:

$$\frac{\partial q}{\partial T} + \frac{\partial B}{\partial t} - \frac{\partial W}{\partial t} = \frac{\partial E}{\partial t} + \sum \partial H \tag{3.41}$$

3.6.1 Numerical method

The solution algorithm is executed in the following steps:

1. Calculate heat release from combustion.

2. Calculate enthalpy change due to gas flows.

3. Calculate heat transfer using cylinder temperature from previous step.

4. Estimate change in cylinder pressure due to energy and volume changes.

$$\partial p = p_{cyl}\left(\frac{\partial Q + \partial B + \partial H}{m_{cyl} c_v T_{cyl}} - k\frac{\partial V}{V_{cyl}}\right) \tag{3.42}$$

5. Estimate displacement work.

$$\partial W = \partial V\left(p_{cyl} + 0.5\partial p\right) \tag{3.43}$$

6. Estimate temperature change.

$$\partial T = \frac{\partial Q + \partial B - \partial W}{c_v} \tag{3.44}$$

7. Enter iteration loop to converge on cylinder temperature.

$$T_{new} = T_{cyl} + \partial T \tag{3.45}$$

8. Calculate cylinder pressure.

$$p_{new} = \frac{m_{cyl} R_{cyl} T_{new}}{V_{new}} \tag{3.46}$$

9. Calculate displacement work.

$$\partial W = \partial V\left(p_{cyl} + 0.5\partial p\right) \tag{3.47}$$

10. Recalculate heat transfer based on mean gas temperature during increment.

11. Calculate energy change due to this gas temperature.

$$\frac{\partial E}{\partial t} = \frac{\partial Q}{\partial T} + \frac{\partial B}{\partial t} - \frac{\partial W}{\partial t} - \sum \partial H \tag{3.48}$$

12. Calculate internal energy change due to change in cylinder temperature.

$$\partial E_2 = E_{new} - E_{cyl} \tag{3.49}$$

13. Where E_{new} and E_{cyl} are the internal energies of the gas in the cylinder at this and the previous time steps respectively.

14. Calculate the error in temperature due to the mismatch in changes in internal energies.

$$\partial T = \frac{E_1 - E_2}{c_v} \tag{3.50}$$

15. If ∂T is greater than 0.01 K repeat calculations from (3.41).

16. When converged on temperature recalculate all conditions within the cylinder.

The above methodology is the simplest approach to solving the energy equation for zero dimensional elements. More complex and computationally efficient "predictor - corrector" algorithms exist but the above approach has been found to be most robust (Lotus Engineering, 2002)

To ensure stability under all test conditions the crankshaft angle increments are limited to so that the change in mass of a zero dimensional element does not exceed 25% of the current mass in a particular time step. The crankshaft increments often require limiting in high compression ratio, four stroke engines during valve overlap.

3.6.2 Heat transfer model in plenums

Heat transfer in plenums is calculated using the connective heat transfer coefficient. For the majority of simulations the heat transfer coefficient may be set to 0. The following notes however provide a guide as to how a heat transfer coefficient of the correct order of magnitude may be calculated. The Nusselt number / Prandtl number / Reynolds number correlation usually applied to turbulent flow in ducts is:

$$Nu = 0.023 \mathrm{Re}^{0.8} \mathrm{Pr}^{0.4} \tag{3.51}$$

where

$$Nu = hd / k$$
$$\mathrm{Pr} = \mu c_p / k \qquad (3.52)$$
$$\mathrm{Re} = \rho v d / \mu$$

and k is the gas conductivity, c_p is the specific heat capacity, v is the gas velocity and d is the characteristic length.

Rearranging the above equations and assuming that the Prandtl number remains constant at around 0.7 yields

$$h = 0.02 \frac{k}{d} \left(\frac{\rho v d}{\mu} \right)^{0.8} \qquad (3.53)$$

The typical gas velocity may be estimated by calculating the mean inlet gas velocity and factoring this by the number of the cylinders feeding the plenum. Subsequently more accurate data may be obtained from the simulation output.

It is important to note that the heat transfer coefficients calculated from the above equation will produce heat transfer rates of the correct order of magnitude. If measured plenum gas temperatures are available then the heat transfer coefficients can be freely adjusted in order to match the measurements.

3.7 Combustion model

A single zone heat release model is used in the simulation. The heat released from combustion affects the whole working volume and there is uniform pressure and temperature distribution. This may affect the accuracy of heat transfer calculation as in reality the charge temperature is different on both sides of the flame front. Considering the gross assumptions used in the heat transfer model relating to wall temperature and heat transfer coefficient it is expected this effect will be comparably small.

3.7.1 Wiebe heat release function

The heat release rate is defined by using the Wiebe function (Wiebe, 1956). It is an empirically derived equation, which defines the mass fraction burnt m_{frac} as a function of the crankshaft angle θ after the start of combustion. It is also normalised by the total combustion duration θ_b.

The mass fraction burnt after start of combustion is:

$$m_{frac} = 1 - \exp^{-A\left(\frac{\theta}{\theta_b}\right)^{M+1}} \tag{3.54}$$

where A and M are coefficients that can be adjusted to match experimental data.

3.7.2 Combustion duration

Combustion duration angle is required as an input by the Wiebe function. Establishing exactly the beginning and end of combustion in SI engine from experimental data is difficult. There are empirically derived formulas for calculating it, however assuming they have been generated from data not including high-speed engines it was preferred to use experimental data. Measured cylinder pressure data was used to determine the combustion duration as the number of crankshaft degrees between 10% and 90% mass fraction burnt.

3.7.3 Combustion phasing

Combustion phasing is required by the model in order to place the process relative to crankshaft position. Combustion phasing is generally a function of the ignition timing. It is common practice though to specify combustion phasing as the number of degrees after TDC when 50% of the mixture has been burnt. Experimental data was used again.

3.7.4 Effect of combustion model assumptions on gas dynamics

Combustion in SI engines is a complex process, which depends on many of parameters. Its modelling complexity has an impact on the predicted torque and power. Due to the fact that in this research focuses only on the gas dynamics and breathing efficiency, the

effect of the combustion model is limited to the prediction of the exhaust temperature and pressure at EVO. The limitations of using single zone model regarding temperature distribution are not imperative as the gas in the combustion chamber at EVO has relatively uniform temperature. The pressure at EVO requires comparison with experimental data as it excites the gas dynamics in the exhaust system.

3.8 Scavenging models

The in-cylinder scavenging model controls the way in which charge gas is mixed with the gas that is currently in the cylinder prior to the cylinder gas being exhausted. There are four scavenging models available in the code but only the following two are used:

- Perfect Mixing
- Perfect Displacement

3.8.1 Perfect mixing model

With the perfect mixing model the assumption is made that any charge gas entering the cylinder is instantaneously, homogeneously mixed with the gas currently in the cylinder. Thus the subsequent transfer of gas to the exhaust will cause some of the charge gas to be removed from the cylinder. This is the default scavenging model for all cylinders and results in the most pessimistic performance results as it will become evident in later chapters.

3.8.2 Perfect displacement model

With the perfect displacement model the assumption is made that any charge gas entering the cylinder is not mixed with the gas currently in the cylinder. The subsequent transfer of gas to the exhaust will cause only residual exhaust gas to be removed from the cylinder. Under prolonged scavenging a point comes at which all the residual gas has been exhausted. Following this fresh charge air must be exhausted. This scavenging model produces the most optimistic results as the least amount of residual gas remains in the cylinder.

3.8.3 Use of scavenging models and limitations

The perfect displacement scavenging model is used for all non-cylinder simulation elements. This ensures that if a reverse flow of cylinder gas to an inlet plenum is produced then that reverse flowed gas is first returned to the cylinder before any fresh charge air is flowed.

It is important to note that all these scavenge models assume an isobaric, isothermal, constant volume flow process. This is very different to the conditions found in the internal combustion engine. The scavenge models have been implemented in such a way that when the simulation model is constructed to simulate an isobaric, isothermal constant volume flow process then the classical scavenging response is obtained. In more conventional simulations the instantaneous scavenging response at each crank angle increment is assumed to be that defined by the scavenge model under isobaric, isothermal constant volume conditions. The overall scavenging response however is often very different to that produced by the classic models.

3.9 Mechanical friction

There are a number of empirically derived formulas allowing the calculation of mechanical friction losses as a function of engine parameters such as engine speed, piston speed, compression ratio, maximum cylinder pressure etc. Methods for detailed calculation based on tribological properties of the friction contributing elements are also available.

3.9.1 Friction representation used

Most current empirical models representing mechanical friction are generally based on a relatively narrow range of engine speeds and there is limited published data for the tribological behaviour of engine components at very high crankshaft speeds. This is why friction data obtained from motoring tests performed on the modelled engine is used.

3.9.2 Effect of friction representation on gas dynamics

The gas dynamics in an engine are generally unaffected by mechanical friction. Therefore the complexity of the model used or the accuracy of measured data has no

effect on the processes investigated by this study. Friction Mean Effective Pressure (FMEP) is a function of volumetric efficiency. Higher Indicated Mean Effective Pressure (IMEP) can bring increase in bearing and piston ring and liner friction, therefore a small inaccuracy in the predicted power and Brake Mean Effective Pressure (BMEP) can be expected.

3.10 Fuel system model

3.10.1 Function

The fuel system model defines the method of fuel introduction and the way the fuel quantity is calculated. The method of introduction influences the combustion and heat transfer model. In the port-injected model fuel is introduced to the cylinder as air flows through the inlet valve. The model assumes that the fuel is fully evaporated and it thus displaces fresh charge that might otherwise flow into the cylinder.

The equivalence ratio specifies the quantity of fuel that should be mixed with fresh charge when it flows through an inlet boundary or inlet port. The flow routines have been developed to ensure that over-fuelling does not occur with reverse flow.

3.10.2 Effect of fuel system model on gas dynamics

In the real engine fuel is introduced towards the end of the intake stroke, which means that the initial gas flow through the valve will be higher than the predicted one. As all the fuel will be introduced towards the end of the intake stroke the predicted air flow will be slightly higher. However, the effect on the total gas flow is likely to be small. There may also be a slight effect of under-prediction of the quantity of fresh charge passed through the cylinder during valve overlap.

3.11 The model

3.11.1 Model structure

This research is based on a Triumph TT600 engine, details for which are provided in Chapter 4. Every component that is part of the gas flow path through this engine is represented by one of the elements described in Section 3.4. An engine model diagram is shown in Figure 3.3 and a list of all elements is provided below. The appropriate

properties and links are assigned to allow the equations simulating the processes to be solved.

Please note that simplified silencer assembly model consisting of one plenum, one pipe and two throttles was used for the research discussed in Chapter 5. This was done to aid the analysis of the shape of the breathing efficiency curve by using simple engine models. For all other work the representation shown with elements 27 to 49 was used.

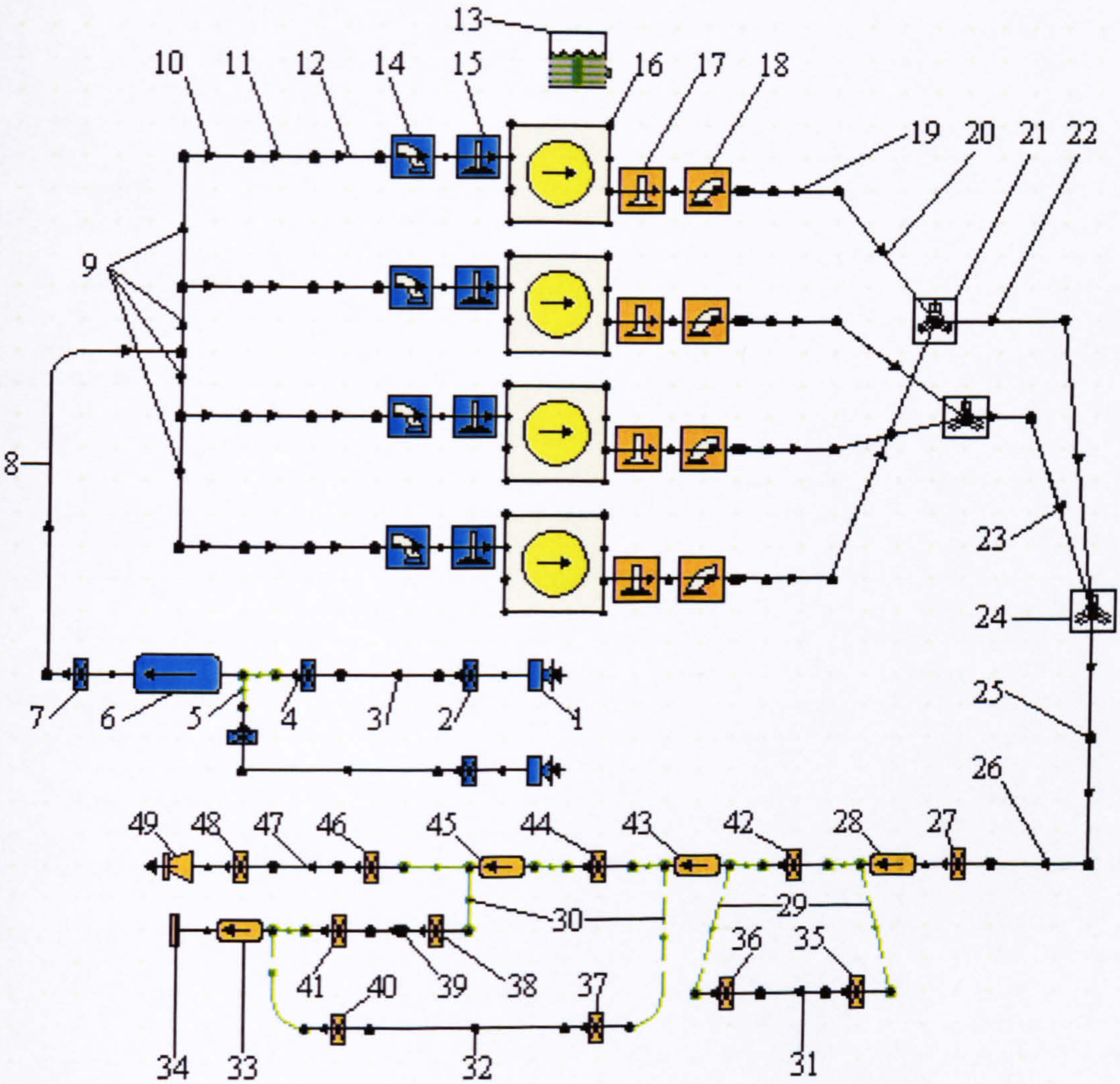

Figure 3.3: Simulation model representation of the TT600 engine

1 Inlet boundary

2 Ram air intake pipe inlet throttle

3 Ram air intake pipe

4 Ram air intake pipe outlet throttle

5 Virtual link

6 Prefilter volume

7 Filter

8 Postfilter volume

9 Throttle body feed volume

10 Throttle body

11 Transition piece

12 Inlet port length

13 Fuel system definition

14 Inlet valve

15 Inlet port flow characteristics

16 Cylinder

17 Exhaust port flow characteristics

18 Exhaust valve

19 Exhaust port length

20 Primary exhaust pipe

21 Primary to Secondary exhaust pipe junction

22 Primary to Secondary exhaust collector

23 Secondary exhaust pipe

24 Secondary to Tertiary exhaust pipe junction

25 Tertiary exhaust pipe

26 Inlet pipe to silencer

27 Exit throttle on Inlet pipe to silencer

28 Silencer volume 1

29 Virtual connection

30 Virtual connection

31 Baffle bypass pipe between Volume 1 and Volume 2

32 Baffle bypass pipe between Volume 2 and Dead end Volume

33 Dead end volume

34 Dead end stop

35 Inlet throttle on Baffle bypass pipe between Volume 1 and Volume 2

36 Exit throttle Baffle bypass pipe between Volume 1 and Volume 2

37 Inlet throttle on Baffle bypass pipe between Volume 2 and Volume 3

38 Exit throttle Baffle bypass pipe between Volume 2 and Volume 3

39 Inlet throttle on Baffle bypass pipe between Volume 2 and Dead end Volume

40 Baffle bypass pipe between Volume 2 and Dead end Volume

41 Exit throttle on Baffle bypass pipe between Volume 2 and Dead end Volume

42 Gauze baffle between Volume 1 and Volume 2

43 Silencer volume 2

44 Gauze baffle between Volume 1 and Volume 2

45 Silencer volume 2

46 Inlet throttle on tail pipe

47 Tail pipe

48 Exit throttle on tail pipe

49 Boundary

3.11.2 Simulation input data

This section provides details of the input data used in the simulation in this research. Due to the confidential nature of some of the parameters, actual values are not disclosed. However, the units and the format in which the data are used is presented.

Table 3.1 shows the submodel types and the appropriate coefficients describing the different physical phenomena in the engine:

- The wall friction factor for the ducts is calculated using the model described in section 5.3.4. The surface roughness is the typical value for the specified material. Note that the friction factor used does not account for losses due to pipe bends.

- The Annand model is used for heat transfer in the cylinders and plenum. The actual coefficients used for the model are based on the recommended values in the LES manual.

- The combustion duration and phasing information was derived from measured cylinder pressure data by using the combustion analysis function of the AVL 670 Indimaster. The measurement procedure was based on the method described in Chapter 4 section 4.3. Average from cylinder pressure data taken over 50 cycles was analysed. The algorithm used is based on the first law of thermodynamics and computes the energy delivered to the gas from the cylinder pressure (AVL 670 Indimaster Operating Manual, 2000). The crankshaft angle at which 10%, 50% and 90% of Mass Fraction Burned (MFB) points occur is calculated. The number of degrees from 10% MFB to 90% MFB point was used as an input for combustion duration in the model. The timing of the 50% MFB point relative to TDC was used as an input to position the heat release curve. Both combustion duration and timing were established to be relatively independent of crankshaft speed for this engine. The coefficients A and *M* of the Wiebe function were adjusted so that the calculated MFB curve passes through the three calculated points for 10%, 50% and 90% MFB.

- The mechanical friction data was obtained from a motoring test. The fuel data is default in the software.

Engine submodel inputs				
Submodel	**Input**		**Value**	**Unit**
Heat transfer in ducts	Wall material density		Default for material	Kg/m^3
	Heat transfer coefficient		Default for material	W/m2/K
	Specific heat constant		Default for material	J/K/kg
Wall friction	Friction factor		Confidential	N/A
	Surface roughness		Default for material	mm
Heat transfer in Cylinders	Open Cycle Annand Coefficients	A	0.1	N/A
		B	0.6	N/A
	Closed Cycle Annand Coefficients	A	0.8	N/A
		B	0.65	N/A
		C	0.1000E-06	N/A
	Combustion chamber / piston / liner area ratios		Confidential	N/A
Heat release	Wiebe coefficients	A	10	N/A
		M	2	N/A
Combustion duration and phasing	50% burn angle		Confidential	Specified in CA °for every engine speed site
	10-90% burn duration		Confidential	Specified in CA °for every engine speed site
Scavenging	Cylinders		Perfect mixing	N/A
	Non cylinder		Perfect displacement	N/A
Mechanical Friction	FMEP from motoring test		Confidential	Specified in [bar] for every engine speed site
Fuel system	Type		Port Injection	N/A
	Fuel type		Gasoline	N/A
	Calorific Value		43000	kJ/kg
	Relative density		0.75	kg/litre
	H/C ratio of Fuel		1.8	molar
	Molecular mass		114.230	kg/k.mol
	Maldistribution coefficient		1	N/A

Table 3.1: Engine submodel inputs

Table 3.2 defines the physical properties of the inlet and exhaust boundary air as well as coolant media.

Boundary conditions data		
Input	**Value**	**Unit**
Inlet boundary temperature	20	° C
Inlet boundary pressure	0.988	Bar (absolute)
Air relative humidity	0.01	Kg/kg
Exhaust boundary pressure	0.988	Bar (absolute)
Coolant air temperature	20	° C
Coolant air pressure	0.988	Bar (absolute)
Engine coolant temperature	100	° C

Table 3.2: Boundary conditions data

Table 3.3 provides information of the chosen speed test points as well as the number of iterations before convergence checks are made, and which iteration is used as a result. The values used are the recommended ones by the LES manual. All simulation is performed for WOT load condition.

Simulation test points and solver parameters		
Input	**Value**	**Unit**
Speed sites	From 1750 to 13000 in 250 steps	rpm
Solver steps	0.5	CA°
Check convergence after	4	cycles
Maximum number of cycles for simulation run	20	cycles
Cycle number from which results are written	20	cycles
Load	WOT	N/A

Table 3.3: Simulation test points and solver parameters

Table 3.4 provides details of the engine geometry data required by the model. It should be noted that apart from the firing phasing of the individual cylinders no other data describing the engine arrangement is required.

Engine geometry data		
Input	**Value**	**Unit**
Bore	68.00	mm
Stroke	41.30	mm
Con-Rod Length	98.50	mm
Compression Ratio	12.55	N/A
Piston Pin Offset	0.80	mm
Number of cylinders	4	N/A
Cylinder firing phasing	0-360-720-540	CA °
IVO	48	CA °BTDC
IVC	80	CA °ABDC
EVO	62	CA °BBDC
EVC	34	CA °ATDC
Inlet valve lift curve	Confidential	Specified by 155 point curve in [mm] valve lift vs. [°] camshaft angle format
Exhaust valve lift curve	Confidential	Specified by 139 point curve in [mm] valve lift vs. [°] camshaft angle format
Maximum inlet valve lift	8.8	mm
Maximum exhaust valve lift	7.75	mm
Inlet port throat diameters	25.4	mm
Exhaust port throat diameters	19	mm
Inlet port flow coefficient	Confidential	Specified by 12 point curve in format flow coefficient vs. L/D ratio format
Exhaust port flow coefficient	Confidential	Specified by 12 point curve in format flow coefficient vs. L/D ratio format
Throttle elements area	Confidential	mm^2
Throttle element discharge coefficients	Confidential	N/A
Plenum elements volume	Confidential	mm^3
Plenum elements wall thickness	Confidential	mm
Pipe elements diameter and length	Confidential	Specified diameter at different points over the length of the pipe [mm]
Pipe elements wall thickness	Confidential	mm
Pipe elements wall material	Confidential	N/A

Table 3.4: Engine geometry data

3.11.3 Approximations and assumptions

Some approximations and assumptions associated with the representation of engine components are necessary due to the complexity of the geometric properties of the components and the operating conditions in which they function. These assumptions are in addition to the simplification described in previous sections.

3.11.3.1 Geometry complexity

Often single volume components are represented as multiple volumes. This is necessary due to the complexity of the geometries involved. Certain judgment must be used to establish which features are significant for the gas flow. For example the shape of the postfilter part of the airbox can be represented with two cylindrical volumes. The first volume indicated as element 9 on Figure 3.3 feeds the throttle bodies. This volume is connected to the filter element by the postfilter volume (element 8 on Figure 3.3) positioned along the symmetry plane of the engine. After considering the shape of the postfilter part of the airbox, it was decided that representing it as two ducts will simulate the significant gas dynamics more accurately. The first volume is represented as four ducts connecting the individual trumpets to simulate the gas dynamic interaction between the individual cylinders. The second cylindrical volume is represented with a single duct allowing the correct simulation of the gas dynamics in this part of the prefilter space.

3.11.3.2 Gas dynamic behaviour in different volumes of the engine

In reality pressure waves transmitted from a pipe into a volume propagate through the volume and are reflected by every opposing wall. The simulation software used represents the engine with 0-D and 1-D elements. A judgement must be made whether a particular volume should be represented as a plenum or a duct. To do this it is important to understand the significance of any gas dynamic effects on the rest of the system.

If a volume is to be represented as a duct it must be decided which direction of wave propagation is significant. For example, waves propagating in very short ducts may be insignificant for the rest of the system. This is why in the volume feeding the throttle bodies (element 9) it is more important to simulate the gas dynamics along a duct

connecting the individual cylinders rather than the wave propagation in the short distance between the throttle body (element 10) and the roof of the volume feeding it (element 9).

If the pressure in a volume is expected to be uniform it can be approximated as a plenum. Such is the case with the representation of the prefilter part of the airbox (element 6).

Similar principals are applied to the modelling of the silencer assembly (elements 27-49).

3.11.3.3 Shape

The shape of some elements such as ports and silencer components has to be approximated to a circular duct.

3.11.3.4 External cooling media

In a real life engine installation, the temperature and flow rate of the external cooling media varies around the engine's inlet and exhaust components. This has an effect on the operating temperatures of ducts and therefore the gas dynamics of the flow inside them. This effect however is considered negligible as correlation results are obtained from a test cell installation where the flow and temperature of the coolant media is relatively uniform.

3.11.3.5 Pressure wave reflection in the end of pipes

In reality as a wave reflects from an open pipe end the rarefaction waves 'grow' from the annulus at the perimeter of the pipe as the incident pressure wave begins to expand, leading to a distributed reflection that appears to originate some distance, typically taken as 0.3 to 0.5 pipe diameters, beyond the pipe end. This is why it is usual in 1-d engine simulations to add an additional length (end effect) to the pipes to allow for. Note that the length of the inlet and exhaust primary pipes (e.g. element 10 and 20) was increased with 0.3 times their diameter to represent correctly the effective reflection point of the pressure waves.

3.11.3.6 Valve timing

Investigation conducted by Lyon (1996) shows that small variation in camshaft timing can be responsible for significant variation in the output of otherwise identical high-speed engine. This is why, while accurate correlation between the predicted output and measured data is not the objective of this research, it is important to carefully select the simulation input parameters relating to the valve events and appreciate their potential to introduce error in the model.

It is assumed that the tappet to base circle clearances on the engine are at their maximum possible setting. This is why the maximum lift is reduced with the value of the maximum tappet to lobe clearance. The test engine for the experimental validation used was set with the maximum tappet to valve clearance.

It must be acknowledged that due to dynamic effects in the camdrive and torsional vibration in the camshaft the actual valve event timing when the engine is running may differ from this measured when the engine is static. The dynamic valve event timing can be established by using engine dynamic simulation software or experimentally however this is beyond the scope of this research.

3.12 Sensitivity of the simulation results to mesh density and time step

The simulation run time is related to the number of calculations the software has to perform. The spatial and temporal accuracy is dependant on the mesh density and the time step. The base simulation setup used in this research utilises automatic mesh generation which generates mesh size which together with the selected time step satisfies the CFL stability criteria for all engine speeds as described in section 3.5.2.2. Figure 3.4 shows a comparison between calculated values for volumetric efficiency using the base setup which is used for all simulation runs in this research and two setups featuring double mesh density and 60% reduced time step. The deviation between the results is within 6% and is confined to certain higher speed regions. The base simulation run time was 9h 30min, while the double mesh density setup was 27h 10min and the reduced time step was 13h 06min. Considering the minimal deviation in the results and the increased run time the base setup is used for the purposes of this research.

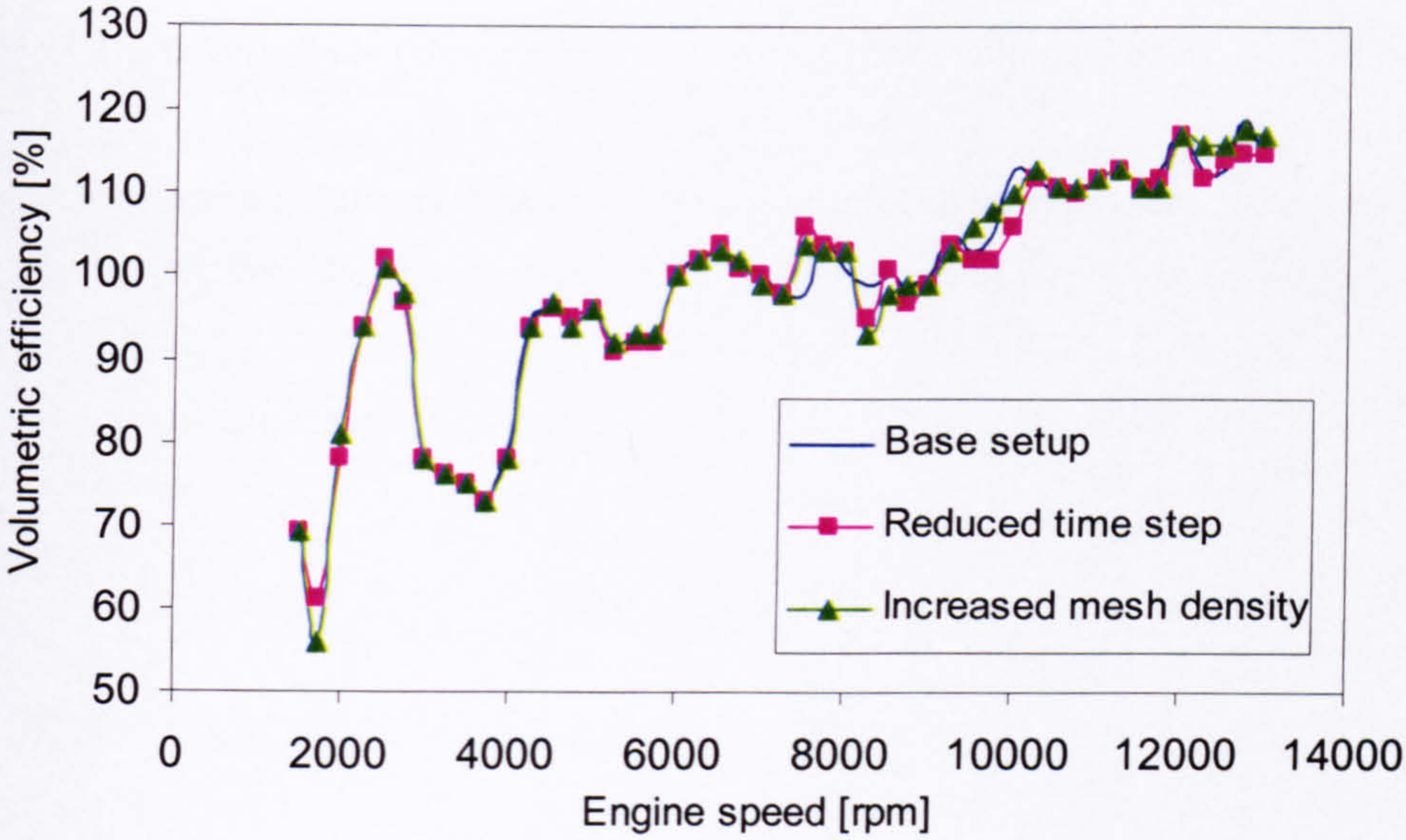

Figure 3.4: Calculated volumetric efficiency vs. engine speed using base setup with automatic mesh generation, reduced time step setup and increased mesh density setup

3.13 Engine simulation software as a tool for investigating gas dynamics

The operation of IC engines is a combination of a complex thermodynamic, chemical, gas dynamic and tribological processes. As with any simulation software LES attempts to create mathematical submodels of each process and join the output in order to predict global parameters such as power and breathing efficiency etc. and local parameters like pressure, temperature, velocity and mass flow.

Previous research (Takizawa *et al.*, 1982; Pearson and Winterbone, 1990; Sung *et al.*, 1995) has shown that the solving of the governing equations of gas flow through ducts using the method of characteristics and reasonable assumptions for wall friction and heat transfer results in a relatively accurate approximation of the gas dynamics. There is evidence that this combined with good approximations for the rest of the engine processes can result in accurate prediction of engine output.

This research concentrates on the gas exchange processes, hence only accurate prediction of the gas flow through the engine is required and the calculation of global parameters is unimportant. This is why the mechanical friction model is unimportant. Accurate prediction is required from the point when the gas enters the engine to the point when the inlet valve closes and from the point when the exhaust valve opens until the burned gas exits the engine. Good modelling of the gas flow through duct, valve/port model and cylinder heat transfer model is required. This is why the accuracy of combustion model is only important as far as predicting the correct pressure and temperature and wall temperatures at EVC. The pressure data shows that this is the case.

In conclusion a judgement was made that the code models the gas dynamic effects in a satisfactory way allowing it to be used for the investigation of the effects of valve events on gas exchange processes.

Chapter 4

Experimental Validation

To be able to use the software as a tool for the investigation presented in the following chapters, the accurate modelling of the gas dynamic process must be proven. The engine used in the research was installed on a dynamometer test bed and instrumented with a number of transducers. A selection of parameters was measured and correlated with predicted data. This chapter presents the experimental set up and comments on the results of the correlation.

4.1 Selection of validation parameters

In order to perform any simulation software correlation it is important to establish a set of parameters that will be used. This research concentrates on the gas dynamics in high-speed engines therefore correlation of parameters characterising the gas flow is essential.

It is logical to seek good correlation for volumetric efficiency however its accurate estimation on a high performance engine is difficult. Calculation based on direct mass flow measurement does not account for the charge escaping directly to the exhaust. Due to the large duration of valve overlap this can be a significant fraction of the fresh charge, which is entering the cylinder under certain conditions. In addition, the device used to measure the mass flow can alter the gas dynamics and have an effect on volumetric efficiency.

Other methods involving fuel flow and AFR measurement are prone to error for the same reason. This is why correlation of volumetric efficiency was not considered reliable. However, accurate prediction of volumetric efficiency and other global parameters relies on good simulation of the gas dynamics through the engine. It was considered that the most important parameter characterising the gas dynamics in the engine is pressure. Correct predication of instantaneous inlet and exhaust port pressure would confirm the

simulation of the flow through the valves. Mean pressure data from both sides of the air filter would validate the throttling coefficient of the air filter element. Mean pressure data from the tertiary exhaust pipe would confirm the silencer modelling. Another important parameter, especially for the gas dynamics in the exhaust system, is gas temperature. Accurate calculation of exhaust gas temperature is necessary to ensure the correct prediction of the wave propagation speed in the exhaust system. Good correlation of this parameter would also indicate the correctness of the combustion model as well as heat transfer in the combustion chamber and exhaust pipes.

4.2 Experimental set up

4.2.1 Test facility

Test cell 6 of the Faculty of Engineering Powertrain Laboratory at Loughborough University, shown in Figure 4.1, was used for the experimental phase of the research. The cell is equipped with ambient air pressure and airflow monitoring and control system as well as closed loop heat exchange system for engine and dynamometer cooling. Remote control as well as in-cell control of the engine and dynamometer is possible.

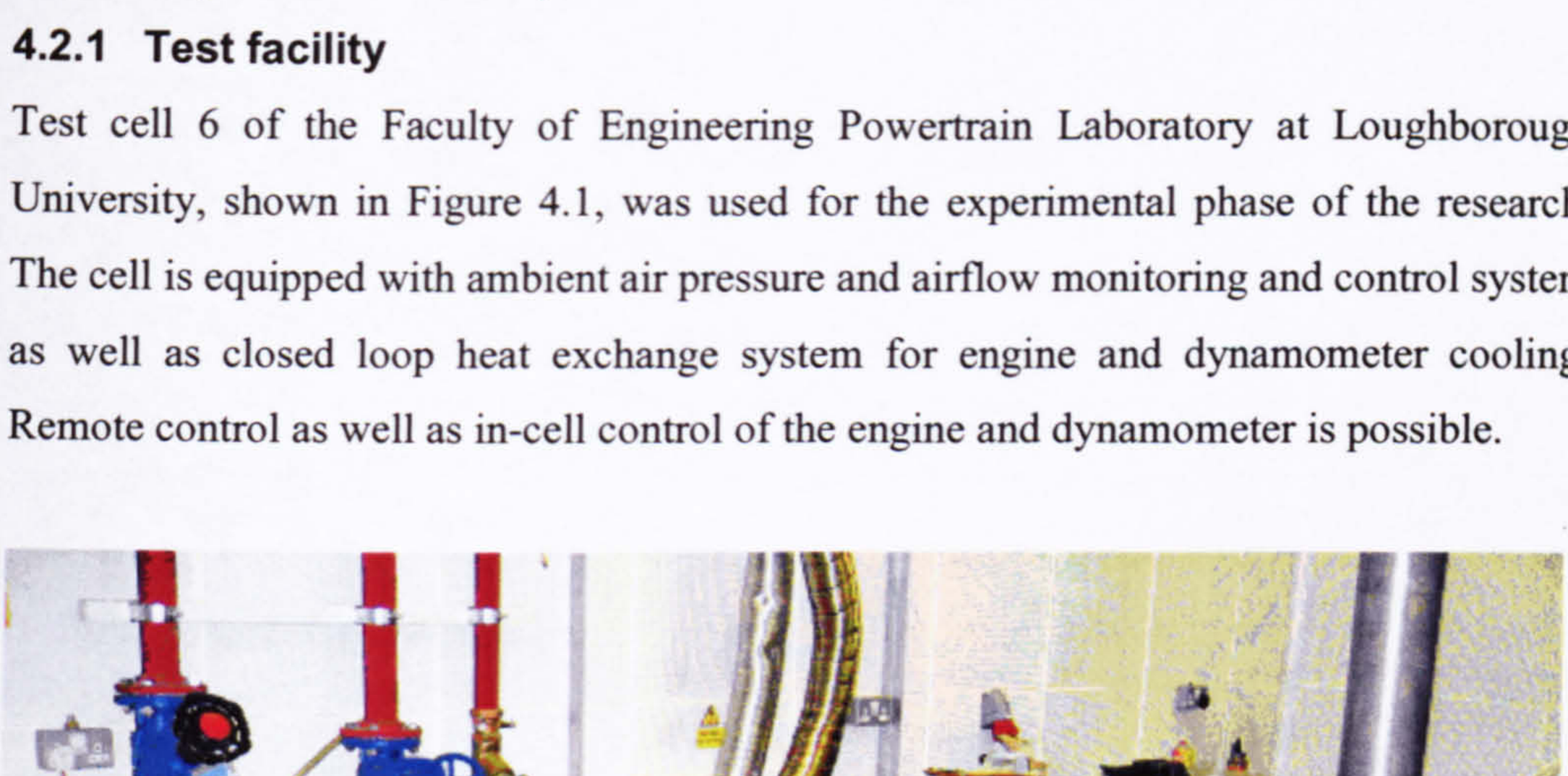

Figure 4.1: Test cell 6 of the Faculty of Engineering Powertrain Laboratory

4.2.2 Engine installation

The engine was installed in a fabricated frame, which was bolted to the test bed. It was connected to the dynamometer via a driveshaft attached to the output shaft of the gearbox. An electric actuator was used for remote control of throttle angle and clutch position. The standard engine management system was replaced with a programmable control unit. The engine was equipped with all necessary transducers required for monitoring engine operation and for the purposes of the correlation. A schematic diagram of the engine installation and the experimental set up is shown in Figure 4.2. The individual elements are discussed in detail in the following sections.

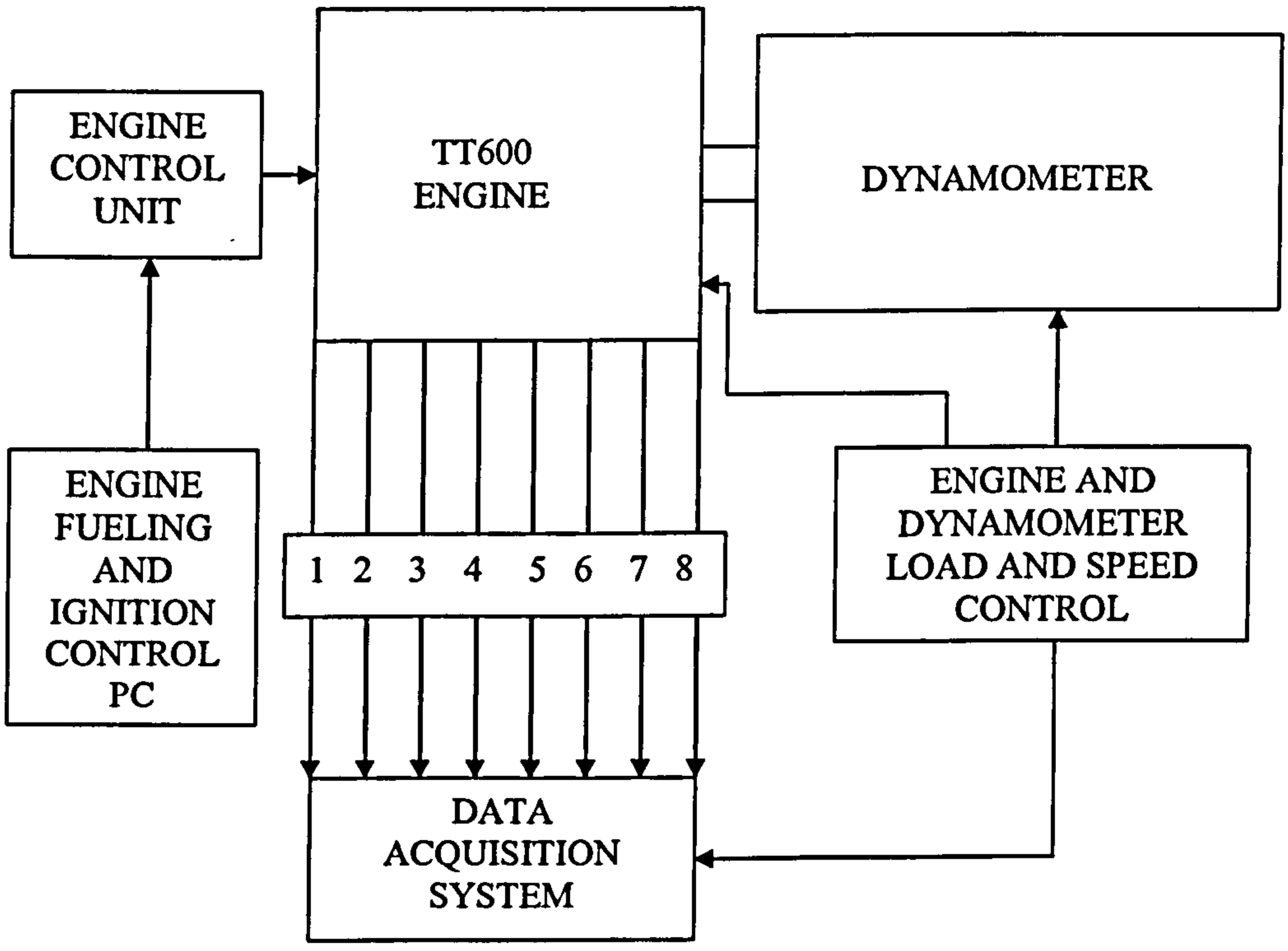

Signals to Data Acquisition System

1 – AFR meter
2 – Crankshaft encoder
3 – Inlet port pressure transducer
4 – Exhaust port pressure transducer
5 – Prefilter pressure transducer
6 – Postfilter pressure transducer
7 – Tertiary exhaust pipe pressure transducer
8 – Exhaust termocouple

Figure 4.2: TT600 engine experimental set up

4.2.3 The engine

The engine used is from a Triumph TT600 sports motorcycle. It is a 600cc, four cylinder, 4 stroke naturally aspirated engine. It became the object of the research due to its wide speed range and performance characteristics. It was identified that it could benefit from the application of a VVA system. With a specific output of 134 kW/l and maximum engine speed of 13500 rpm, it is a typical naturally aspirated high performance, high-speed engine. It can be assumed that the knowledge gained from an investigation based on this engine is applicable to other powerplants of this type.

The engine has an aluminium alloy cylinder head and crankcases. It features wet Nikasil coated aluminium liners. The gearbox and all engine auxiliaries are incorporated within the engine structure. The inlet system features a common airbox and individual throttle butterflies for each cylinder. Fuel is introduced in the engine with a sequential port injection system. The exhaust system is of the 4 into 2 into 1 type and includes a pre-catalyst element in the tertiary pipe and a catalyst in the silencer. Basic engine data is presented in Table 4.1.

Number of cylinders	4 in line
Bore / Stroke	68 mm / 41.3 mm
Compression ratio	12.55:1
Maximum power output	81 kW at 12750 rpm*
Maximum torque output	68 Nm at 11000 rpm*
Maximum engine speed	13500 rpm
Number of inlet valves	8
Number of exhaust valves	8
IVO / IVC / Inlet max. lift	48° BTDC / 80° ABDC / 9 mm
EVO / EVC / Exhaust max lift	62° BBDC / 34° ATDC / 8 mm
Inlet primary length	261 mm
Exhaust primary length	647 mm

Table 4.1: TT600 engine specifications

(*manufacturer claimed figures, measured to DIN 70020)

4.2.4 Engine fuelling and ignition control

The engine fuelling and ignition was controlled with a purpose build Electronic Control Unit (ECU) supplied by General Engine Management Systems Ltd (see General Engine Management Systems Ltd Website, 2004). The ECU was connected with a computer via a serial link allowing real time control over fuel injection duration and phasing as well as ignition timing. The software allowed direct change of the appropriate values for each speed/load site in the fuel and ignition maps.

4.2.5 Dynamometer and control unit

A Heenan Dynamatic Mark 2 Eddy current water cooled dynamometer was used. It is capable of absorbing 186kW and has a maximum shaft speed of 10000 rpm. Due to the high inertia of the rotor compared with the equivalent inertia of the engine components and the inability to change gear during the test, excessive clutch slippage was required during engagement. In addition, full load operation at speeds below 3000 rpm caused excessive vibration of the engine / dynamometer system and difficulties with maintaining constant speed.

The control system for the dynamometer was developed at the Faculty of Engineering at Loughborough University. It allows both manual and automated test control. The former was used for the purposes of this research. The system provides engine speed and absorbed torque as analogue outputs.

4.2.6 Data acquisition systems and other instrumentation

Two data acquisition systems were employed. The first system was used for general engine and dynamometer monitoring. It allowed monitoring of critical engine operating parameters such as coolant, oil and exhaust gas temperatures, oil pressure and AFR. It also provided an alarm if predefined limits for a particular parameter were exceeded. The arrangement was based on a 16 channel PCI-MIO-16E-4 card (see National Instruments Corporation Website, 2004), configured with LabView software. A National Instruments BNC breakout box was used to connect to the transducers. The front panel of the virtual instrument, which was developed is shown on Figure 4.3.

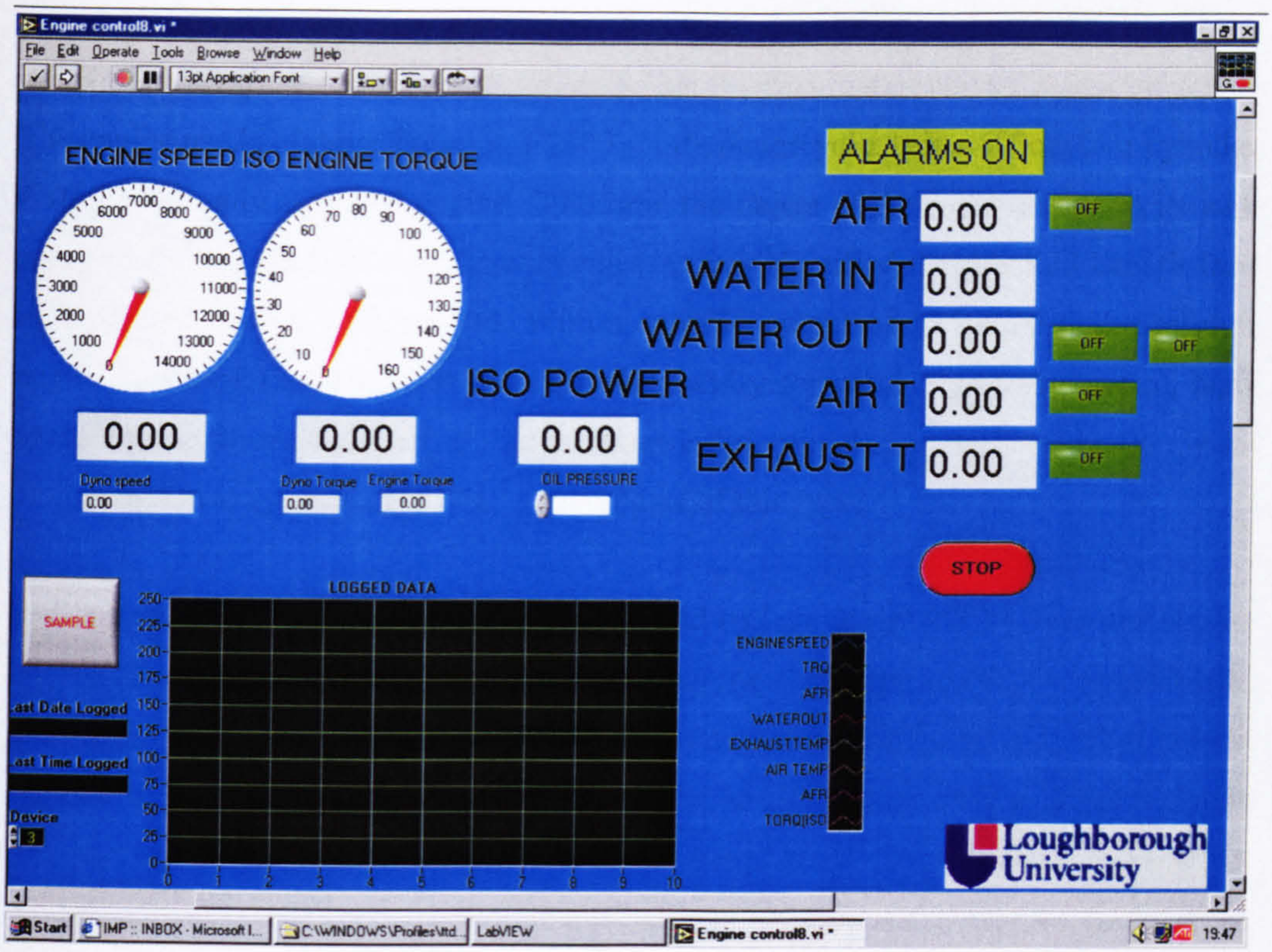

Figure 4.3: LabView control panel

All transducer signals measuring parameters used for correlation with simulation results were done with an AVL 670 Indimaster (AVL 670 Indimaster Operating Manual, 2000) unit shown on Figure 4.4. This system allows crankshaft position triggered as well as time base sampling. In this research signal from the crankshaft encoder was used for data sampling triggering as well as for establishing TDC.

The unit can incorporate the required amplifiers, signal conditioning circuits and analogue to digital signal converters for a variety of transducers. As well as being capable of receiving raw signals as an input the system has the facility to sample already amplified and conditioned signals.

AVL Multi Purpose Amplifier 3009 was used to boost the signal from the Kistler pressure transducer, described in the following section. A standard thermocouple amplifier with internal cold junction compensation was used for temperature measurements. The AFR sensor was used with an NTK AFR M01000 amplifier.

Figure 4.4: AVL 670 Indimaster

4.2.7 Transducers

As mentioned in an earlier section, after installation on the test bed, the engine was equipped with transducers monitoring essential parameters such as coolant, oil and exhaust gas temperatures as well as oil pressure. While their output values were not recorded or used directly for the purposes of this research, they were required to ensure safe operation of the engine during testing.

Table 4.2 provides a list of the transducers installed on the engine specifically for the purposes of simulation correlation. The Kistler 4045A20 piezoelectric transducer was

used for measurement of instantaneous pressure in the inlet and exhaust port as well as cycle mean pressure in the tertiary pipe. In the first application the transducer was positioned in the left hand side of cylinder 1 inlet port and approximately 65 mm in from the inlet valve seat plane. The axis of the transducer was at 90° to the flow direction and the measuring diaphragm was level with the port inner wall.

In both exhaust measurements a cooling adapter Kistler 7511 was used. The closest practical mounting position to the exhaust port was in the left hand side of the cylinder 1 header pipe and approximately 100 mm from the exhaust valve seat plane. The transducer was oriented at 90° to the flow. Due to the cooling adapter the measuring face was offset from the inner wall by 40mm. The calibration of all pressure transducers was checked with a calibration tool.

Measured parameter	Transducer manufacturer / code	Sensing principal	Sensitivity	Range	Thermal shift
Crankshaft speed angular position	Baumer - BDK 16.05A360-5-4	Optical	0.5 CA°	12000 rpm	N/A
AFR	NTK	Electrochemical	0.5 V/AFR	10-30	±0.2 AFR
Inlet port pressure	Kistler – 4045A20	Piezoresistive	25 mV/bar	0-20 bar	Zero ≤±0.5%FSO Sensitivity ≤±1%
Exhaust port pressure	Kistler – 4045A20	Piezoresistive	25 mV/bar	0-20 bar	Zero ≤±0.5%FSO Sensitivity ≤±1%
Prefilter and Postfilter pressure	Basingstoke - 2000	Piezoresistive	3.125 V/bar	0-1.6 bar	N/A
Tertiary pressure	Kistler – 4045A20	Piezoresistive	25 mV/bar	0-20 bar	Zero ≤±0.5%FSO Sensitivity ≤±1%
Exhaust temperature	K-type Thermocouple	Thermovoltage	41μV/°C	-200-+1200° C	±1 C

Table 4.2: Transducers fitted to the engine

The second location was 130mm downstream from the beginning of the exhaust tertiary pipe. The orientation relative to the flow and the distance from the pipe wall is the same as in the previous location.

Note that the Basingstoke 2000 pressure transducer, which was used for measuring pressure on both sides of the filter element, has an inbuilt amplifier.

The thermocouple monitoring exhaust gas temperature was mounted at 120mm away from the exhaust valve seat plane in the primary pipe.

4.3 Experimental procedure

The experimental procedure included the following steps:

1 Warm up engine at 3000 rpm and no load for 5 minutes followed by running at 6000 rpm at 20% load until normal coolant and oil temperatures are achieved.
2 Set engine speed to 3000 rpm and increase load to 100%.
3 Increase engine speed to the highest speed site to be measured (do not allow AFR to rise above 13:1 at engine speeds higher than 6000 rpm).
4 When at desired speed site adjust AFR to 12.5±0.1 and allow to settle for 5 seconds.
5 Sample data for 50 cycles.
6 Move to lower engine speed site and repeat steps 4 and 5.
7 When test complete reduce speed to 3000 rpm and load to zero and run engine for two minutes.

4.4 Test conditions

All measurements and simulation runs were done for full load condition. The simulation was performed for engine speeds ranging from 1500 rpm to 13000 rpm in 250 rpm intervals. Test results were obtained for speeds from 2500 rpm to 13000 rpm in 500 rpm intervals. Air to fuel ratio was kept at 12.5:1. The engine specification as described in section 4.2.3 is identical to the simulation inputs described in section 3.11.2.

4.5 Experimental data processing and sources of errors

The measured data was processed in two different ways. The inlet and exhaust port data was averaged at every crankshaft angle. The pressure data for both sides of the filter element and the tertiary exhaust pipe was averaged for every crankshaft angle and the cycle average was established. Exhaust gas temperature measurements were also averaged for 50 cycles.

There are three potential sources for measurement error. The first one is due to incorrect establishing of TDC. This was done by inserting a purpose made tool in the spark plug hole and turning the crankshaft, until piston contact was made. The angular position when this happened was recorded. The same procedure was repeated in the opposite direction. The middle of these two angular positions was considered to be TDC. Establishing TDC in such a way is well established procedure, however it is subject to inaccuracy due to piston tilt in the cylinder and piston to crankshaft axis offset. The AVL Indimaster unit has a facility to establish TDC by using peak compression cylinder pressure. Comparison with this showed variable error not exceeding 7° CA, which is deemed satisfactory.

The second source of error is associated with the temperature effect on the pressure transducers. Table 4.2 shows that for the Kistler pressure transducer this is equal or less than 0.5 % FSO for the thermal zero shift and equal or less than 1 % for the thermal sensitivity shift, which is considered acceptable. There is no data available for the thermal effects on the Basingstoke pressure transducer. However, due to its installation position it is not subjected to severe thermal loads or temperature fluctuations.

The third source of inaccuracy, which will affect the correlation, arises from the difficulty in establishing the exact mounting position of the inlet and exhaust port pressure measurement positions relative to the combustion chamber. The approximate distances from the valve seat planes were used to extract the data from the simulation model. This can result in a small phase error. The depth of the measuring diaphragm when the sensor is installed with a cooling adapter also introduces a small error of the same type.

4.6 Correlation results

From this point on in this thesis the pressure in all results plots is absolute.

Figure 4.5 shows calculated and measured inlet port pressure data at 9000 rpm plotted vs. crankshaft angle. It can be seen that the measured and calculated pressure exhibit the same number of dips and peaks and the general shape of the two curves is similar. There is good correlation in the actual values, especially in the region from TDC to EVC and BDC to IVC, which is important for this study. However, the magnitudes of the peaks and dips of the pressure curve after IVC are overestimated. This underdamping effect is due to the modelling of the pressure wave reflection at the open end of the inlet runner. As the code is 1-dimensional such reflection occurs in a planar fashion and it produces a single reflection point at the pipe-end. In reality, as a wave reflects from an open pipe end the rarefaction waves 'grow' from the annulus at the perimeter of the pipe as the incident pressure wave begins to expand. This leads to a distributed reflection, which appears to originate some distance (typically taken as 0.3 to 0.5 pipe diameters) beyond the pipe-end.

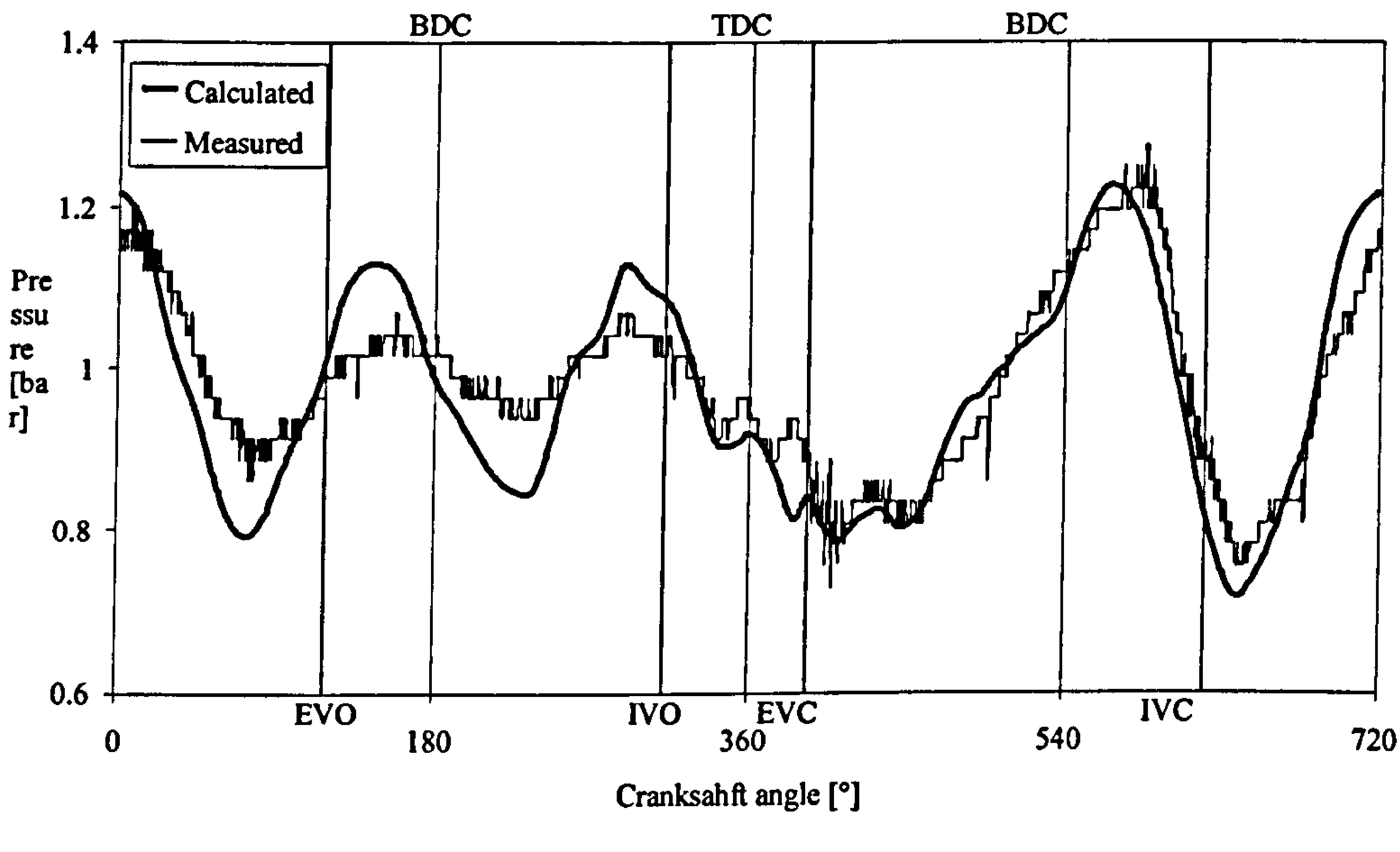

Figure 4.5: Measured and calculated inlet port pressure vs. crankshaft angle at 9000 rpm

Additionally, the bellmouths on the inlet runners are designed to give a very high discharge coefficient in the forward flow direction, but not in the reverse flow direction. In reality, any reverse flow will separate from the wall, which will lead to high losses. This is not captured by the model as the flow is assumed 1-D it is always attached.

Figure 4.6 shows calculated and measured exhaust port pressure data at 9000 rpm plotted vs. crankshaft angle. It can be noticed that the timing of both peaks at BDC after EVO and just after IVC is well simulated. The first peak is caused by the flow leaving the cylinder and the second is caused by the other cylinder connected via the first junction in the exhaust. The magnitude of the second peak is slightly overestimated by the simulation. This is possible because of the same reasons relating to the reflection of waves as described above. The peak also occurs a little earlier indicating slightly overestimated wave propagation speed. The high frequency elements of the curve are less well simulated. However, the behaviour during valve overlap is well modelled.

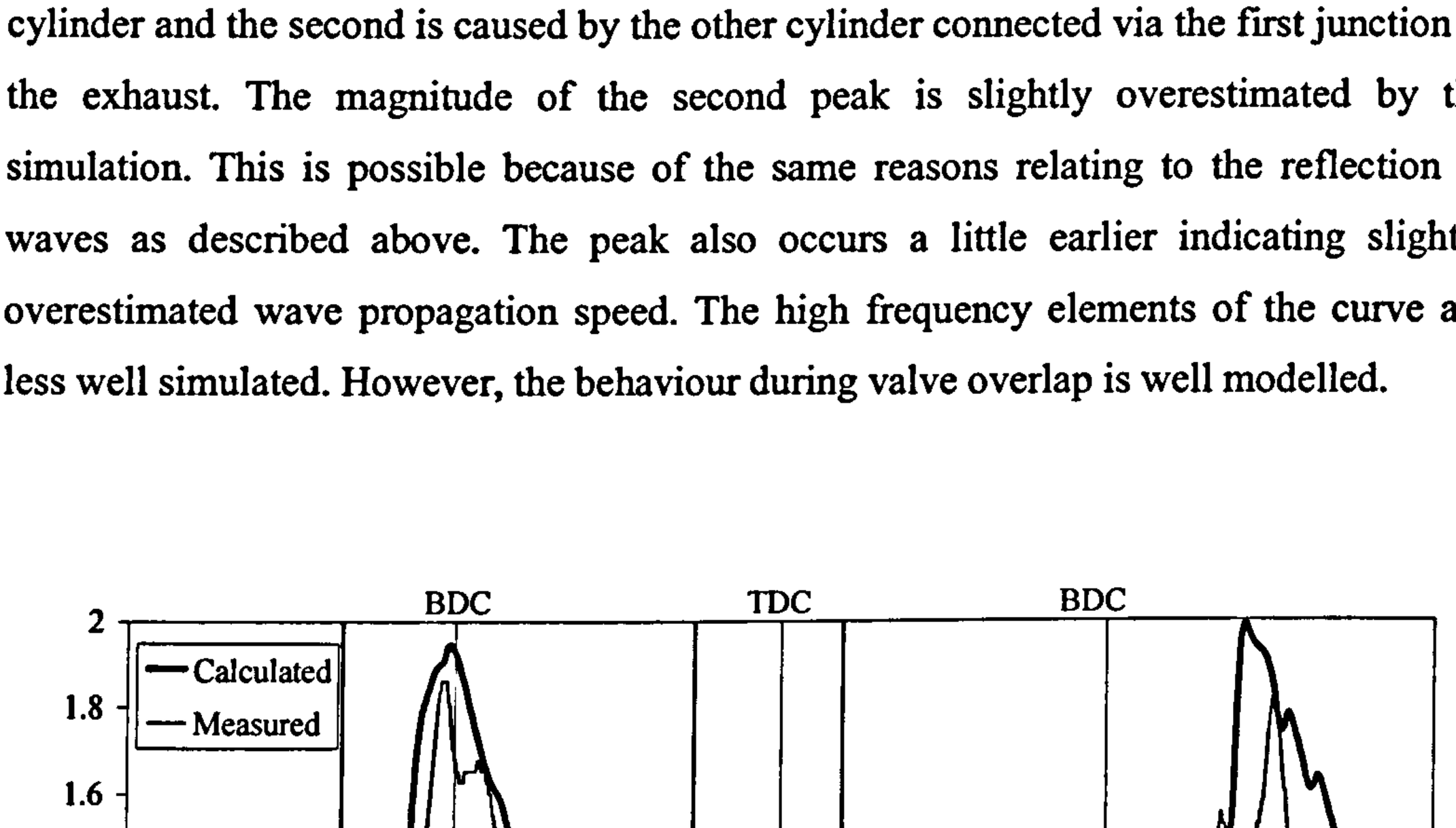

Figure 4.6: Measured and calculated exhaust port pressure vs. crankshaft angle at 9000 rpm

Figure 4.7 shows comparison between predicted and measured mean pressure upstream of the air filter element, throughout the engine speed range. The difference between the two curves is less than 1 mbar for the entire engine speed range except at 11000 rpm and at 13000 rpm. The reason for the dip at these speeds is possibly due to the underdamping of the pressure pulsations when the inlet valve is closed. As it will become clear in the following chapters, the coincidence of a positive pressure pulse with the valve overlap period has significant effect on cylinder filling. Hence, an overprediction of the peak magnitude has the same effect on inlet flow. This causes a reduction of mean pressure in the inlet at these speeds. Considering the isolated nature of this error it will not have a significant effect on the findings of this research. It can be conclude that there is good simulation of the intake system upstream of the air filter element.

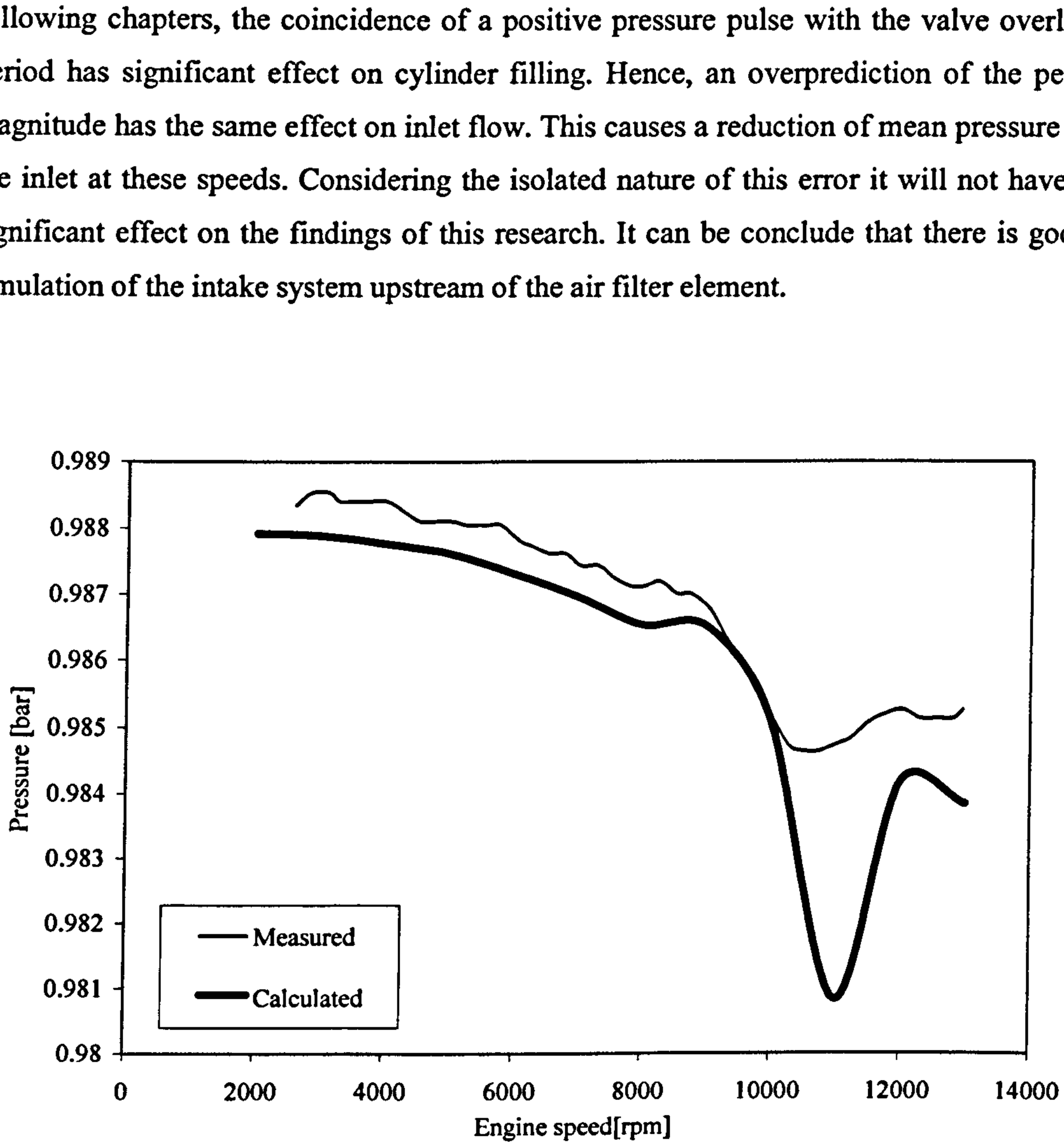

Figure 4.7: Measured and calculated prefilter mean absolute pressure vs. engine speed

Figures 4.8 presents calculated values and experimental data for the mean pressure in the volume downstream of the air filter element. The difference between the two curves is within 5 mbar, demonstrating correct representation of the air filter element. Note that the air filter element is represented as a throttle with specific area and discharge coefficient. The same inaccuracy is observed as with the prefilter pressure at 11000 rpm and 13000 rpm. This is because of the same reason and as commented earlier this should have limited effect on the findings from this research.

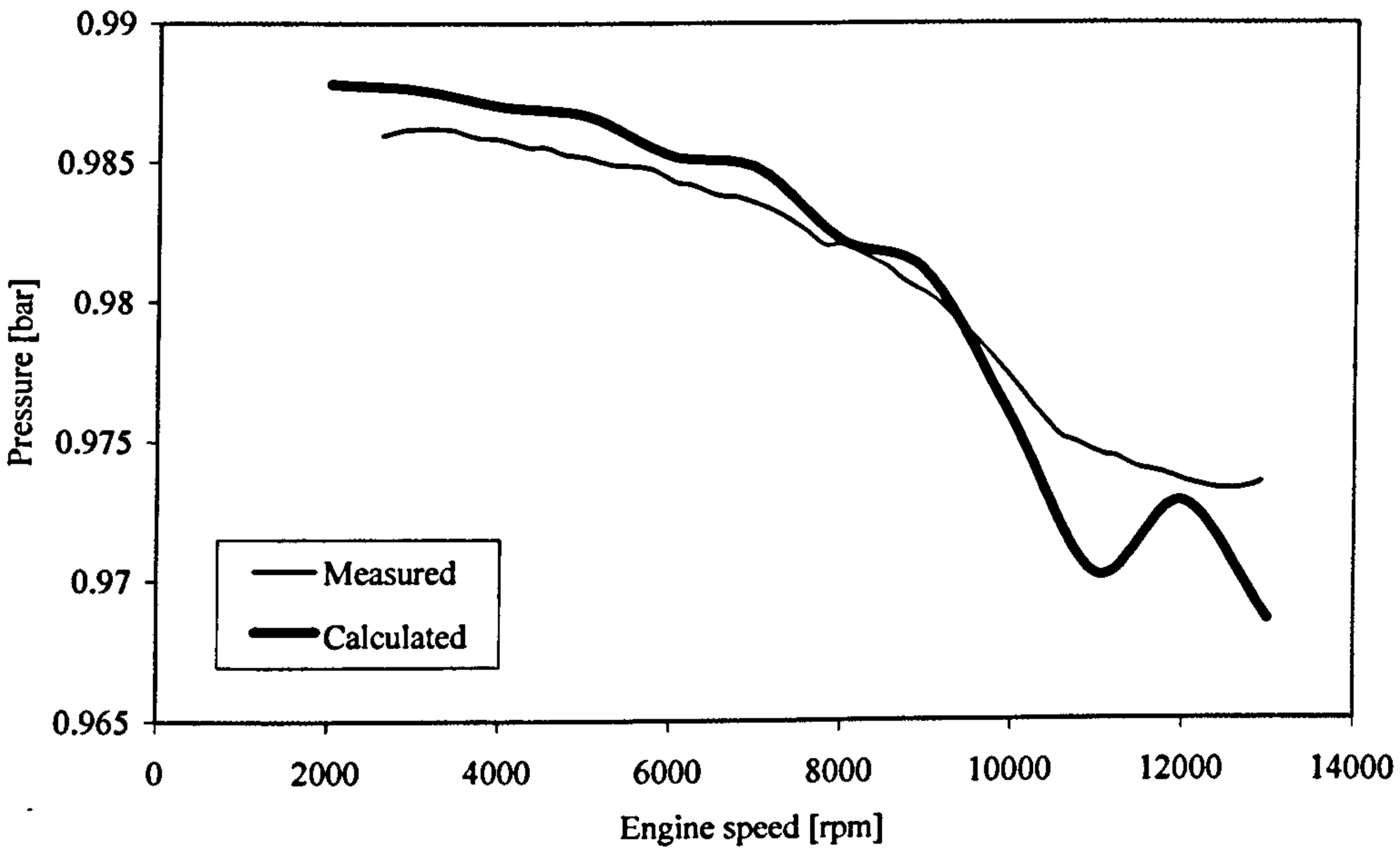

Figure 4.8: Measured and calculated postfilter mean absolute pressure vs. engine speed

Figure 4.9 shows measured and predicted mean pressure in the exhaust tertiary pipe throughout the speed range. The largest error occurs around 8000 rpm where the predicted backpressure is higher than the measured. This is possibly due to acoustic tuning effects simulated by the code, which do not appear in the exhaust system of the real engine. However, the difference in the two curves does not exceed 20 mbar. This is relatively small considering the acoustically complex nature of the silencer assembly. The slight overprediction at 11000 pm and 13000 rpm is due to the increase in flow at these speeds as explained earlier. Therefore it can be concluded that the simulation provides accurate modelling of the silencer characteristics.

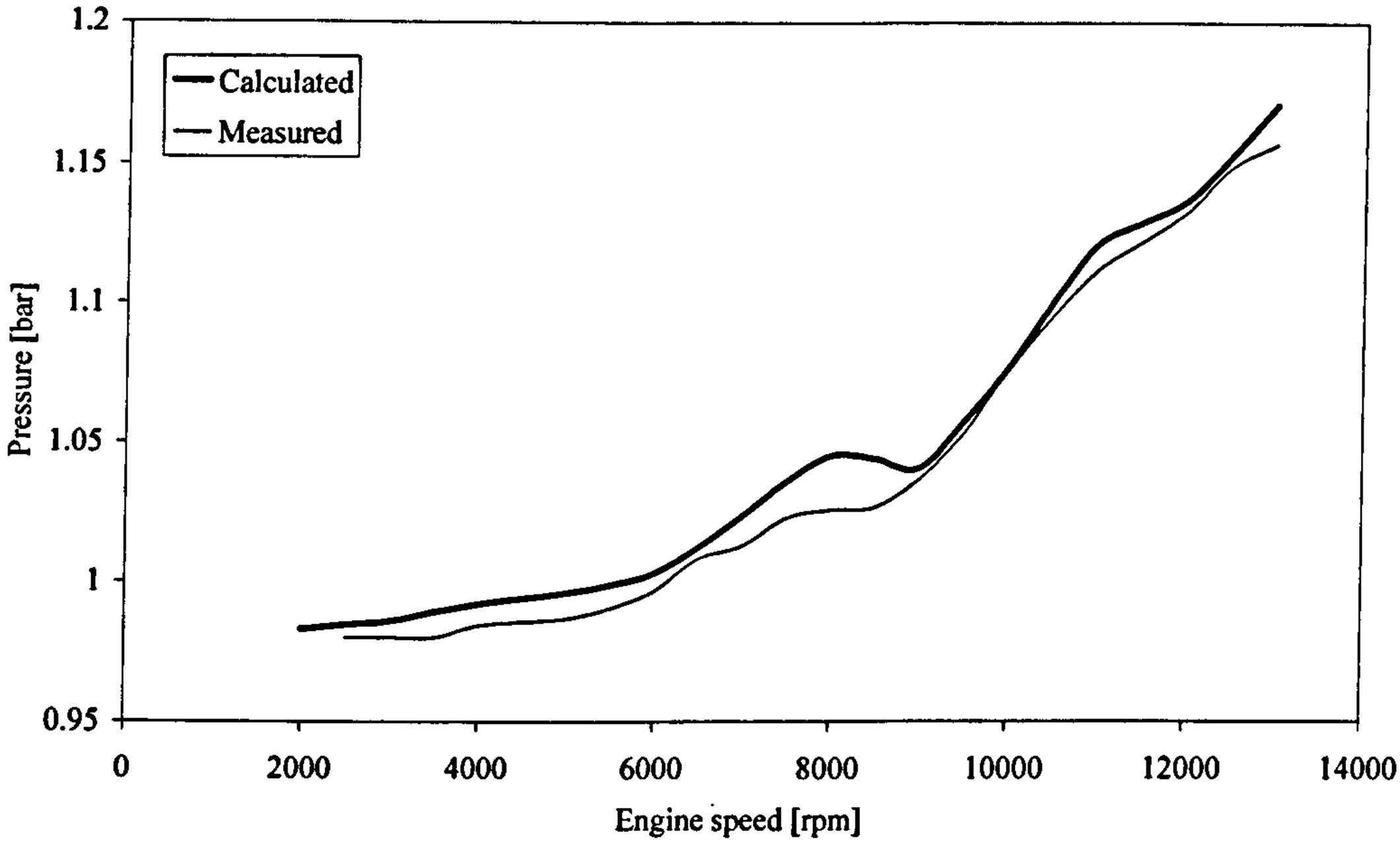

Figure 4.9: Measured and calculated mean pressure in tertiary pipe vs. engine speed

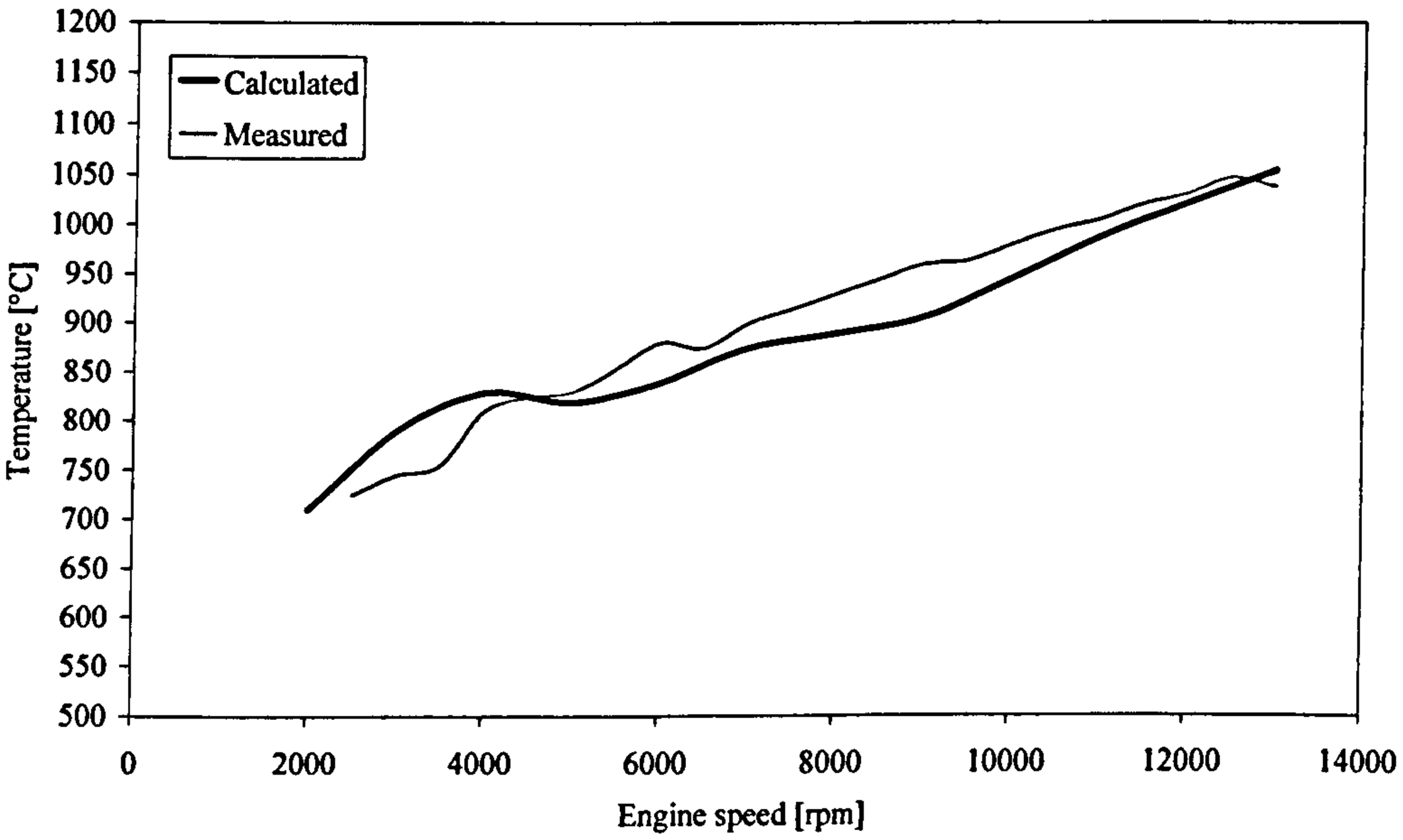

Figure 4.10: Measured and calculated mean gas temperature in the primary exhaust pipe vs. engine speed

Figure 4.10 shows the measured and calculated gas temperature in the primary exhaust pipe. It can be seen that up to 4500 rpm the code overestimates the gas temperature. Above that speed the measured temperature is higher than the calculated by the model. This could be due either to the combustion model or the heat release model in the cylinder. Either way the difference does not exceed 55 °C which less than 8% of the gas temperature. The highest difference is at 3500 rpm and 9000 rpm. The second speed corresponds to the speed for which the instantaneous inlet and exhaust pressure results are presented. This means that the slight shift in the prediction of the second pressure peak in Figure 4.6 and attributed to incorrect wave propagation speed is not going to be worse for any other speed.

4.7 Summary of conclusions

The results presented above demonstrate accurate correlation between measured and predicted instantaneous inlet port pressure, apart from the slight underdamping effect after IVC. This proves that the model replicates the propagation of the pressure waves relatively well. The instantaneous exhaust port pressure is also well simulated in terms of magnitudes and approximate shape. The observed shift of the second peak caused by the pressure wave in the adjacent cylinder is probably worse for this speed. Comparing the mean pressures taken from different parts of the engine with simulation results show that the flow coefficients along the inlet and exhaust system are fairly well simulated. The largest inaccuracy is due to the pressure pulse underdamping effect on engine breathing.

The exhaust gas temperature is predicted within 55 °C. This may have a small effect on the wave propagation speed. However, this will only have a slight effect on the exact engine speed where the tuning effects in the exhaust system occur.

In conclusion, a judgement was made that the simulation software models the gas dynamic effects accurately allowing it to be used for the investigation of the effects of valve events on gas exchange processes. While not dismissing the importance of correlation and the fact that this research is based on a real engine it should be noted that this research focuses on the exploration of gas dynamic phenomena, rather than prediction of actual parameters.

Chapter 5

Gas Dynamic Behaviour and Cylinder Filling Mechanisms

This chapter presents the results from investigation of the effect of gas dynamic behaviour in the inlet and exhaust system on the gas exchange process in high-speed engines. This is essential in order to be able to discuss the effect of the individual valve events in later chapters. It begins by defining the key parameters used to quantify the efficiency of the breathing process.

The breathing process in a multi-cylinder engine, like the one used in this research is a function of the complicated gas dynamic behaviour in the inlet and exhaust systems and the cylinders. This is reflected in the complex shape of the breathing efficiency curve typical for such engines. Detailed explanation of the exact reasons for this shape is complex and unnecessary as it relates to a particular engine arrangement. It is more important to understand the basic mechanisms of the gas exchange process. This is done by examining this process in simulation models of two single, cylinder engines one with infinitely short exhaust duct and the other with infinitely short inlet duct by using engine simulation software.

Using these simple models it is possible to explore the effect of the inlet and exhaust gas dynamics on the engines' breathing efficiency. This effect is explained by examining the pressure gradient across the cylinder and the gas flow through the valve. Whilst the gas dynamic behaviour in the inlet and exhaust is not the main subject of this research, it has an enormous impact on the effect of the individual valve events on engine breathing, which will become clear in the following chapters.

5.1 Engine breathing efficiencies

Up to this point the general term 'breathing efficiency' rather than 'volumetric efficiency' has been used to quantify the engine breathing process. This was done intentionally as the parameter 'charging efficiency' defined in the following sections, evaluates the same process more accurately in terms of fresh charge trapped at IVC. When applied to naturally aspirated SI engines with short valve overlap the difference between charging and volumetric efficiency is usually not significant, but in high-speed engines with large valve overlap this is not the case. In these engines under certain conditions a fraction of the freshly induced charge is able to flow directly in the exhaust port during valve overlap. It is only the fresh charge left in the cylinder after IVC that is available for combustion and has significance for engine performance.

In order to differentiate between the fresh charge entering the engine and the fresh charge trapped at IVC the following efficiencies characterising the engine breathing are defined:

5.1.1 Volumetric efficiency

This is a measure of the breathing capacity of the engine. It is defined as the ratio of the mass of the fresh air supplied per cycle per cylinder relative to the mass of air that the cylinder would hold at a reference density. The volumetric efficiency η_v is defined as:

$$\eta_v = \frac{m_s}{V_c \times \rho_r} \tag{5.1}$$

where V_c is the cylinder volume, ρ_r is a reference density and the supplied fresh air mass m_s is defined as:

$$m_s = \int_{IVO}^{IVC} \dot{i}_i \times dt_i \tag{5.2}$$

where $\dot{i}_i$ is the mass flow through the inlet valves and t_i is the time the valves are open.

5.1.2 Trapping efficiency

The trapping efficiency η_t is the ratio of the mass of fresh air trapped in the cylinder at IVC m_t relative to the mass of fresh air supplied per cycle per cylinder m_s. It accounts for the fraction of fresh air mass that can flow through the exhaust port during valve overlap and is defined by the following equation

$$\eta_t = \frac{m_t}{m_s} \tag{5.3}$$

The trapped mass m_t is defined by the following equation

$$m_t = \int_{IVO}^{IVC} \dot{i}_i \times dt_i - \int_{EVO}^{EVC} \dot{i}_e \times dt_e \tag{5.4}$$

where $\dot{i}_e$ is the fraction of fresh mass flow through the exhaust valves and t_e is the time the valves are open.

5.1.3 Charging efficiency

Charging efficiency is the ratio of the fresh air mass trapped in the cylinder per cycle relative to the mass of air the cylinder would hold at reference density.

$$\eta_c = \frac{m_t}{V_c \times \rho_r} \tag{5.5}$$

The charging efficiency is the product of the volumetric and trapping efficiency and is an indication of the actual mass of fresh air available for combustion.

$$\eta_c = \eta_v \times \eta_t \tag{5.6}$$

The charging efficiency of any IC engine throughout its operating speed range is directly related to the maximum torque available at any given speed and hence the maximum power output. High charging efficiency at high engine speeds is one of the conditions required if high specific power output is to be achieved. Note that the charging efficiency is proportional to the IMEP only if the combustion and thermodynamic efficiencies remain the same. While appreciating the significant effect, which the gas exchange process has on other factors related to engine performance, this research focuses on charging efficiency and uses this parameter as an indication for the effect on power output.

5.2 Gas exchange process mechanisms in high-speed engines

As mentioned earlier the gas exchange process in a multicylinder engine is a function of the complex gas dynamic behaviour in the whole engine. The complexity of this phenomenon is illustrated by the instantaneous pressure data from inlet and exhaust manifolds of such engine presented by Heywood (1988). In order to understand the basics of this process the charging efficiency curve for two simple single cylinder engine models is examined. Its shape is explained by looking at the pressure differences and mass flow across the cylinder. Engine simulation software is used as a research tool. The four cylinder engine on which this research is based in the configuration used to validate the simulation software in Chapter 4 will be referred to as the *'4 cyl. engine'*.

5.2.1 Simulation model, input data and test conditions

The first engine, shown in Figure 5.1, has an inlet pipe length of 452 mm, which is equal to the equivalent primary inlet pipe in the *4 cyl. engine* and has an infinitely small exhaust pipe. This will be referred to as the *'1 cyl. inlet only'* engine. The term 'equivalent primary pipe' length is used to define the distance from the valve seat to the first upstream junction in a multicylinder inlet system. In the TT600 engine this includes the throttle body, transition piece and inlet port length. The gas dynamic behaviour in the exhaust pipe can affect the cylinder filling only during the valve overlap period. By keeping the length of this pipe as short as possible any pressure waves excited by the gas exiting the cylinder propagate across the pipe several times and their amplitudes reduce below the amplitude of the inlet port pressure during valve overlap. Hence, the mass

flow into the cylinder in this simplified engine model should be mostly governed by the gas dynamic behaviour in the inlet pipe.

The second engine, shown in Figure 5.2, has an exhaust pipe length of 646 mm equal to the equivalent primary exhaust pipe length of the base engine and an infinitely small inlet pipe. This will be referred to as the *'1 cyl. exhaust only'* engine. The equivalent primary exhaust pipe length is defined as the distance from the exhaust valve seat and the first downstream junction and in the case of the TT600 engine includes the exhaust port length and the primary exhaust pipe. The gas dynamic behaviour in an infinitely short inlet pipe should have minimal effect on the gas exchange mechanism. The standing waves excited by the piston motion should have minimum amplitudes.

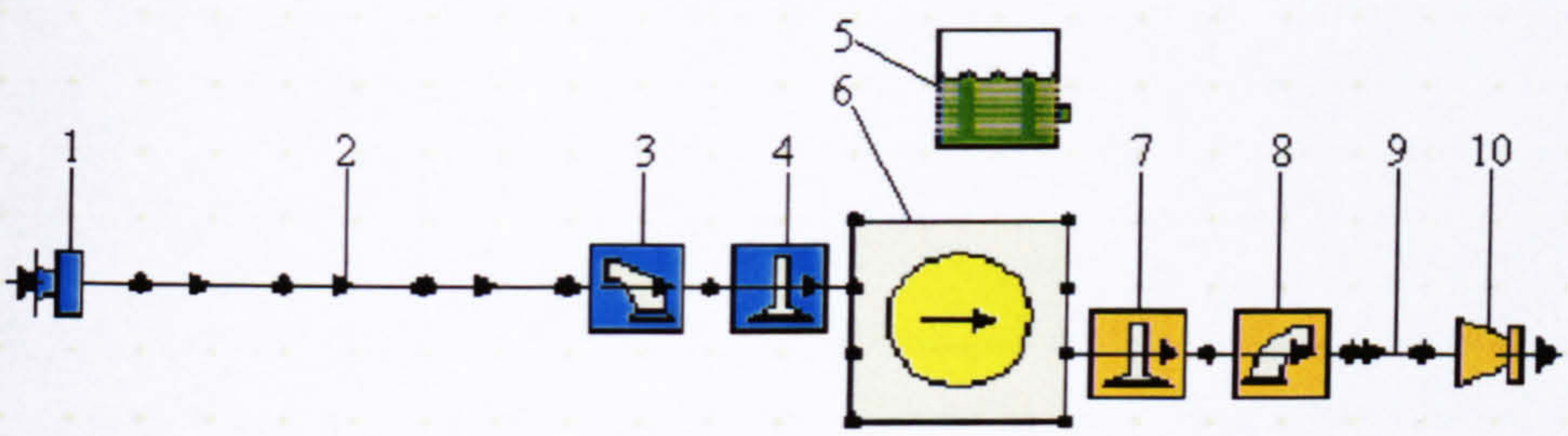

Figure 5.1: Simulation model representation of the *1 cyl. inlet only* engine

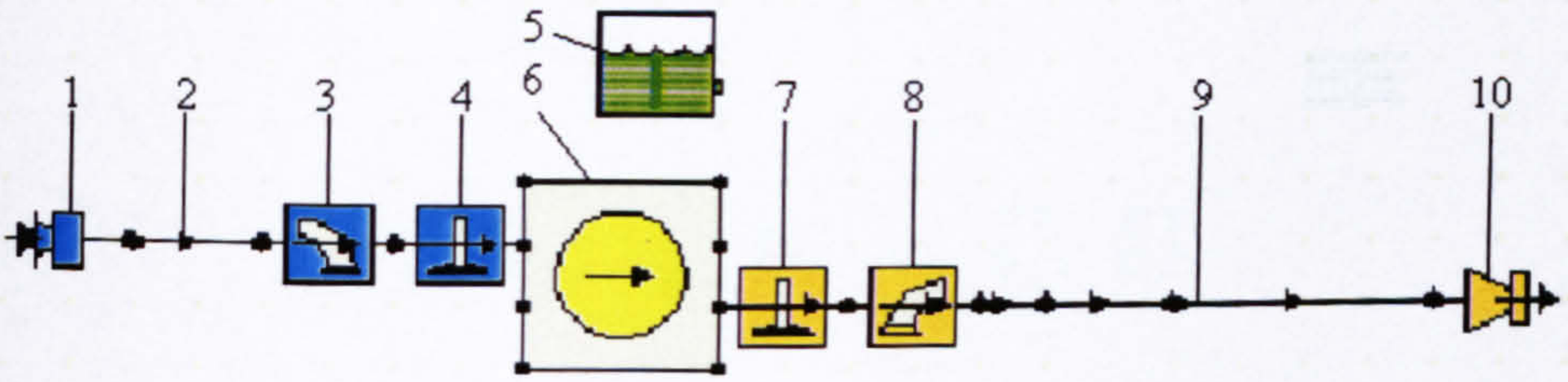

Figure 5.2: Simulation model representation of the *1 cyl. exhaust only* engine

The simulation input data for the *1 cyl. inlet only* engine and the *1 cyl. exhaust only* engine is the same as for the main simulation model as described in Chapter 3, other than some of the parameters relating to the inlet and exhaust system arrangement. To clarify this, the individual elements representing components along the gas flow path in the engine are shown in Table 5.1. The simulation was run for engine speeds ranging from 2000 rpm to 13000 rpm at WOT condition. The AFR used was 12.5:1.

No.	Parameter		*1 cyl. inlet only* engine	1 cyl. exhaust only engine
1	Inlet boundary		The same as 4 cyl. engine	Same as 4 cyl. engine
2	Inlet pipe	length	452 mm	50 mm
		diameter	The same as 4 cyl. engine	The same as 4 cyl. engine
3	Inlet port flow characteristics		The same as 4 cyl. engine	The same as 4 cyl. engine
4	Inlet valve		The same as 4 cyl. engine	The same as 4 cyl. engine
5	Fuel system definition		The same as 4 cyl. engine	The same as 4 cyl. engine
6	Cylinder		The same as 4 cyl. engine	The same as 4 cyl. engine
7	Exhaust valve		The same as 4 cyl. engine	The same as 4 cyl. engine
8	Exhaust port flow characteristics		The same as 4 cyl. engine	The same as 4 cyl. engine
9	Exhaust pipe	length	47 mm	646 mm
		diameter	The same as 4 cyl. engine	The same as 4 cyl. engine
10	Exhaust boundary		The same as 4 cyl. engine	The same as 4 cyl. engine

Table 5.1: Simulation input parameters for the *1 cyl. inlet only* engine and the *1 cyl. exhaust only* engine, which are different from the *4 cyl. engine* (the numbering system corresponds to the elements in Figures 5.1 and 5.2)

5.2.2 Simulation results and analysis

5.2.2.1 Charging efficiency results

Figure 5.3 shows the charging efficiency curves for the *4 cyl. engine*, *1 cyl inlet only* engine and *1cyl. exhaust only* engine. It can be seen that the charging efficiency curves generally consists of a series of peaks and dips.

At speeds around 2500 rpm, 4750 rpm, 6500 rpm, 8000 rpm and 12000 rpm, the charging efficiency of the base engine peaks, and at around 2000 rpm, 3750 rpm 5750 rpm and 9000 rpm, the efficiency dips. The large dip in the efficiency curve in the region of 3500 rpm is a typical characteristic of many 4-cylinder high-speed motorcycle engines and it seriously decreases the engine torque in this speed range. According to Yamabe and Ueda (1988) such dips are caused by negative tuning effects in the exhaust system. The phenomena responsible for this effect will be explained by analysing the gas exchange mechanism in the *1 cyl exhaust only* engine in section 5.2.4.

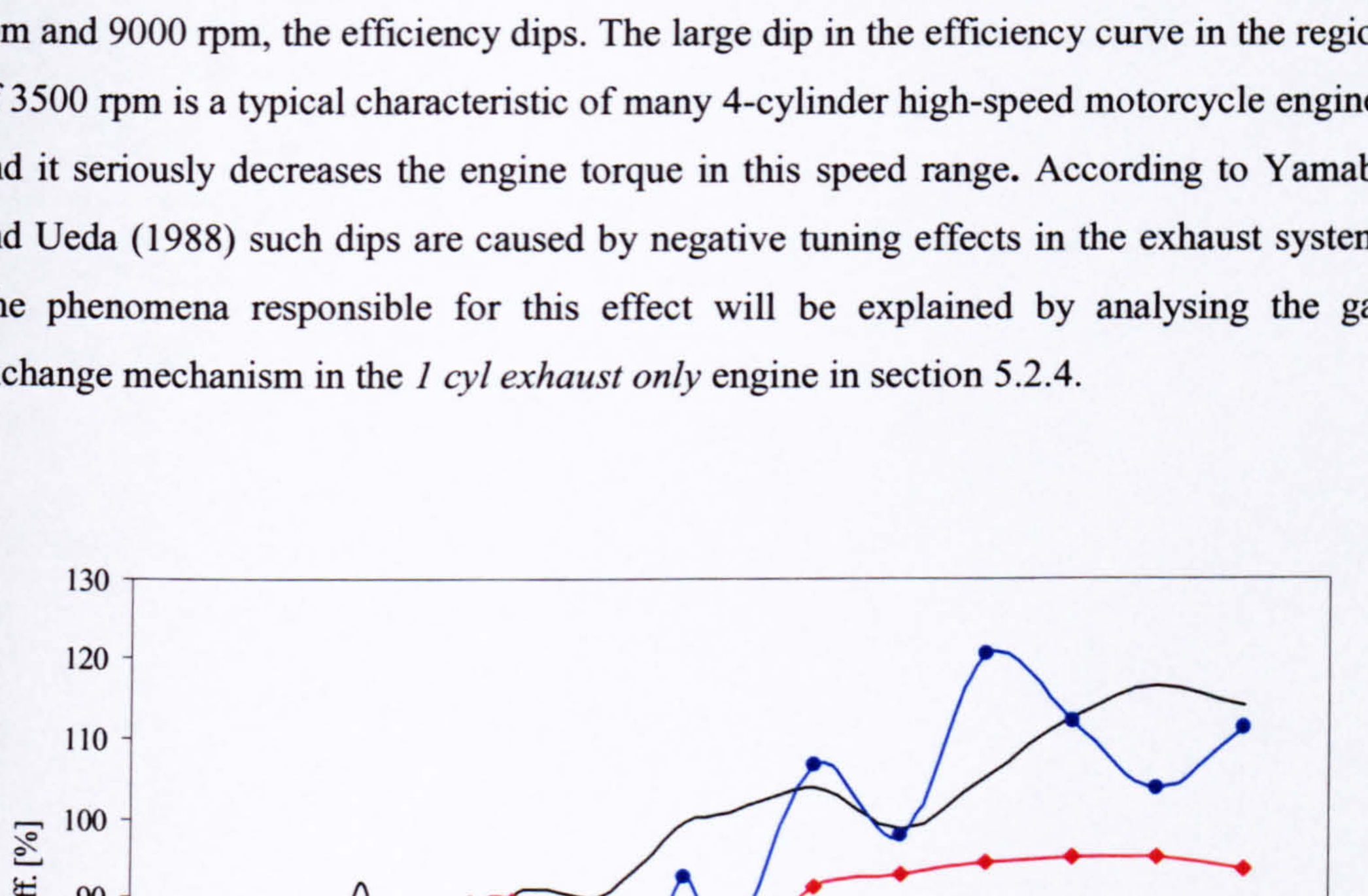

Figure 5.3: Charging efficiency of *4 cyl. engine*, *1 cyl. inlet only* engine and *1 cyl. exhaust only* engine

The charging efficiency of the *1 cyl. inlet only* engine exhibits peaks at 4500 rpm, 6500 rpm, 8000 rpm, 10000 rpm and 13000 rpm and dips at 2000 rpm, 6000 rpm, 7000 rpm, 9000 rpm and 12000 rpm. However, it is noticeable that the mean line increases with engine speed.

The charging efficiency of the *1 cyl. exhaust only* engine peaks at 2500 rpm, 4500 rpm and 8000 rpm and dips at 2000 rpm, 3250 rpm and 6000 rpm. It remains almost flat above 8000 rpm.

The reason for these shapes are discussed in the following sections.

5.2.2.2 Cylinder filling during different parts of the inlet process

In order to be able to identify which part of the inlet process is responsible for the shape of the charging efficiency curves, it has been divided into three periods. The first period is from IVO to EVC (valve overlap period), the second is from EVC to BDC and the third is from BDC to IVC. Figure 5.4 shows the mass that has entered the cylinder during the first two periods for each of the engines. Figure 5.5 shows the mass entering the cylinder in the last period plotted with the same vertical scale for comparison.

IVO to EVC (valve overlap period)

This is the period in which the mass entering the cylinder experiences the highest variations throughout the speed range. The curve representing the mass inhaled by the cylinder of the *4 cyl. engine* and the *1 cyl. exhaust only* engine is oscillatory up to 7000 rpm. It can be seen that peaks in the curve occur at approximately the same speeds where the charging efficiency is high. For the *4 cyl. engine* this is at 2500 rpm, 4750 rpm and 6500 rpm, and for the *1 cyl. exhaust only* engine at 2500 rpm and 4000 rpm. The same is valid for the dips occurring at 2000 rpm, 3750 rpm and 5750 rpm for the *4 cyl. engine* and at 2000 rpm, 3000 rpm and 6000 rpm for the *1 cyl. exhaust only* engine. This, combined with the relative flatness of the curves for these engines in the other periods, suggests that the mass entering the cylinder during valve overlap determines the shape of the charging efficiency curve up to 7000 rpm. Above 7000 rpm the curves are almost flat.

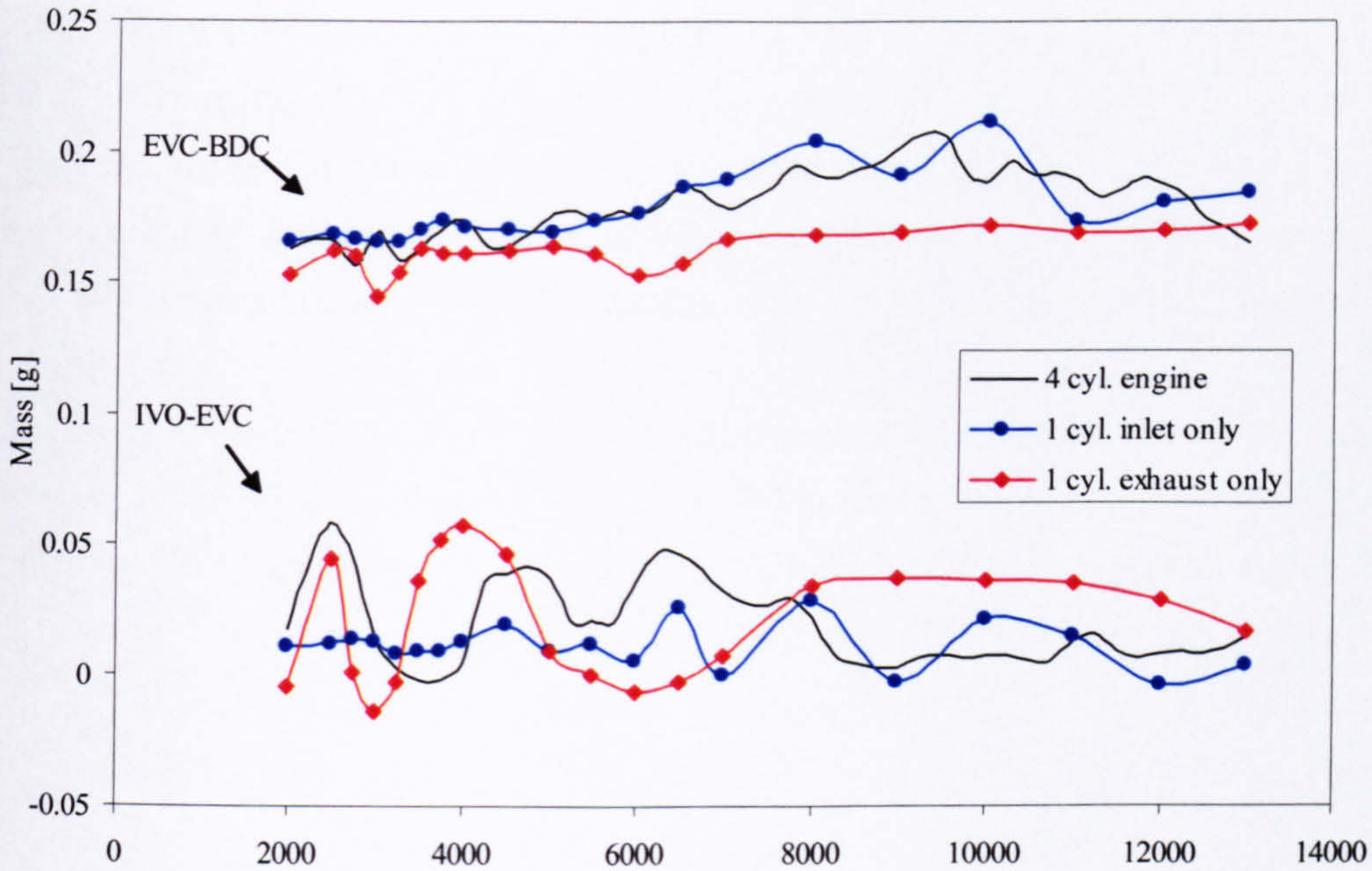

Figure 5.4: Mass inhaled by the cylinder from IVO to EVC and from EVC to BDC for the *4 cyl. engine*, *1 cyl. inlet only* engine and *1 cyl. exhaust only* engine

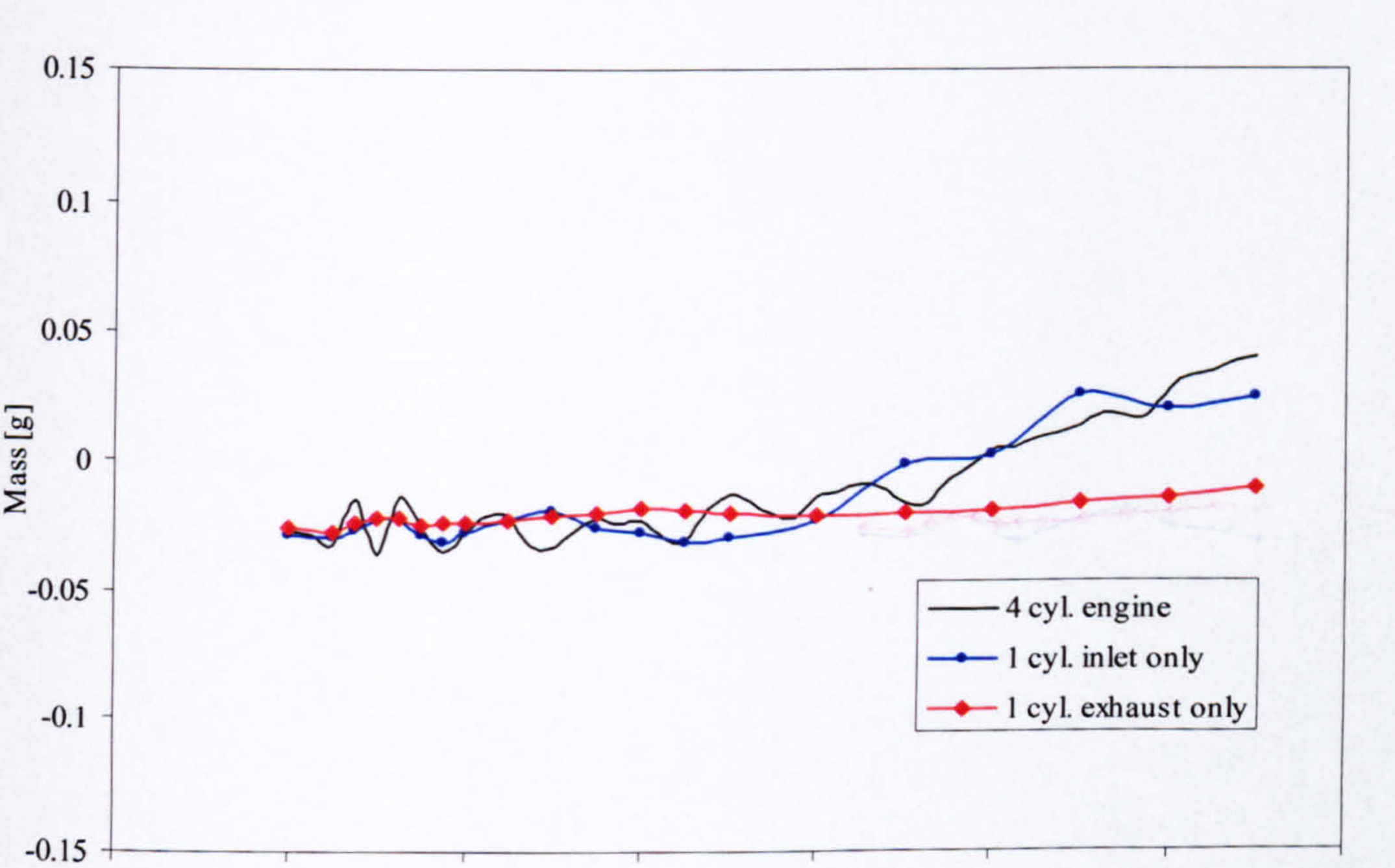

Figure 5.5: Mass inhaled by the cylinder from BDC to IVC for the *4 cyl. engine*, *1 cyl. inlet only* engine and *1 cyl. exhaust only* engine

This is not the case for the *1 cyl. inlet only* engine. Its curve appears almost flat up to 6000 rpm and becomes oscillatory above that speed. The peaks at 6500 rpm, 8000 rpm, 10000 rpm and 13000 rpm and the dips at 6000 rpm, 7000 rpm, 9000 rpm and 12000 rpm correspond to the high and low point of the charging efficiency curve. However the mass entering the cylinder during the other periods of the intake process also varies with speed and contributes to the shape of the charging efficiency curve.

EVC to BDC

For the *4 cyl. engine* and the *1 cyl. inlet only* engine the curve representing the charge mass inhaled during the second period peaks respectively at 9000 rpm and 10000 rpm. The shape of the curve for the *4 cyl. engine* is oscillatory, however the amplitudes are relatively low.

Above 8000 rpm the shape of the curve for the *1 cyl. inlet only* engine is also oscillatory and has higher amplitudes. However, correlation to the charging efficiency curve is not possible due to the oscillatory nature of the shape of the curve in the other periods.

For the *1 cyl. exhaust only* engine the curve remains almost unchanged throughout the entire speed range as expected due to the small influence of the gas dynamics in the infinitely short inlet pipe.

BDC to IVC

As speed increases the mass entering the cylinder for the *4 cyl. engine* and the *1cyl. inlet only* engine rises. This is not the case for the *1 cyl. exhaust only* engine where the mass remains almost constant. Combined with the relative flatness of the curves in the other periods this explain the flat shape of the charging efficiency curve above 8000 rpm for this engine.

While this section attempts to identify the parts of the inlet process responsible for the shape of the charging efficiency curves it does not provide an answer for cylinder fillings involved. This is discussed in the following sections.

5.2.3 Analysis of the gas exchange in the *1 cyl. inlet only* engine

To simplify the explanation, the term 'pressure gradient' has been used in this thesis. A positive pressure gradient means that the instantaneous pressure in the inlet port is higher than that in the exhaust port, and the inverse is defined as a negative pressure gradient.

The pressure waves in the inlet pipe are excited by the reciprocating motion of the piston combined with the valve events. According to the theory described by Winterbone and Pearson (2000) a pressure wave propagating from the inlet port will travel at the local speed of sound and after reaching the open end of the pipe will return as a wave with opposite sign. Depending on the engine speed and the length of the inlet pipe, this process may be repeated several times per engine cycle. The pressure at the inlet port at any time is a function of the state of this propagating wave and the flow conditions across the valve. The term 'positive pressure wave' is used for pressure pulsation with positive amplitude and 'negative pressure wave' for the pulses with negative amplitude.

The effect of the gas dynamics in the inlet system has been a subject of number of investigations. Prosser (1974) suggests that the speeds when positive pressure wave returns to the inlet port just before IVC, coincides with peak volumetric efficiency and uses the term 'induction ramming' to describe this phenomena. This is also supported by Ohata and Ishida (1982) who claim that the volumetric efficiency is almost entirely determined by the inlet pressure during the short period before IVC. Both studies refer to medium speed engines. According to Yagi *et al.* (1970) a synchronisation of the positive pressure pulsations, initially caused by IVC, with TDC of the next inlet cycle is responsible for charging efficiency peaks. Boretti and Villa (1998) claim that the charging efficiency peaks when positive pressure waves are present at the inlet port just before IVC and after IVO. The last two investigations are based on high-speed engines.

In order to understand what are the filling mechanisms responsible for the charging efficiency of the *1 cyl. inlet only* engine, the mass entering the cylinder during the different parts of the inlet process and the gas dynamic behaviour in the inlet pipe must be related. This is done by examining combined plots of the inlet and exhaust port pressures and flow rates.

Figures 5.6, 5.7, 5.8 and 5.9 show inlet and exhaust port pressure and normalised flow rate vs. crankshaft angle at engine speeds of 6000 rpm, 7000 rpm, 9000 rpm and 12000 rpm, which are the speeds where dips in the charging efficiency occur (refer to Figure 5.3). It can be seen that at 6000 rpm the inlet port pressure is lower than the exhaust port pressure during the second part of the overlap period. For the other three engine speeds it is lower during the entire overlap period. This is due to the presence of a negative pressure wave in the inlet port during this period. The resulting negative pressure gradient causes reverse inlet and exhaust flow (the flow rate values become negative). This explains the dips in the curve representing the inhaled mass during valve overlap at 6000 rpm, 7000 rpm, 9000 rpm and 12000 rpm (see Figure 5.4).

Figures 5.10, 5.11, 5.12, 5.13 and 5.14 show inlet and exhaust port pressures and flow rates vs. crankshaft angle at 4500 rpm, 6500 rpm, 8000 rpm, 10000 rpm and 13000 rpm, which are the speeds where the charging efficiency peaks (refer to Figure 5.3). It can be seen that a positive pressure wave is present at the inlet port during valve overlap generating a positive pressure gradient across the cylinder. This results in positive inlet flow during valve overlap period. This is responsible for the peaks in the curve representing the mass of the inhaled charge during the overlap period at 4500 rpm, 6500 rpm, 8000 rpm, 10000 rpm and 13000 rpm (see Figure 5.4).

Note that in the plots for all engine speeds the amplitudes of the exhaust port pressure are always significantly lower than amplitudes of the inlet port pressure during valve overlap. Therefore it has a small effect on the polarity of the pressure gradient and hence on cylinder filling. This demonstrates the independence of the *1cyl. inlet only* engine model from the gas dynamics in the exhaust system. In a real engine the pressure gradient will be influenced by the gas dynamics in the exhaust system.

The pressure data corresponding to 10000 rpm and 13000 rpm (Figures 5.13 and 5.14) shows three and four positive pressure peaks in the inlet port during one cycle. These are the speeds where highest charging efficiency is achieved. This confirms Borreti's (1998) suggestion that the highest charging efficiency peaks occur at the engine speeds where three or four positive pressure peaks can be measured in the inlet port during one cycle.

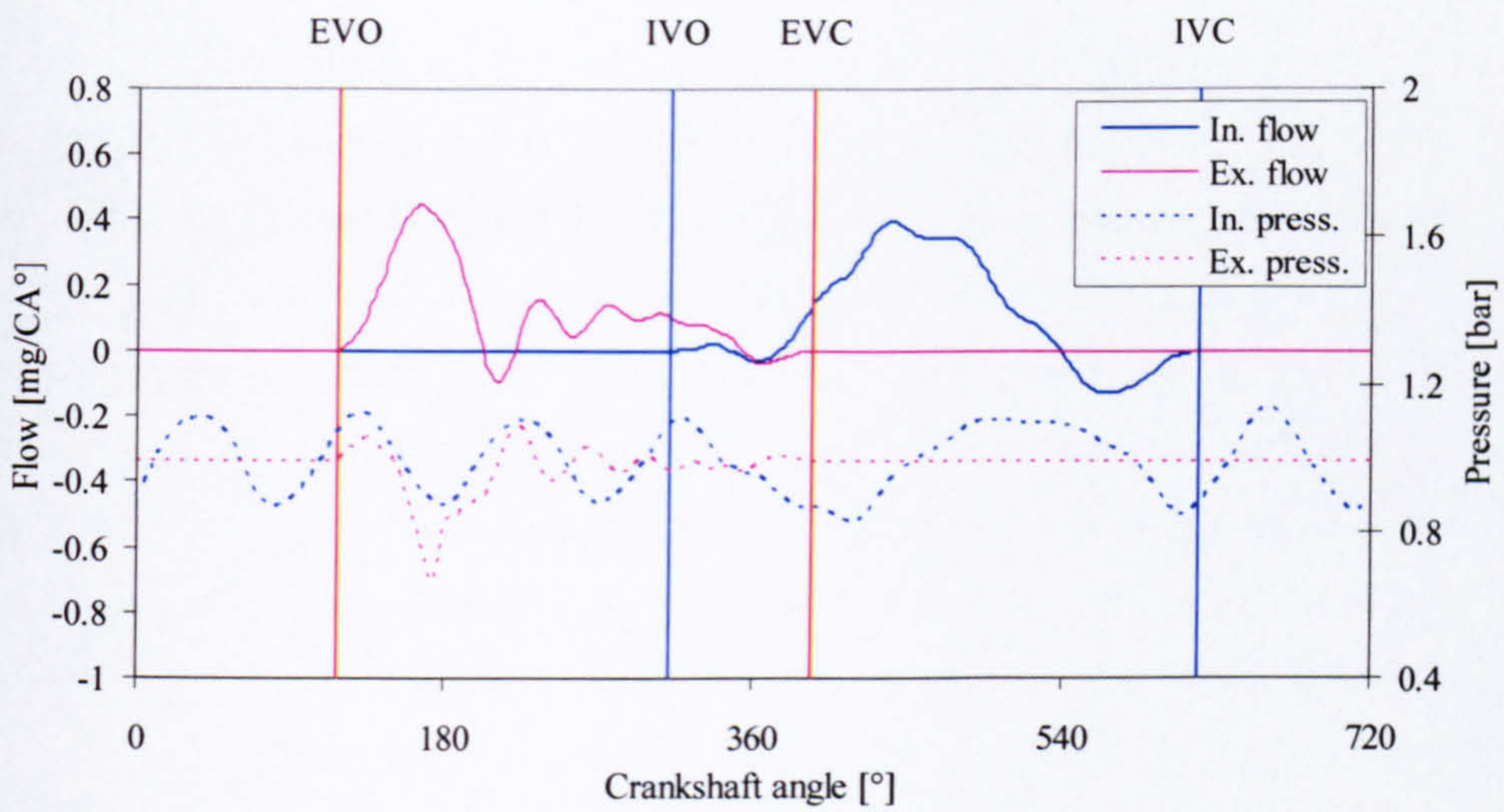

Figure 5.6: Inlet and exhaust port pressures and flow rates vs. crankshaft angle for the *1 cyl. inlet only* engine at 6000 rpm (flow rate is normalised with engine speed)

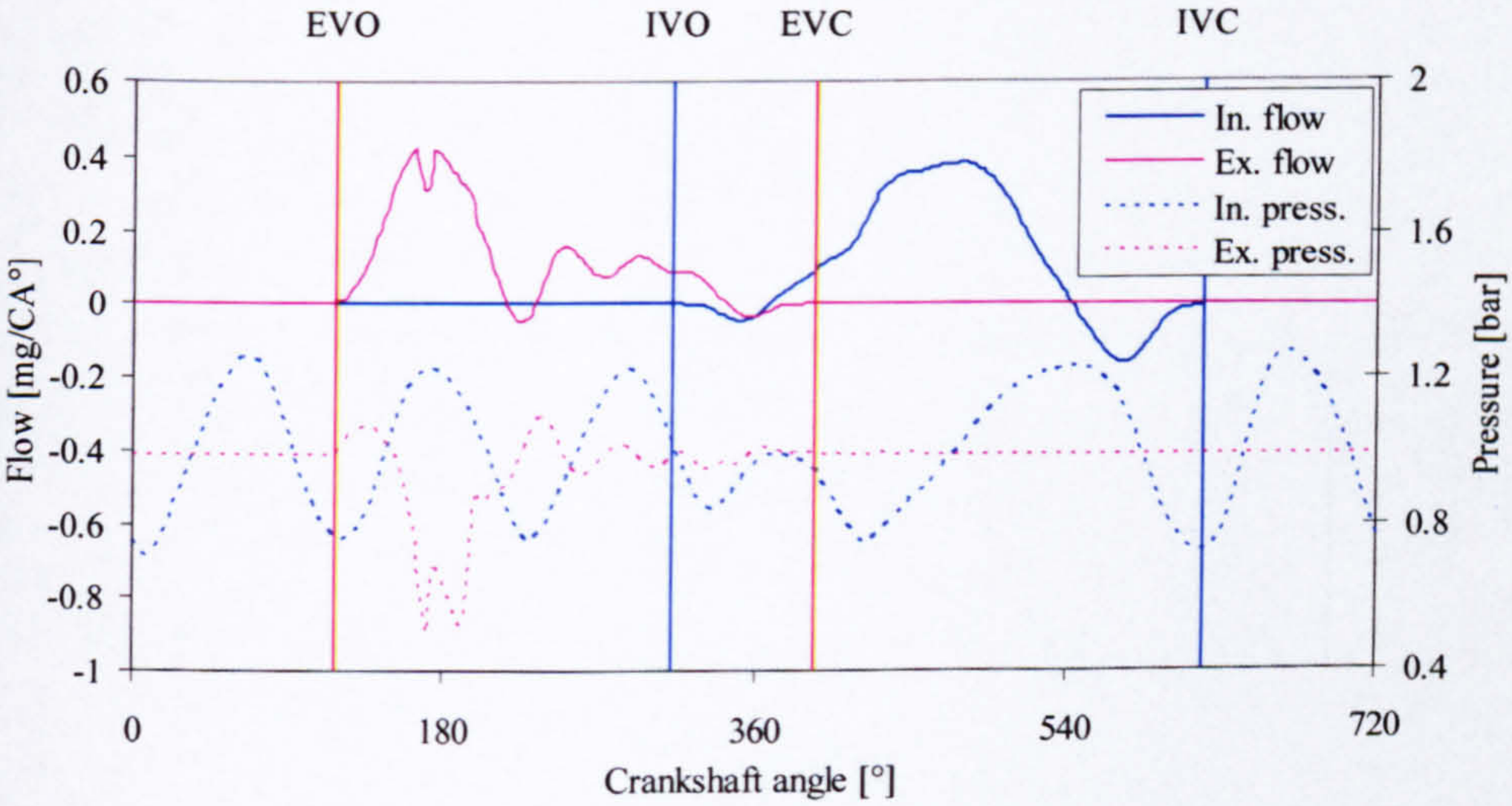

Figure 5.7: Inlet and exhaust port pressures and flow rates vs. crankshaft angle for the *1 cyl. inlet only* engine at 7000 rpm (flow rate is normalised with engine speed)

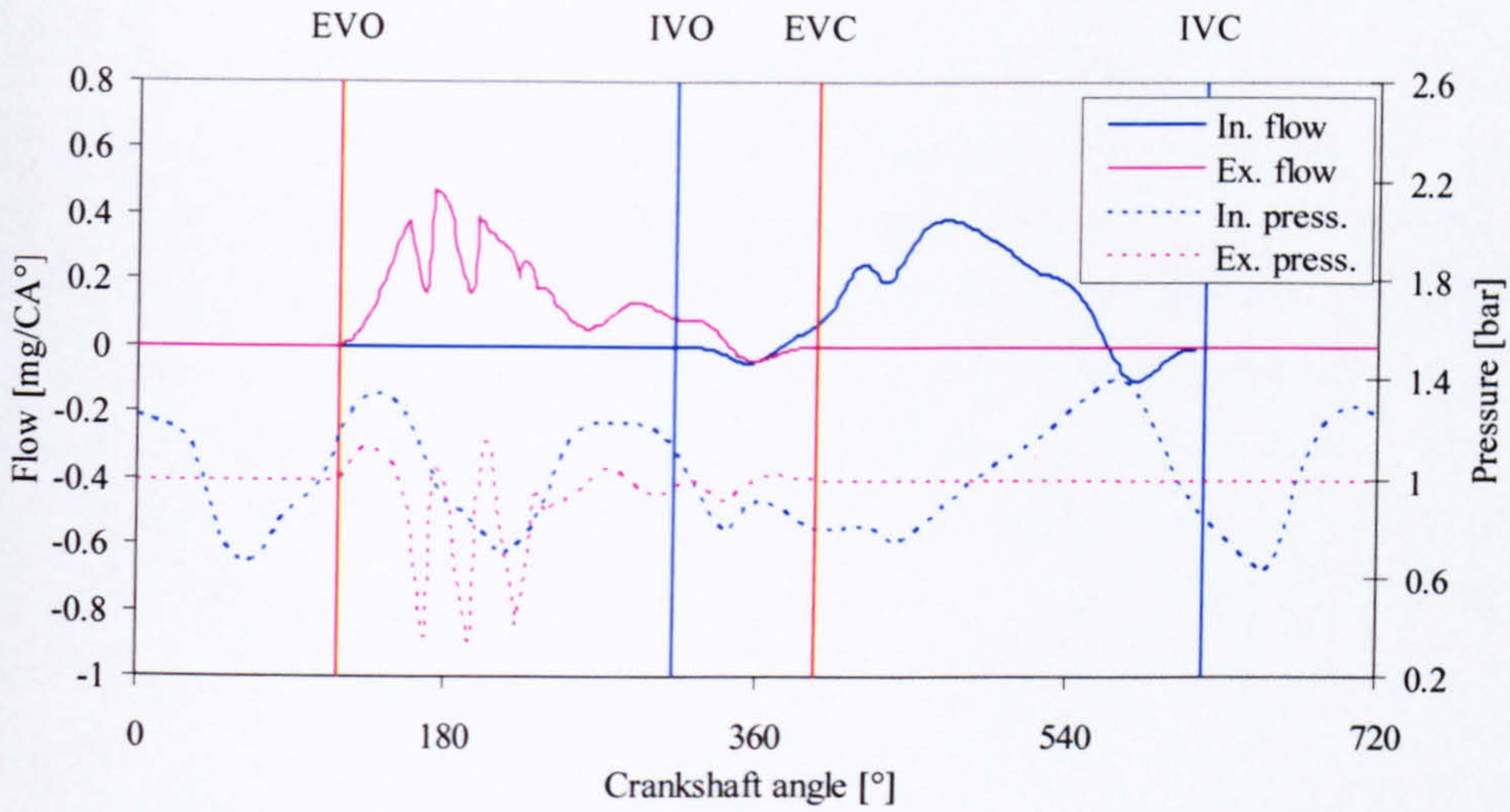

Figure 5.8: Inlet and exhaust port pressures and flow rates vs. crankshaft angle for the *1 cyl. inlet only* engine at 9000 rpm (flow rate is normalised with engine speed)

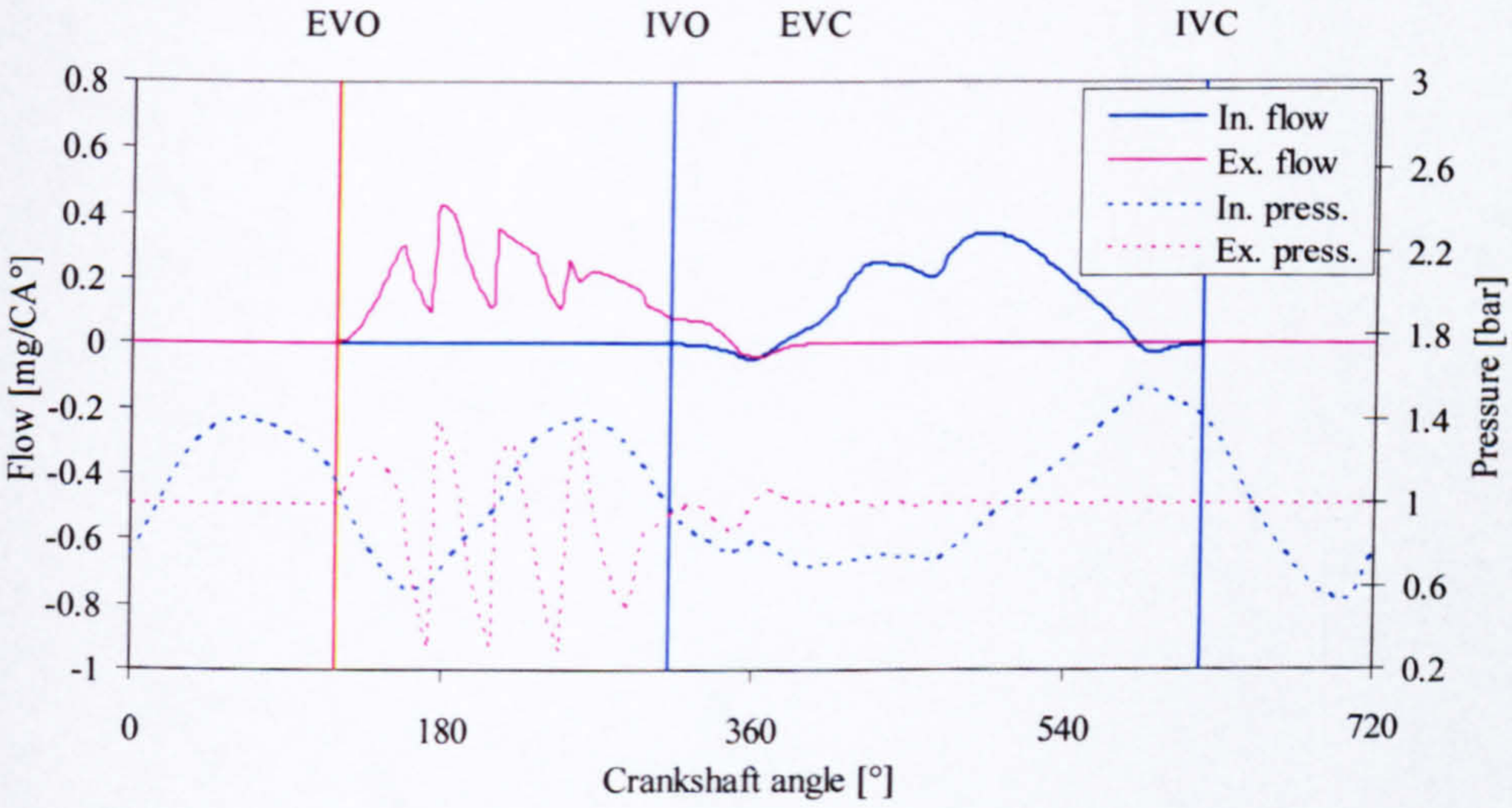

Figure 5.9: Inlet and exhaust port pressures and flow rates vs. crankshaft angle for *the 1 cyl. inlet only* engine at 12000 rpm (flow rate is normalised with engine speed)

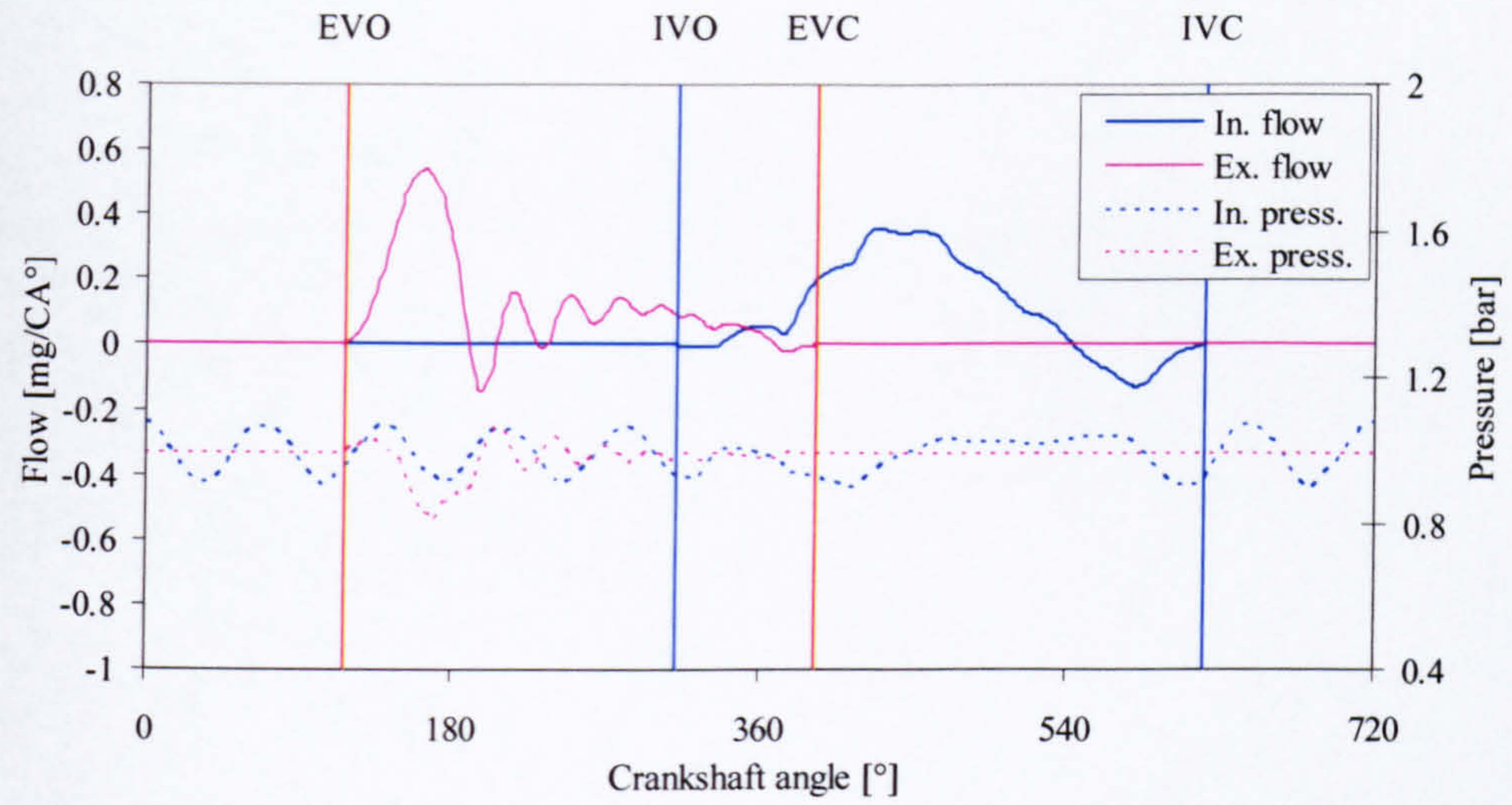

Figure 5.10: Inlet and exhaust port pressures and flow rates vs. crankshaft angle for the *1 cyl. inlet only* engine at 4500 rpm (flow rate is normalised with engine speed)

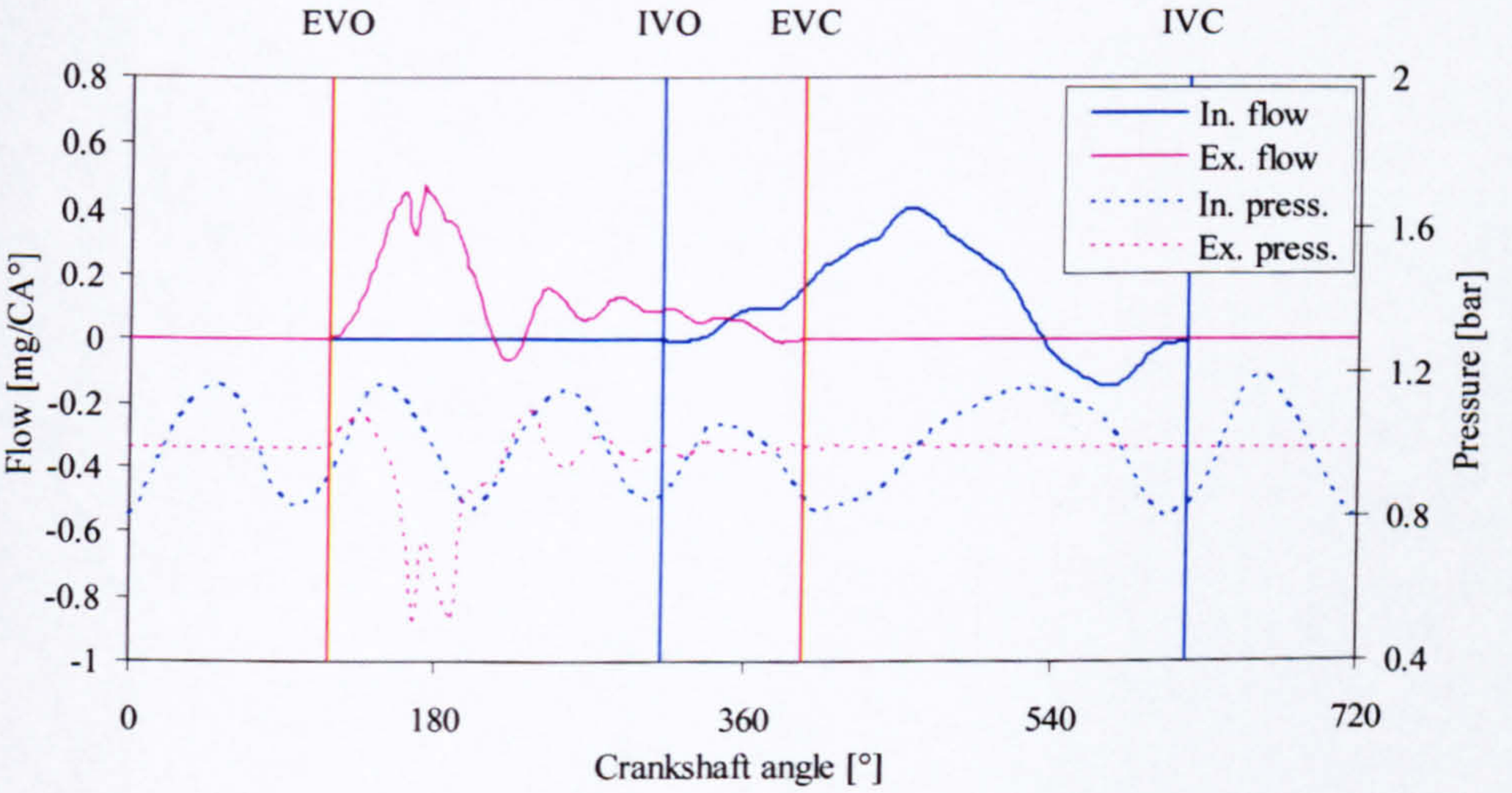

Figure 5.11: Inlet and exhaust port pressures and flow rates vs. crankshaft angle for *'1 cyl. inlet only'* engine at 6500 rpm (flow rate is normalised with engine speed)

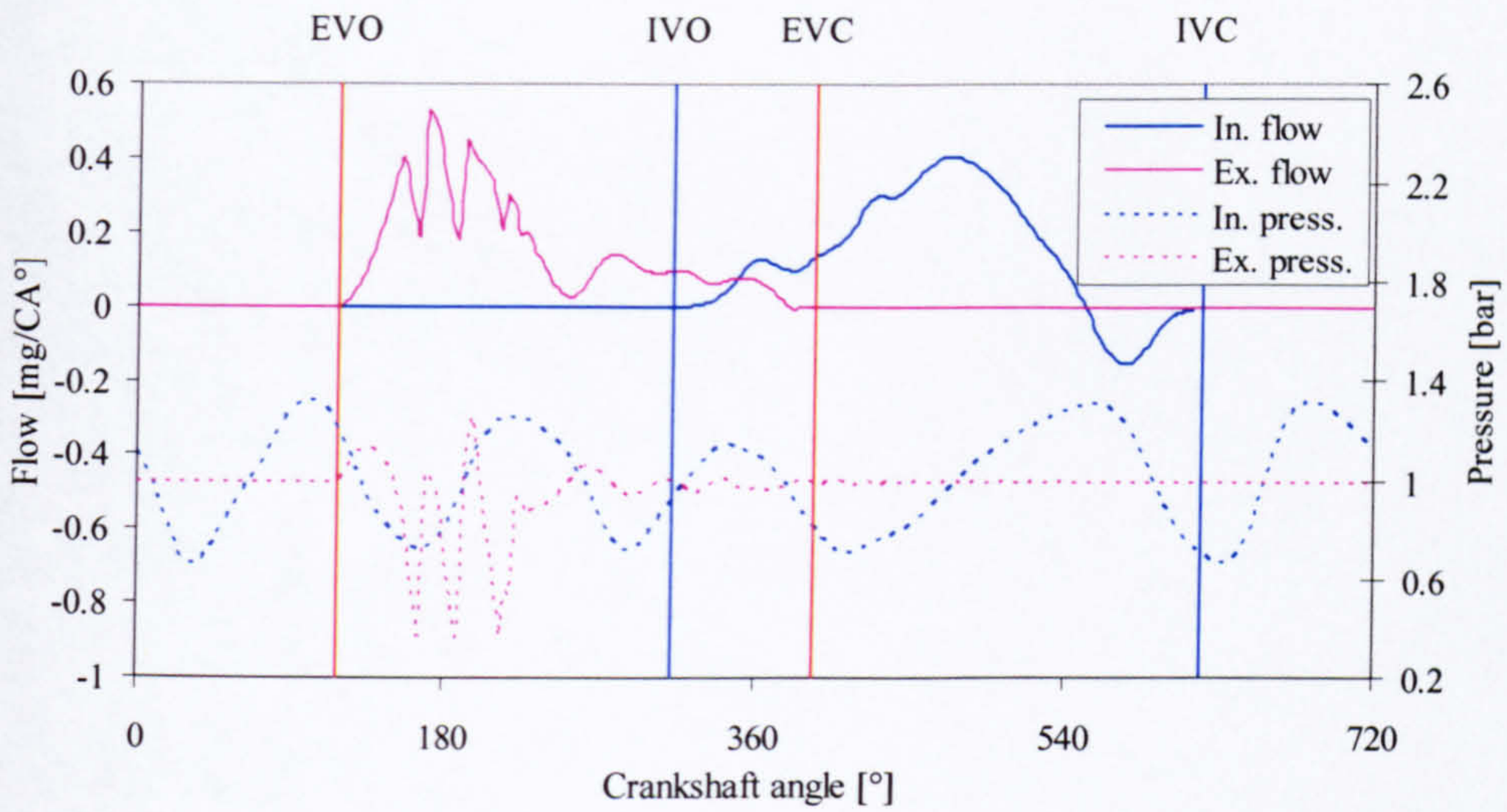

Figure 5.12: Inlet and exhaust port pressures and flow rates vs. crankshaft angle for the *1 cyl. inlet only* engine at 8000 rpm (flow rate is normalised with engine speed)

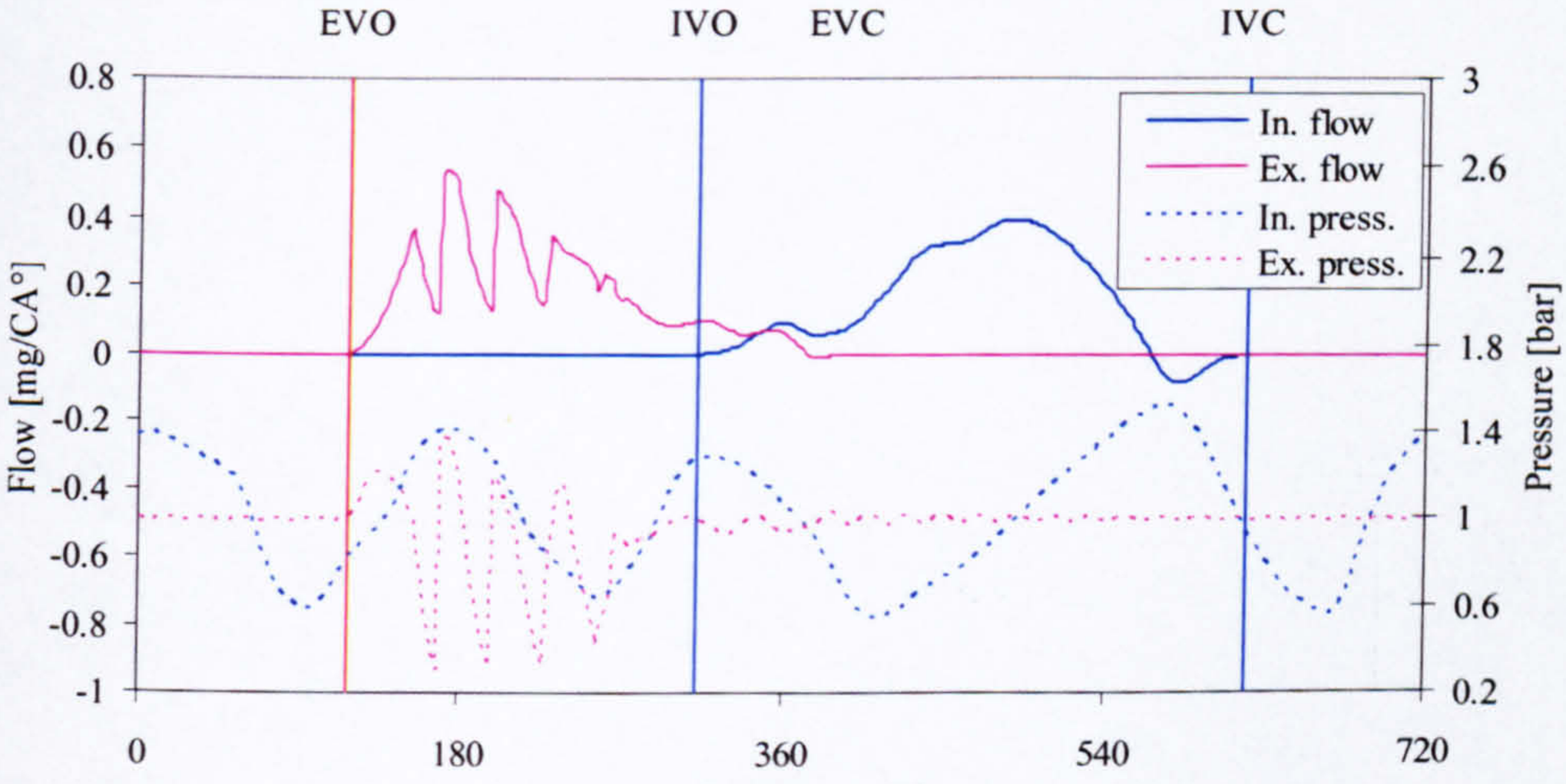

Figure 5.13: Inlet and exhaust port pressures and flow rates vs. crankshaft angle for the*1 cyl. inlet only* engine at 10000 rpm (flow rate is normalised with engine speed)

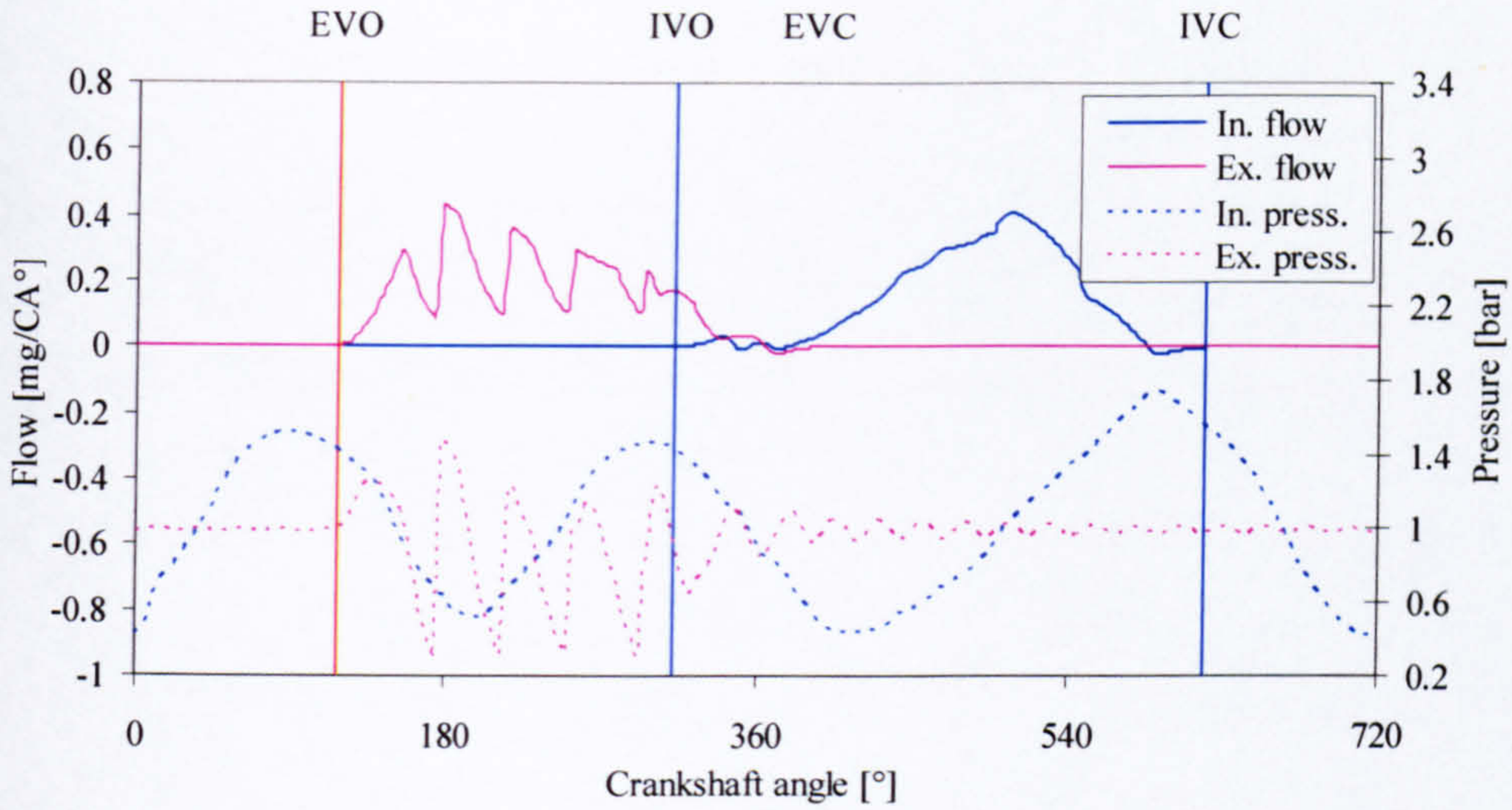

Figure 5.14: Inlet and exhaust port pressures and flow rates vs. crankshaft angle for the *1 cyl. inlet only* engine at 13000 rpm (flow rate is normalised with engine speed)

These above findings also confirm the theory proposed by Yagi *et al.* (1970). However, as the charging efficiency is proportional to the mass of the charge entering the cylinder during different periods of the inlet process, the flow rate through the rest of the inlet period should also be examined.

Figure 5.15 shows the inlet flow rate during the intake process for a range of engine speeds. As in the previous figures the flow rate has been normalised with crankshaft speed and is in [mg/CA°] units to allow comparison between different engine speeds. It can be seen that as engine speed increases the reverse flow just before IVC reduces. This is reflected in the general shape of the curve for mass entering the cylinder during the period BDC- IVC. In addition the position where peak flow occurs shifts later in the cycle as engine speed increases. This is due to the inertia effects in the inlet pipe.

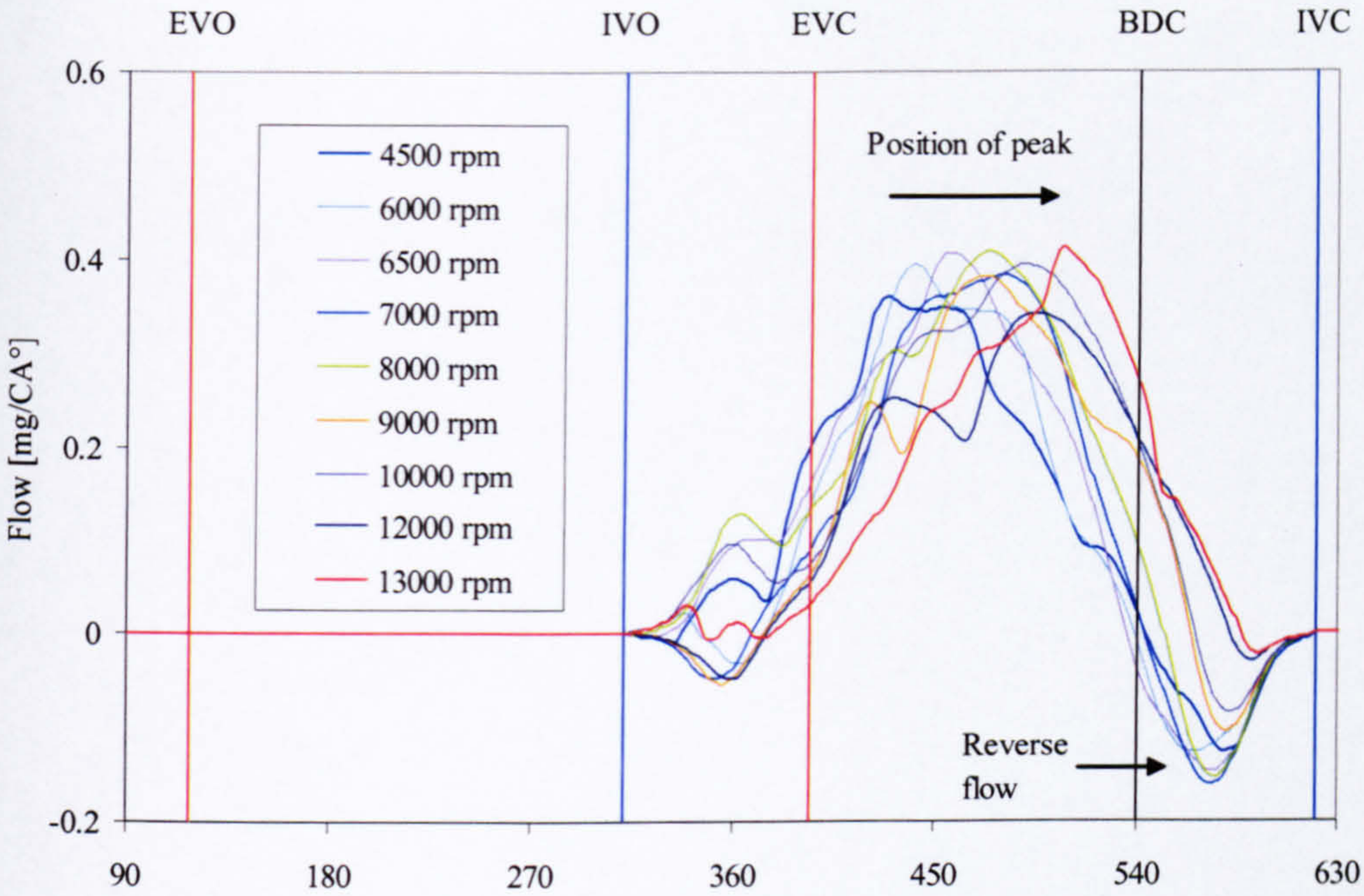

Figure 5.15: Inlet port flow rate vs. crankshaft angle for the *1 cyl. inlet only* engine at different engine speeds (the flow rate is normalised with crankshaft speed)

In conclusion, two mechanisms are identified in which the gas dynamics in the inlet system affects the charging efficiency. The first one is due to the timing of positive or negative pressure wave with the valve overlap period. This is responsible for the oscillatory nature of the charging efficiency curve. At low engine speeds the effect of the gas dynamics on this cylinder filling mechanism is less pronounced as the piston motion is unable to excite pressure waves with high amplitudes. This is shown in the flatness of the curve representing the mass of the charge entering the cylinder during overlap. At high speed this effect is significant. This mechanism is also affected by the gas dynamics in the exhaust system, which is discussed in the next section.

The second mechanism involves the positive pressure wave present in the inlet port just before IVC, which reduces the backflow in the inlet. This appears to be responsible for the increase of the mean value of the charging efficiency curve with engine speed.

5.2.4 Analysis of the gas exchange in the *1 cyl. exhaust only* engine

The pressure wave propagation in the exhaust pipe can again be explained by the theory described by Winterbone and Pearson (2000). The pressure wave can traverse the pipe several times depending on engine speed, pipe length and local speed of sound. The major difference is that the local speed of sound can significantly vary depending on engine speed and load as well as along the exhaust system.

There appears to be a general consensus on the effect of the gas dynamics on the cylinder filling mechanisms. Both Yagi *et al.* (1970) and Borreti (1998) suggest that the timing of the arrival of negative pressure pulse during valve overlap is beneficial for charging efficiency. However, the significance of this effect on charging efficiency in medium speed engines is considered small by Taylor (1985), possibly due to the small duration of valve overlap used

This filling mechanism is very well illustrated by examining the exhaust port pressure and the flow through the inlet valve corresponding to engine speeds where charging efficiency curve dips and where it peaks. Figures 5.16, 5.17 and 5.18 show the inlet and exhaust port pressure and flow vs. crankshaft angle for engine speeds of 2000 rpm, 3000 rpm and 6000 rpm. Note that inlet port pressure is plotted only to demonstrate the minimal effect of the gas dynamics in the inlet system. It can be seen that at these engine speeds there is a positive pressure wave in the exhaust port during valve overlap causing negative pressure gradient across the cylinder. This results in reverse inlet and exhaust flow and low residual gas purging. This explains the dips in the curve of the mass entering the cylinder during this period shown in Figure 5.4 and the dips in the charging efficiency shown in Figure 5.3 at these speeds.

Figures 5.19, 5.20, 5.21, 5.22 and 5.23 show the inlet and exhaust port pressure and flow for engine speeds of 2500 rpm, 4000 rpm, 8000 rpm, 11000 rpm and 13000 rpm. At all these speeds the arrival of a negative pressure wave in the exhaust port coincides with the valve overlap period. This aids the cylinder purging during this period. These speeds coincide with high quantities of mass entering the cylinder during this period shown in Figure 5.4 and peaks or high areas in the charging efficiency curve shown in Figure 5.3.

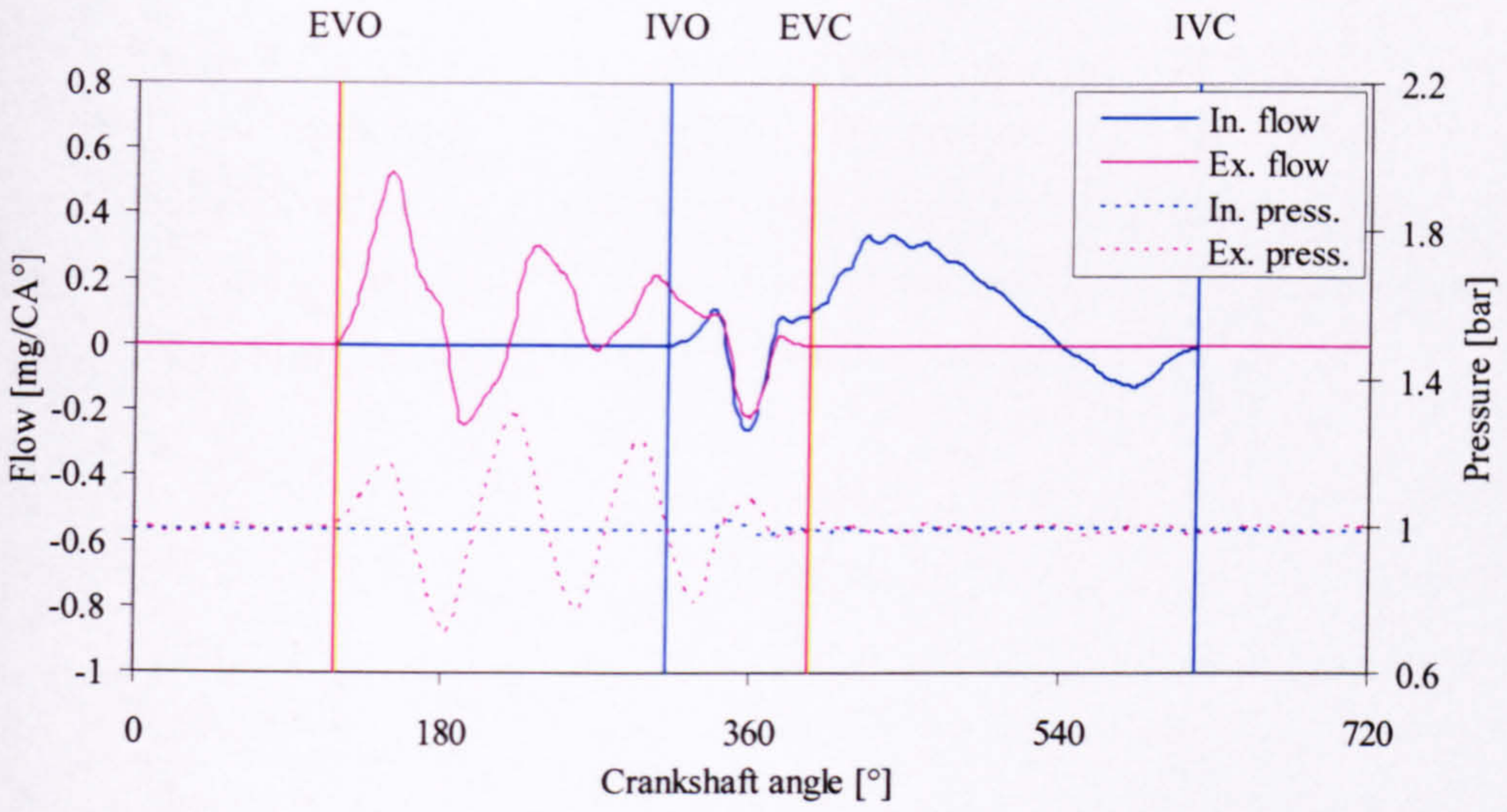

Figure 5.16: Inlet and exhaust port pressure and flow rate vs. crankshaft angle for *1 cyl. exhaust only* engine at 2000 rpm (flow rate is normalised with engine speed)

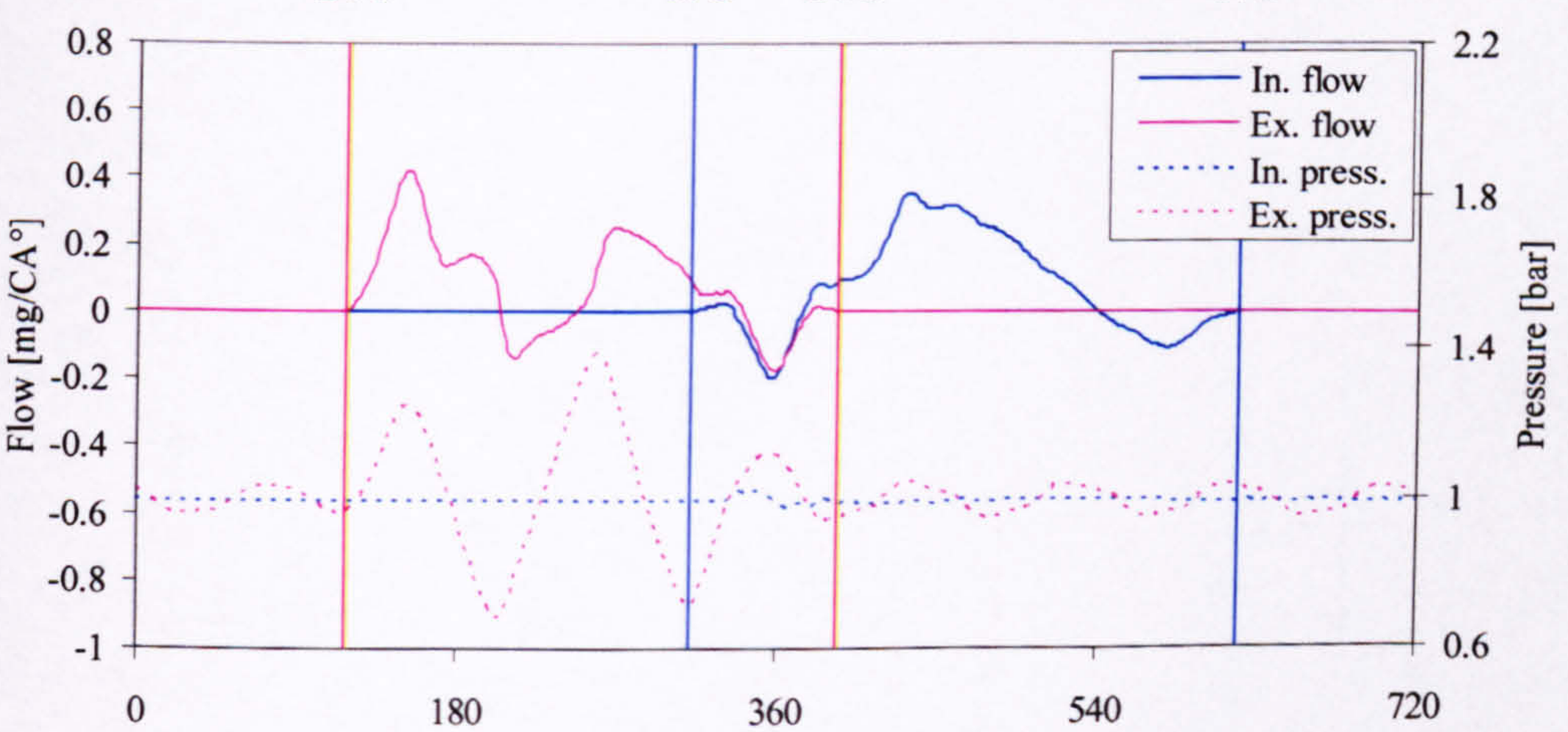

Figure 5.17: Inlet and exhaust port pressure and flow rate vs. crankshaft angle for *1 cyl. exhaust only* engine at 3000 rpm (flow rate is normalised with engine speed)

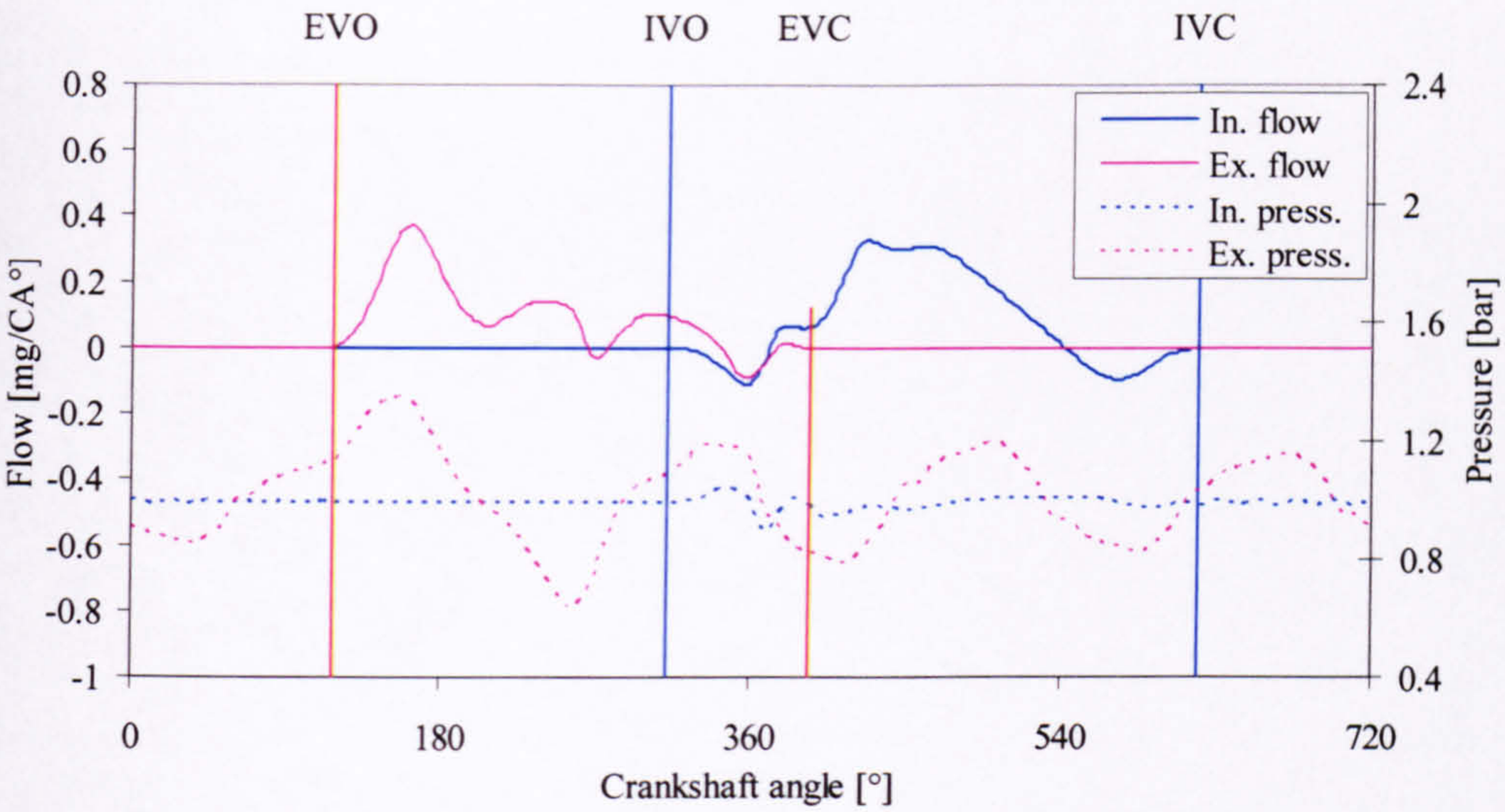

Figure 5.18: Inlet and exhaust port pressure and flow rate vs. crankshaft angle for *1 cyl. exhaust only* engine at 6000 rpm (flow rate is normalised with engine speed)

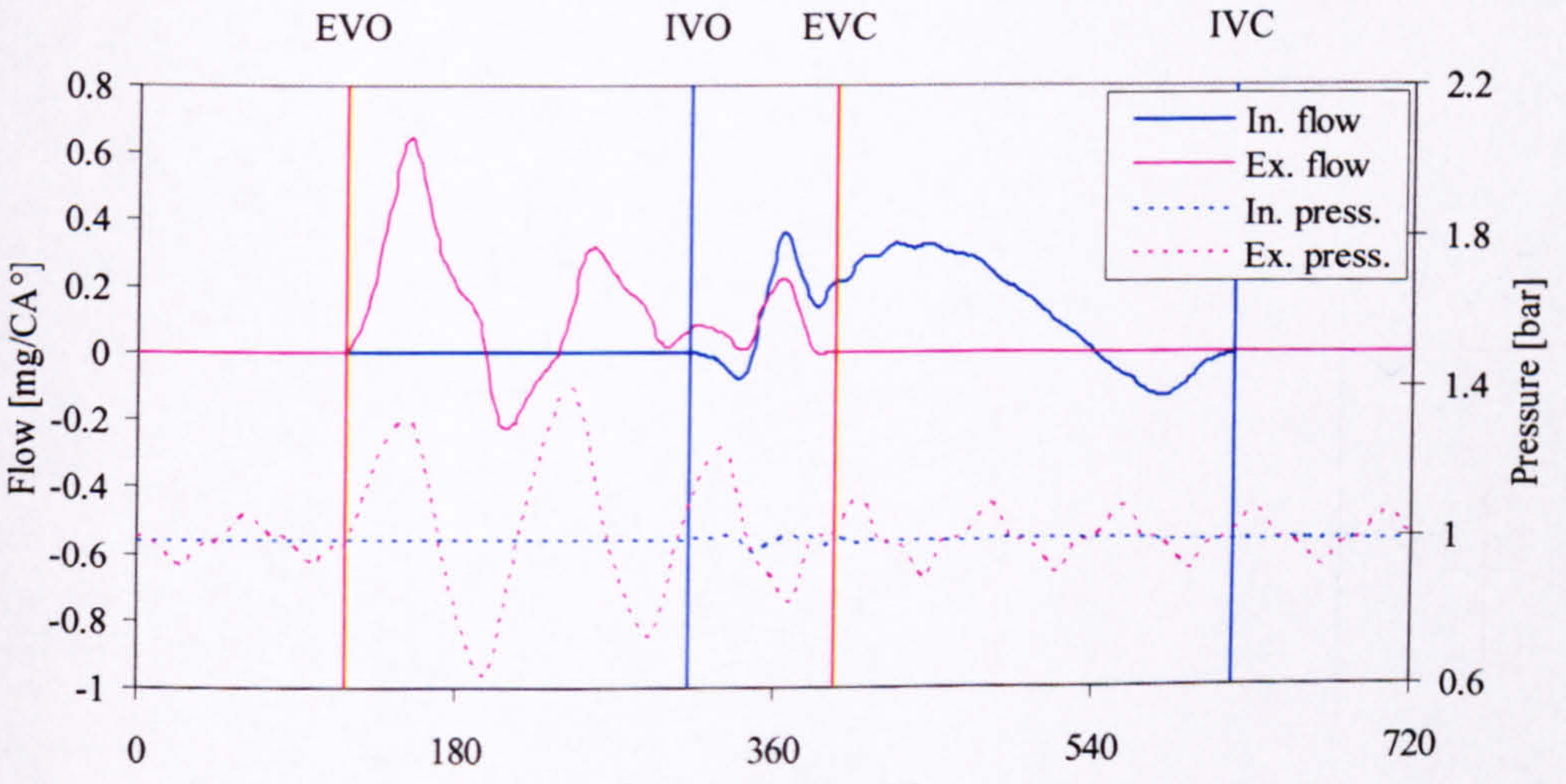

Figure 5.19: Inlet and exhaust port pressure and flow rate vs. crankshaft angle for *1 cyl. exhaust only* engine at 2500 rpm (flow rate is normalised with engine speed)

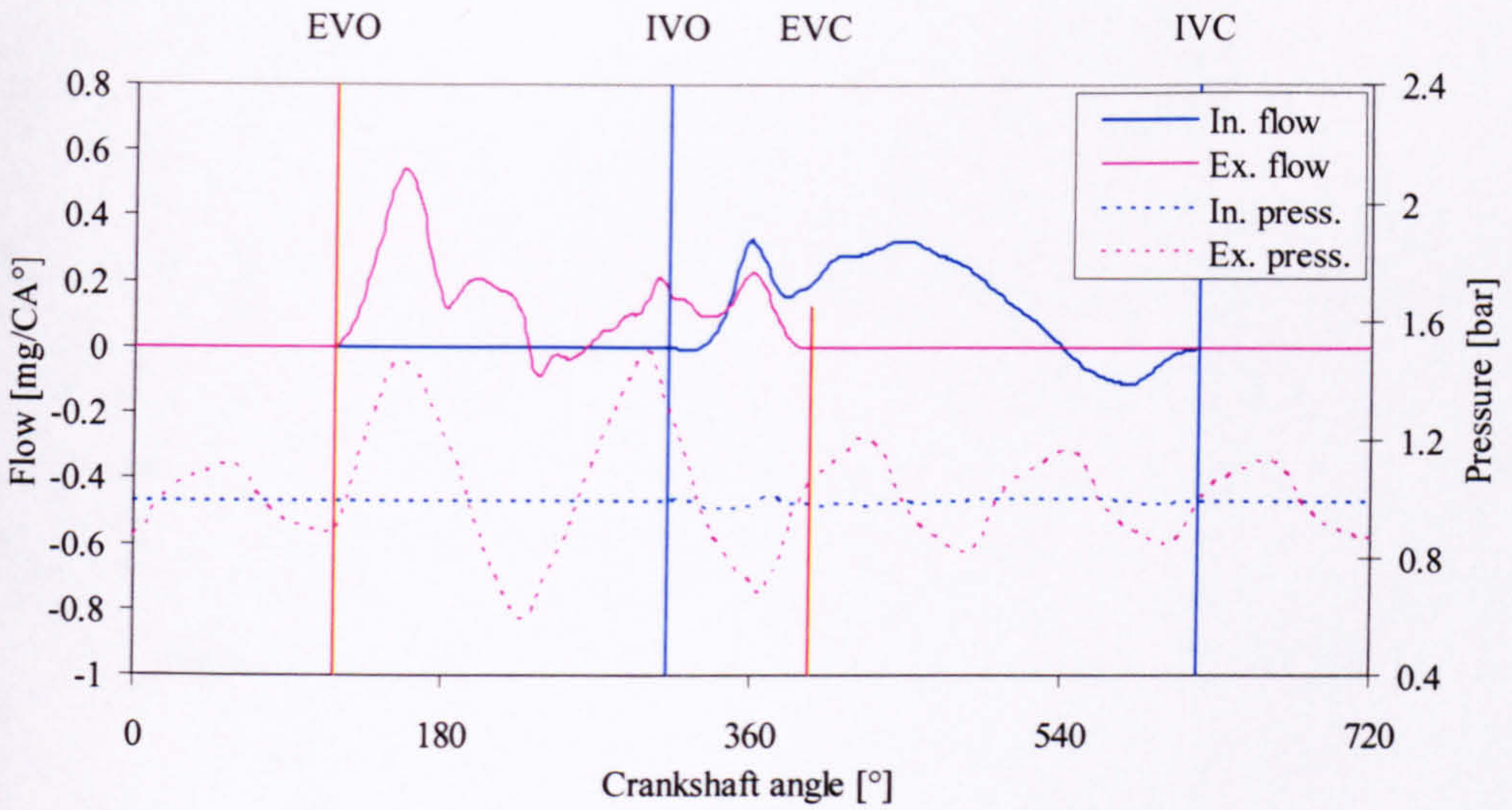

Figure 5.20: Inlet and exhaust port pressure and flow rate vs. crankshaft angle for *1 cyl. exhaust only* engine at 4000 rpm (flow rate is normalised with engine speed)

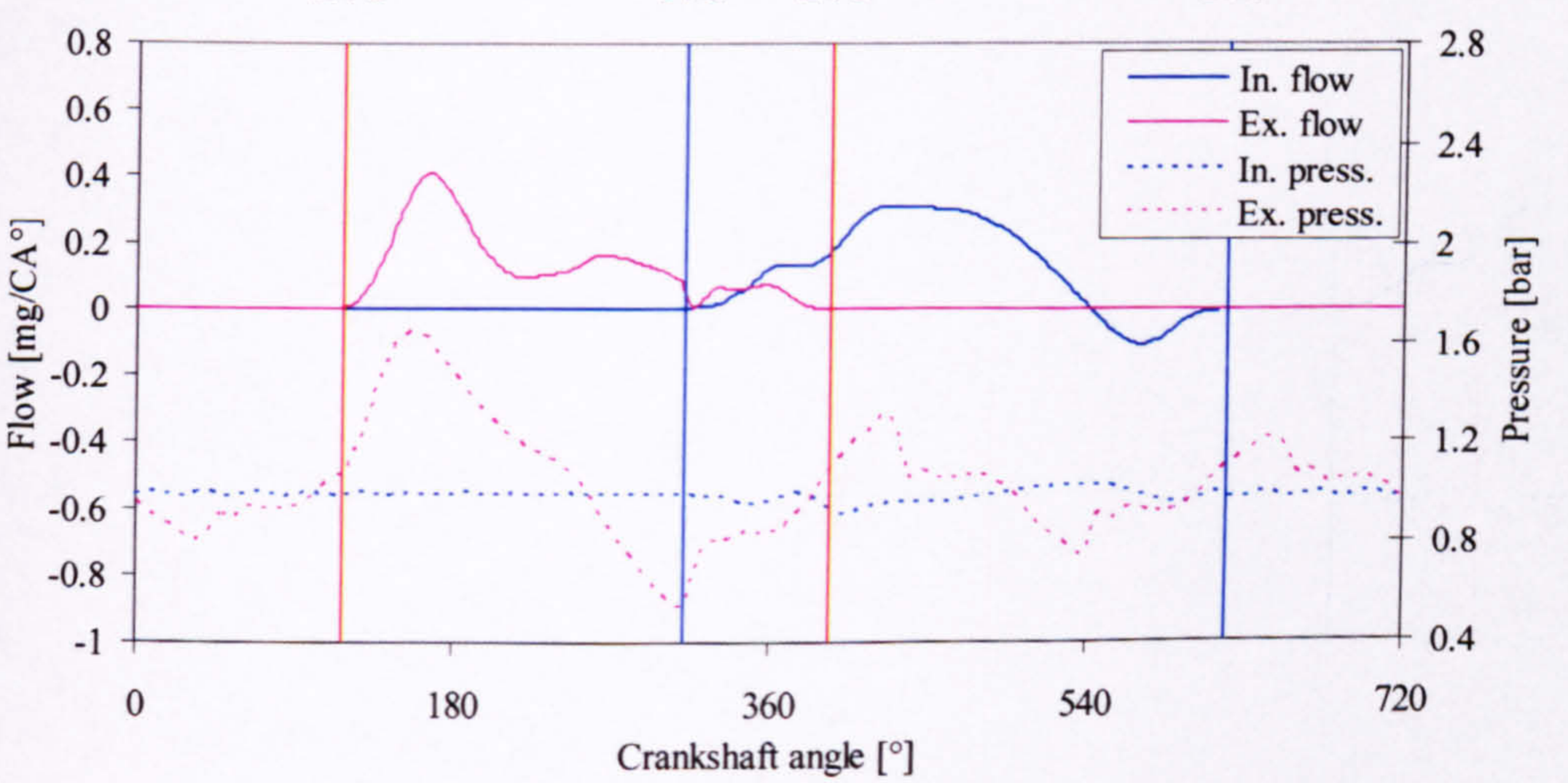

Figure 5.21: Inlet and exhaust port pressure and flow rate vs. crankshaft angle for *1 cyl. exhaust only* engine at 8000 rpm (flow rate is normalised with engine speed)

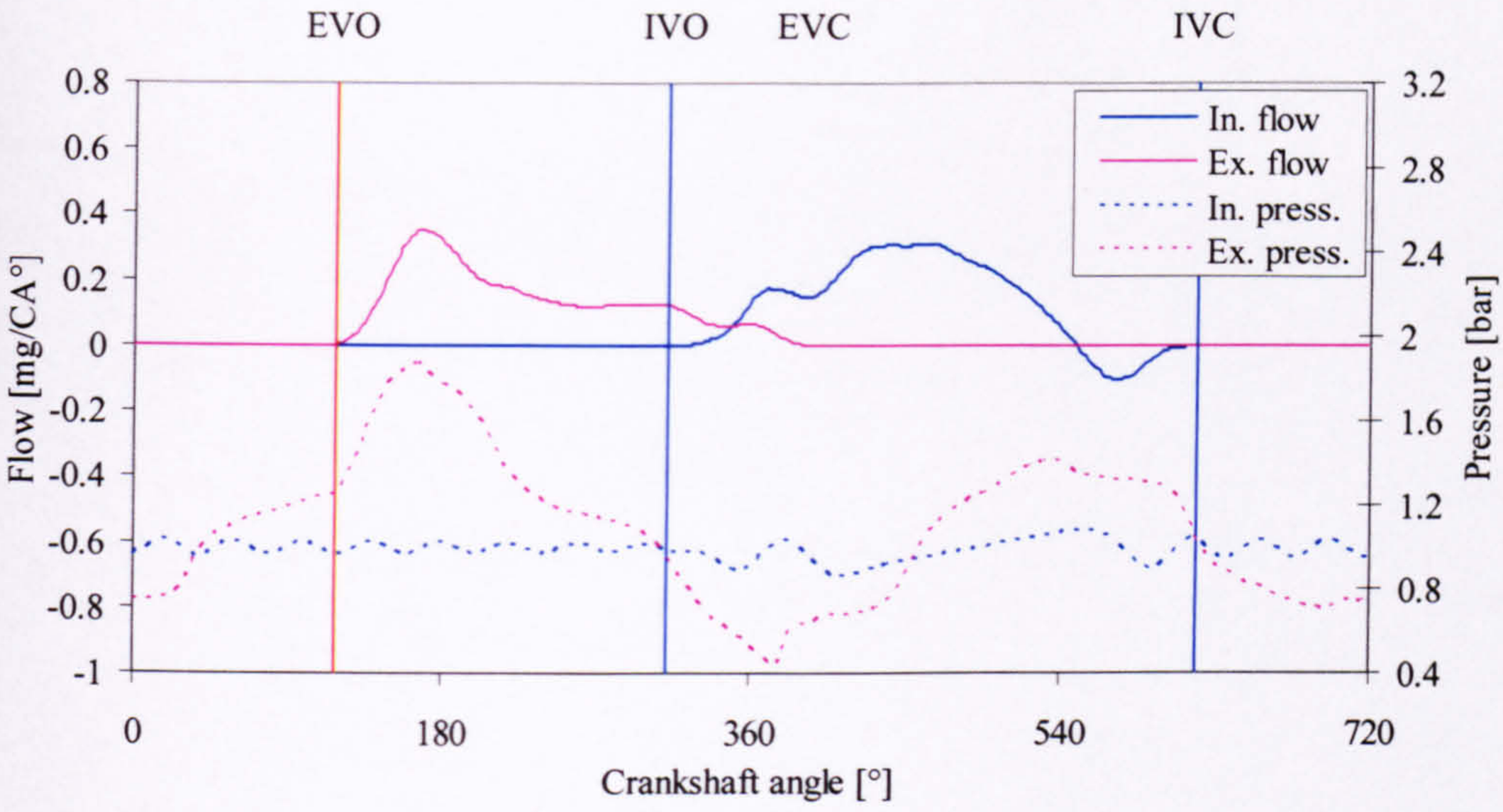

Figure 5.22: Inlet and exhaust port pressure and flow rate vs. crankshaft angle for *1 cyl. exhaust only* engine at 11000 rpm (flow rate is normalised with engine speed)

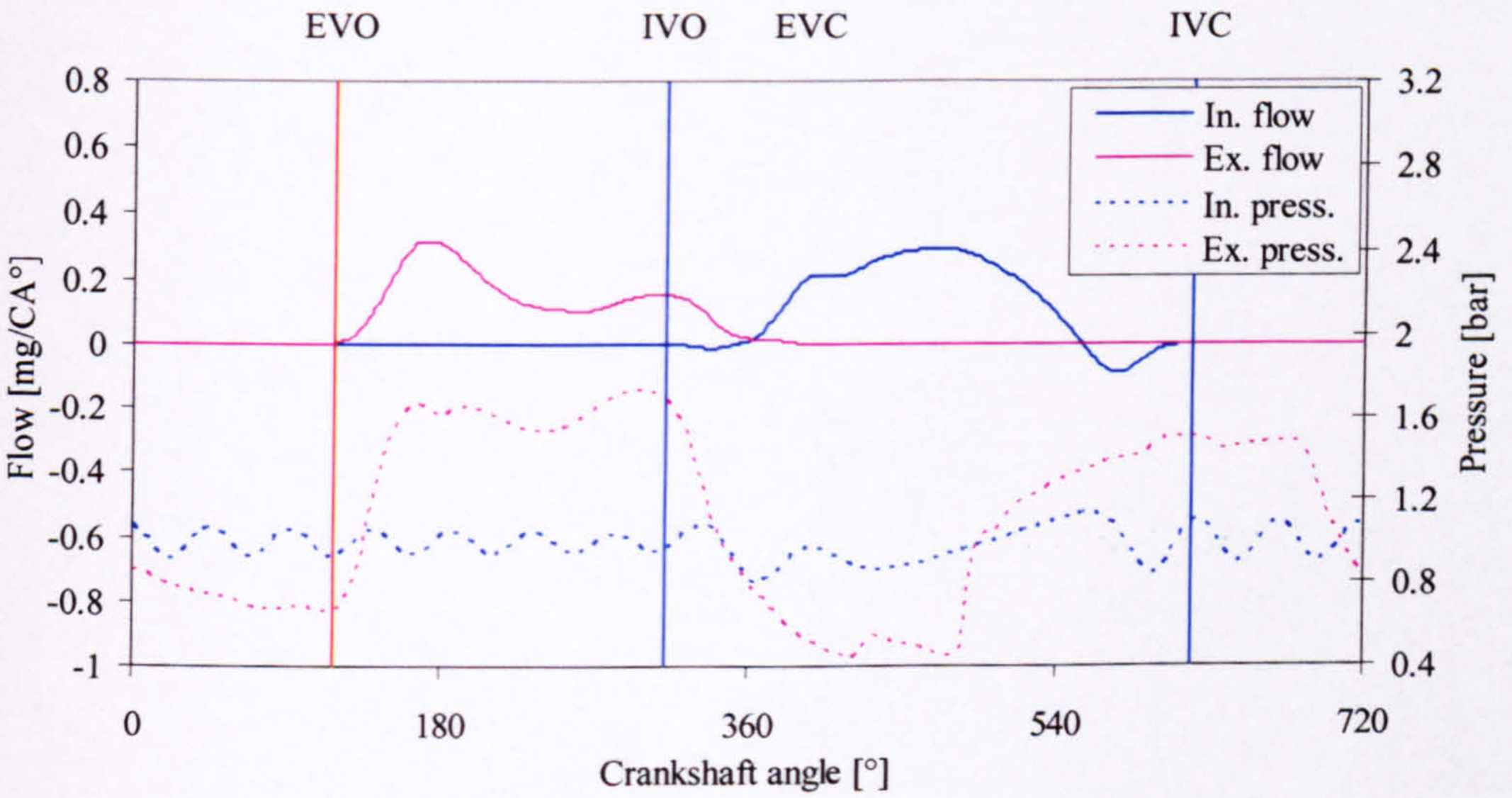

Figure 5.23: Inlet and exhaust port pressure and flow rate vs. crankshaft angle for *1 cyl. exhaust only* engine at 13000 rpm (flow rate is normalised with engine speed)

It should be noted that the flatness of the charging efficiency curve above 8000 rpm is due to length of the pipe. Figure 5.23 shows that it is too short to allow a standing wave to develop. If the engine is run at higher engine speed a fall in volumetric efficiency can be expected, as the pressure gradient across the cylinder will become negative.

Figure 5.24 shows normalised inlet port flow rate vs. crankshaft angle. It can be seen that the mass flow after EVC is almost unchanged for different engine speeds, which explains the flatness of the mass entering the cylinder during the periods EVC-BDC and BDC-IVC (see Figure 5.5). The mass flow during these periods has a very small effect on the charging efficiency. However, it should be noted that for speeds 2000 rpm, 3000 rpm and 6000 rpm where the flow rate is negative during the valve overlap period also have lower flow rate immediately after EVC. This is due to the low density and higher temperature of the reverse flow gas, which is the first to re-enter the engine.

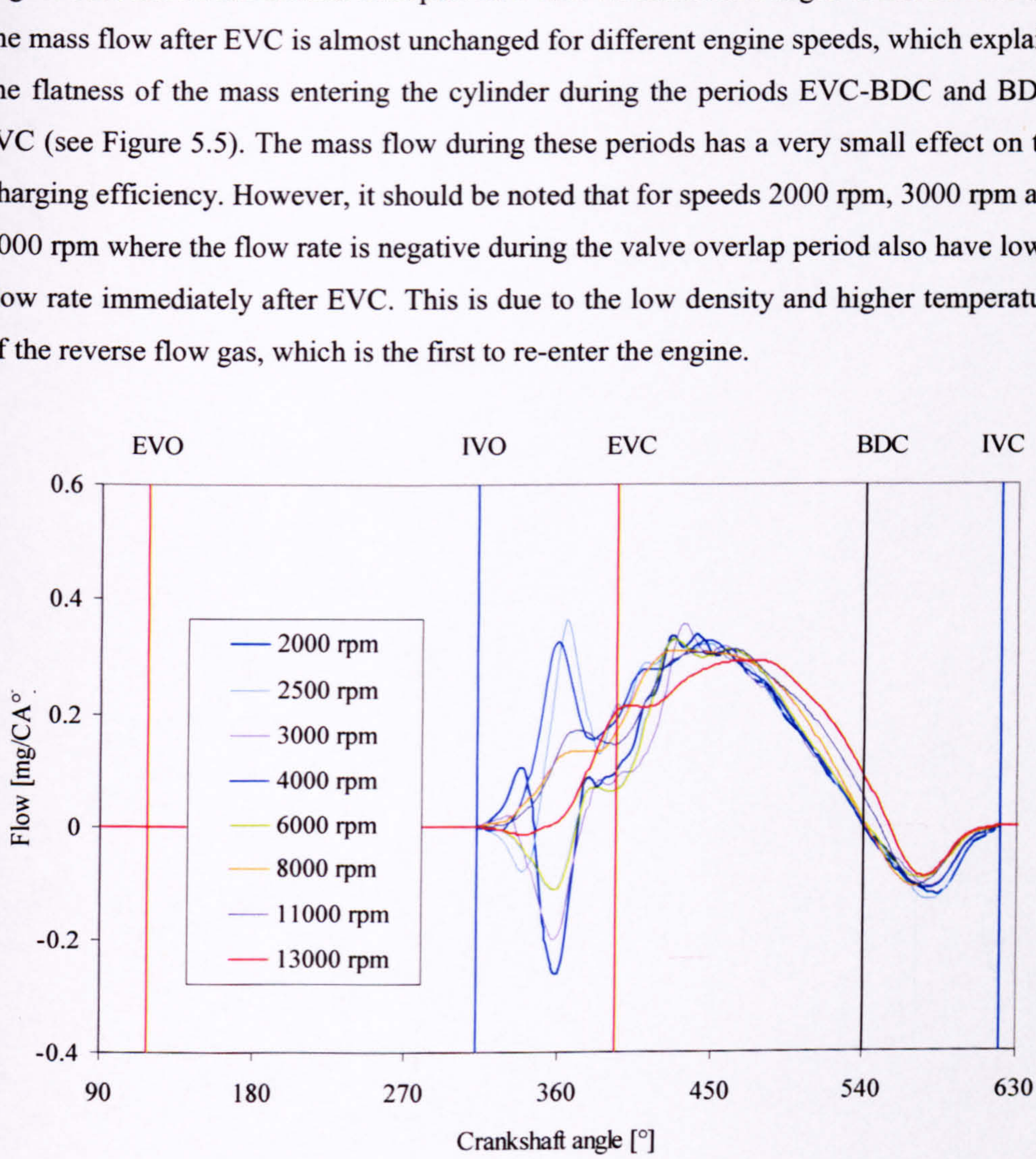

Figure 5.24: Inlet port flow vs. crankshaft angle *1 cyl. exhaust only* engine at different engine speeds

In summary, the main mechanism through which the gas dynamics in the exhaust system affect the charging efficiency is by the arrival of a negative or positive pressure wave during valve overlap, which determines the pressure gradient across the cylinder and the direction of the inlet flow during valve overlap. This is valid even for low engine speeds as the gas dynamics in the exhaust system are excited by the pressure gradient across the exhaust valve at EVO.

5.3 Summary of conclusions

The charging efficiency in a multi-cylinder engine is a function of the complex gas dynamic phenomena occurring in the inlet and exhaust system. The use of the *1 cyl. inlet only* and 1 cyl. exhaust only engine allows the effects of the gas dynamics in the inlet pipe and exhaust pipes on the cylinder filling process to be investigated in isolation from each other. The following conclusions can be made from the results and discussion presented above:

- For the *1 cyl. inlet only* engine the charging efficiency peaks and dips are governed mainly by the pressure gradient across the cylinder during valve overlap. This is less pronounced at low engine speeds. The general rise of charging efficiency with speed depends on the arrival of a positive pressure wave just before IVC. Both filling effects are a function of pipe length and engine speed. These findings agree with previous research conducted by Prosser (1974) and Yagi et al. (1970). However, a conclusion is made that the charging efficiency should be considered to be a function of the combined effect of both cylinder filling mechanism.

- The effect of the gas dynamic behaviour in the exhaust system is mainly confined to the overlap period. Examining the gas exchange process in the *1cyl. exhaust only* engine showed that the arrival of a negative pressure wave during this period is beneficial to charging efficiency. This agrees with previous research by Yagi et al. (1970) and Borreti and Villa (1998). It should be noted that depending on the length of the exhaust pipe the speed range of this effect can be limited.

- The pressure gradient across the cylinder in a real engine is a function of the effects of both inlet and exhaust pressure during valve overlap and the pressure across the inlet valve during the rest of the inlet period. This, together with the complex gas dynamics in a branched inlet and exhaust systems and the interaction between different cylinders is the reason for the intricate shape of the charging efficiency curve of such engines. However, from the analysis presented it is possible to conclude that the shape of the charging efficiency curve at low speed is mainly influenced by the pressure waves in the exhaust system. At higher engine speeds it becomes a function of the combined effect of the gas dynamics in the inlet and exhaust system.

Establishing the effect of inlet and exhaust system on the cylinder filling mechanisms taking place in high-speed engines provides the background enabling the exploration of the effect of the IVO and IVC timing on the charging efficiency. This is done in the following two chapters.

Chapter 6

Results and Discussion: I. Parametric Study of the Effects of Inlet Valve Opening Timing on the Gas Exchange Process

Understanding the sensitivity of different engine performance characteristics to variation of individual valve event parameters is critical in the context of VVA application. The focus of this chapter is the effect of Inlet Valve Opening timing on the gas exchange process, the mechanisms involved and the overall effect on charging efficiency.

Previous research conducted by Asmus (1982) showed increased backflow of burned gases in the inlet system caused by early IVO timing. It was also found that IVO can be delayed significantly without detrimental effect on volumetric efficiency, but will cause a slight dip in the pumping loop near TDC. Similar conclusions were made by Roth (1998) who related the optimum IVO timing to the peak value of the Intake Pseudo Flow Velocity. It is important to note that both studies relate to production medium speed engines where, due to the design of the intake and exhaust system, a negative pressure gradient exists across the cylinder during valve overlap period at most engine speeds and loads. As explained in the introduction to this thesis differences exist between the design of these systems in medium and high-speed engines.

The effect of five different IVO timings on charging efficiency was explored with the use of engine simulation software. The camshaft profiles were generated in such a way that the rest of the features of the valve remain unchanged. The inlet process was divided into three sectors and the effect of IVO timing on each was studied. The overlap period was closely examined by comparing inlet and exhaust port pressures and mass flow through

the inlet valve. The gas dynamic events taking part in the inlet and exhaust system were shown to be responsible for the effect of IVO on charging efficiency.

6.1 Generation of lift curves for different IVO timings

Five different inlet lift curves were generated to give five different IVO timings at 12° intervals from 12° BTDC to 60° BTDC as detailed in Figure 6.1 and Table 6.1. In order to investigate only the effect of IVO timing and minimise the influence of variation of other parameters on the gas exchange process extra care was taken to leave other features of the lift curve unchanged. The lift curves were created in such a way that the lift profile from IVO to maximum lift was kept the same. A compensation for the reduced valve event duration has been made by increasing the closing velocity immediately after maximum lift. This will have a negligible effect on the gas exchange process, as at this part of the lift curve it is a very small percentage of the effective flow area. The opening lift rate, maximum lift and IVC timing remain the same. This resulted in the creation of a lift profile, which will result in poor dynamic performance of the valvetrain but allow the exploration of IVO timing in relative isolation.

There are some practical limitations on the IVO timing caused by the geometry of the combustion chamber and the high compression ratios used in high-speed high performance engines. This type of engines, normally have high bore/stroke ratios in order to maintain low piston speeds and accommodate larger valves. This combined with high compression ratios results in very short combustion chambers. The earliest IVO is often limited by piston to valve clearance. This is reflected in the selection of IVO timings to be tested. The base engine IVO is 48° BTDC and is the earliest possible with this rate of opening, which allows sufficient clearance from the piston accounting for variation of manufacturing tolerances and dimensional changes during operation. Only one more advanced IVO timing at 60° BTDC was explored in order to assess if any potential advantage can be gained if earlier timing was possible.

IMOP ATDC	IVO BTDC	IVC ABDC
94°	60°	80°
106°*	48°*	80°*
118°	36°	80°
130°	24°	80°
142°	12°	80°

Table 6.1: Inlet valve lift curve parameters

(*Base line engine)

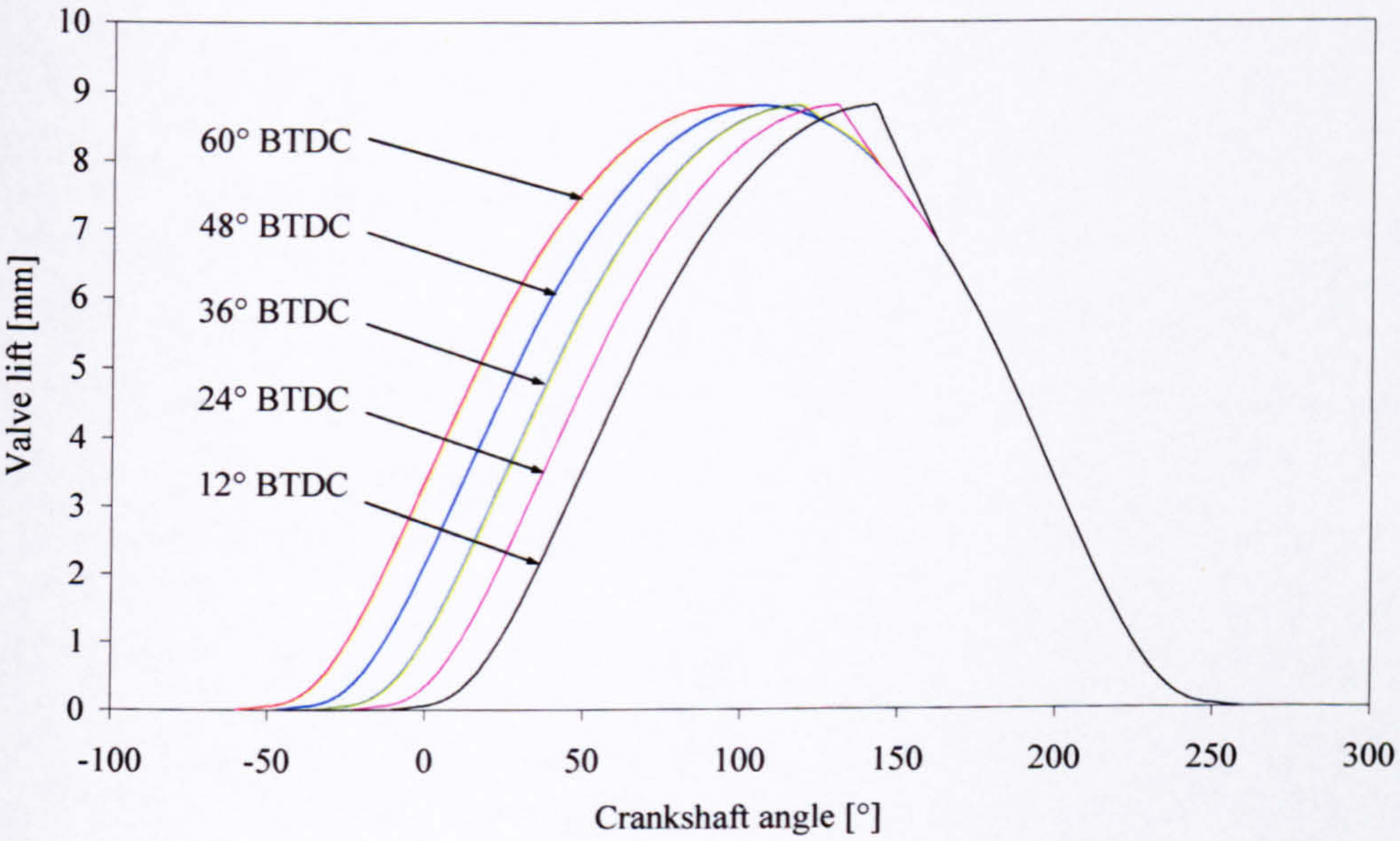

Figure 6.1: Inlet valves lift curves investigated

6.2 Simulation results

For each of the test cases the simulation was run for steady state, WOT condition at engine speeds ranging from 1500 rpm to 13000 rpm at intervals of 250 rpm.

6.2.1 Effect of IVO timing on charging efficiency

Figure 6.2 shows the effect of IVO timing on calculated charging efficiency, which is an indication of the trapped fresh charge at IVC. All five charging efficiency curves generally consists of a series of peaks and dips exhibited at approximately the same engine speeds up to 9000 rpm. It is also noticeable that up to the same speed there are significant differences in the magnitude of those peaks and dips depending on IVO timing. The following general patterns are present. The more advanced IVO timings such as 60° BTDC and 48° BTDC have the largest amplitudes at the speeds where peaks and dips occur. This is best illustrated at 1750 rpm, where IVO at 60° BTDC results in the lowest charging efficiency. At an engine speed of 2750 rpm, IVO at 48° BTDC produces the highest charging efficiency. Retarding IVO to a later angle such as 12° BTDC reduces the magnitude of the peaks but fills the dips. This can be seen around 3000 rpm for the peak and around 3750 rpm for the trough. Above 9000 rpm there appears to be a shift of the speeds where charging efficiency peaks and dips for the different IVO timings. Any pattern is less apparent, although the later IVO such as for 12° BTDC and 24° BTDC appear less oscillatory. The reasons for these effects are discussed later in the chapter.

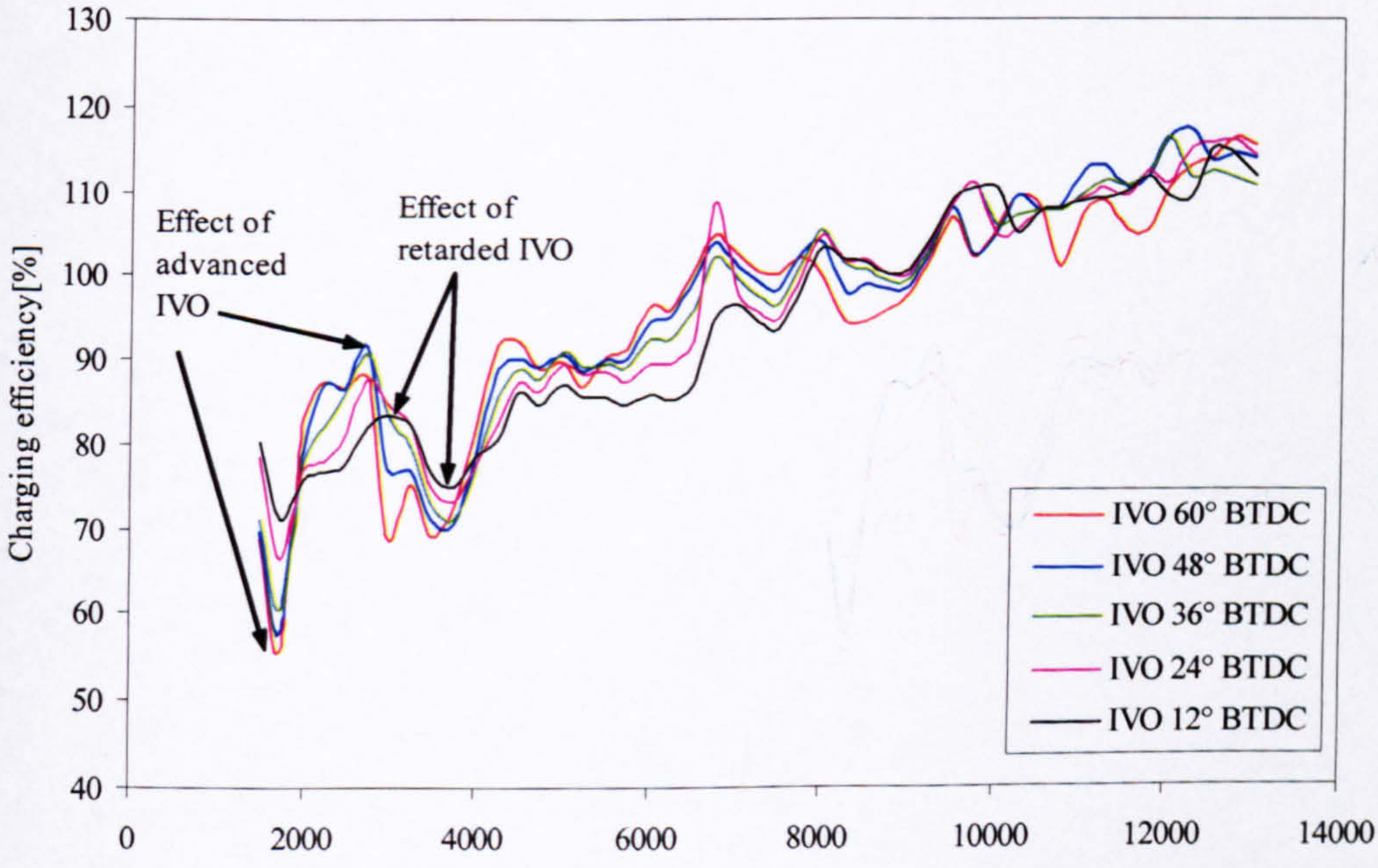

Figure 6.2: Effect of IVO timing on charging efficiency at various engine speeds

6.2.2 Effect of IVO timing on volumetric and trapping efficiency

Volumetric efficiency, as defined in Chapter 5, is not proportional to the mass of fresh charge trapped in the cylinder but it indicates the quantity of charge entering it. Bearing in mind the conservative nature of the scavenging model in terms of trapped mass, volumetric efficiency gives an insight to the potential effects IVO can have on charging efficiency. Examining the effect of IVO on volumetric efficiency in the context of the effect on charging efficiency can pin point the speed regions where the difference between these effects is due to extra charge flow during the overlap period. The implications of this will become apparent in the following discussion. Figure 6.2 and 6.3 show that up to 9000 rpm the speeds where peaks and dips occur are the same for both the volumetric and charging efficiency curves. The major difference is that at the speeds where volumetric efficiency peaks e.g. 2500 rpm, 4500 rpm and 6500 rpm, the amplitudes of these peaks are more sensitive to IVO timing than in the case of charging efficiency. For example in the region of 2500-3250 rpm the variation between the peaks is approximately 30% where it is only 10% for the charging efficiency.

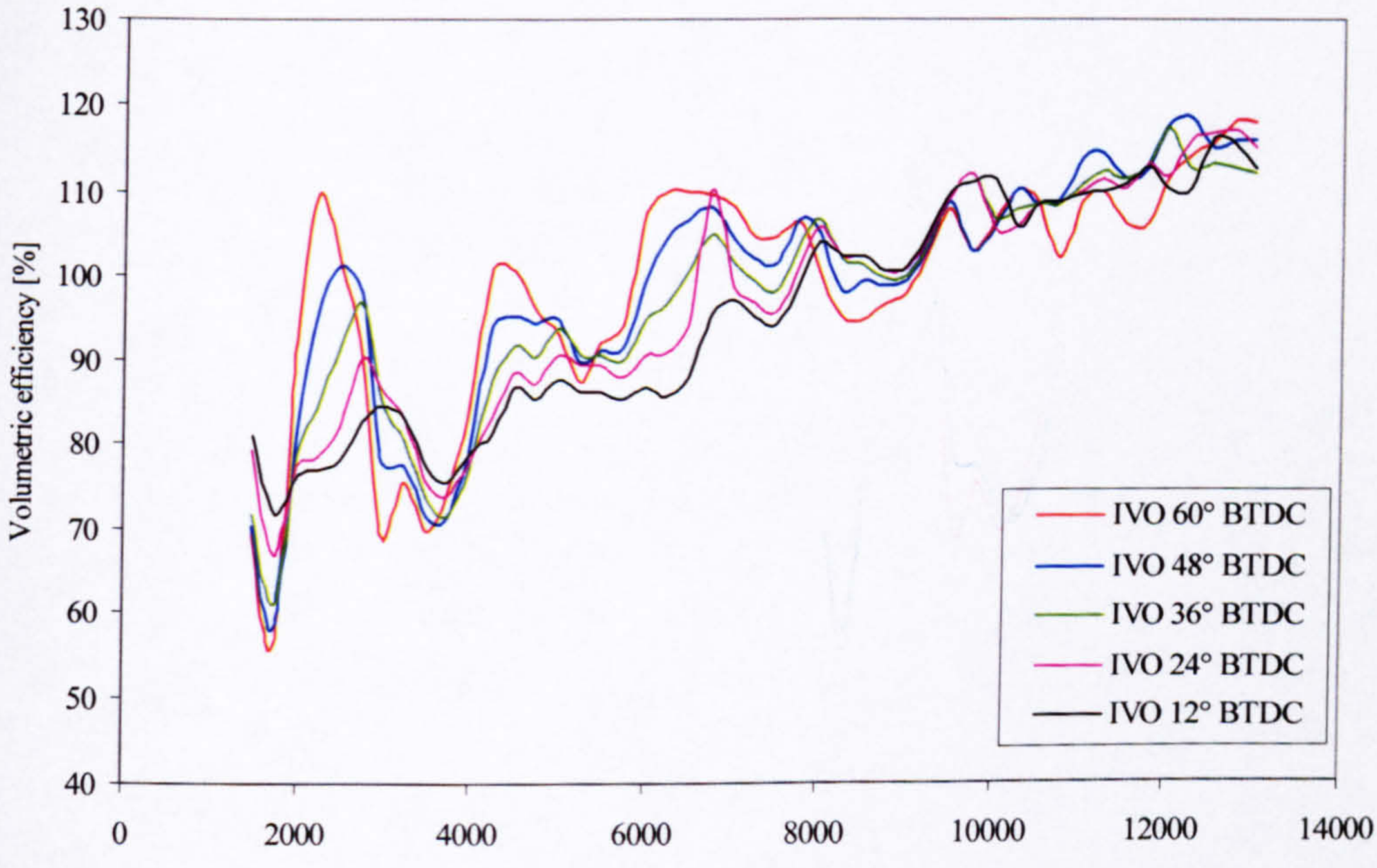

Figure 6.3: Effect of IVO timing on volumetric efficiency at various engine speeds

This can be explained by examining the trapping efficiency curves for different IVO timings shown in Figure 6.4. There is a noticeable reduction in the trapping efficiency at the same speeds where volumetric efficiency peaks. In addition to this the reduction in trapping efficiency is highest for the most advanced IVO opening, i.e. 60° BTDC. This means that the increase of airflow due to earlier IVO at these speeds is not proportional to an increase in the trapped mass after IVC.

Above 9000 rpm the sensitivity of volumetric efficiency to IVO is similar to that of charging efficiency.

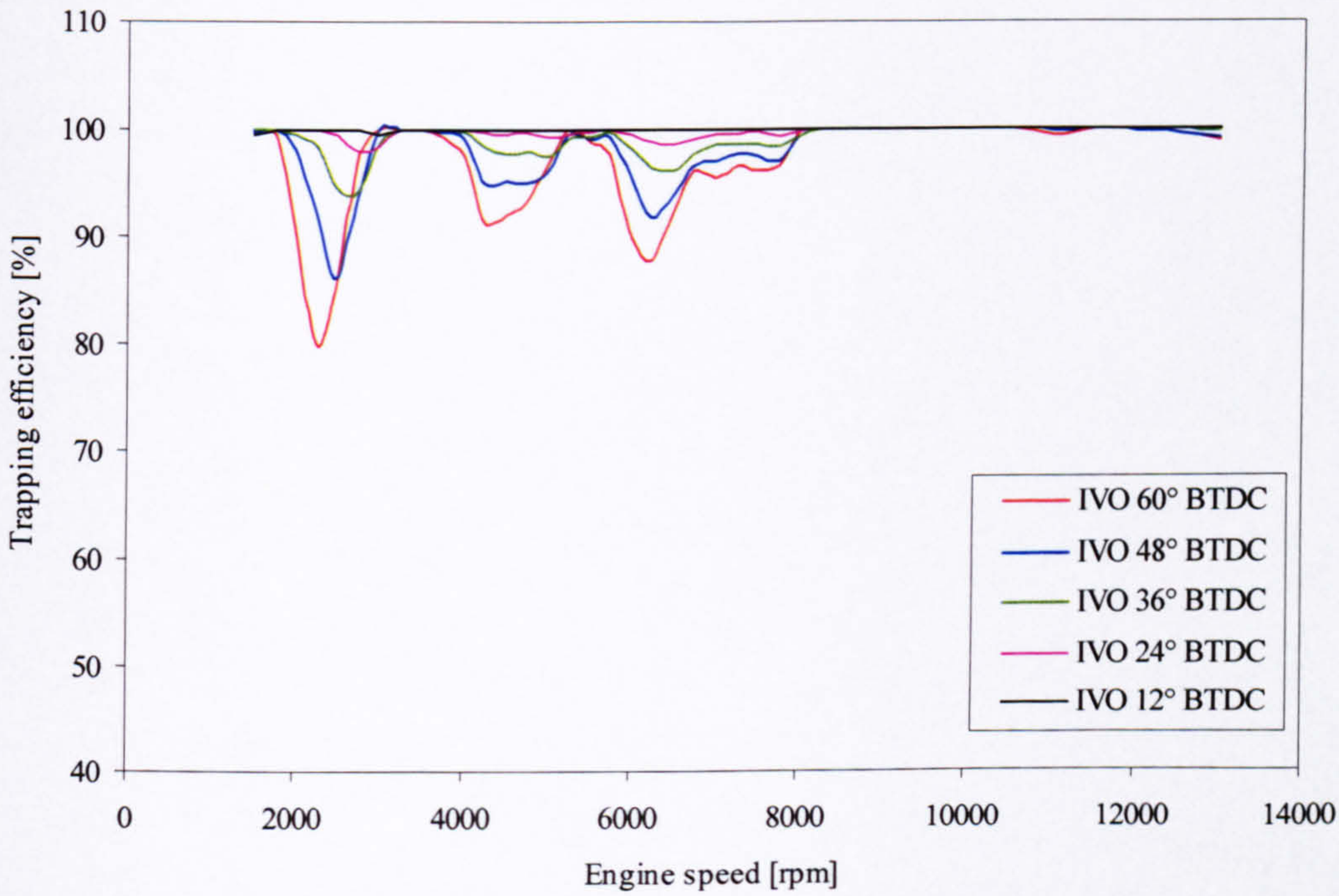

Figure 6.4: Effect of IVO timing on trapping efficiency at various engine speeds

6.2.3 Effect IVO timing on exhaust residuals

Figure 6.5 shows the exhaust residual fraction in the engine cylinder after IVC for various IVO timings. The residual curves appear similar in shape. There are three speeds where the exhaust residual fraction peaks: 1750 rpm, 3500 rpm and 8500 rpm. The more advanced IVO timings, such as 60° BTDC and 48° BTDC, produce the highest peaks at these speeds. However, they have the lowest residual levels in the rest of the engine

speed range. Later IVO timings such as 24° BTDC and 12° BTDC have lower residual fraction at the speeds indicated above where the curves peak. However, they generally have higher residual levels in the rest of the speed range. There are certain limitations associated with the use of the perfect mixing scavenging model to representing the flow from the cylinders into the exhaust port and the perfect displacement model used for reverse flows. Because of this, the effect of early IVO in the areas of volumetric efficiency peaks and dips has been underestimated.

In comparison with Figure 6.3, it can be seen that the residual gases peak at the same speeds where low volumetric efficiency is experienced, i.e. 1750 rpm, 3500 rpm and 8500 rpm. This suggests that a negative pressure gradient across the cylinder causing poor expulsion of residual gas during the overlap may be partially responsible for the dips in volumetric efficiency. This will become more apparent in the following section.

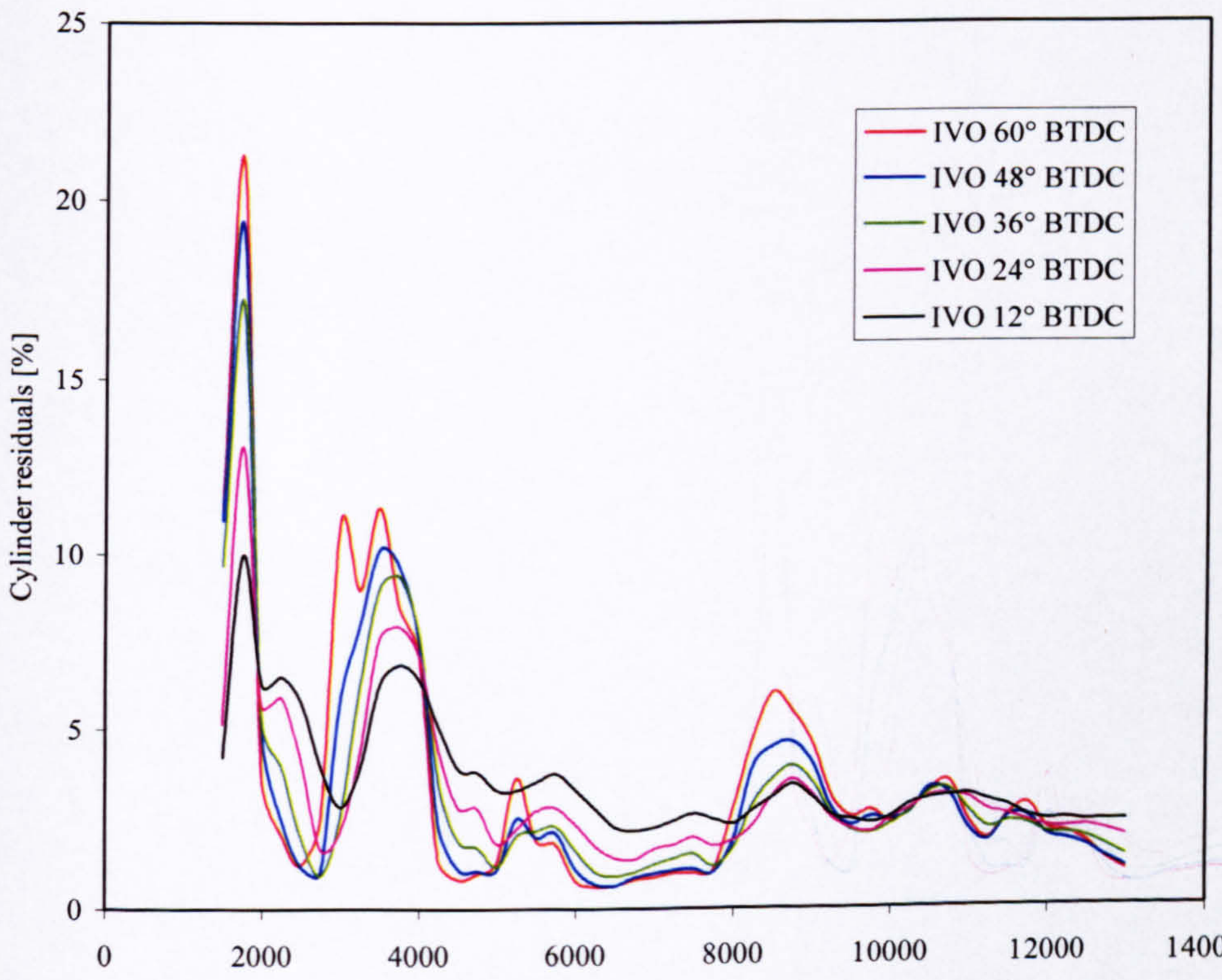

Figure 6.5: Effect of IVO timing on exhaust residuals at various engine speeds

6.3 Discussion

In order to explain the mechanisms through which IVO timing affects the charging efficiency, volumetric efficiency and residual gases it is important to first identify the part of the intake process, which is most sensitive to IVO timing. For that purpose the intake process has been divided into three periods as described in Chapter 5: IVO-EVC, which is the valve overlap period, EVC-BDC and BDC-IVC. Figure 6.6 shows the calculated mass entering the cylinder through the inlet during each of these periods for the five different IVO timings.

6.3.1 Overlap period

Examining Figure 6.6 shows that the valve overlap period is the most sensitive part of the inlet process to variation of IVO timing up to 8500 rpm. The engine speeds where there is large difference in the mass flow during overlap coincides with the speeds of charging efficiency peaks e.g. 2500 rpm, 4500 rpm and 6500 rpm and to a lower extent when it dips e.g. 1750 rpm and 3750 rpm.

Figure 6.6 also indicates that the most advanced IVO timing (i.e. 60° BTDC) produces the highest peaks in the curves in the regions from 2250 rpm to 3750 rpm, from 4000 rpm to 5500 rpm and from 6000 rpm to 7500 rpm. The most retarded IVO timing (i.e. 12° BTDC) produces the lowest peaks in the same speed regions. There is a slight speed change for the corresponding peaks for the different IVO timings as indicated on Figure 6.6. To understand what causes the differences in the height of these peaks the pressure difference across the cylinder and the actual mass flow for each IVO timing at a typical speed in each region is examined.

Figures 6.7, 6.8 and 6.9 illustrate calculated inlet and exhaust port pressure vs. crankshaft angle at 2500 rpm, 4500 rpm and 6500 rpm for different IVO timings. It can be seen that the pressure traces in the exhaust port for each speed are fairly insensitive to IVO timing. The sensitivity of inlet port pressure is marginally higher. The most important observation is that for all these engine speeds and IVO timings there is positive pressure gradient during most of the valve overlap period. The reasons for this pressure gradient will be examined individually at every speed.

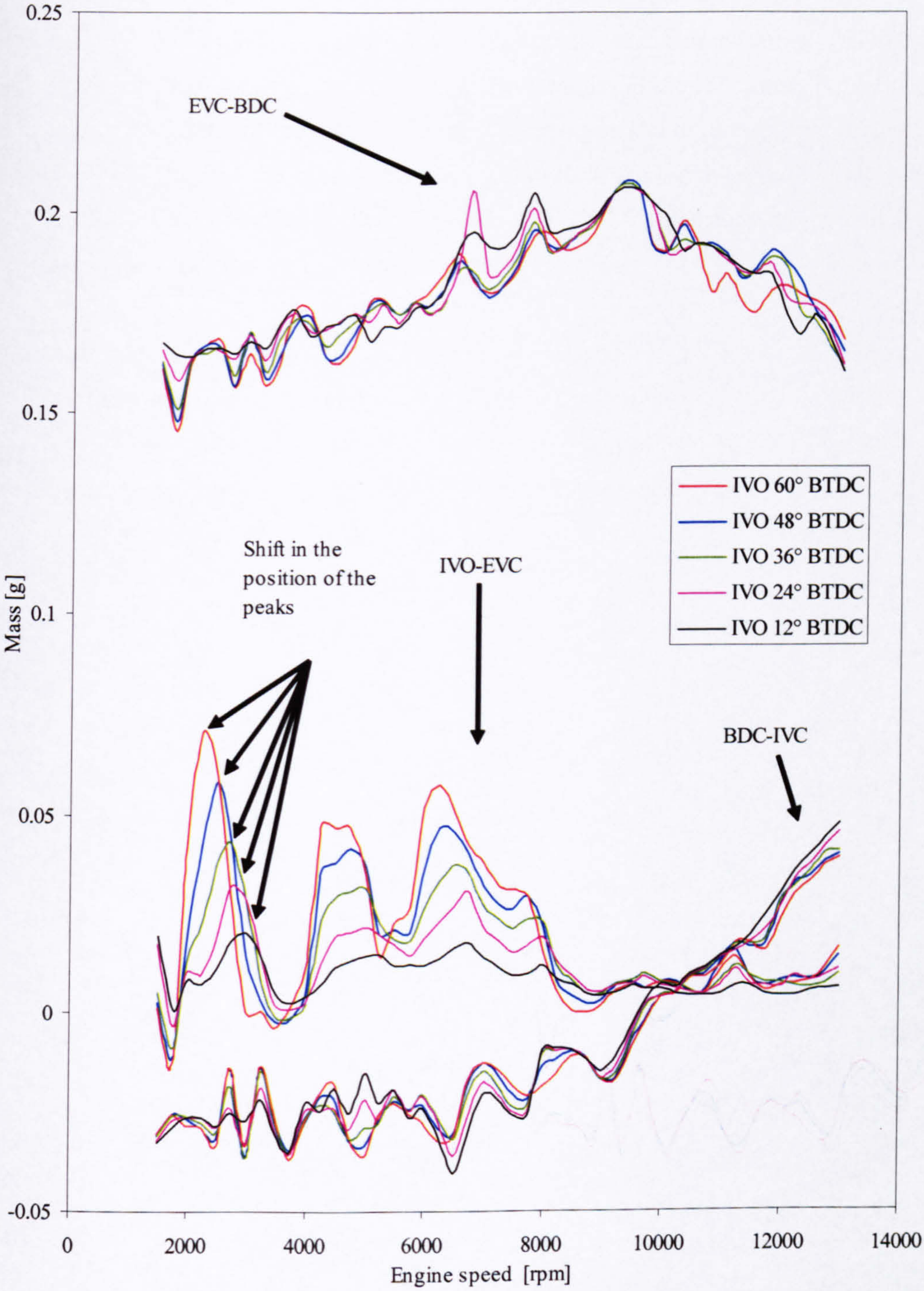

Figure 6.6: Effect of IVO timing on the mass inhaled by the cylinder during different periods of intake process at various engine speeds

Figure 6.7 shows that at 2500 rpm the pressure waves in the inlet port have small amplitudes compared with the pressure pulsations in the exhaust port. As discussed earlier in Chapter 5 this is due to the low excitation input of the piston at this speed. In fact the highest amplitudes of the pressure in the inlet port are excited by the interaction with the exhaust port pressure during overlap. It is a negative pressure wave in the exhaust port that is responsible for the negative pressure gradient during valve overlap.

At 4500 rpm shown on Figure 6.8, the pressure gradient is due to the coexistence of a positive pressure wave in the inlet port and negative pressure wave in the exhaust port. This is also the case for 6500 rpm shown in Figure 6.9.

Having determined the pressure gradient across the cylinder for these three engine speeds helps to explain the flow conditions through the valves during the overlap period.

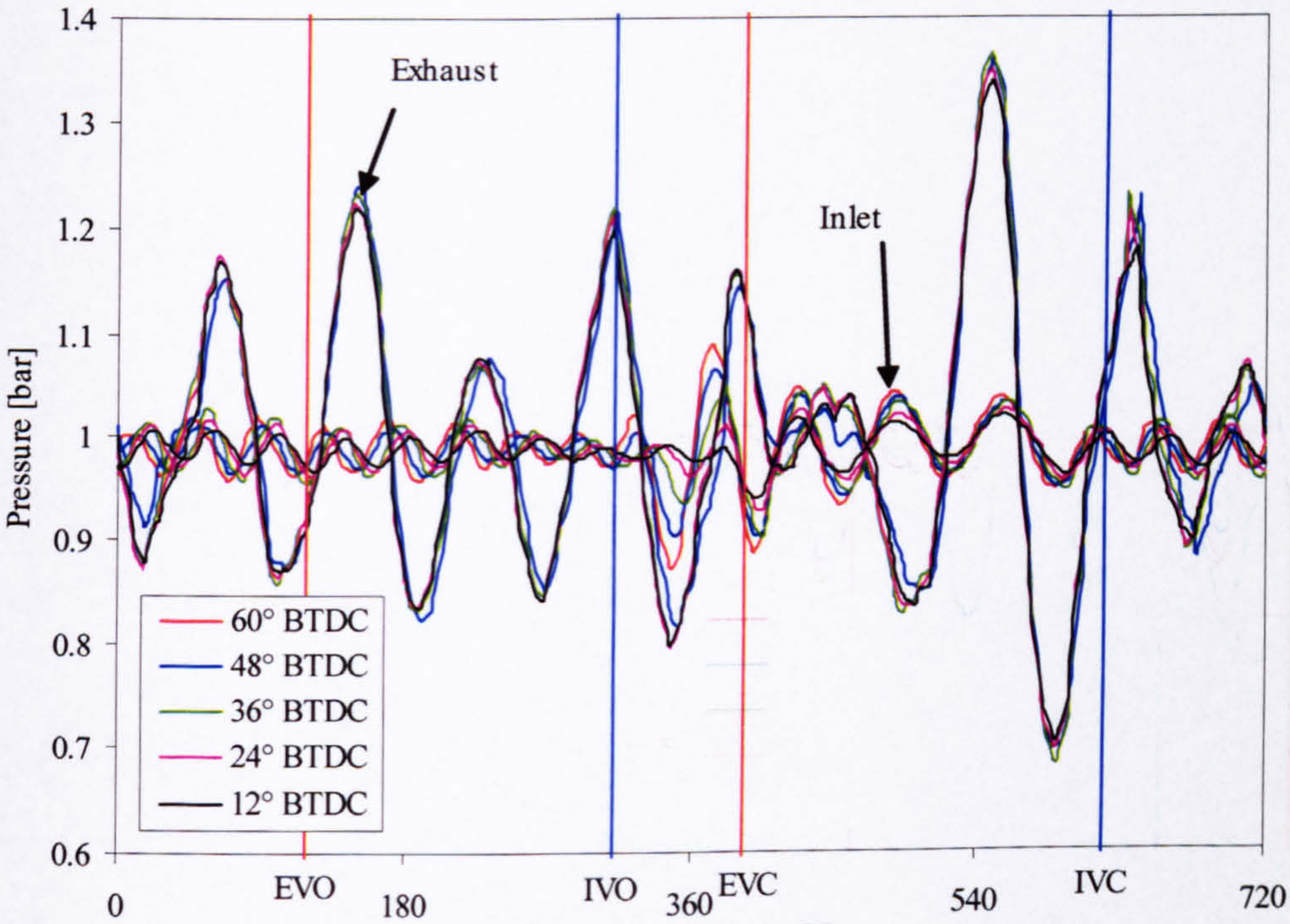

Figure 6.7: Inlet and exhaust port pressure vs. crankshaft angle with different IVO timings at 2500 rpm *(IVO line shown is for the base line engine at 48˚BTDC)*

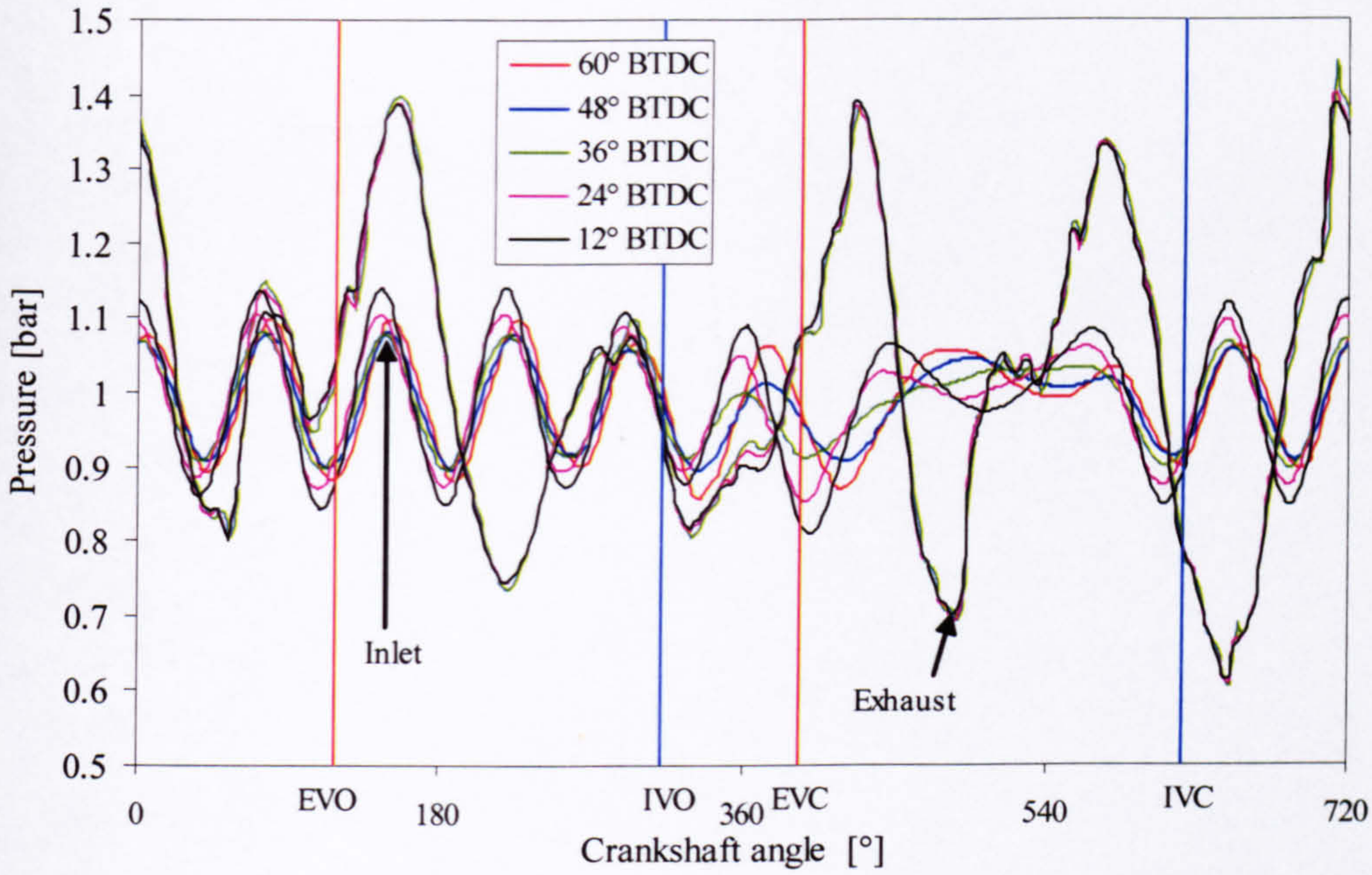

Figure 6.8: Inlet and exhaust port pressure vs. crankshaft angle with different IVO timings at 4500 rpm

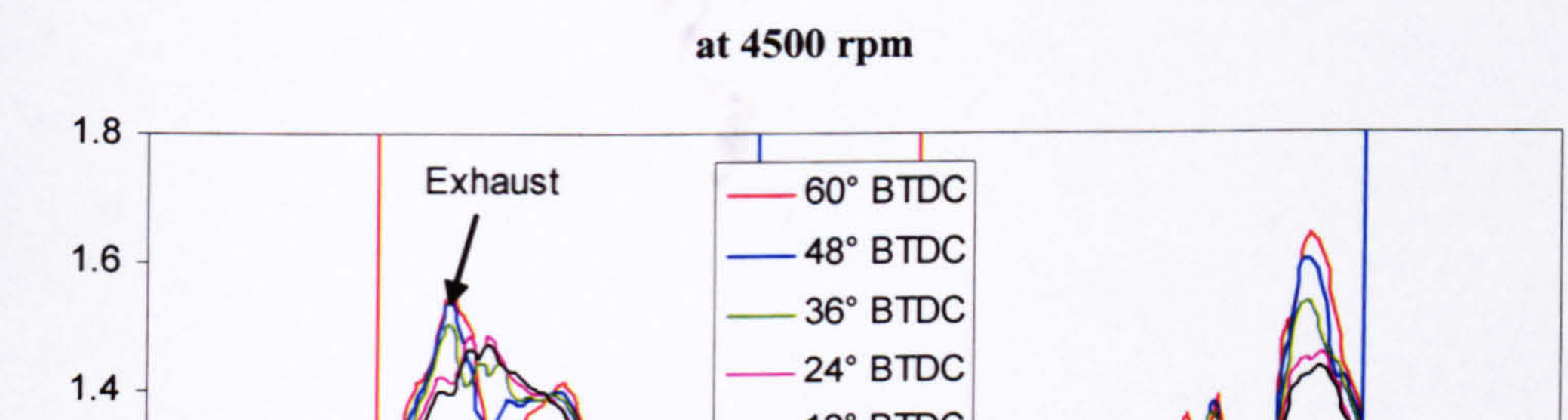

Figure 6.9: Inlet and exhaust port pressure vs. crankshaft angle with different IVO timings at 6500 rpm

Figures 6.10, 6.11 and 6.12 show the mass flow rate through the inlet valves for different IVO timing, at the speeds when a positive pressure gradient occurs during overlap period, i.e. at 2500 rpm, 4500 rpm and 6500 rpm. It can be seen on all three figures that early IVO opening results in higher inlet flow during this period.

It is important to note that the effect of early IVO timing on mass flow during overlap is not proportional to the effect on charging efficiency. This is particularly noticeable at 2500 rpm (Figure 6.10), where despite significantly higher mass flow into the cylinder during overlap and similar flow in the rest of the inlet period, IVO timing of 60° BTDC, 48°BTDC and 36°BTDC produce almost the same charging efficiency (Figure 6.2). The reason for this is that the scavenging model assumes perfect mixing, which is aerodynamically impossible, and is the most pessimistic estimate in terms of trapping efficiency. Similar overestimate of the fresh charge leaving the cylinder for large overlap durations is reported by Sandquist *et al.* (1997), who also suggests the insufficient heat

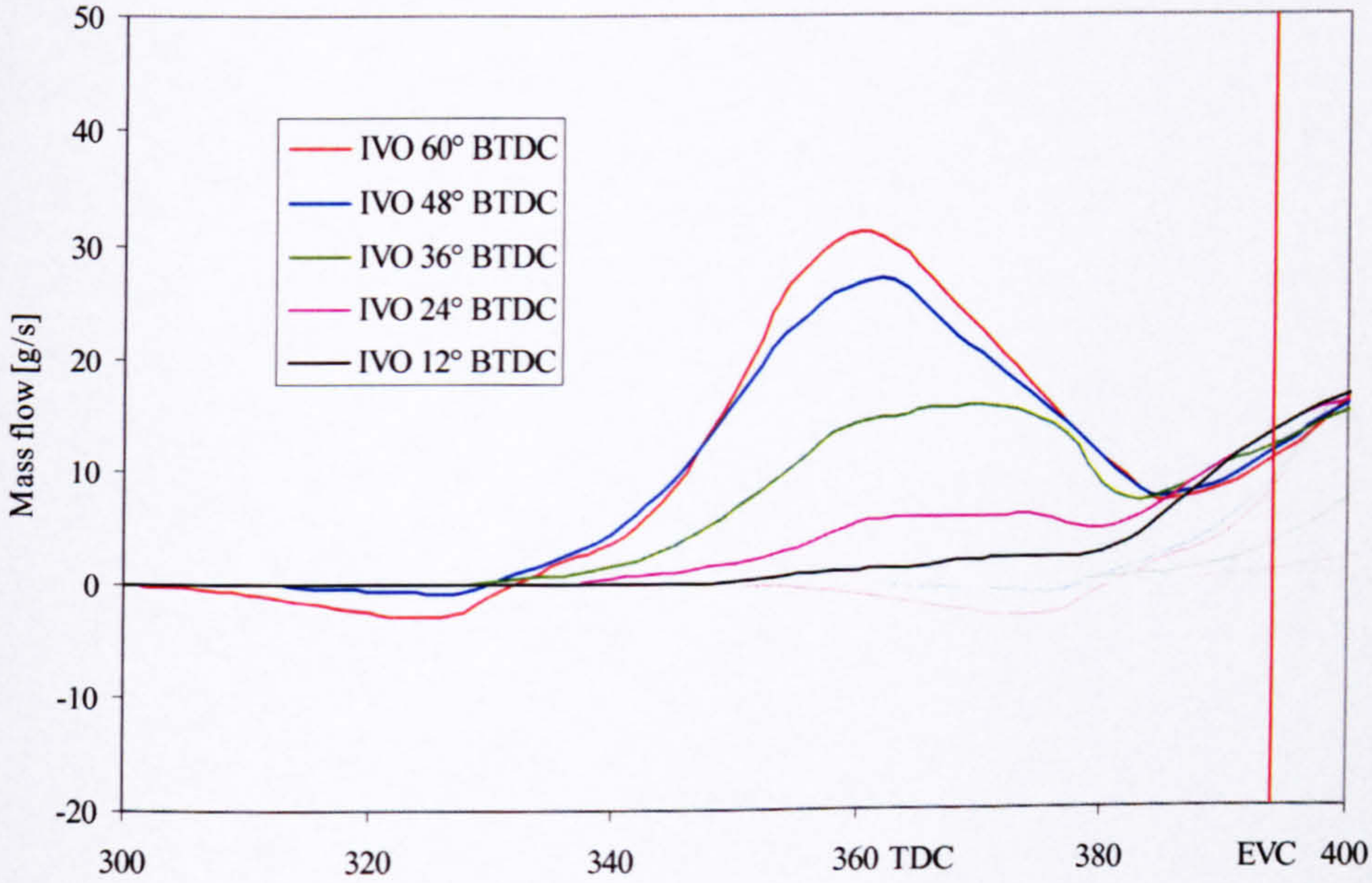

Figure 6.10: Inlet mass flow rate vs. crankshaft angle with different IVO timing at 2500 rpm

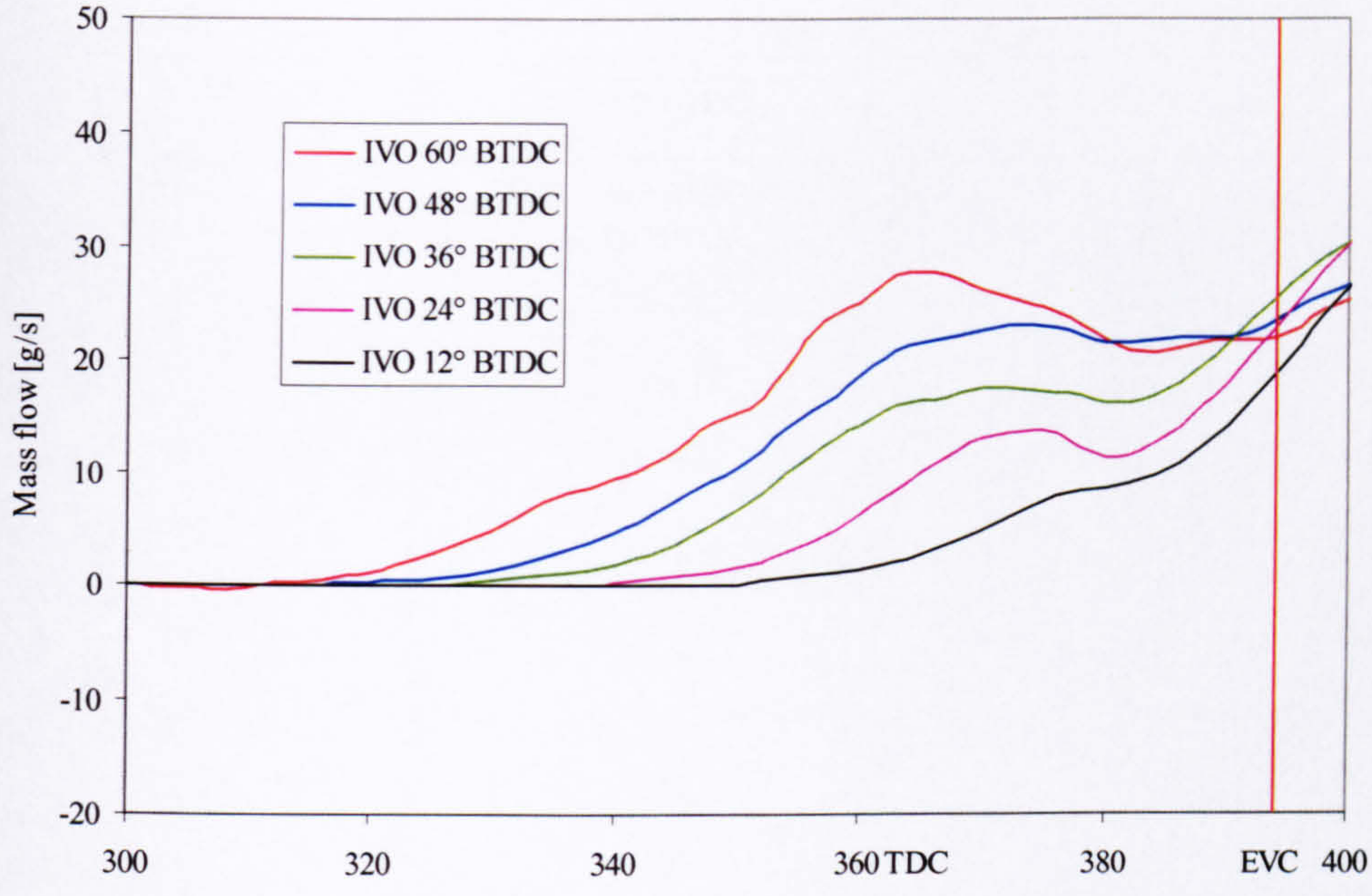

Figure 6.11: Inlet mass flow rate vs. crankshaft angle with different IVO timing at 4500 rpm

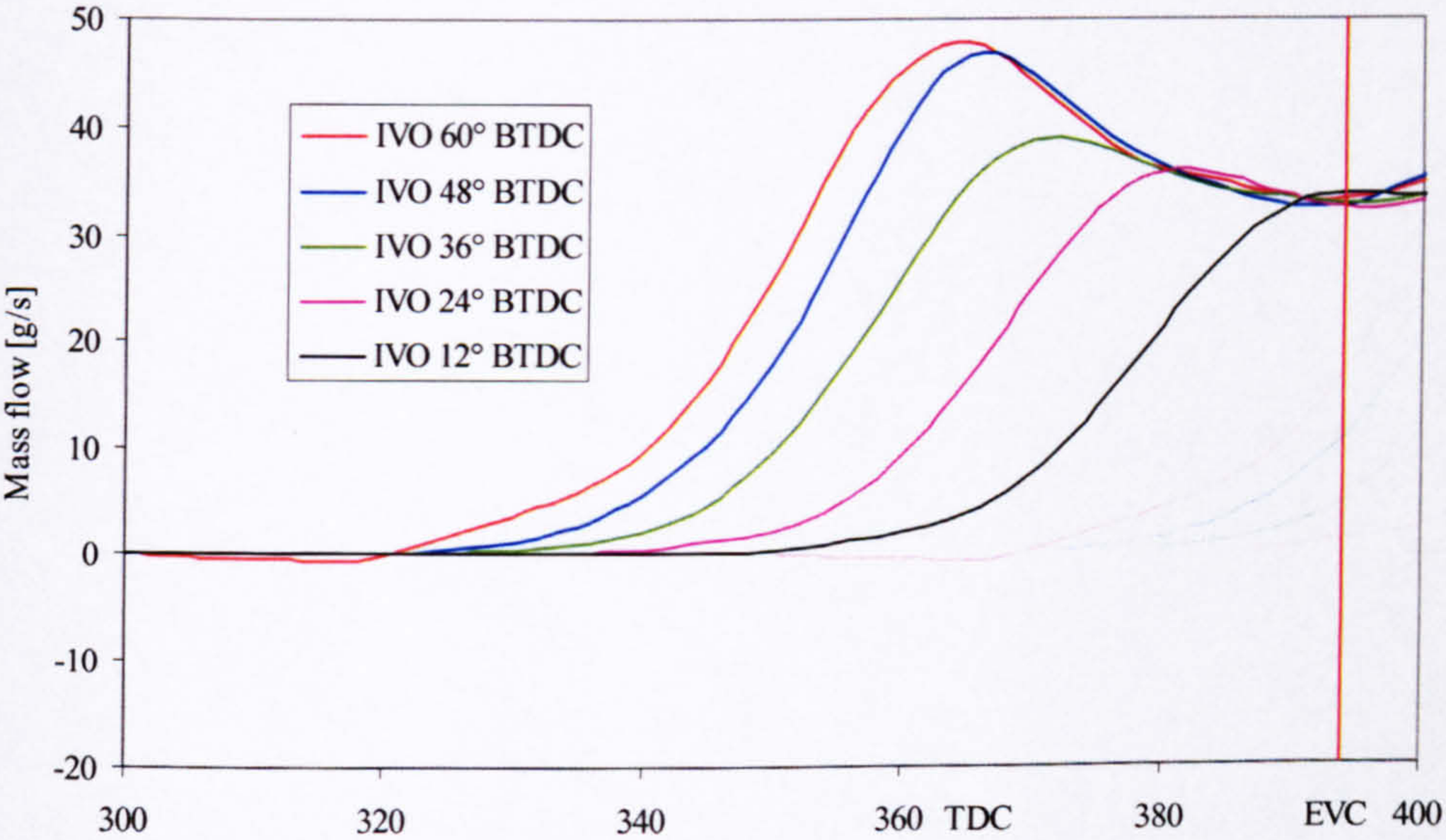

Figure 6.12: Inlet mass flow rate vs. crankshaft angle with different IVO timing at 6500 rpm

transfer model as a possible cause. In a pent roof combustion chamber there is a relatively short path between the inlet and exhaust ports, however without three-dimensional flow simulation it is impossible to assess how much fresh charge leaves the cylinder. It is likely that the real value for charging efficiency is between the calculated values for charging and volumetric efficiency.

After establishing the mechanisms explaining the effect of IVO at the speeds where charging efficiency peaks the investigation focuses on the speeds where it dips. Examining again Figures 6.2 and 6.6 indicates that in the regions where the charging efficiency dips there is a reduction in the amount of charge entering the cylinder during valve overlap. In all areas where this is present, apart from 3500 rpm, the biggest reduction in charge flow is observed with early IVO timing while later IVO appears less affected. This can be explained by examining the inlet and exhaust port pressures at 1750 rpm and 3500 rpm shown in Figures 6.13 and 6.14. In both figures it can

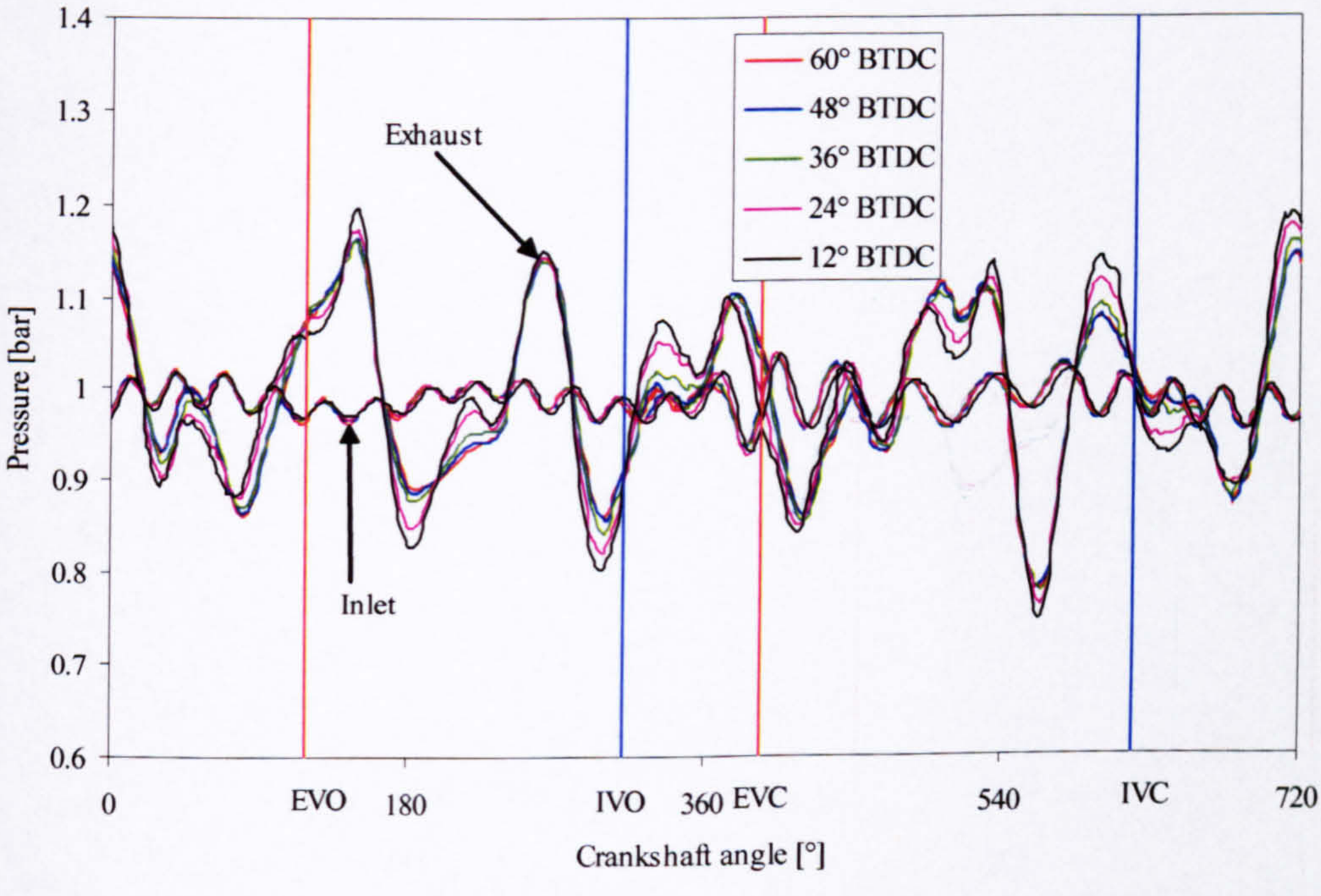

Figure 6.13: Inlet and exhaust port pressure vs. crankshaft angle with different IVO timings at 1750 rpm

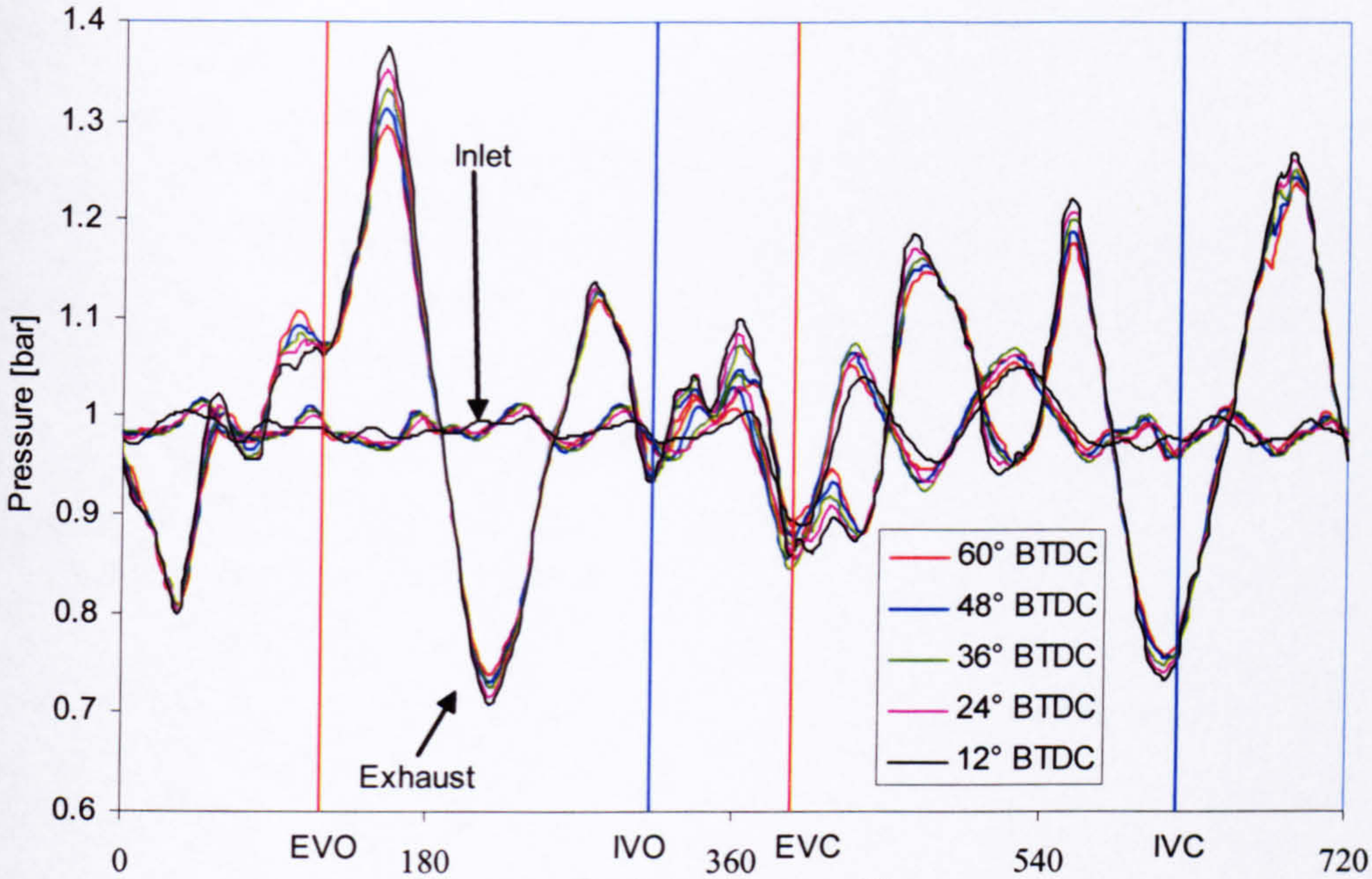

Figure 6.14: Inlet and exhaust port pressure vs. crankshaft angle with different IVO timings at 3500 rpm

be seen that during the valve overlap, the exhaust port pressure is generally higher than that of the inlet port. This is caused by the positive pressure pulse arriving at the exhaust port during this period.

Figures 6.15 and 6.16 show the calculated inlet mass flow rate with various IVO timings at 1750 rpm and 3500 rpm. It becomes apparent that the negative pressure gradient during overlap occurring at these speeds causes exhaust gas backflow and reduces the engine's charging efficiency. The quantity of backflow is affected by the IVO timing. It can be seen that a more advanced IVO timing, (e.g. 60° BTDC) allows more exhaust gas backflow into the inlet port and a later IVO (e.g. 12° BTDC) reduces it. This is because the available flow area during the overlap period increases as IVO advances and consequently the negative pressure gradient generates higher backflow. The differences in the mass flow through the inlet valve during overlap is very small compared with the difference of the trapped mass at the speeds corresponding to charging efficiency dips.

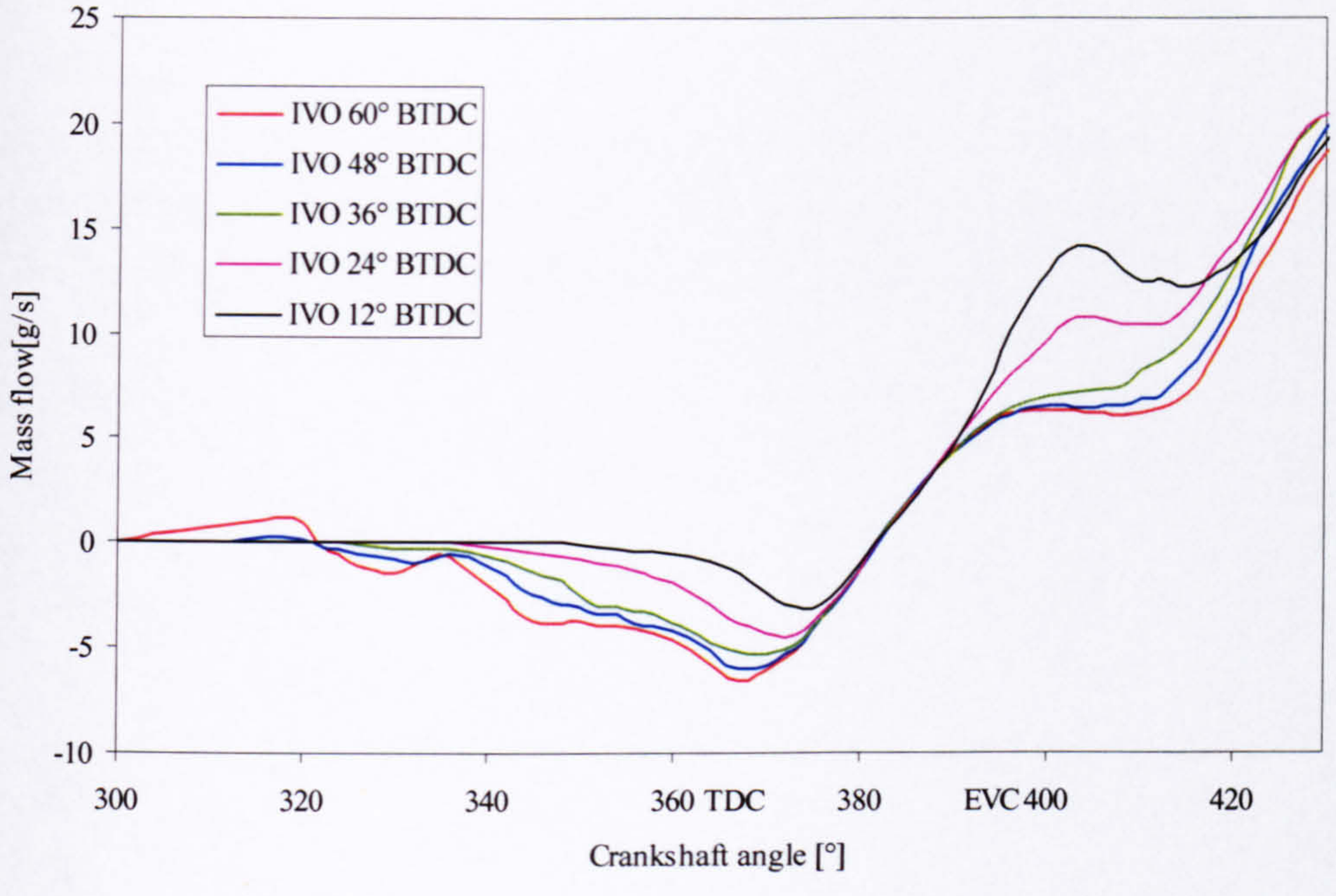

Figure 6.15: Inlet mass flow rate vs. crankshaft angle with different IVO timing at 1750 rpm

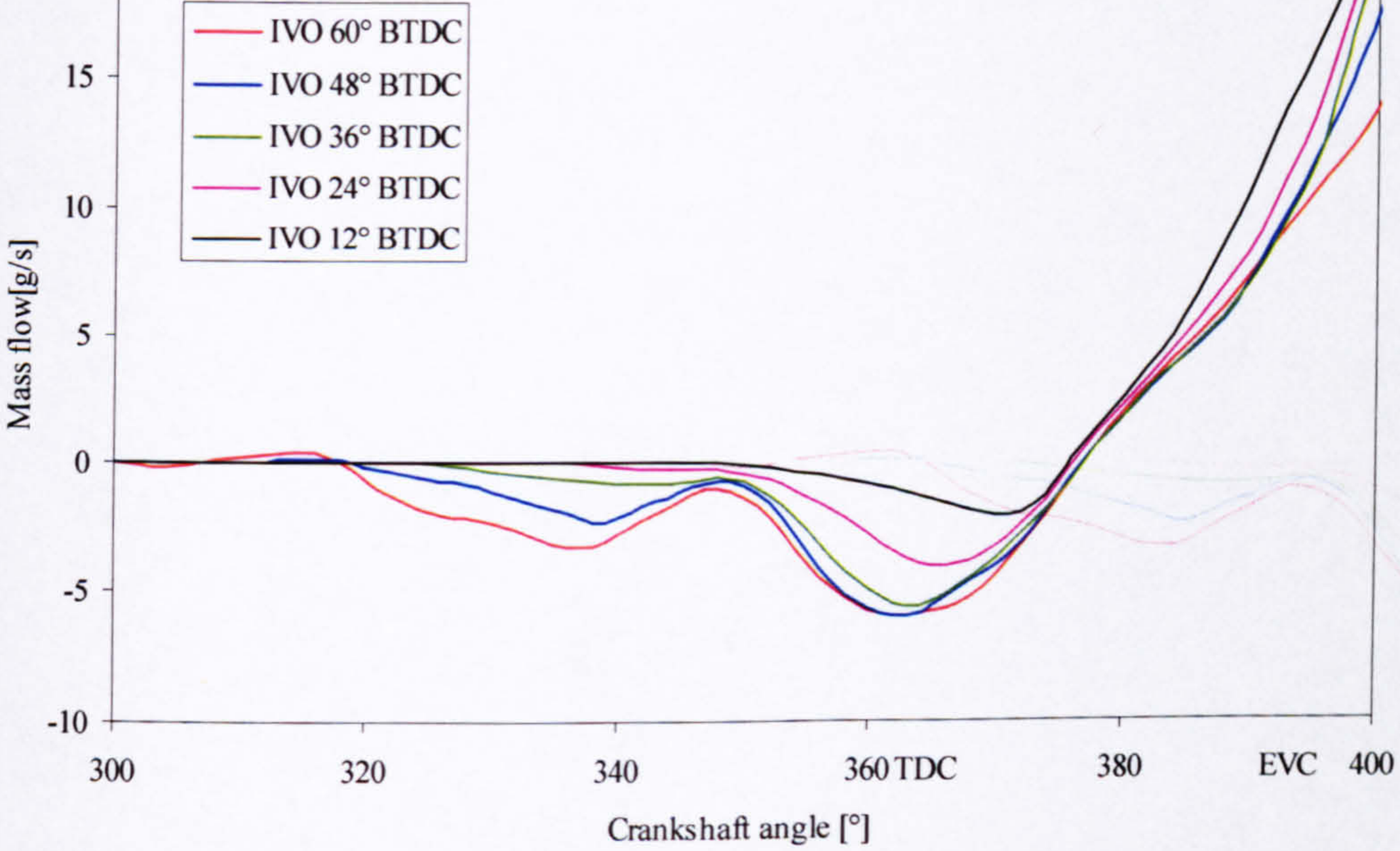

Figure 6.16: Inlet mass flow rate vs. crankshaft angle with different IVO timings at 3500 rpm

This suggests that the reduction in charging efficiency involve reduction in the mass flow during other periods of the inlet process.

6.3.2 EVC to BDC

Figure 6.6 shows that the sensitivity of the mass entering the cylinder to variations in IVO timing during this period is lower than that in the overlap period. Once the exhaust valve is closed the mass flow in the cylinder becomes a function of the inlet and cylinder pressures. It is also affected by the gas contents in the inlet port, which is related to the flow conditions during overlap and hence IVO timing. The sensitivity varies with engine speed. However, it lacks a particular pattern during most of the speed range. This can be explained with the complexity of gas dynamics commencing with IVO. The opening of the inlet valve presents a constantly changing boundary condition connecting the inlet port with the cylinder and stipulates the beginning of complex interaction between the standing pressure waves propagating in the inlet, the flow across the inlet valve and the forcing function of the piston motion.

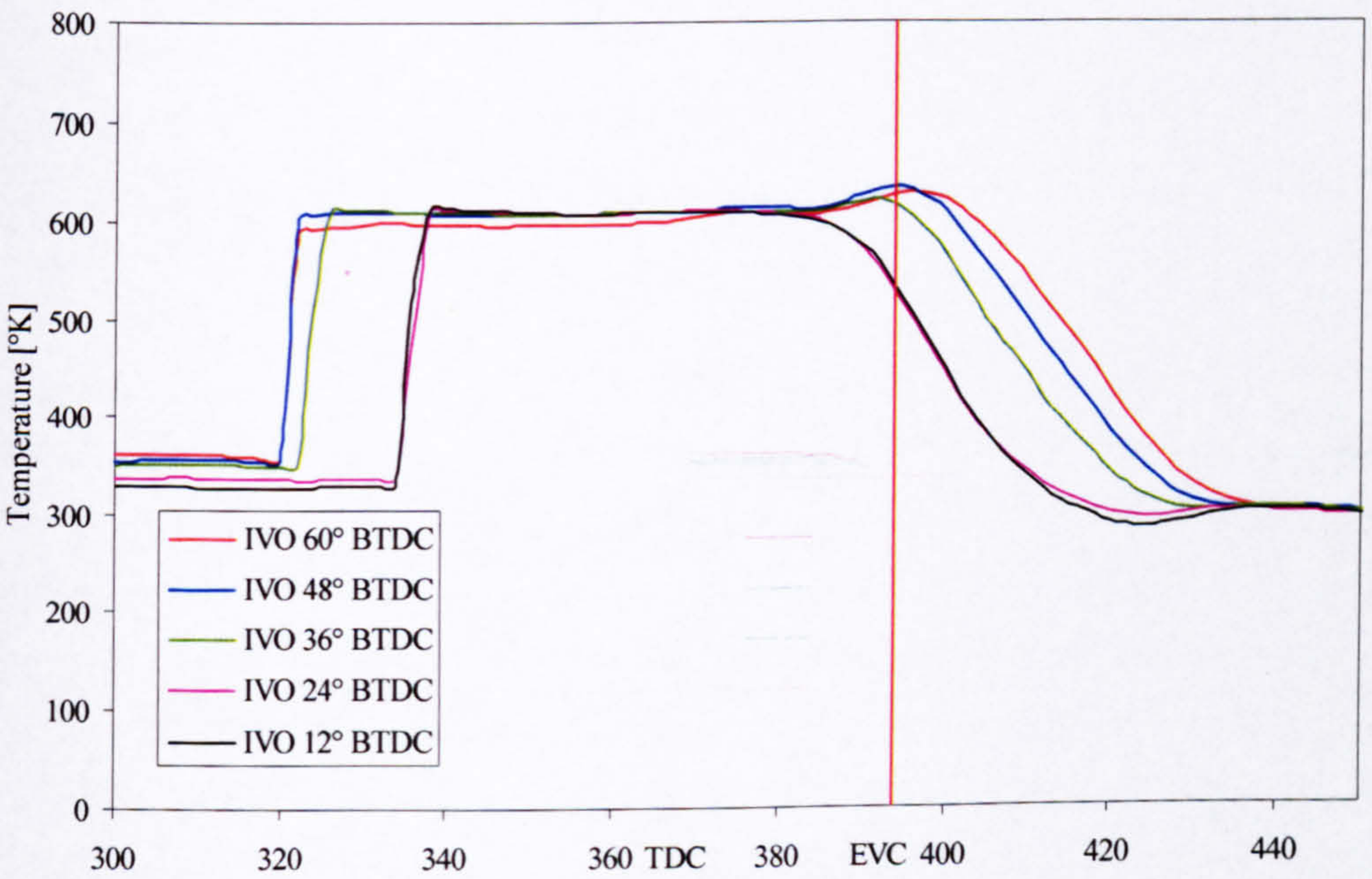

Figure 6.17: Gas temperature at inlet port vs. crankshaft angle with different IVO timing at 1750 rpm

Examining Figure 6.6 shows that the engine speeds that exhibit a particular pattern are 1750 rpm and 3500 rpm, which correspond to speeds where there are dips in the charging efficiency curve (Figure 6.2). Similarly to the overlap period discussed earlier, retarded IVO (e.g. 12° BTDC) yields the highest inhaled mass during this period at both speeds. Considering that the charging efficiency is a function of the flow during all periods of the inlet process, this can explain the low sensitivity of the mass flow during overlap to IVO found when examining Figure 6.16, compared with the high sensitivity of the charging efficiency to this parameter. Examining the actual flow through the inlet at 1750 rpm shows a dip in the flow after EVC. This is because of the lower density of the charge entering the cylinder, which contains hot residual exhaust gas. Figure 6.17 shows the temperatures of the gas flowing through the inlet ports confirms that early IVO results in higher amount of hot gases re-entering the cylinder.

6.3.3 BDC to IVC

Figure 6.6 shows that sensitivity of this period of the inlet process to IVO timing is comparatively low. It is impossible to establish a particular pattern up to 9000 rpm. It is noticeable that above that speed a more retarded IVO results in slightly higher flow during this period. This may be explained by the effect, which later IVO has on the gas dynamics in the inlet port and the cylinder filling mechanism relating to this period in the inlet process. According to the theory discussed in Chapter 5, a later IVO may cause lower inlet port pressure after the piston has passed TDC. This would results in a reflected pressure wave with higher amplitude returning at the inlet port before IVC and increasing the amount of charge entering the cylinder.

6.4 Summary of conclusions

Based on the analysis of the simulation results presented above the following conclusions for the effect of IVO timing on the gas exchange process in high-speed engines can be made:

- The main effect of the IVO timing on charging efficiency is in the speed regions where peaks or troughs occur. Early IVO timing increases the amplitudes of the peaks and dips and later IVO reduces them. This is explained by the fact that IVO timing controls the length of the valve overlap and in this way governs the

number of crankshaft degrees when the cylinder is exposed to the pressure gradient between the inlet and exhaust port.

- At engine speeds when positive pressure gradient is present across the cylinder during valve overlap an early IVO would increase the charging efficiency peaks. Whenever negative pressure gradient occurs, IVO needs to be retarded to improve the dips in the charging efficiency curve.

- IVO timing has small effect on the mass flow into the cylinder after EVC. This effect is confined to the following two phenomena. The first one relates to the speeds where backflow in the inlet occurs during valve overlap. Such backflow has a detrimental effect on cylinder filling after EVC due to the lower density of the charge re-entering the cylinder. As mentioned previously, later IVO timing can reduce this backflow. The second phenomena relates to the pressure pulsation excited by the piston in the inlet. A later IVO was found to produce slightly higher flow before IVC at higher engine speeds, possibly due to increasing the amplitudes of pressure pulsations.

- The optimal IVO timing in a high-speed engine has more complex behaviour than the ideal for medium speed engines as suggested by Asmus (1982) and Roth, (1998). The effect of this on VVA system performance is discussed in Chapter 8.

Having explored the effect of IVO timing on charging efficiency the next chapter focuses on the effect of IVC timing.

Chapter 7

Results and Discussion: II. Parametric Study of the Effects of Inlet Valve Closing Timing on the Gas Exchange Process

After discussing the effects of IVO timing on the gas exchange mechanism in Chapter 6, now the focus is on the effects of inlet IVC. According to Asmus (1982) the optimum IVC timing should be retarded with an increase of engine speed. To investigate if this is the case for high-speed engines, five valve lift profiles with different IVC timings were generated in a similar way to that described in Chapter 6 and their effect on charging efficiency was explored by using engine simulation software.

To explain the results the inlet process was divided into three sectors as suggested in Chapter 5 and the effect of the gas flow to variations of IVC timing was examined. The last period was found most sensitive to IVC timing. The effect on charging efficiency was found to be proportional to the ability to reduce the backflow after TDC caused by the gas dynamics in the inlet system.

7.1 Generation of lift curves for different IVO timings

Five different inlet lift curves were generated to give five different IVC at 12 deg intervals from 54° ATDC to 60° ATDC as detailed in Figure 7.1 and Table 7.1. In order to investigate only the effect of IVC timing and minimise the influence of variation of other parameters on the gas exchange process extra care was taken to leave other features of the lift curve unchanged. The curves were created in such a way that the lift profile from maximum lift to IVC was kept constant. Increasing the opening velocity just before maximum lift has compensated for the reduced duration. This will have a negligible effect on the gas exchange process, as it is a very small percentage of the effective flow

area. The opening lift rate, IVO timing, maximum lift and IVC rate remain the same. These lift profiles will result in poor dynamic performance of the valvetrain, but allow the exploration of IVC timing in relative isolation.

Unlike IVO there are no mechanical constraints on IVC timing. However, a judgement was made that considering the engine speed range only one more retarded IVC timing should be explored at 90° ATDC. The other three timings are more advanced.

IMOP ATDC	IVO BTDC	IVC ABDC
70°	48°	54°
82°	48°	66°
94°	48°	78°
106°*	48°*	80°*
118°	48°	92°

Table 7.1: Inlet valve lift curve parameters

(*Base line engine)

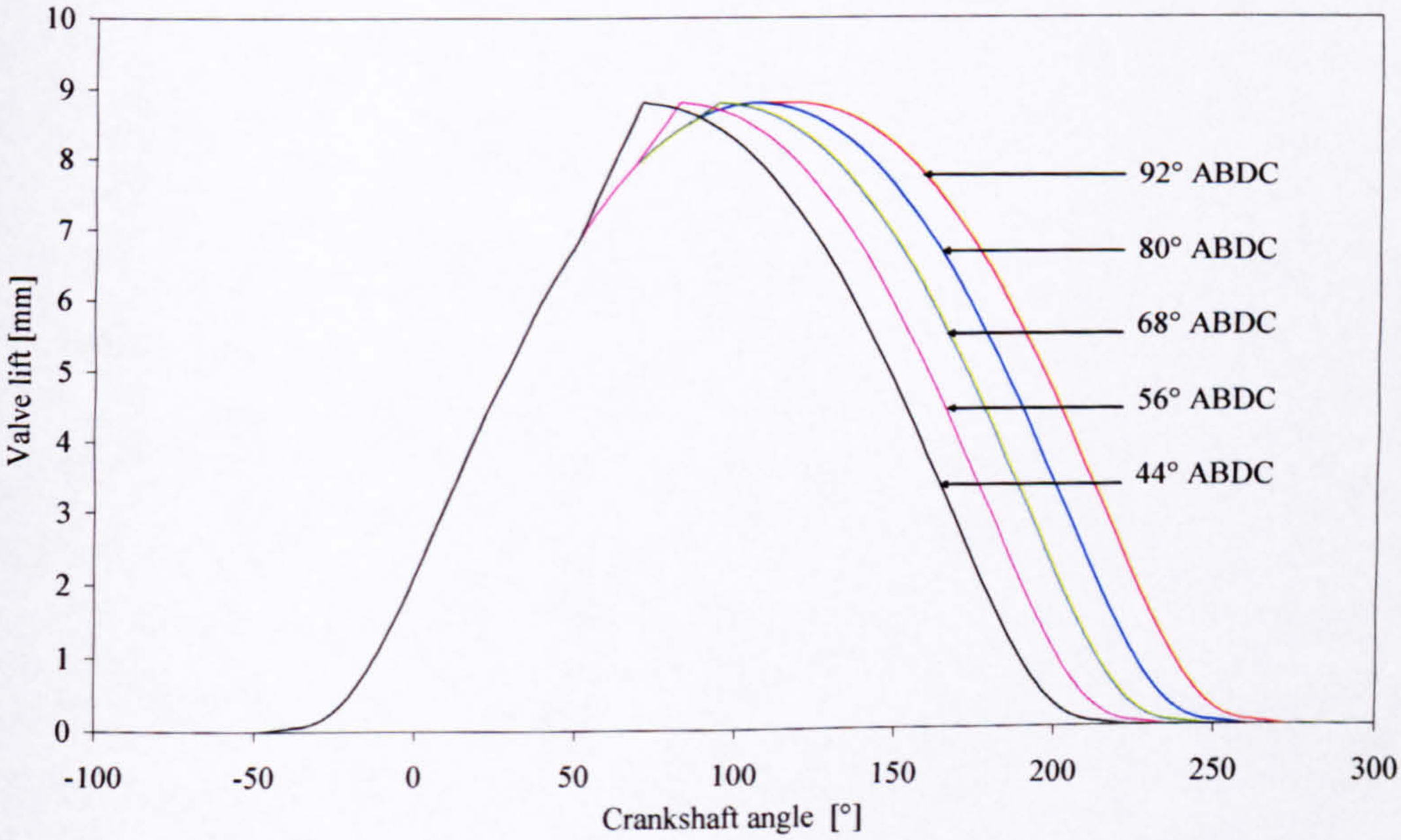

Figure 7.1: Inlet valves lift curves investigated

7.2 Simulation results

The simulation was run for steady state, WOT operation and engine speeds ranging from 1500 rpm to 13000 rpm at intervals of 250 rpm.

7.2.1 Effect of IVC timing on charging efficiency

Figure 7.2 shows the effect of IVC timing on charging efficiency. It can be seen that each curve exhibits the same peaks and troughs up to approximately 9250 rpm. The earlier IVC timings produce higher charging efficiency. For example IVC at 44° ABDC yields 113% and IVC at 90° ABDC only 96% at 7000 rpm. However, it can be noticed that this sensitivity is not proportional for different IVC ranges. For example 12° retardation from IVC at 92° ABDC to IVC at 80° ABDC results in 8 % improvement at 7000 rpm while 12° retardation from IVC at 80° ABDC to IVC at 68° ABDC produces only 6 % at the same speed. This disproportional sensitivity is a feature of the entire speed range up to 9250 rpm. As speed increases above 9250 rpm later IVC timings result in higher charging efficiency and dominate for a short speed range. For example IVC at 56° ABDC results in the highest charging efficiency in the range from 9250 rpm to 10250

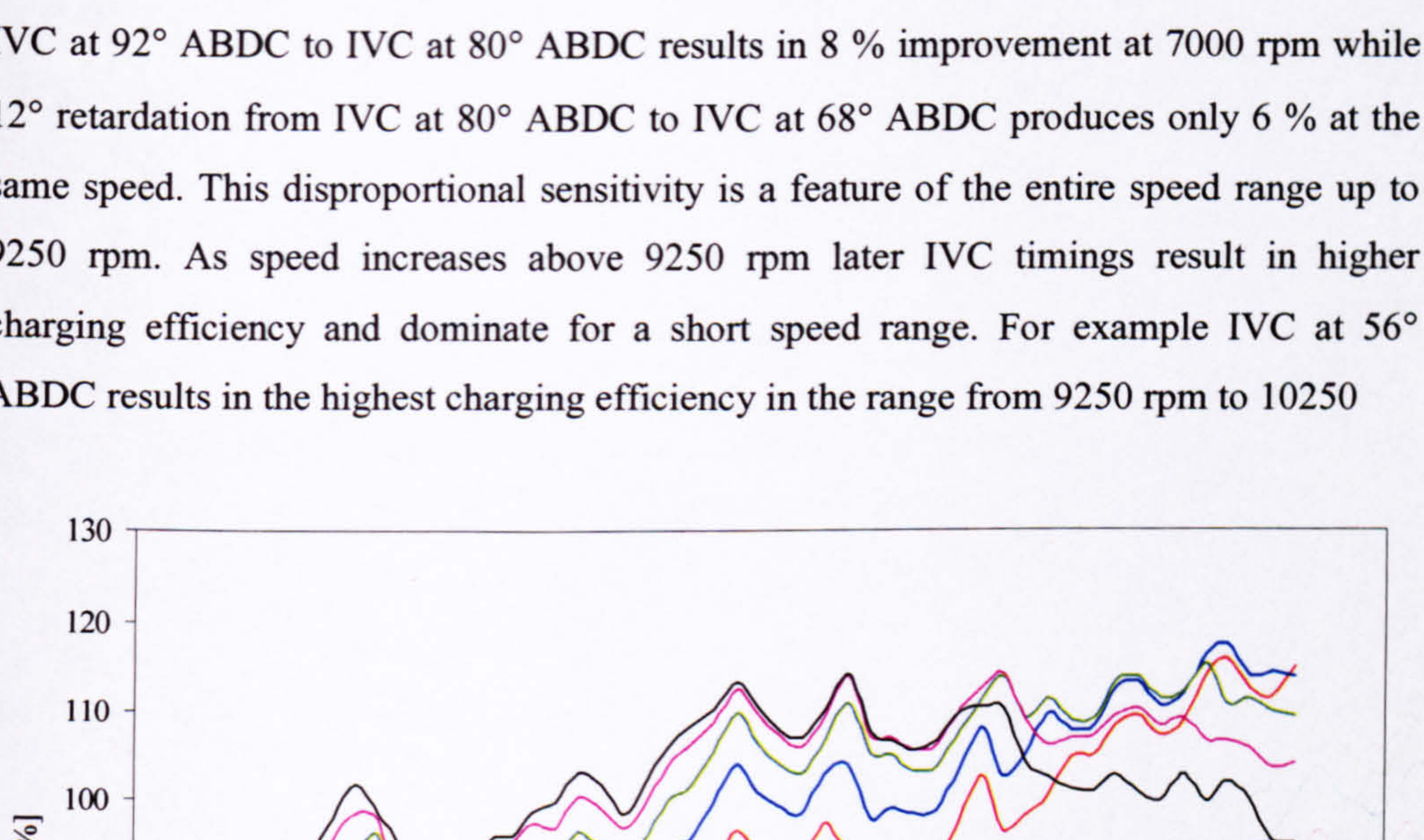

Figure 7.2: Effect of IVC timing on charging efficiency at various engine speeds

rpm. The highest charging efficiency from 10250 rpm to 12000 rpm is generated by IVC at 68° ABDC. The base IVC timing (i.e. 80° ABDC) is optimum for engine speeds above 12000 rpm apart from 13000 rpm where the most retarded IVC (i.e. 92° ABDC) yields slightly higher charging efficiency. This demonstrates that the base setting is biased towards high-speed power as can be expected in a high performance engine. The reason for such a pattern in the sensitivity to IVO timing becomes clear in the discussion section.

7.2.2 Effect of IVC timing on volumetric efficiency

The sensitivity of volumetric efficiency to IVC timing shown on Figure 7.3 is very similar to that of charging efficiency. For example, at 2500 rpm the difference between the volumetric efficiency produced by the earliest IVC (i.e. 44° ABDC) and the latest IVC (i.e. 90° ABDC) is approximately 22%, which is the same for the charging efficiency variation at this speed. Considering that the valve overlap period is responsible for any differences between the two efficiencies, this similarity suggests that the mass flow during this period is not affected.

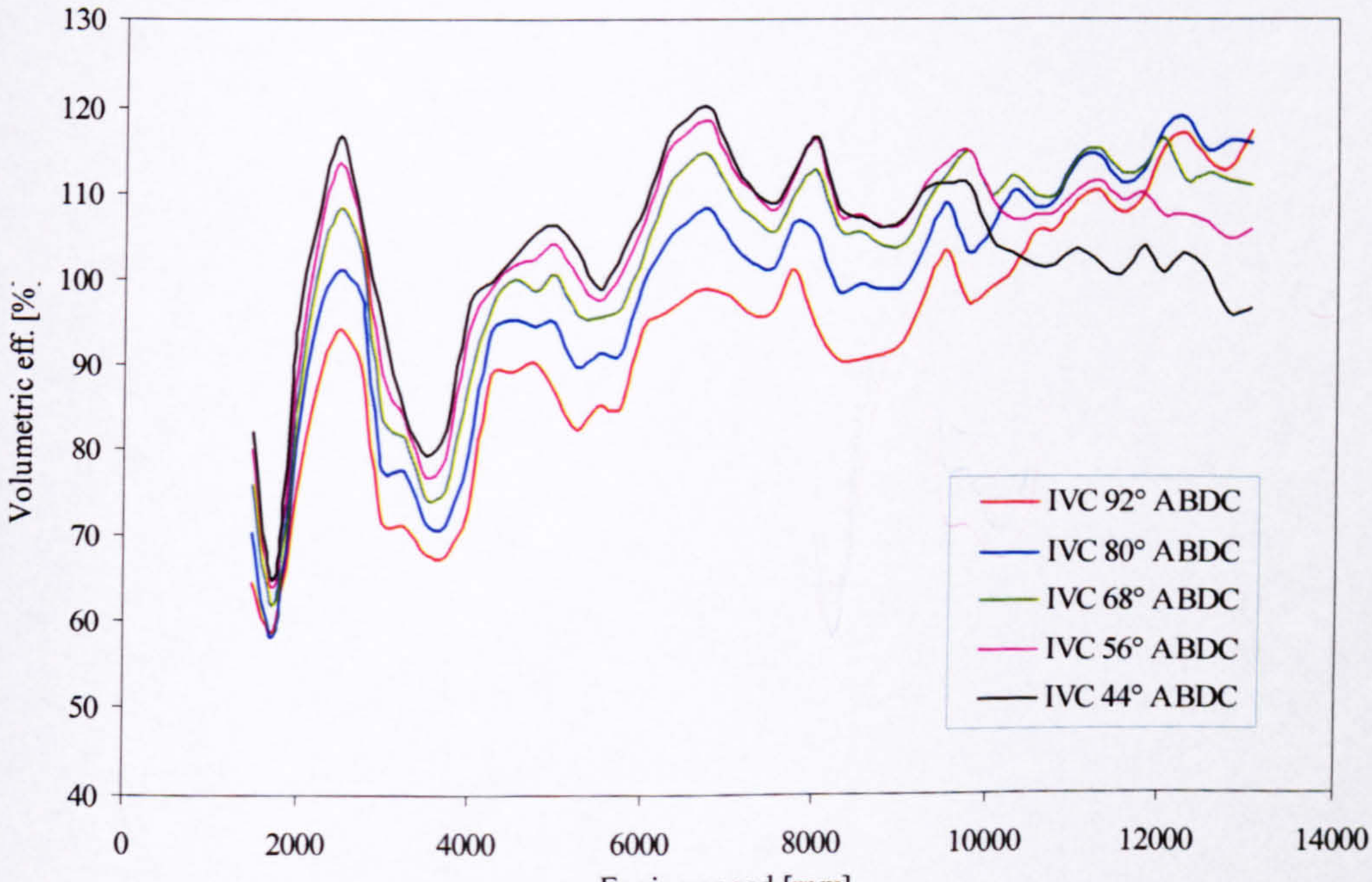

Figure 7.3: Effect of IVC timing on volumetric efficiency at various engine speeds

7.2.3 Effect of IVC timing on exhaust residuals

The fraction of exhaust residuals left in the cylinder, shown in Figure 7.4 are generally unaffected by IVC timing. This confirms the conclusion made when comparing the sensitivity of volumetric and charging efficiency regarding the mass flow during valve overlap. The speeds where different IVC timing produce exhaust residuals variation larger than 2% are 1750 rpm and 9000 rpm. The possible reasons for this are discussed in the following section.

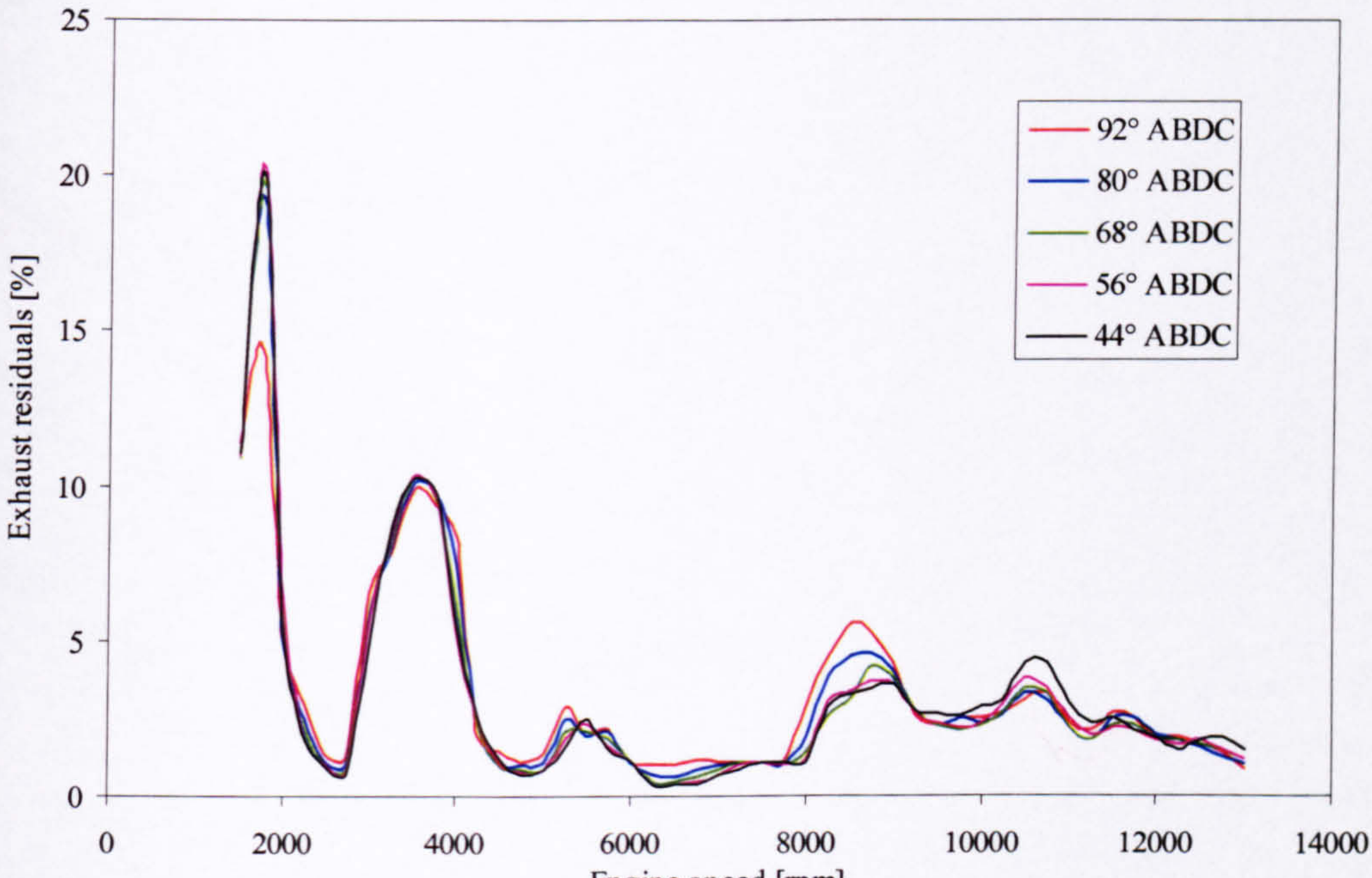

Figure 7.4: Effect of IVC timing on exhaust residuals

7.3 Discussion

In order to understand the reason for the effects of IVC timing on charging efficiency, the mass flow into the cylinder in the three different periods as described in Chapter 5 is considered. Figure 7.5 indicates the calculated mass entering the cylinder for the first two periods of the inlet process with different IVC timing. It can be seen that the mass entering the cylinder during overlap (i.e. IVO-EVC) is generally unaffected. Any variation coincides with the speeds when the exhaust residuals were affected e.g. 1750 rpm and 9000 rpm.

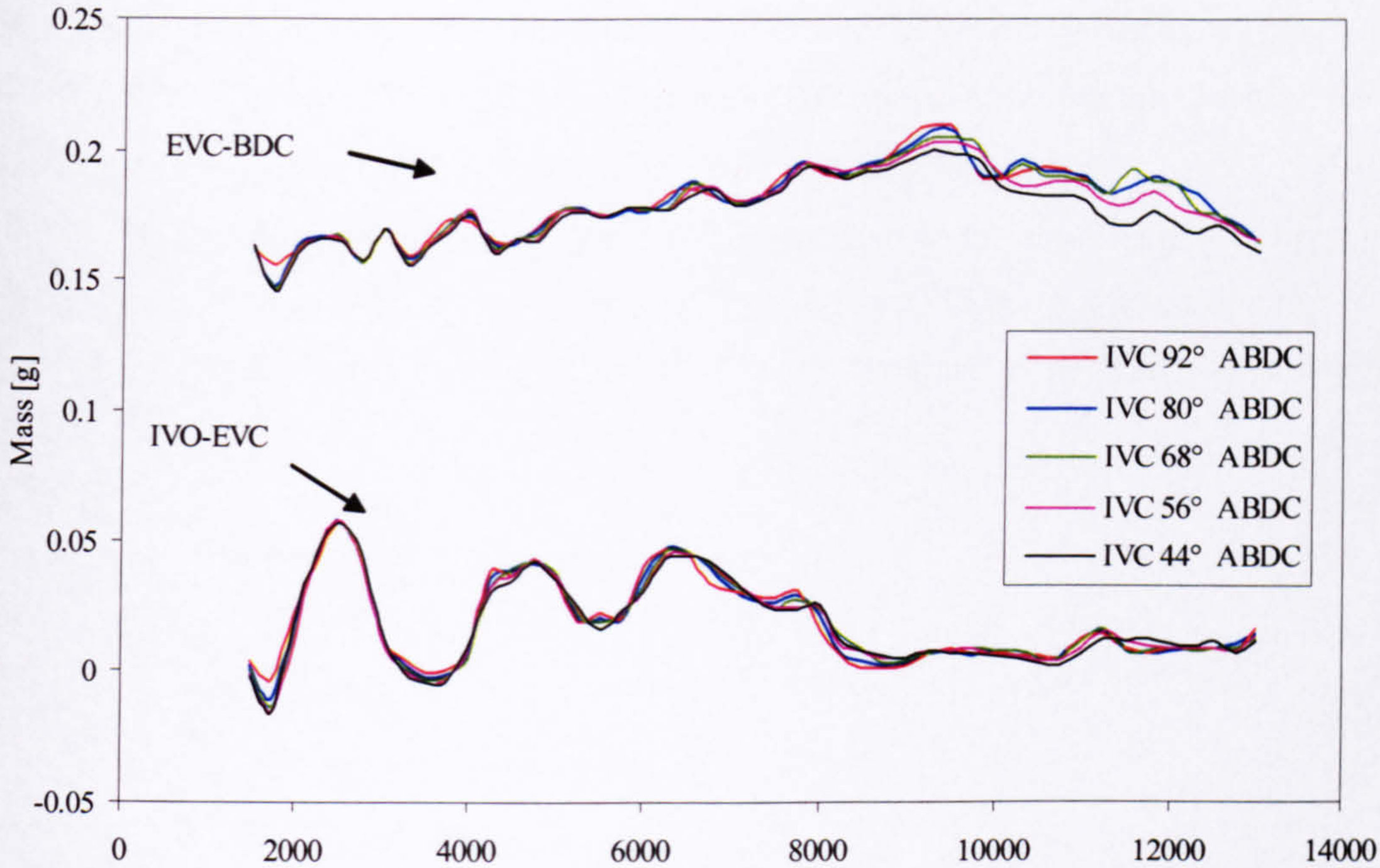

Figure 7.5: Effect of IVC timing on the mass inhaled by the cylinder during different periods of the intake process at various engine speeds

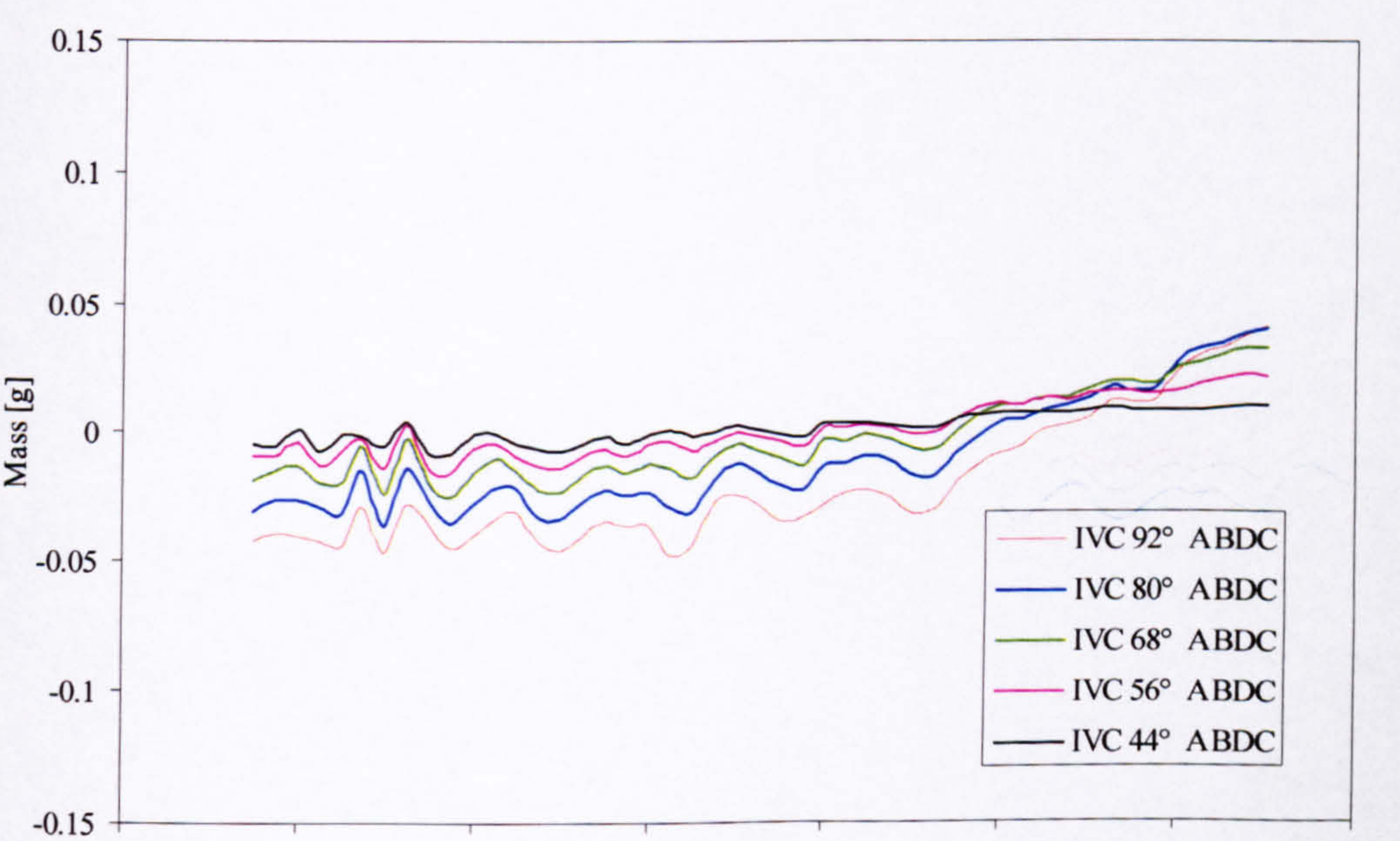

Figure 7.6: Effect of IVC timing on the mass inhaled by the cylinder in the period BDC-IVC at various engine speeds

The mass entering the cylinder during the period from EVC to BDC (Figure 7.5) is generally insensitive to variations of IVC timing. However above 8000 rpm later IVC timings result in a slightly higher mass inhaled by the cylinder during this period.

Figure 7.6 demonstrates the large effect of IVC timing on the mass flow in the last period of the inlet process. Comparing Figures 7.5 and 7.6, which are plotted with the same scale shows that this is the most sensitive period of the inlet process. Up to engine speeds of 8000 rpm the more advanced IVC timings produce higher mass flow. For example IVC at 44° ABDC yields the highest mass inhaled during this period. As speed increases above 8000 rpm later IVC result in higher mass flow. The reasons for this sensitivity are explained in the following discussion by exploring the mass flow through the inlet valve and the pressure gradient across the cylinder at three different engine speeds.

1750 rpm

Figures 7.7, 7.8, 7.9, 7.10 and 7.11 show the inlet port and cylinder pressure for IVC at 92° ABDC, 80° ABDC, 68° ABDC, 56° ABDC and 44° ABDC at 1750 rpm. All findings based on this speed are generally valid up to 8000 rpm. It can be seen that for all IVC timings the cylinder pressure and inlet pressure are very similar during most of the inlet period. However, the cylinder pressure quickly rises above the port pressure soon after BDC (point indicated on Figure 7.7). This produces negative pressure gradient across the inlet valve. Comparing all five figures shows that the crankshaft angle when this negative pressure gradient first occurs is approximately the same. However, the magnitude that is reached at IVC depends on the IVC timing. For example Figure 7.7 shows that the pressure difference (as indicated on the figure) has reached 0.4bar when IVC occurs at 90° ABDC. This is significantly higher that the 0.1 bar pressure difference (as indicated on the figure) when the inlet valve closes at 44° ABDC shown in Figure 7.12. These examples demonstrate the ability of IVO to control the crankshaft angle window when there is a negative pressure gradient across the inlet valve.

As discussed in chapter 5 such negative pressure gradient across the inlet valve results in reverse flow from the cylinder into the inlet port. Such reverse flow reduces the charging efficiency of the engine. The flow during the inlet period for all five IVC timings at

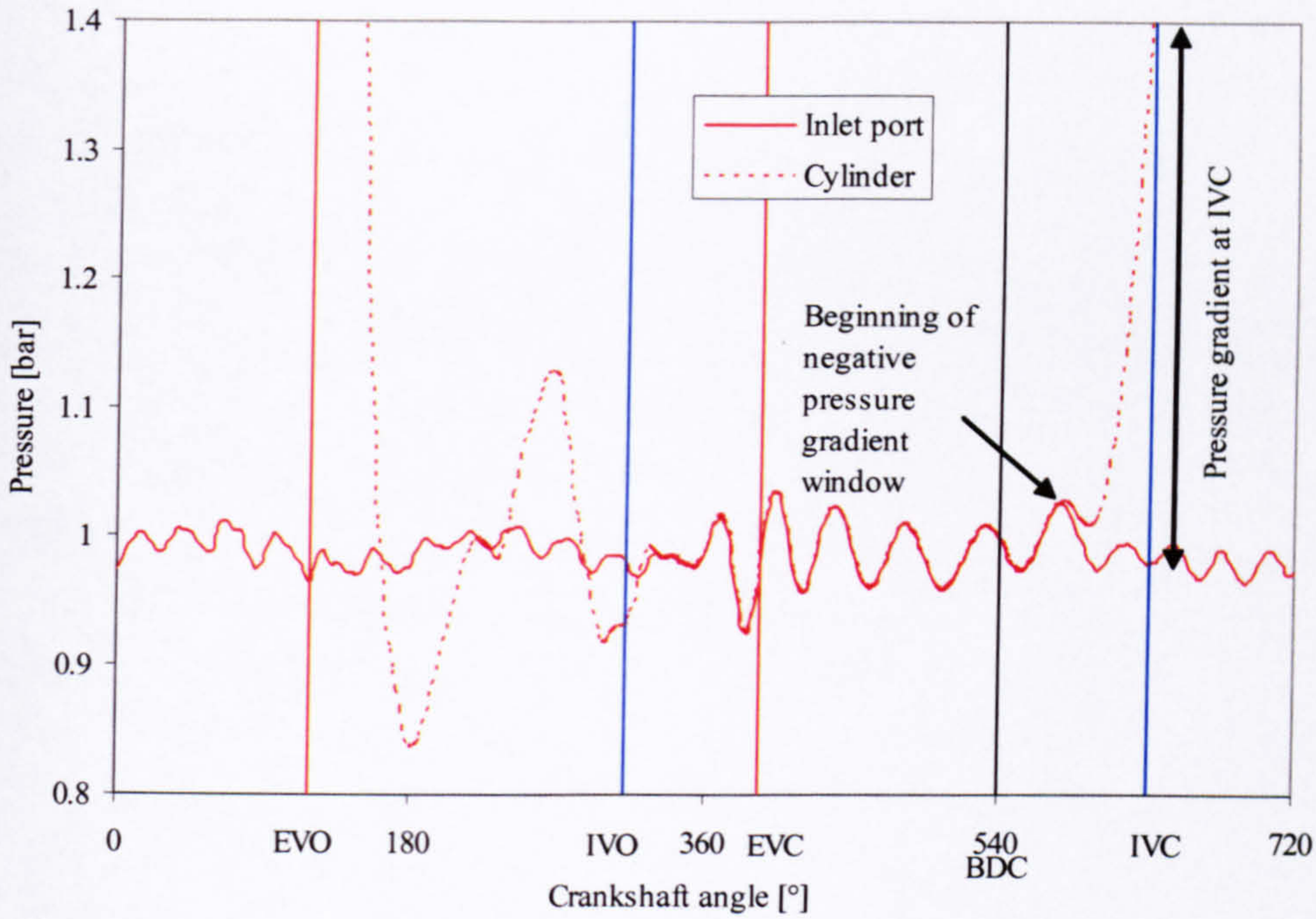

Figure 7.7: Inlet port and cylinder pressure vs. crankshaft angle at 1750 rpm with IVC 92° ABDC

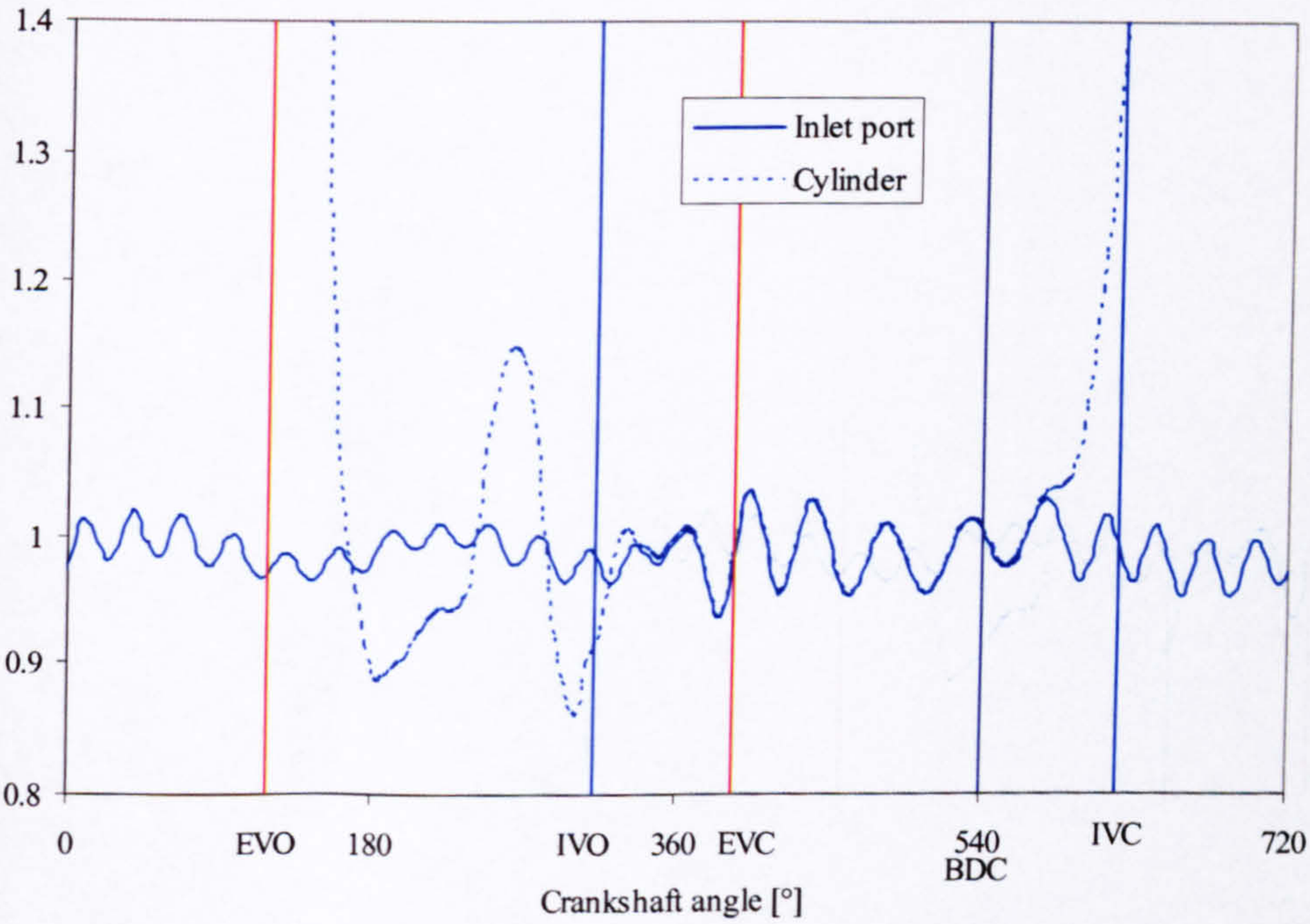

Figure 7.8: Inlet port and cylinder pressure vs. crankshaft angle at 1750 rpm with IVC 80° ABDC

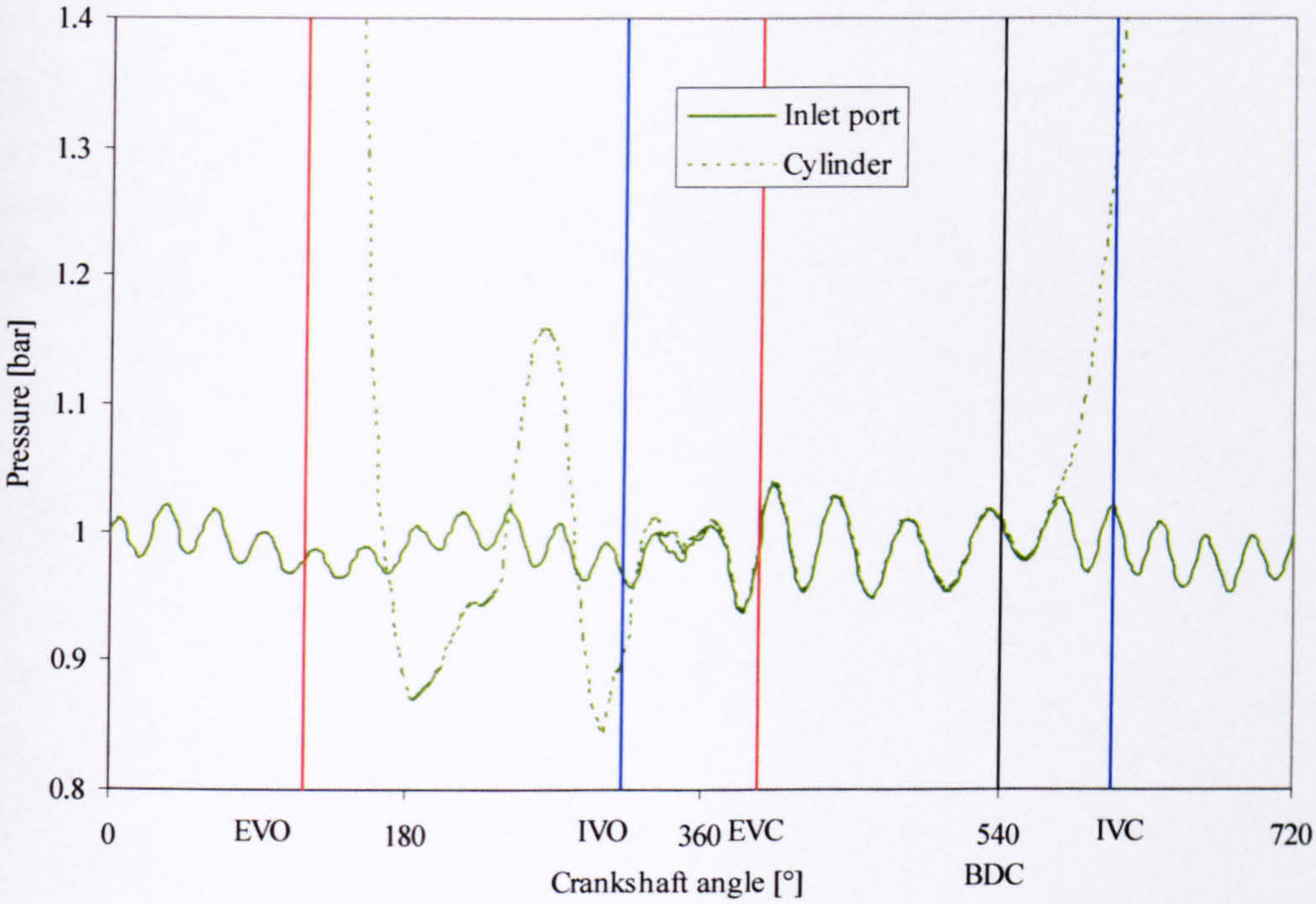

Figure 7.9: Inlet port and cylinder pressure vs. crankshaft angle at 1750 rpm with IVC 68° ABDC

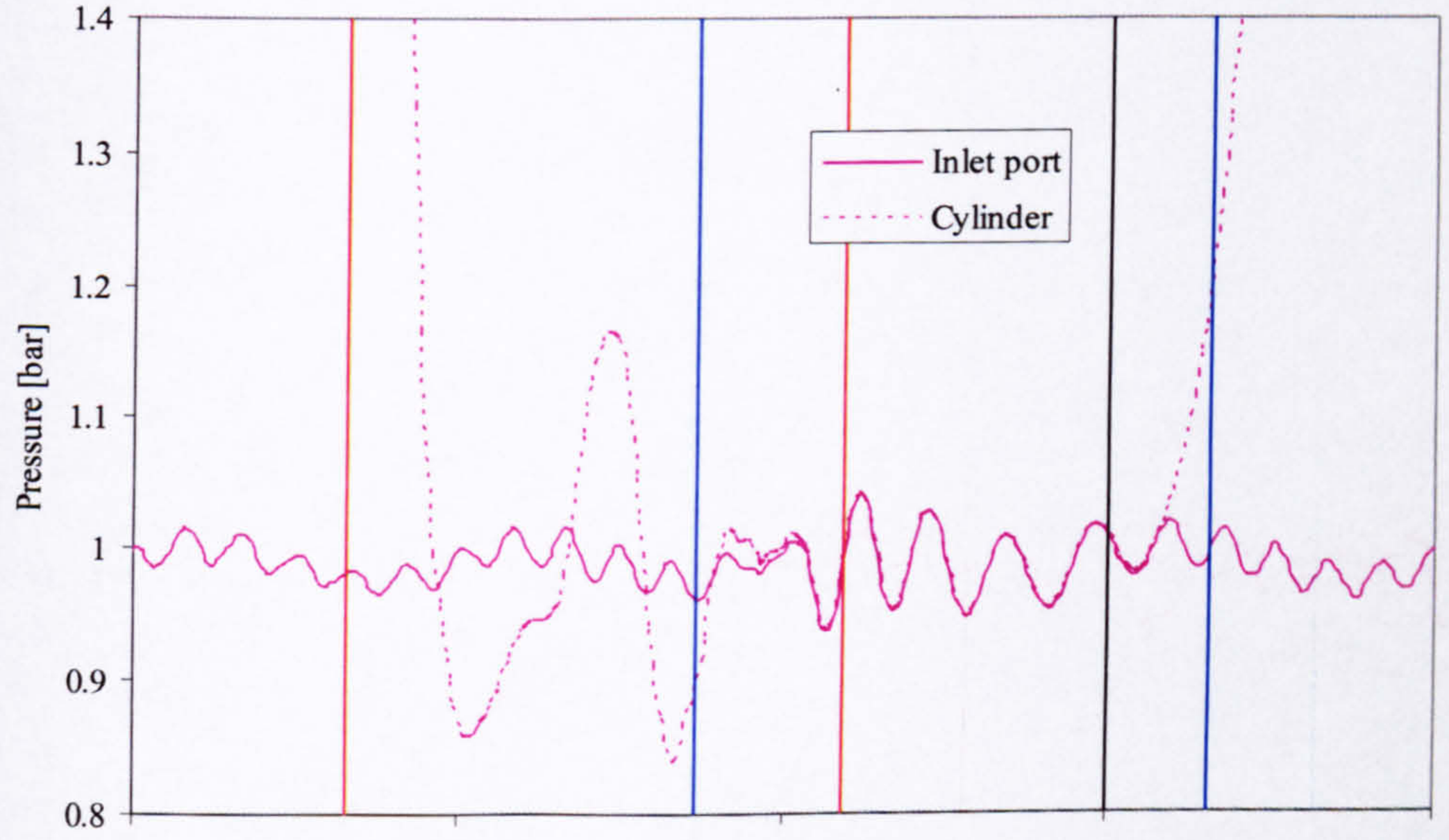

Figure 7.10: Inlet port and cylinder pressure vs. crankshaft angle at 1750 rpm with IVC 56° ABDC

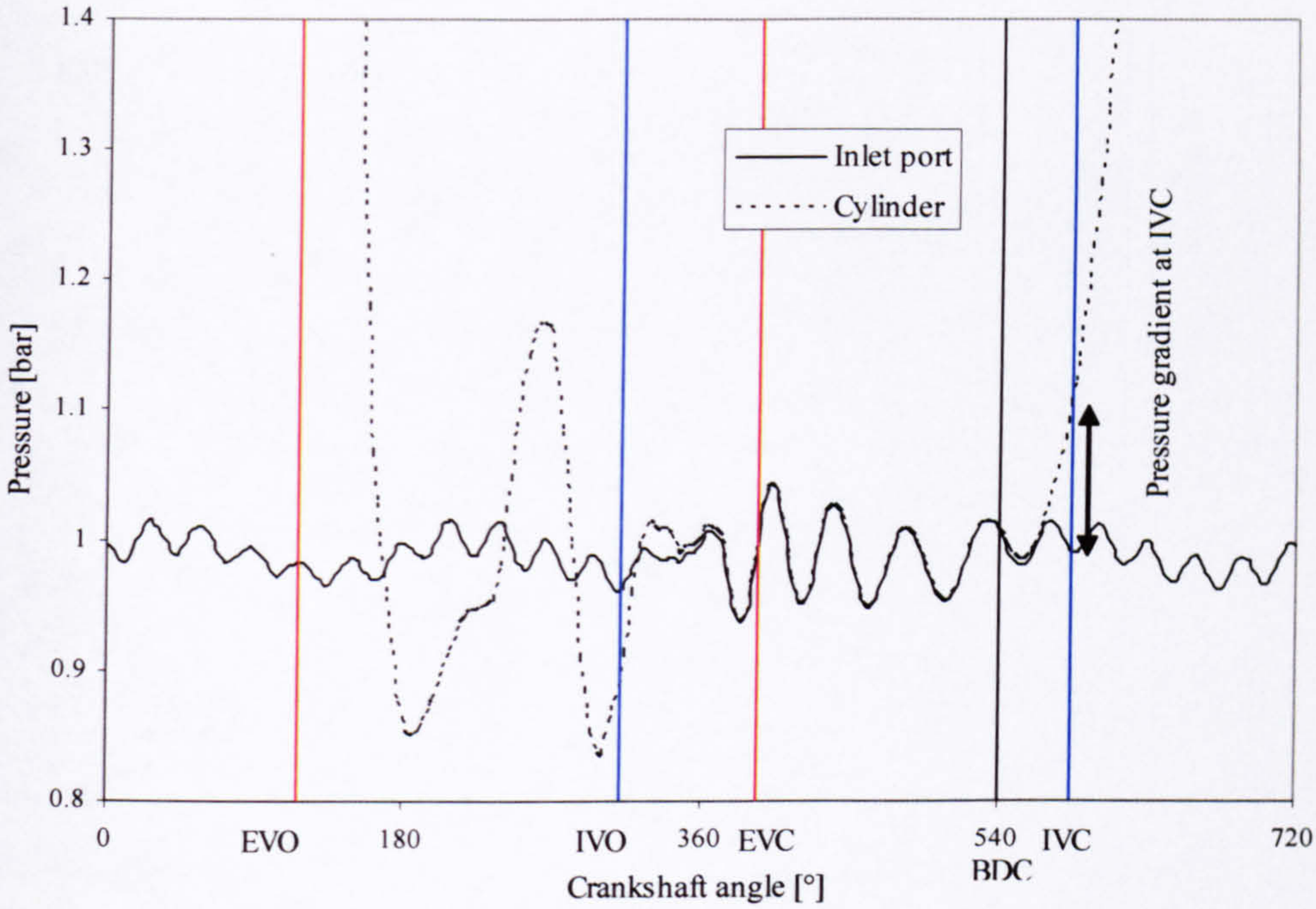

Figure 7.11: Inlet port and cylinder pressure vs. crankshaft angle at 1750 rpm with IVC 44° ABDC

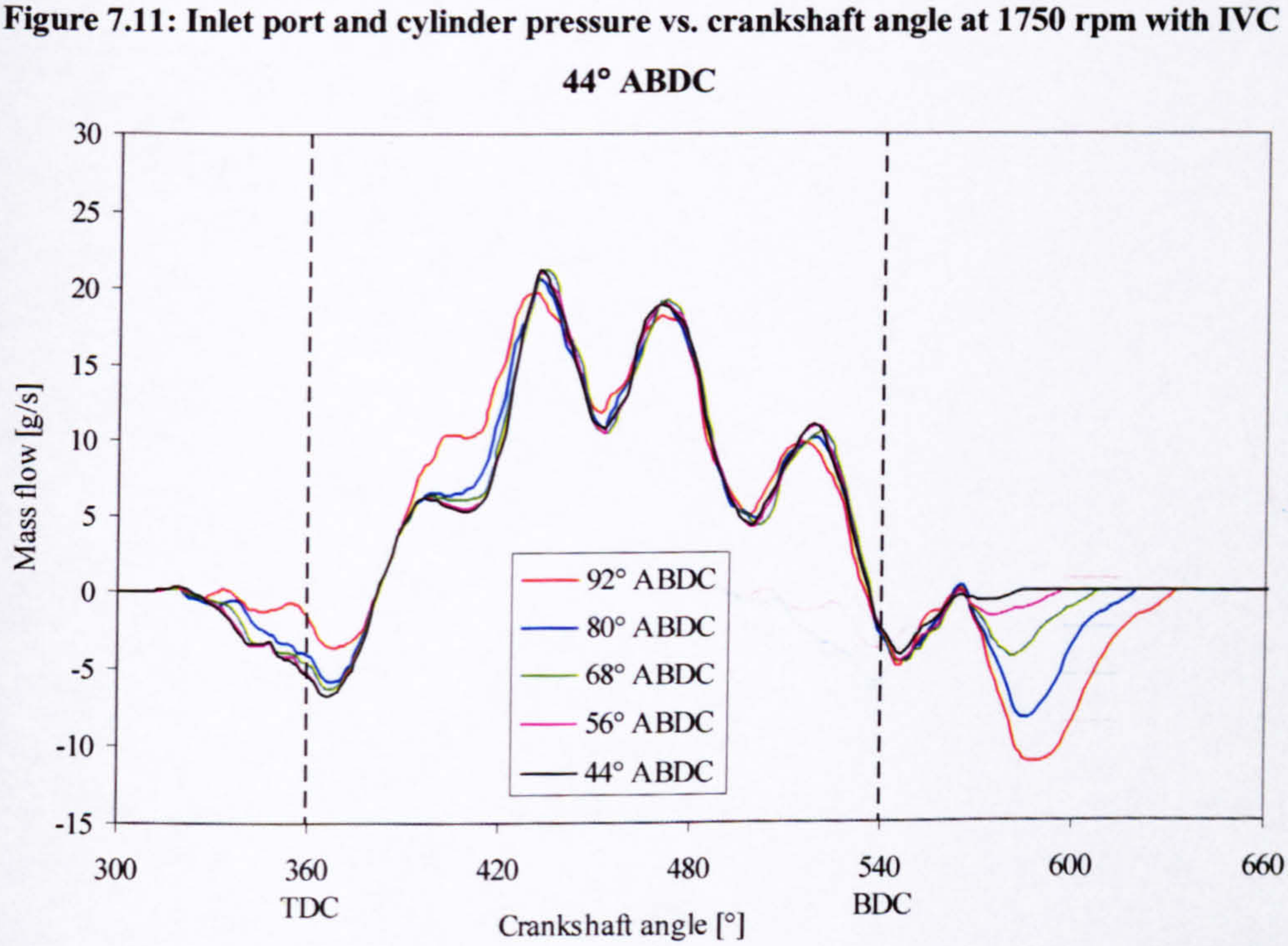

Figure 7.12: Inlet valve flow vs. crankshaft angle with different IVC timings at 1750 rpm

1750 rpm is shown in Figure 7.12. It can be seen that the flow during the inlet process is very similar during both IVO to EVC and IVC to BDC period for all IVC timings. There is a very slight reduction in backflow during valve overlap for later IVC timings. This is especially pronounced for IVO timing of 90° ABDC. Its flow curve shows the lowest backflow during overlap and is least affected by the dip soon after EVC, the reasons for which were described in detail in Chapter 6. This backflow is caused by a negative pressure gradient and there are two possible causes. The first one relates to a very small phase shift in inlet pressure pulsations caused by variations in IVC timing. This is most easily noticeable by examining a combined plot of the inlet port pressure vs. crankshaft angle for all five IVC timings at 1750 rpm shown in Figures 7.13. The second possible cause is the fact that the different IVC produce different charging efficiencies and therefore peak cylinder pressures. This means that there is different magnitude of excitation for the pressure in the exhaust pipe. It should be noted that cylinder pressure follows closely exhaust port pressure during most of the time the exhaust valve is open, therefore it varies with IVC timing. These are likely to be the reasons for the small sensitivity of the exhaust residuals observed in Figure 7.4 and mass inhaled during overlap observed in Figure 7.5 at certain speeds.

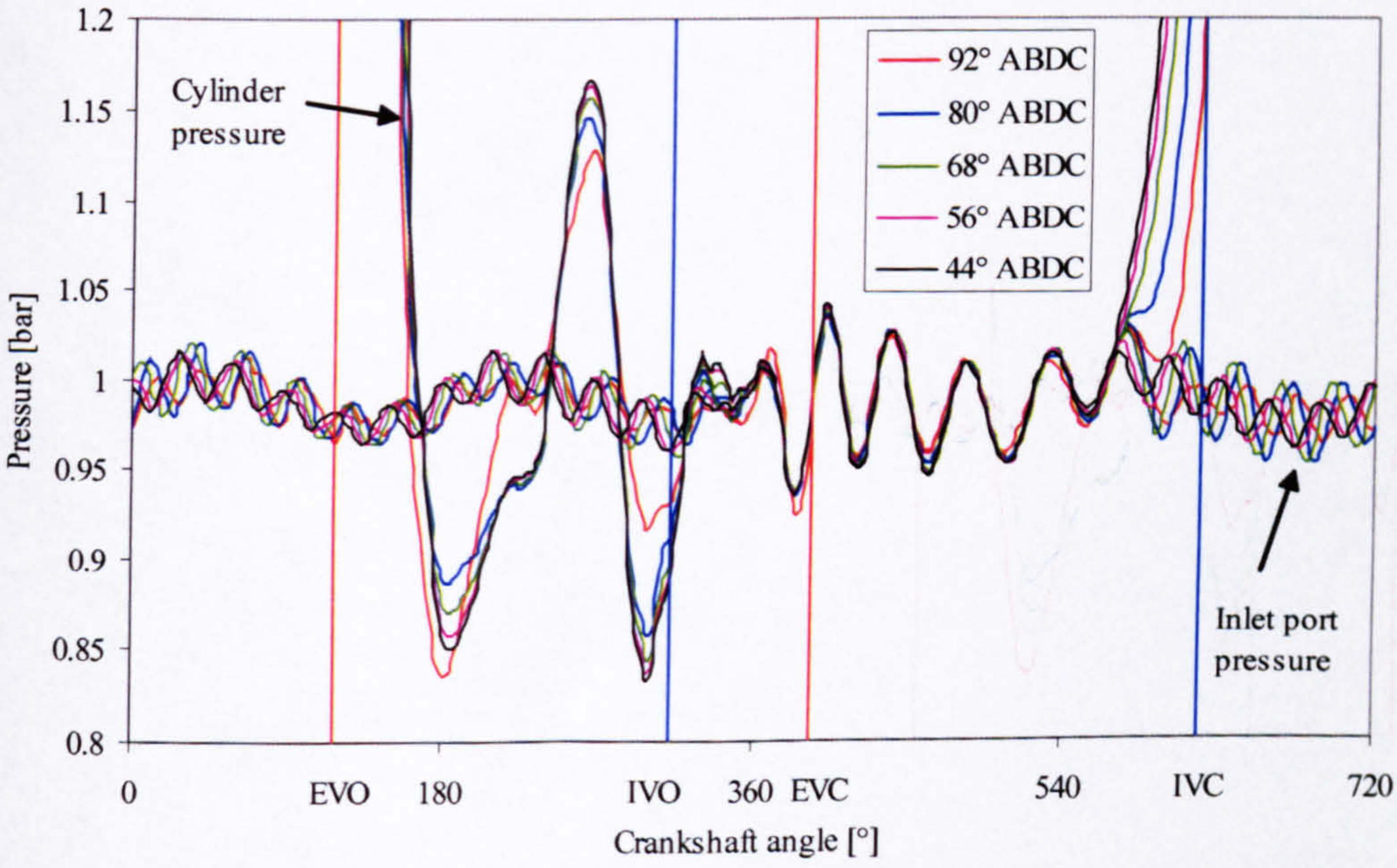

Figure 7.13: Inlet port and cylinder pressure vs. crankshaft angle at 1750 rpm with IVC 92° ABDC

Figure 7.12 shows that after BDC there is reverse flow into the inlet for all test cases and IVC timing has large effect on how much charge is returned into the cylinder. It can be seen that the earlier the inlet valve closes the less is the backflow. This explains why earlier IVC produces the highest charging efficiency typical for engine speeds up to 8000 rpm.

8000 rpm

Figures 7.14, 7.15, 7.16, 7.17 and 7.18 show inlet and cylinder pressures for IVC at 92° ABDC, 80° ABDC, 68° ABDC, 56° ABDC and 44° ABDC for 8000 rpm. Examining these figures shows that the inlet port pressure after TDC is higher than the cylinder pressure during the IVC to BDC period. The inlet pressure is slightly higher than the cylinder pressure for a few degrees after BDC after which the cylinder pressure rises suddenly in a similar way to 1750 rpm. The reason for this is the return of the reflected negative pressure wave initiated by the piston motion as a positive wave near BDC. At this speed the pressure pulsations in the inlet pipe become significant for cylinder filling after BDC. This observation is most apparent for 56° ABDC and 44° ABDC shown in

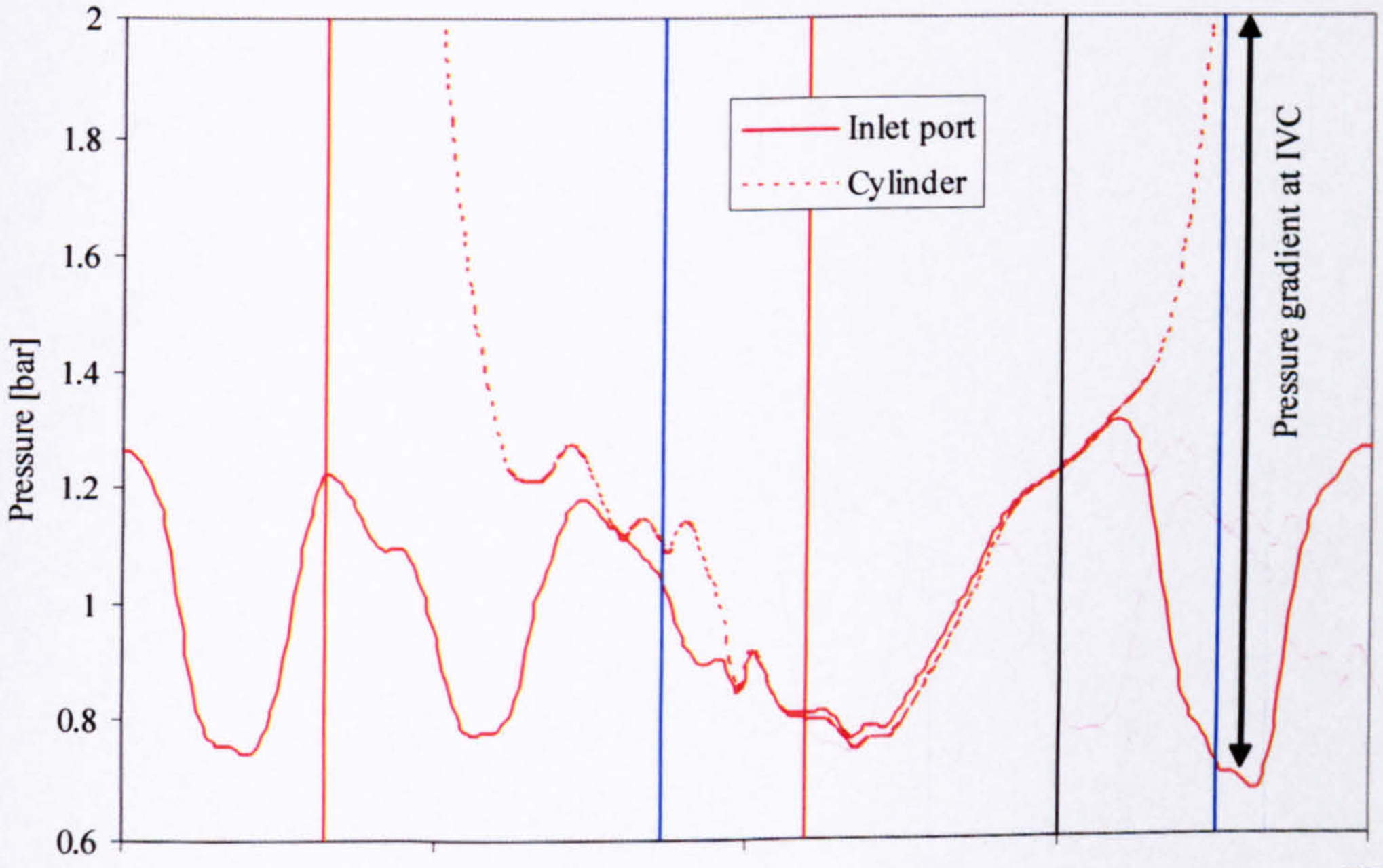

Figure 7.14: Inlet port and cylinder pressure vs. crankshaft angle at 8000 rpm with IVC 92° ABDC

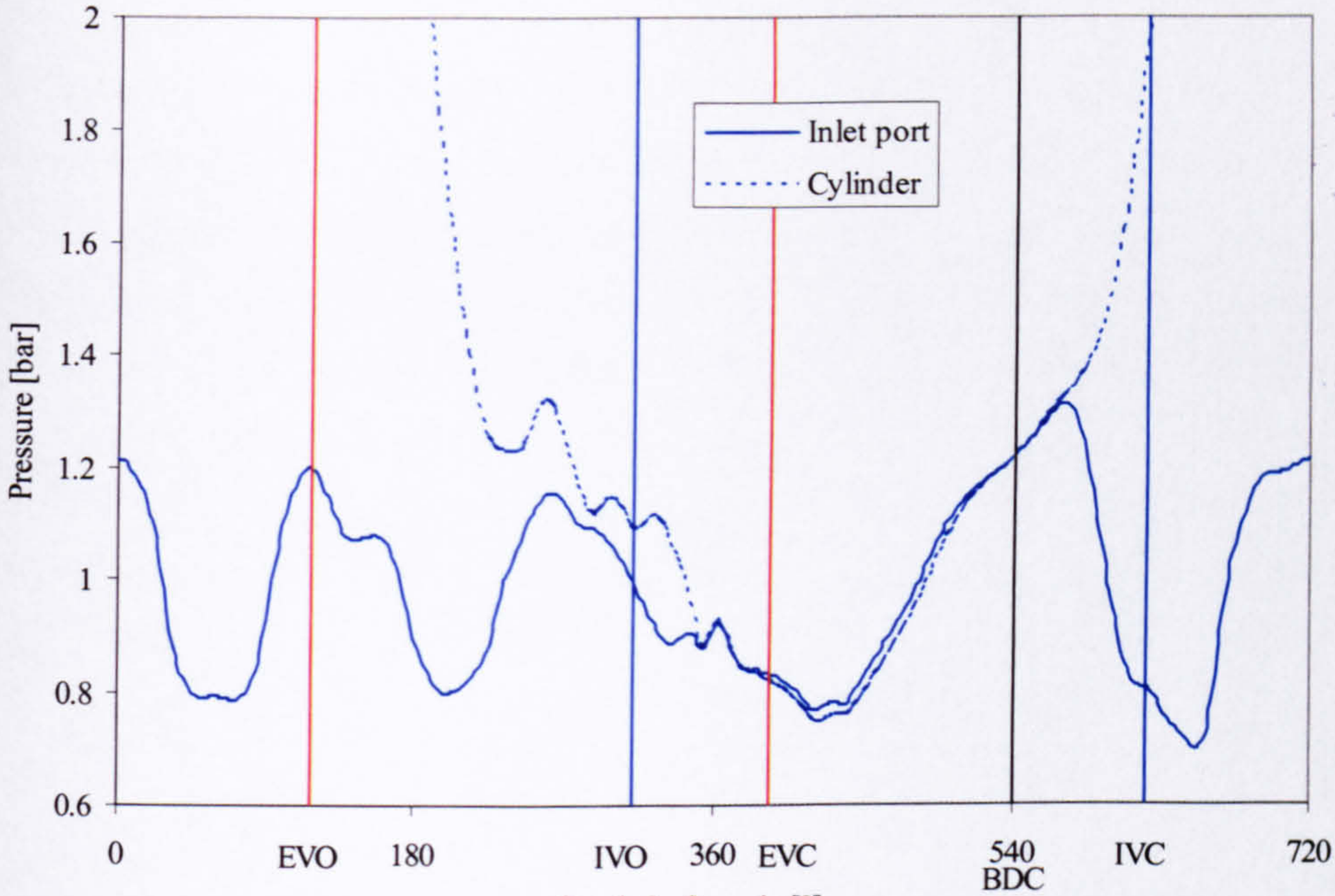

Figure 7.15: Inlet port and cylinder pressure vs. crankshaft angle at 8000 rpm with IVC 80° ABDC

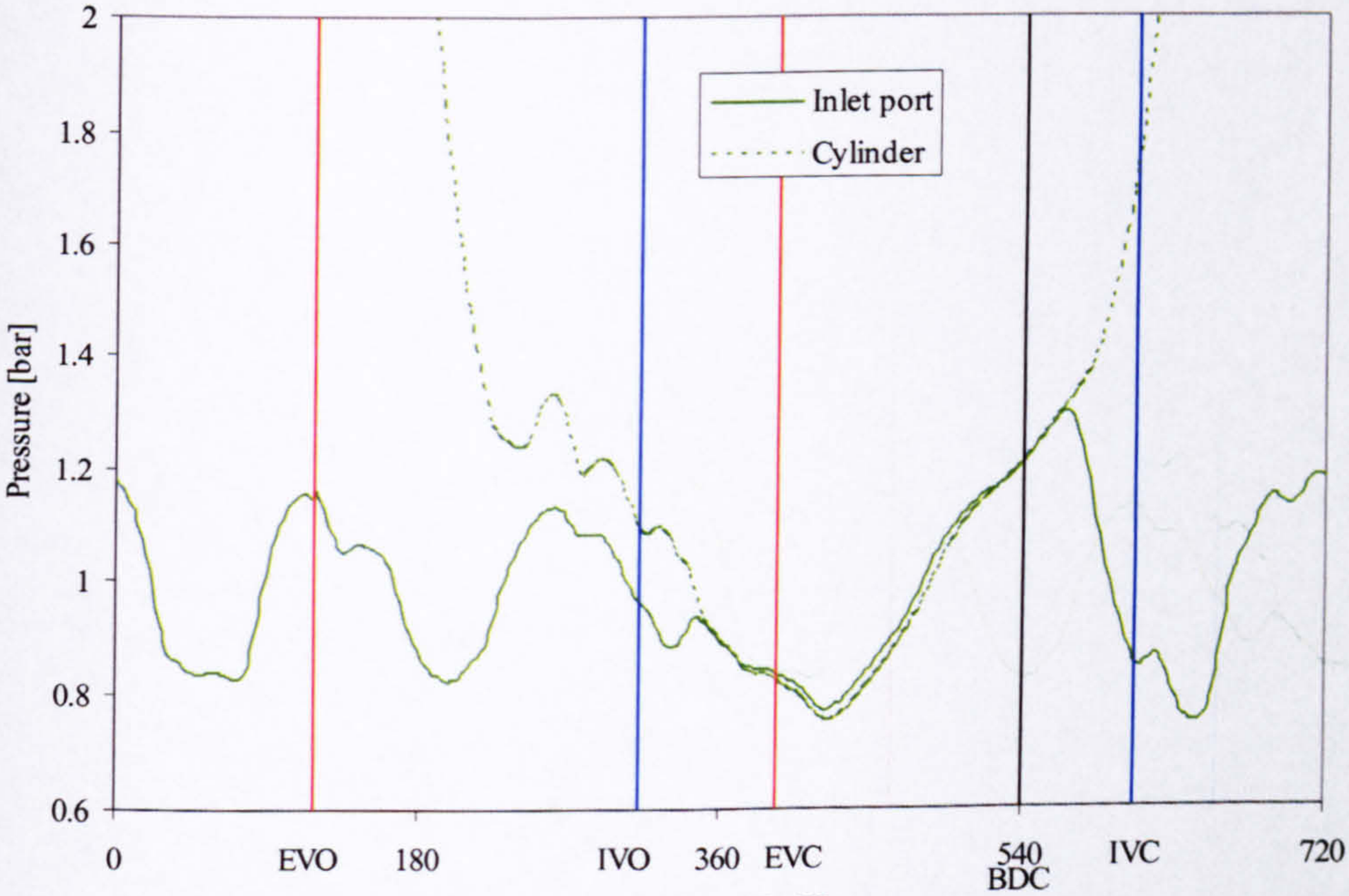

Figure 7.16: Inlet port and cylinder pressure vs. crankshaft angle at 8000 rpm with IVC 68° ABDC

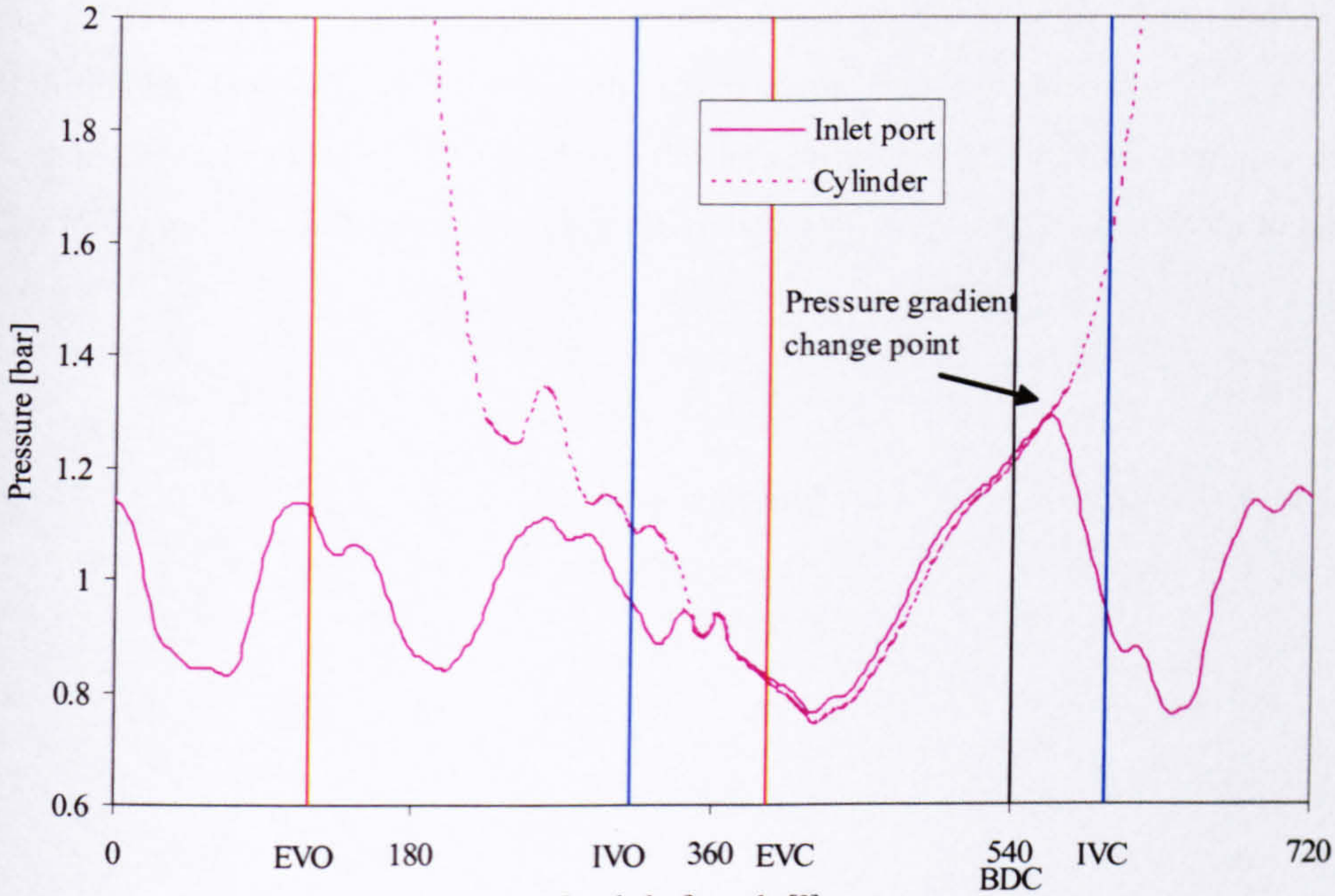

Figure 7.17: Inlet port and cylinder pressure vs. crankshaft angle at 8000 rpm with IVC 56° ABDC

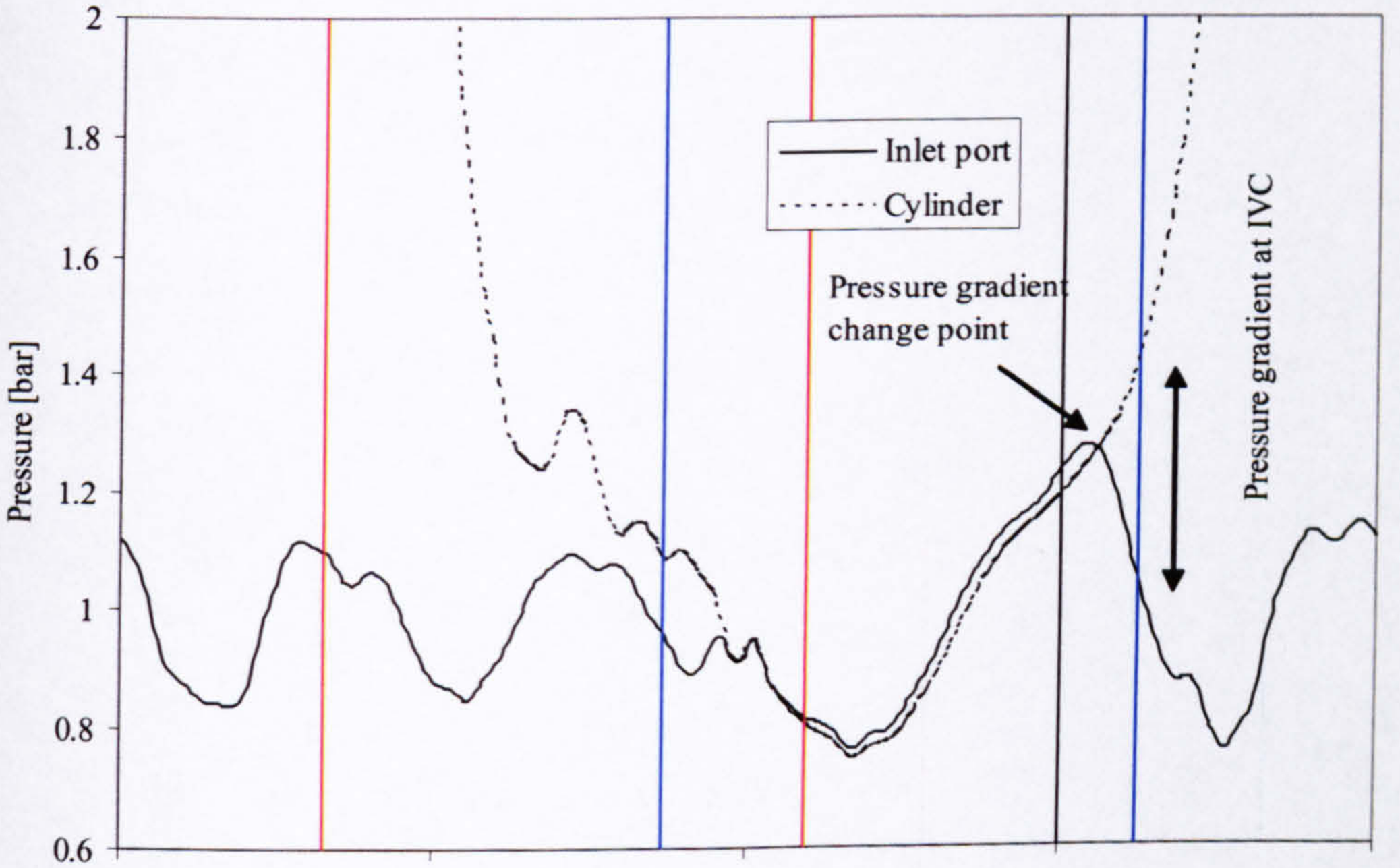

Figure 7.18: Inlet port and cylinder pressure at 8000 rpm with IVC 44° ABDC

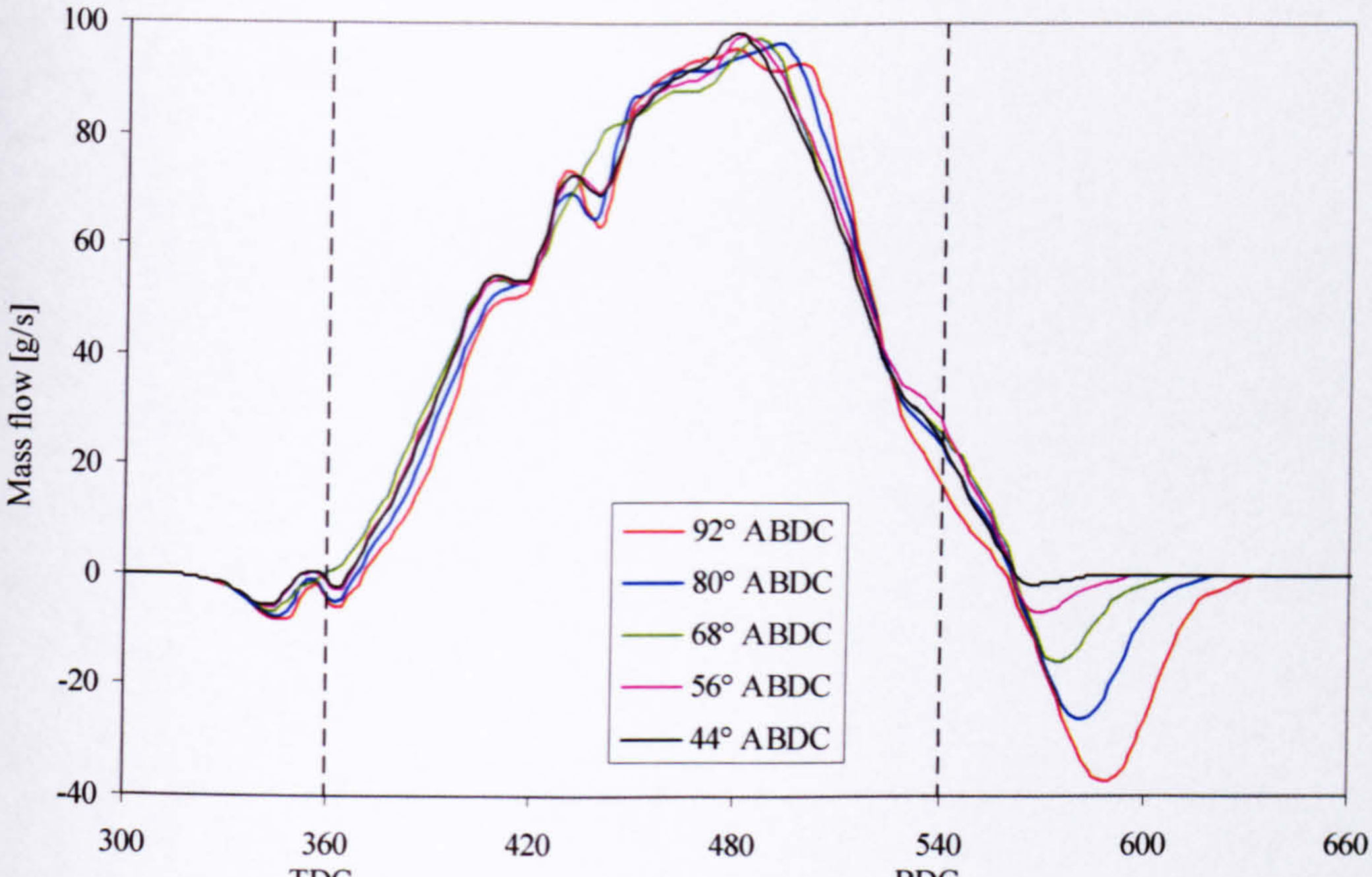

Figure 7.19: Inlet valve flow vs. crankshaft angle with different IVC timings at 8000 rpm

Figure 7.17 and 7.18. This is because early IVC reduces the available flow area and flow after BDC. This explains the higher port pressure after BDC compared with later IVC.

In a similar way to 1750 rpm early IVC timing reduces the crankshaft angle window during which negative pressure gradient is present across the inlet valve as well as the pressure difference at IVC. For example, Figure 7.14 shows that the pressure difference (as indicated on the figure) has reached 1.3 bar when IVC occurs at 90° ABDC. This is significantly higher that the 0.3 bar pressure difference (as indicated on the figure) when the inlet valve closes at 44° ABDC shown in Figure 7.18.

Figure 7.19 shows the flow rate into the cylinder for all 5 IVC timings at 8000 rpm. It can be seen that the most sensitive part of the flow rate curve to variation of IVC timing is after BDC. The change in the polarity of pressure gradient results in positive mass flow into the cylinder, followed by a backflow as shown. The amount of backflow depends on the IVC timing. At this engine speed the earliest IVC (i.e. 44° ABDC) still yields the lowest back flow and hence produces the highest mass trapped in the cylinder.

11000 rpm

Figures 7.20, 7.21, 7.22, 7.23 and 7.24 show cylinder pressure and inlet port pressure for IVC at 92° ABDC, 80° ABDC, 68° ABDC, 56° ABDC and 44° ABDC for 11000 rpm. Examining all 5 figures shows that the inlet pressure is higher than the cylinder pressure for a short crankshaft angle window after BDC. This is soon reversed causing a negative pressure differential. This is similar to the findings from the lower engine speeds. The negative pressure gradient at IVC is higher for the later IVC timings and lower for the earlier IVC timings. In the extreme case of the earliest IVC timing (i.e.44° ABDC), shown in Figure 7.24 the negative pressure gradient is nearly zero. The reason for this can be seen by examining Figures 7.11, 7.18 and 7.24. The point at which the negative pressure differential occurs is different at different speeds. It can be seen that as the engine speed increases the point at which the negative pressure gradient occurs is delayed i.e. at 1750 rpm this happens at BDC, at 8000 rpm at approximately 20° ABDC and at 11000 rpm at 40° ABDC. This is due to the gas dynamic effects in the inlet.

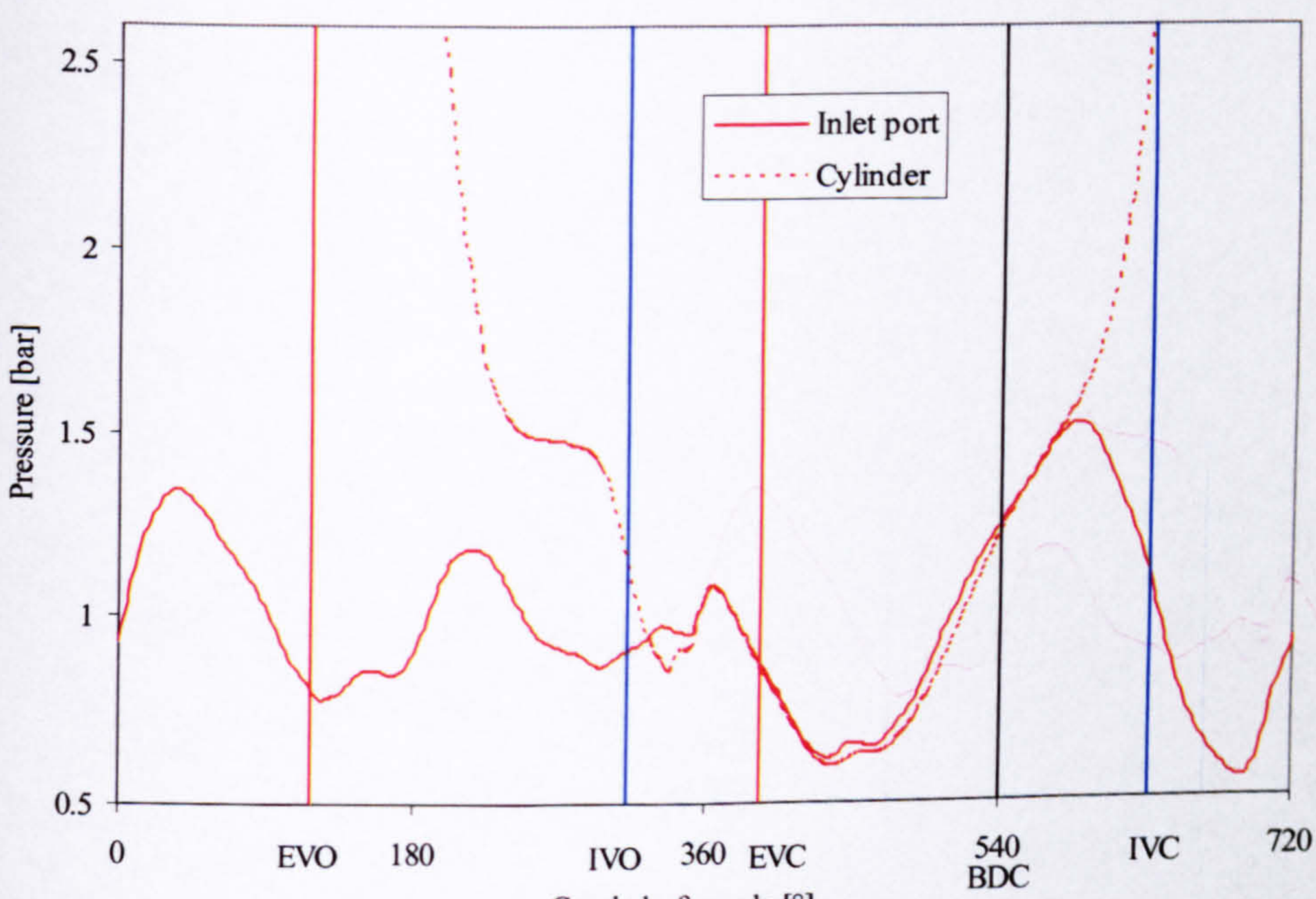

Figure 7.20: Inlet port and cylinder pressure vs. crankshaft angle at 11000 rpm with IVC 92° ABDC

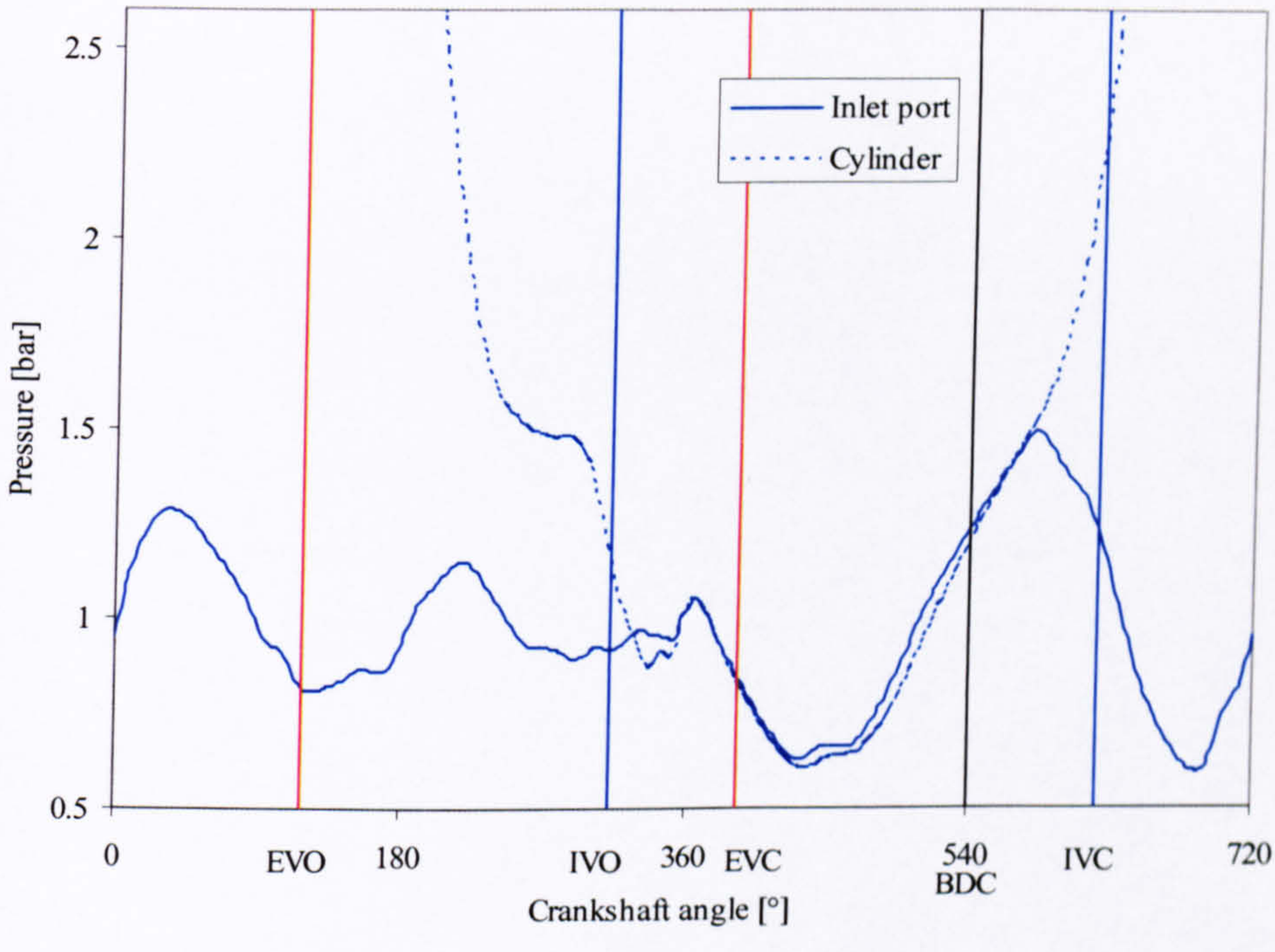

Figure 7.21: Inlet port and cylinder pressure vs. crankshaft angle at 11000 rpm with IVC 80° ABDC

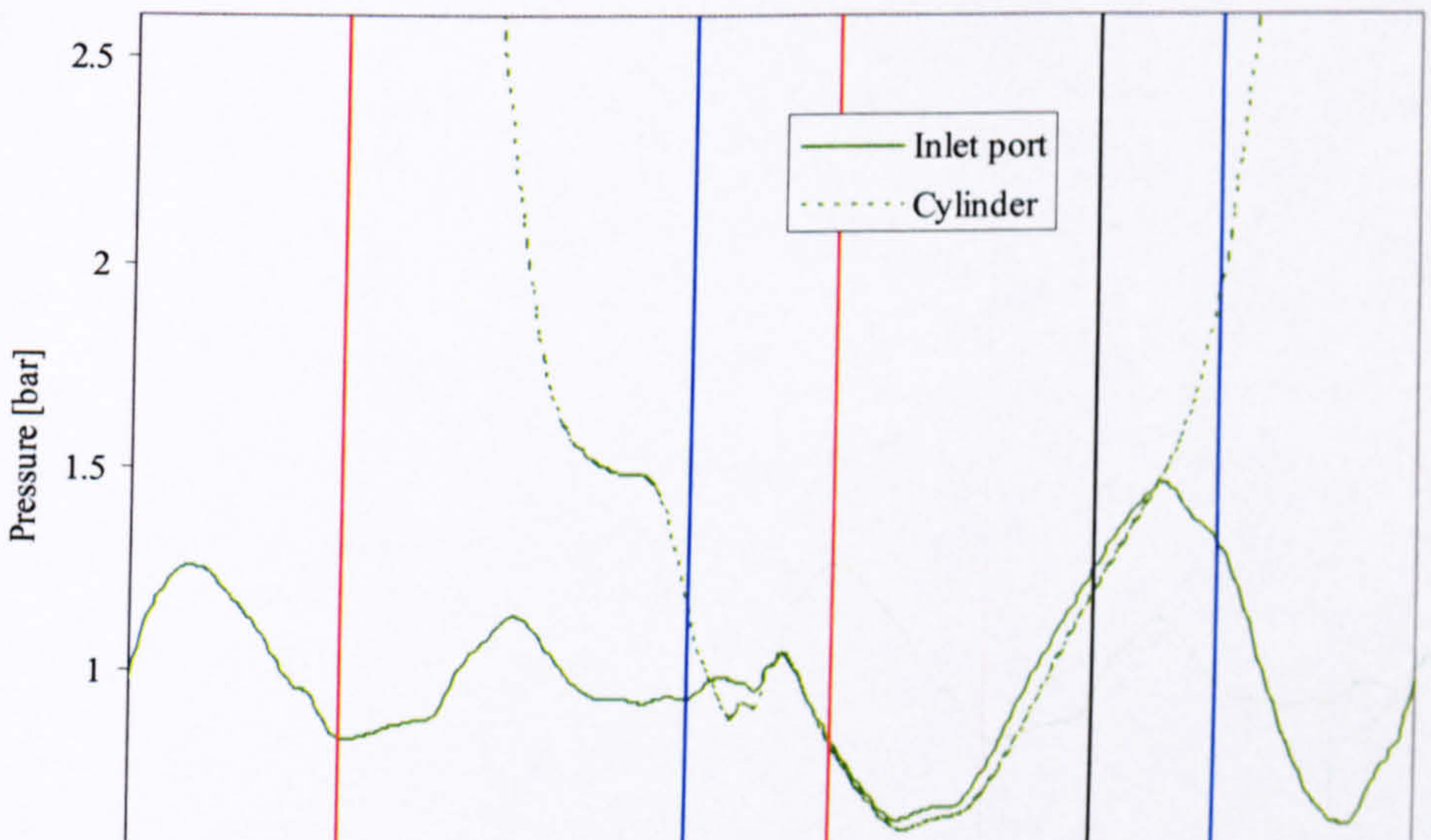

Figure 7.22: Inlet port and cylinder pressure vs. crankshaft angle at 11000 rpm with IVC 68° ABDC

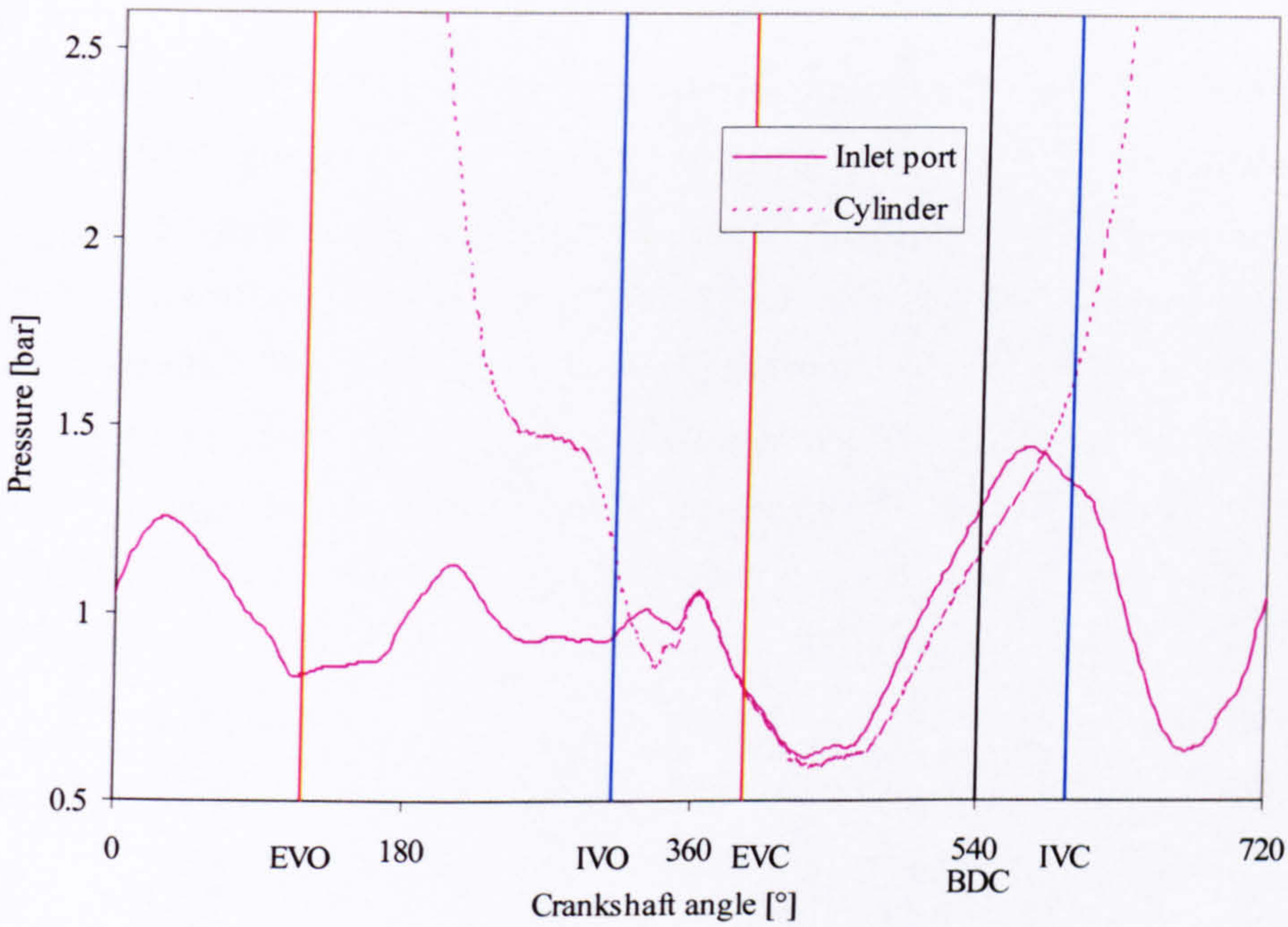

Figure 7.23: Inlet port and cylinder pressure vs. crankshaft angle at 11000 rpm with IVC 56° ABDC

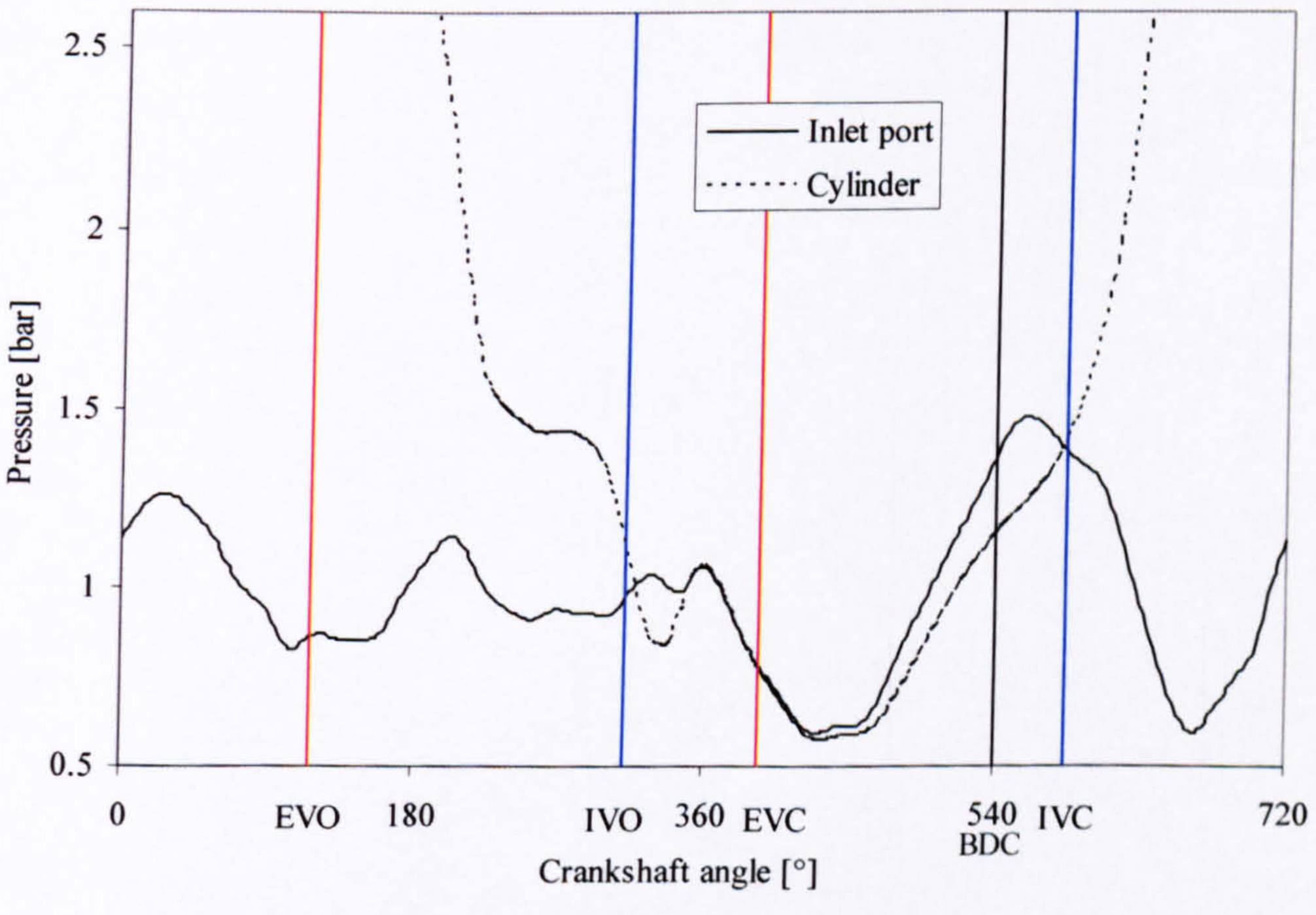

Figure 7.24: Inlet port and cylinder pressure vs. crankshaft angle at 11000 rpm with IVC 44° ABDC

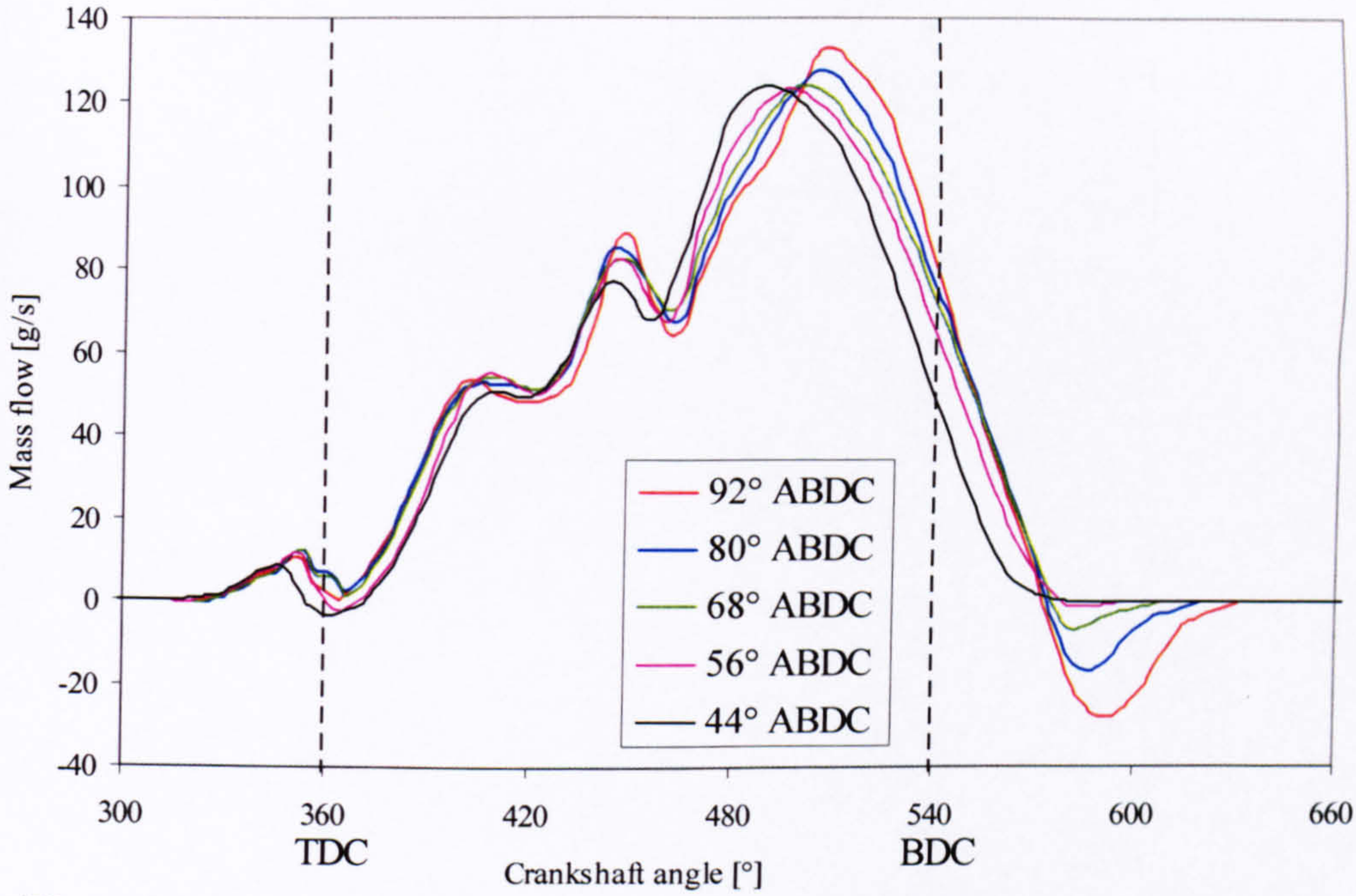

Figure 7.25 Inlet valve flow vs. crankshaft angle with different IVC timings at 11000 rpm

It is also important to notice that positive pressure differential for earlier IVC is higher than for later IVC. This is caused by the reduced available flow at this crankshaft angle. This is confirmed by examining Figure 7.25, which shows the flow rate for different IVC timings vs. crankshaft angle. The earlier IVC still produces lower backflow, however it also restricts the flow immediately before and after BDC. This is best illustrated with IVC 44° ABDC, which despite generating nil backflow does not yield the highest charging efficiency. The increase in the pressure difference between the inlet port and cylinder for early IVC timing indicates restriction of the flow in this part of the cylinder filling process. Referring to Figure 7.2 shows that the highest charging efficiency is generated by IVC at 68° ABDC, which appears to produce some backflow but does not restrict the flow around BDC and results in the highest net flow after BDC. Therefore, the ideal valve closing curve should provide a good compromise between restricting the flow entering the cylinder around BDC and reduce the backflow. A lift profile with inlet valve closing point at 44° ABDC but higher closing velocity would improve cylinder filling after BDC but still produce low backflow. The design of such lift profiles, with

high closing velocity and the effect on valvetrain dynamics is discussed in detail by Boretti and Villa (1998).

The process described above for 11000 rpm is similar at higher engine speeds where later IVC timings allow higher flow into the cylinder.

7.4 Summary of conclusions

Based on the above discussion the following conclusions regarding the effect of IVC timing on the gas exchange process in high-speed engines can be made:

- The main mechanism through which IVC timing affects charging efficiency is by controlling the net flow through the valve in the period BDC-IVC.
- At low speeds there is no pressure build up in the inlet after BDC due to the length of the primary inlet pipe. Early IVC reduces the backflow after BDC and yields higher charging efficiency. Potentially earlier IVC timing than the range explored can result in higher benefit.
- The optimal IVC for different engine speeds follows the same pattern for medium and high-speed engines.
- IVC timing variation can cause a phase shift of the pressure waves propagating in the inlet port at certain speeds. This may result in small changes in gas flow into the cylinder during the valve overlap period and hence the exhaust residuals. The effect on charging efficiency appears insignificant compared with the other mechanisms explained above.

As a result of the parametric studies presented in this and the previous chapters it is possible to generate a map of the optimal IVO and IVC timings in terms of charging efficiency within a 60° range. This information is used in the next chapter to assess the abilities of selected VVA systems, which were identified to be dynamically suitable for high-speed operation.

Chapter 8

Assessment of the Ability of Selected VVA Systems to Satisfy Optimum IVO and IVC Timing

This chapter discusses the ability of the VVA systems identified as dynamically suitable for high-speed operation to satisfy the ideal valve events. This is done by comparing their adjustment range with the optimum IVO and IVC timing established for the engine from the parametric studies done in previous chapters. The relative independence of the effects of IVO and IVC timing on charging efficiency allowing an approximate assessment of the possible gain from variation of both events. A possible control strategy resulting in the highest charging efficiency is proposed.

8.1 Optimum IVO timing

The optimum IVO timing for the engine used in this research in a 60° range is shown in Figure 8.1. The most advanced setting is constrained by piston to valve clearance.

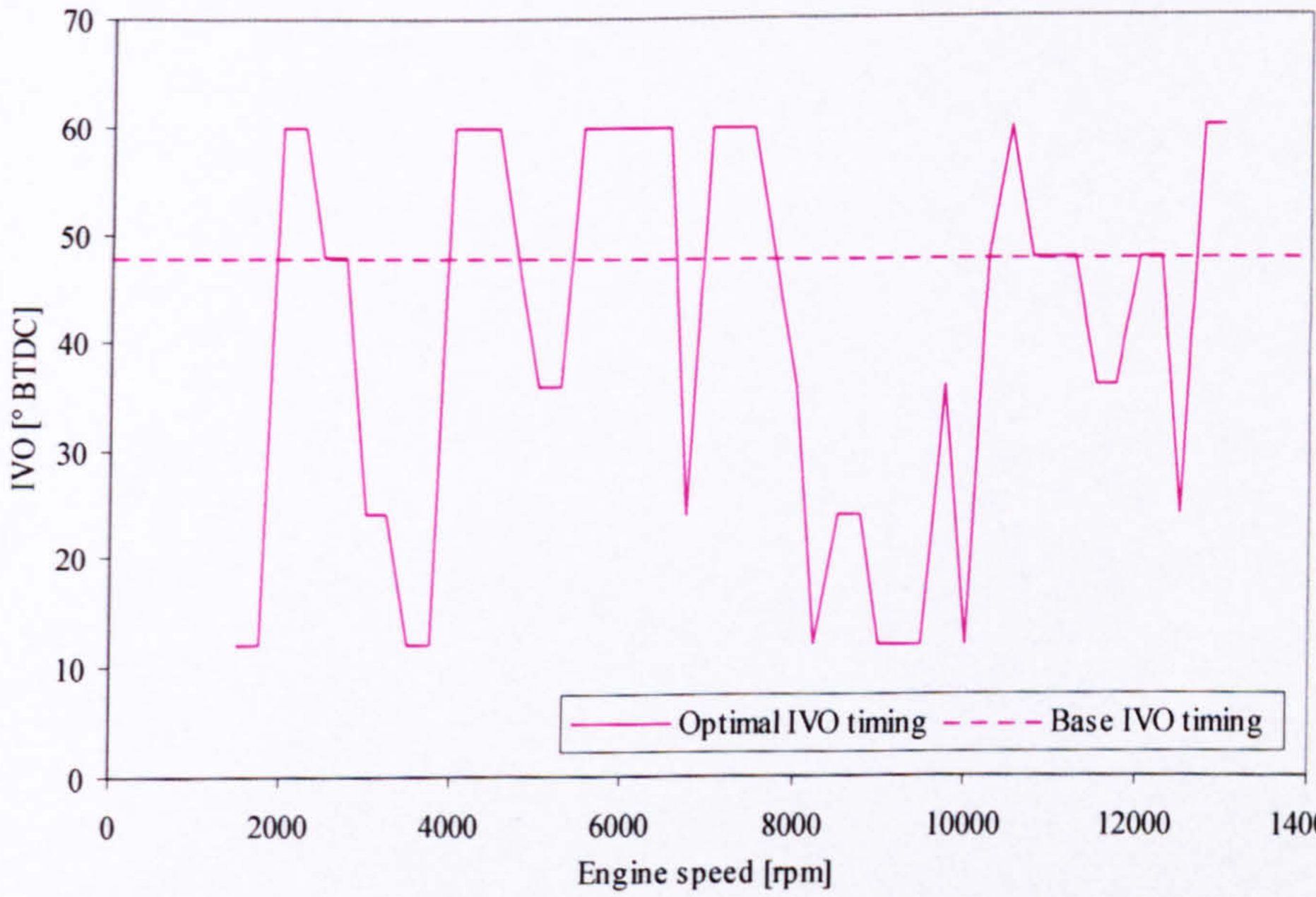

Figure 8.1: Optimal IVO timing for charging efficiency at different engine speeds

The shape of the curve is oscillatory and the optimal IVO timing shifts as much as 60° within 1000 rpm in several places. The reason for this shape was explained in Chapter 6. It is important to note that the base IVO timing is ideal for the engine speed when maximum power is developed. The base setting is also close to the ideal for most of the speed range.

Figure 8.2 shows the possible charging efficiency improvement with optimal IVO selected from within 60° range. As commented in Chapter 6 significant improvement can be achieved in the speed ranges where there are troughs in the curve e.g. 1750 rpm, 3750 rpm, 8500 rpm and 9750 rpm. Small increase of charging efficiency is also possible in other areas. The reason for this difference is the fact that the base IVO is further away to the optimal for the dips (i.e. the most retarded possible). A small improvement is also possible at 12750 rpm where peak power is generated and also at 13000 rpm, which may extend the maximum power range.

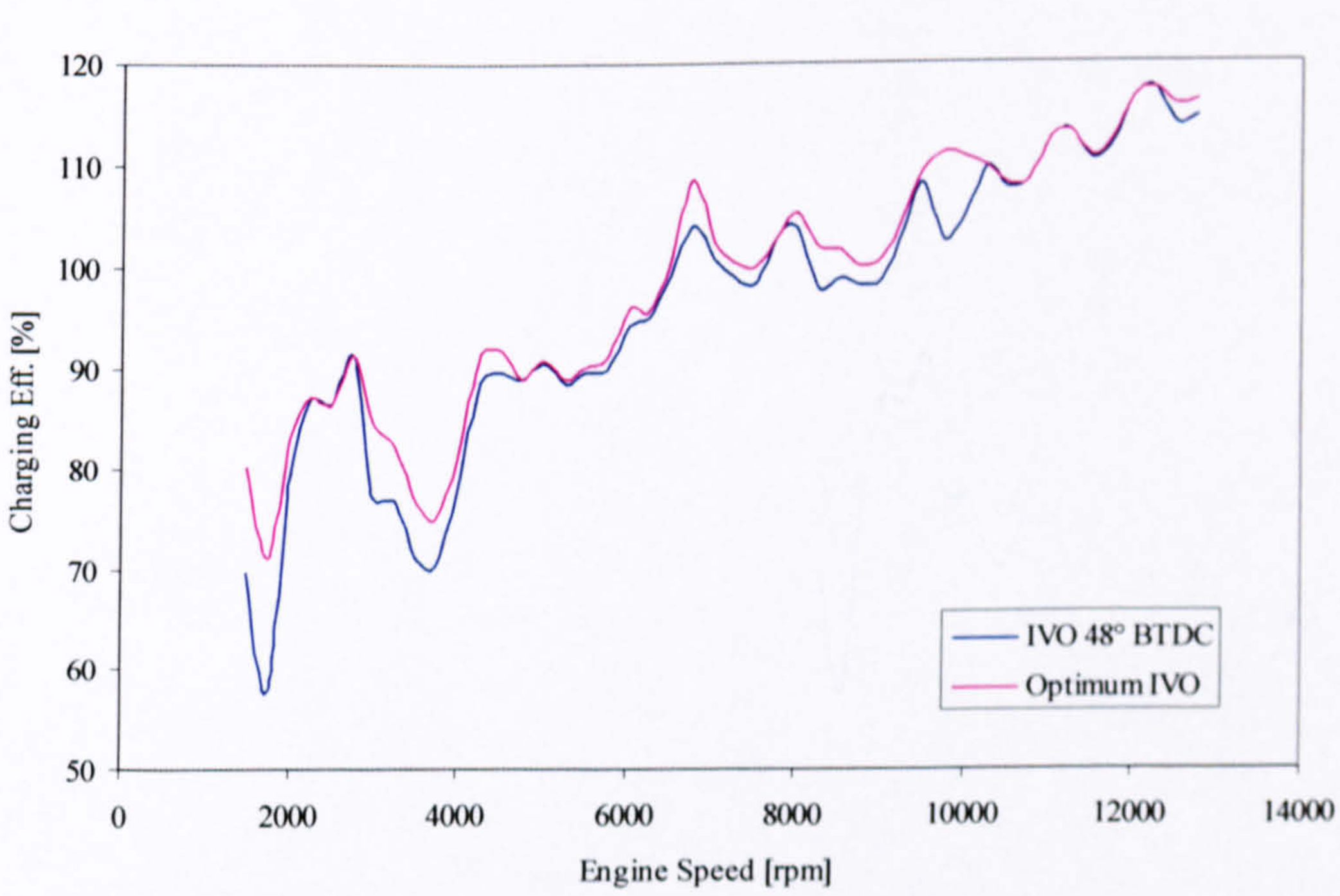

Figure 8.2: Charging efficiency improvement with optimal IVO at different engine speeds

8.2 Optimum IVC timing

Figure 8.3 presents the optimal IVC timing for maximum charging efficiency in a range of 60°. The shape of the curve is a lot simpler than for the optimal IVO. Up to 8000 rpm the optimal timing is the most retarded in the range explored. Above that speed later IVC produces higher charging efficiency. Again the base setting matches the optimal in the range between 12000 rpm and 12750 rpm.

One of the conclusions from Chapter 7 suggests that because of the mechanisms in which IVC affects charging efficiency at low speeds an earlier setting than these explored in the parametric study will produce higher benefit.

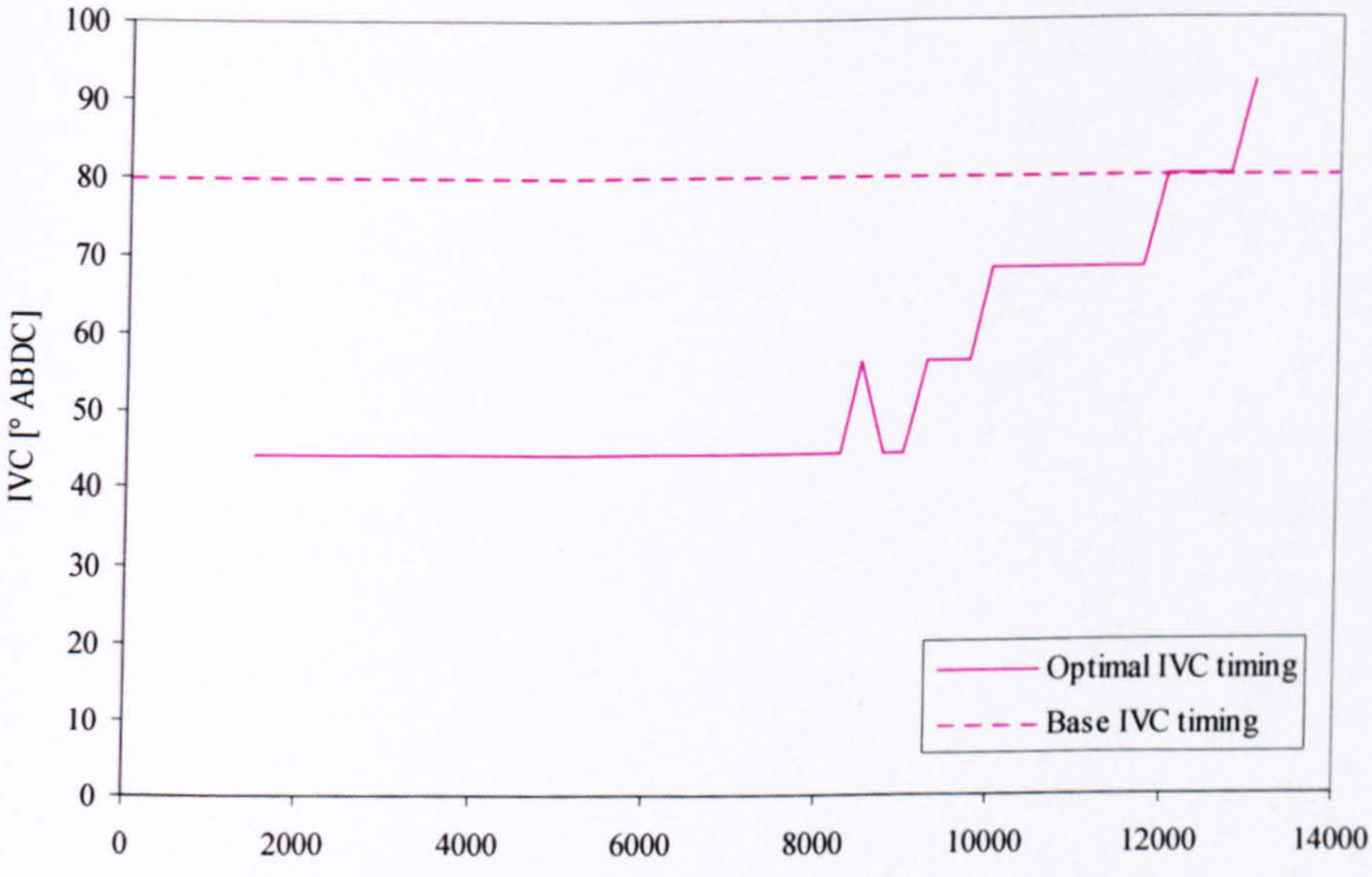

Figure 8.3: Optimal IVC timing for charging efficiency at different engine speeds

Figure 8.4 shows that significant improvement in charging efficiency can be achieved all the way up to 9750 rpm. Above that speed the improvement diminishes. This is because the base IVO timing is closer to the optimal. It should be noted that a small improvement is again possible at 13000 rpm. The reason why any improvement at high speed is significant because a small increase in torque relates to a notable increase in power e.g. 1 Nm at 13000 rpm is equivalent of 1.9kW.

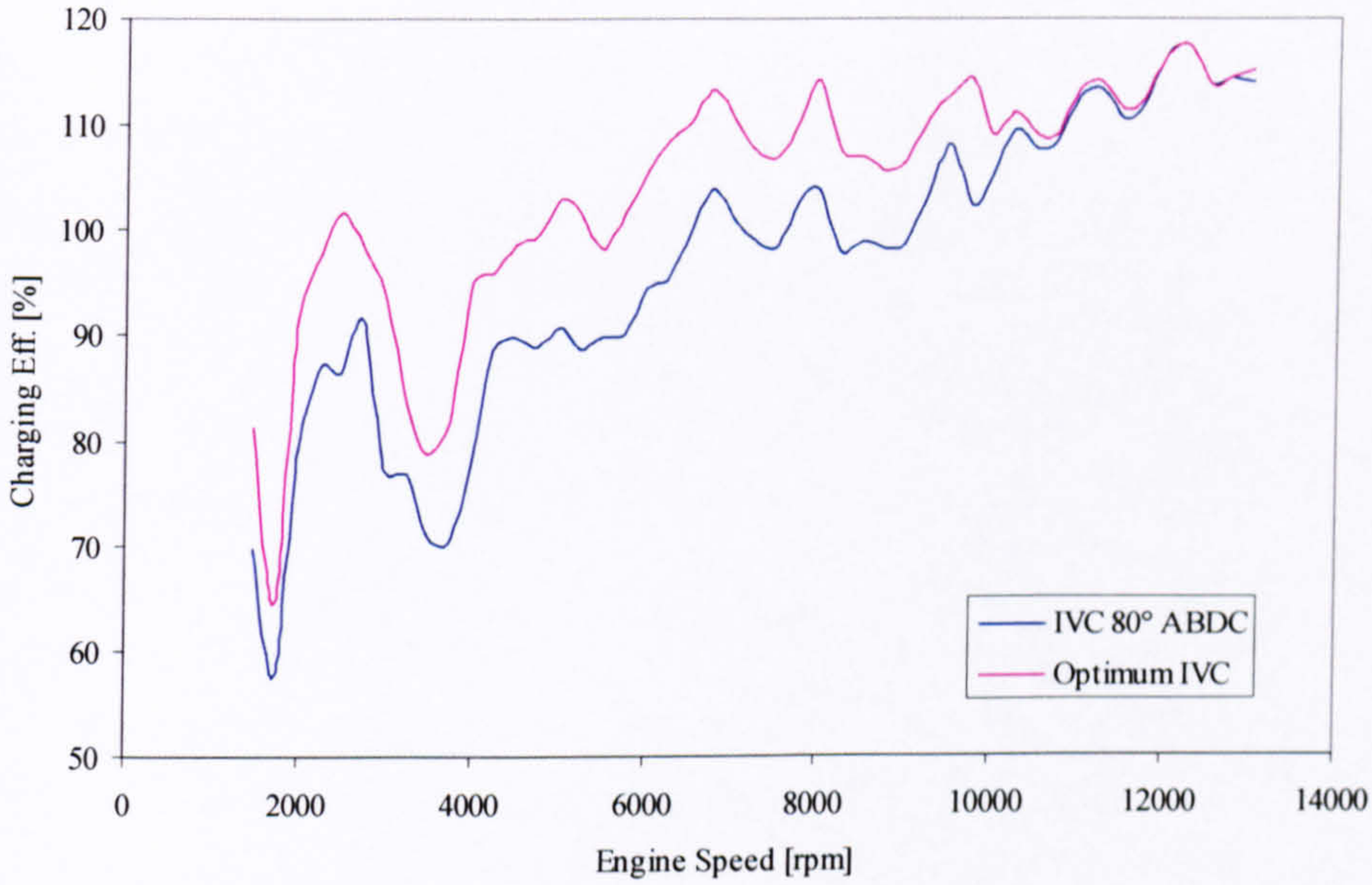

Figure 8.4: Charging efficiency improvement with optimal IVC at different engine speeds

8.3 Combined effect of optimum IVO and IVC timing

To be able to combine the results from the two parametric studies exploring the effects of IVO and IVC on charging efficiency the independence of these findings must be established. In order to do this the mechanisms in which they influence charging efficiency will be briefly discussed.

Inlet valve opening timing affected mainly the gas flow during valve overlap and the first part of the period EVC – BDC. Figures 6.7, 6.8, 6.9, 6.13 and 6.14 in Chapter 6 all demonstrate that IVO timing has a small effect on the inlet port pressure after BDC at engine speeds up to 6500 rpm. However, in Chapter 7 it became apparent that the inlet port pressure is lower than cylinder pressure for a significant part of the BDC – IVC period at such low speeds. It was established that IVC only controls the reduction of backflow and up to 8000 rpm the earliest IVC yields the highest charging efficiency. Hence the optimum IVC is still the most advanced setting.

At higher engine speeds the inlet port pressure after BDC is mainly a function of the pressure pulsations excited by the reciprocating motion of the piston and is unlikely to be significantly affected by variations in the beginning of valve overlap.

Figure 7.4 in Chapter 7 shows the minimal effect of IVC timing on exhaust residuals. This together with the low sensitivity of the mass flow during valve overlap shown in Figure 7.5 proves that IVC timing has a small effect on the flow conditions during overlap and hence optimum IVO timing.

Whilst appreciating that the above comments are based on an individual engine and assumptions regarding the independence of the two studies the mechanisms in which they affect charging efficiency are different. Combining the results of the two studies allows the net effect to be approximately established.

Considering this, plotting net charging efficiency cannot be justified. Instead the net improvement for every 12° variation of individual valve events will be used to represent the combined effect of IVO and IVC timing.

8.4 VVA system assessment

Examining Figure 8.5 presenting the optimum IVC and IVO combined timing suggests that in order to satisfy the valve event requirements completely a mechanism able to vary independently duration and timing is required. In order to ensure at least the same power output as the base engine the same IVO and IVC timing and event duration is kept at the speed where it is developed.

The two mechanisms identified as dynamically suitable for high-speed operation are the VCP and the Non-constant velocity drive type. The first one is capable of varying valve event timing and the second is capable of varying valve event duration. Whilst resulting in high complexity and cost a combination of both mechanism types is possible, especially when the VAST system is used.

Each individual system will be examined separately and in combination.

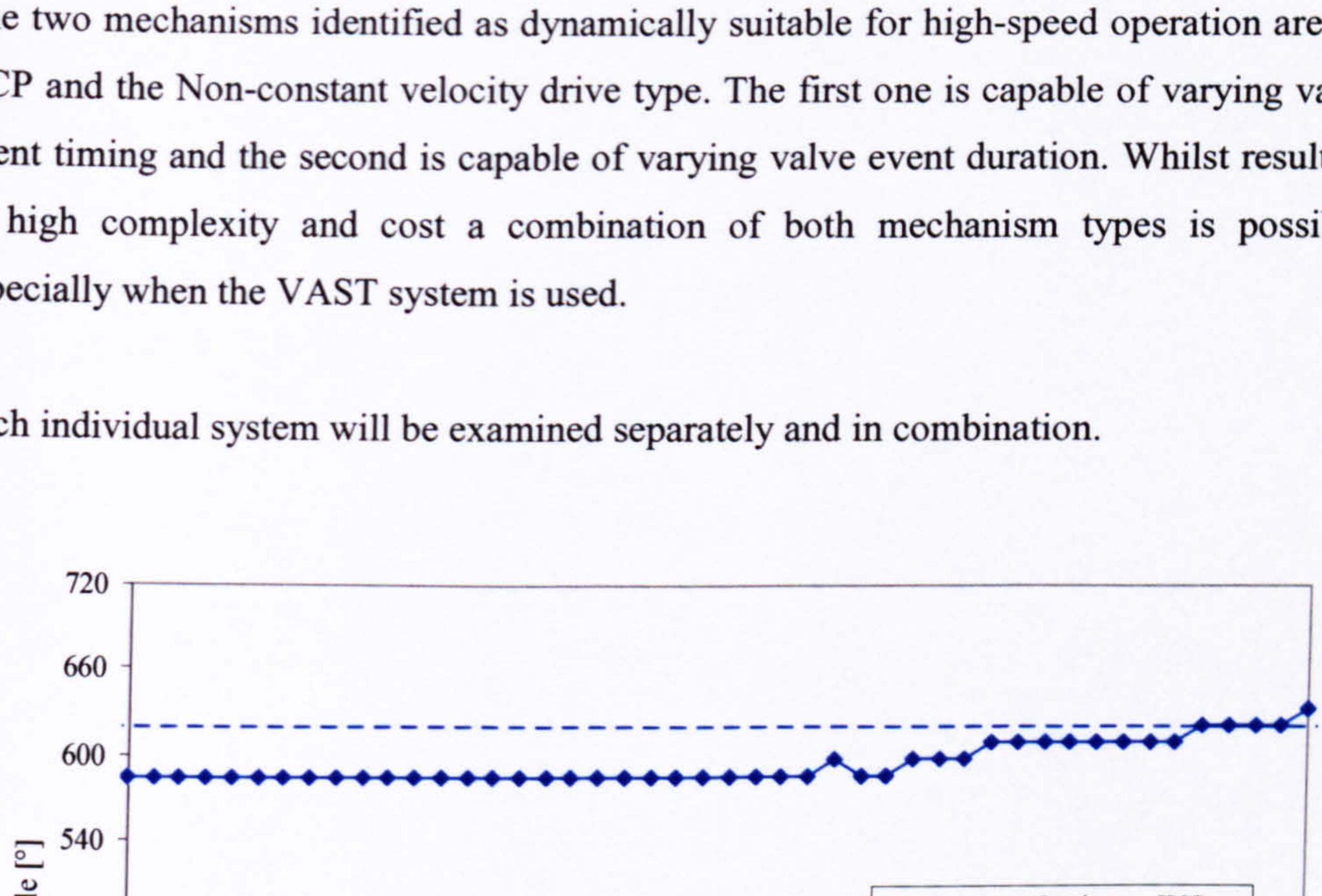

Figure 8.5: Optimum IVC and IVO combined timing at different engine speeds

8.4.1 VCP system

In order to ensure at least the same power output as the base engine the base valve event duration is kept. For reasons explained in the beginning of Chapter 6, IVO can be advanced with only 12° from the base setting. Figure 8.3 showed that only 12° more retarded setting is explored. Hence VCP system with a variation range of 24° is studied. The accuracy of this prediction depends on the assumption that changes in the maximum opening point has a small effect on charging efficiency.

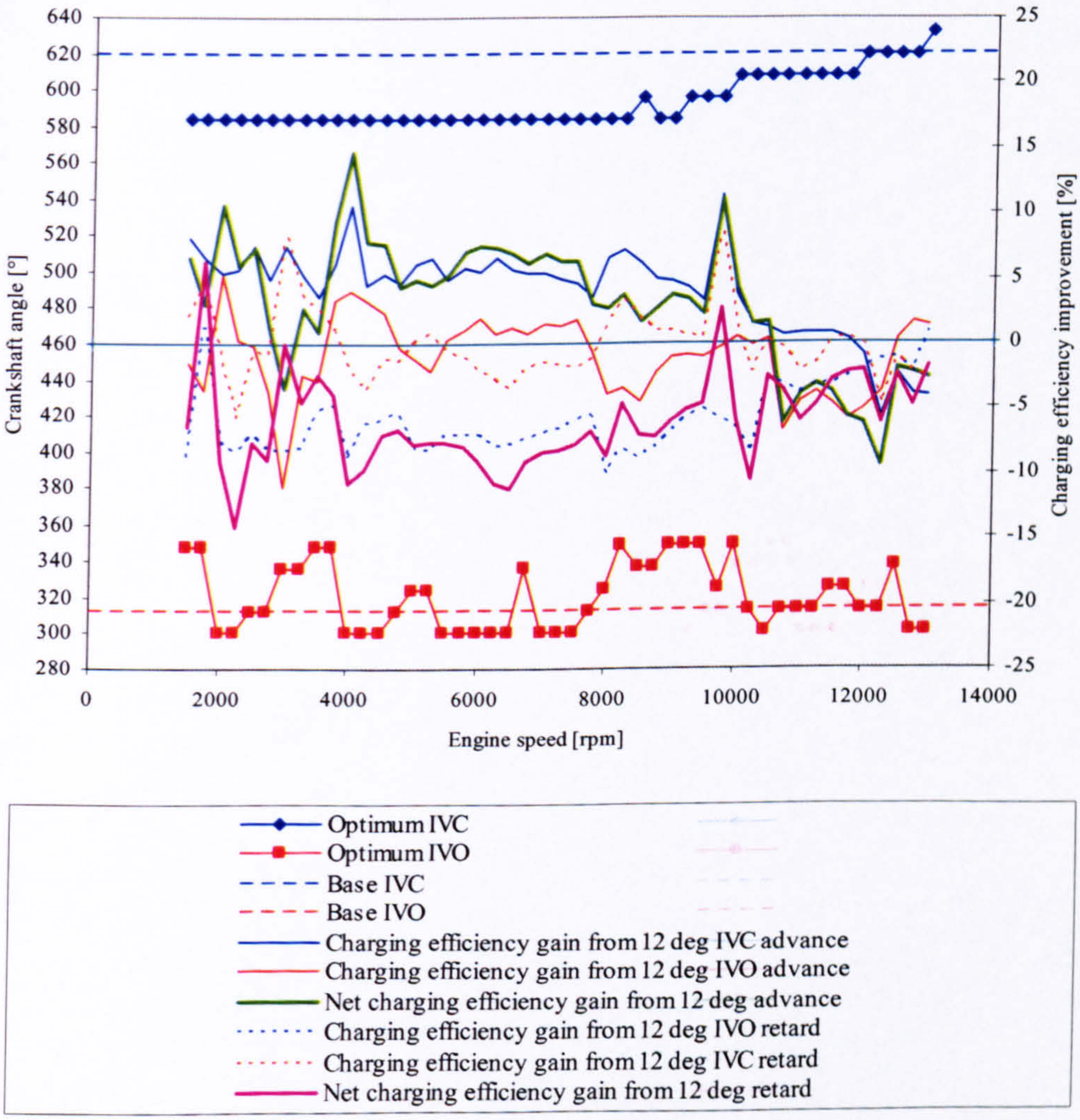

Figure 8.6: Gains from 12° advance and retard with VCP system at different engine speeds

Figure 8.6 shows the individual and net gains from advancing and retarding the camshaft phasing by 12°. The solid blue line shows the effect on charging efficiency from 12° advance of IVC and the solid orange line that of 12° advance of IVO. Whenever the two lines are on the opposite side of the zero line means that a part of their combined effect will be cancelled. The green line shows their combined effect.

The dotted blue line shows the effect on charging efficiency from 12° retard of IVC and the dotted red line that of 12° retard of IVO. The pink line shows their combined effect.

Examination of the green and pink lines show that advancing the inlet cam timing will improve charging efficiency in the range up to 10500 rpm apart from an engine speed of 1750 rpm where retardation gives slightly better improvement and 2750 rpm where a gain cannot be achieved. At these speeds the timing should be retarded. Above 10500 rpm standard timing should be retained.

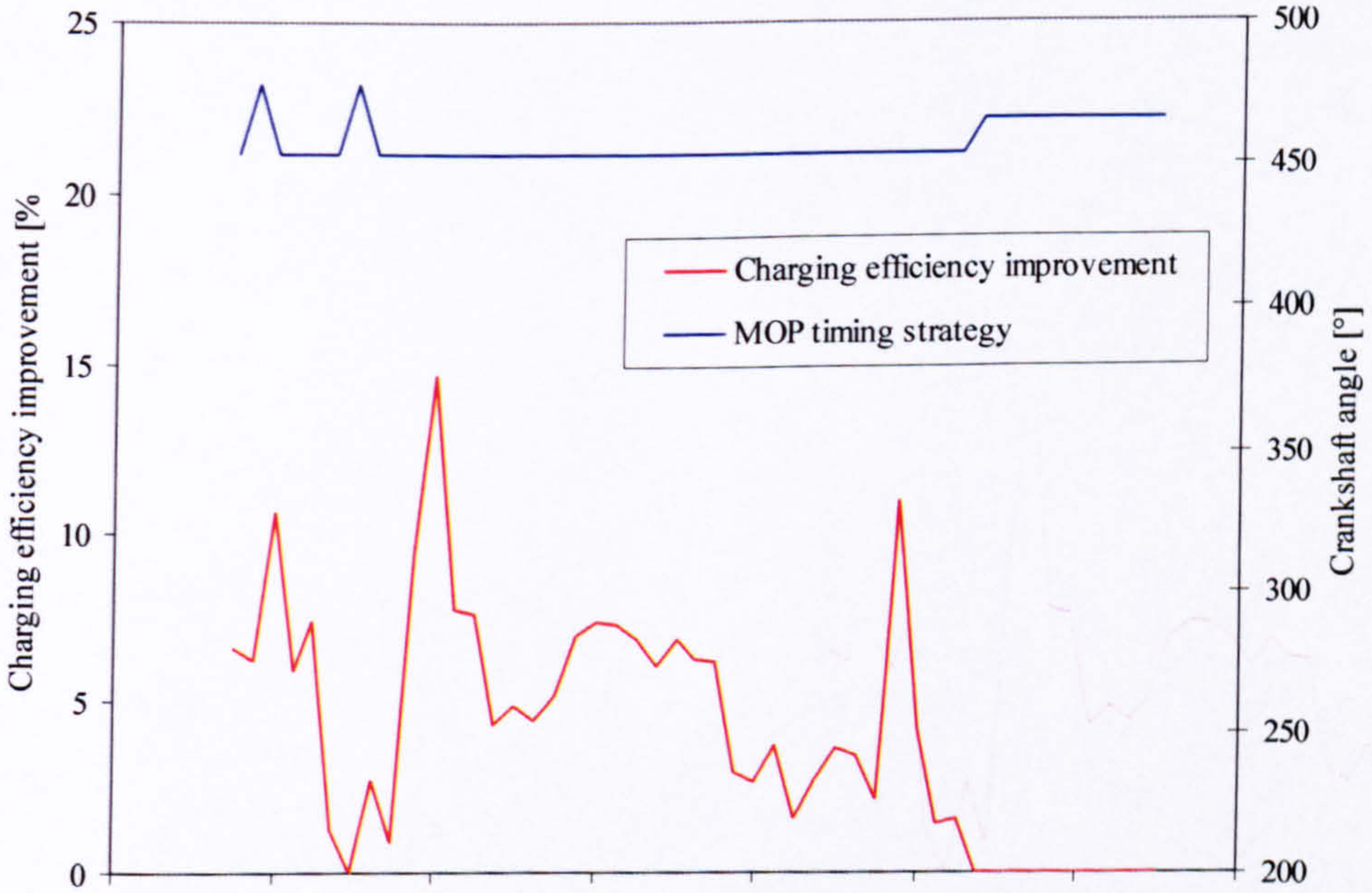

Figure 8.7: Possible charging efficiency improvement and MOP timing strategy at different engine speeds

The control strategy and overall improvement is shown on Figure 8.7. It is noticeable that up to 10500 rpm with the exception of two low speed sites the camshaft timing is retarded. This is closer to the optimum IVC timing, which provides significantly higher gains than the optimum IVO. This is similar to the full load strategy for low speed engines. However, this is not the case in the two low speed regions where the combined benefit from retarding IVO and IVC is larger.

It could be concluded that the VCP system applied on a high-speed engine has the potential to improve the charging efficiency of the engine at speeds below the maximum power speed. The gains in some of the areas where charging efficiency dips (e.g. 3750 rpm) are not large. This is because the optimum IVO and IVC require shifting of the valve event in opposite directions. It can be seen that at this speed advancing IVC produces improvement of nearly the same magnitude as the detriment caused by advancing IVO. This inability to fill the dips severely reduces the potential of the system. This is because in reality a VVA control strategy may not take advantage of the ability to increase the peaks in the torque curve however will aim to fill the dips.

8.4.2 Non-constant velocity drive system

This system allows valve event duration variation. In order to produce the same engine power IVO and IVC timing are maintained the same as the base engine. This also fixes the timing of maximum opening point to remain the same. The range of valve event duration variation is from 236° to 332°.

The accuracy of this prediction is limited by the fact that in the case of the shortest valve event duration there is a significant reduction of total valve flow area available and a change of valve closing velocities. As discussed in Chapter 7 this may have an effect on the backflow after BDC.

Due to the large number of data, the combined effect of IVO and IVC on charging efficiency is only presented. Figure 8.8 shows the possible improvements in charging efficiency with different valve event durations. Gains can be achieved in the entire speed range up to 11000 rpm.

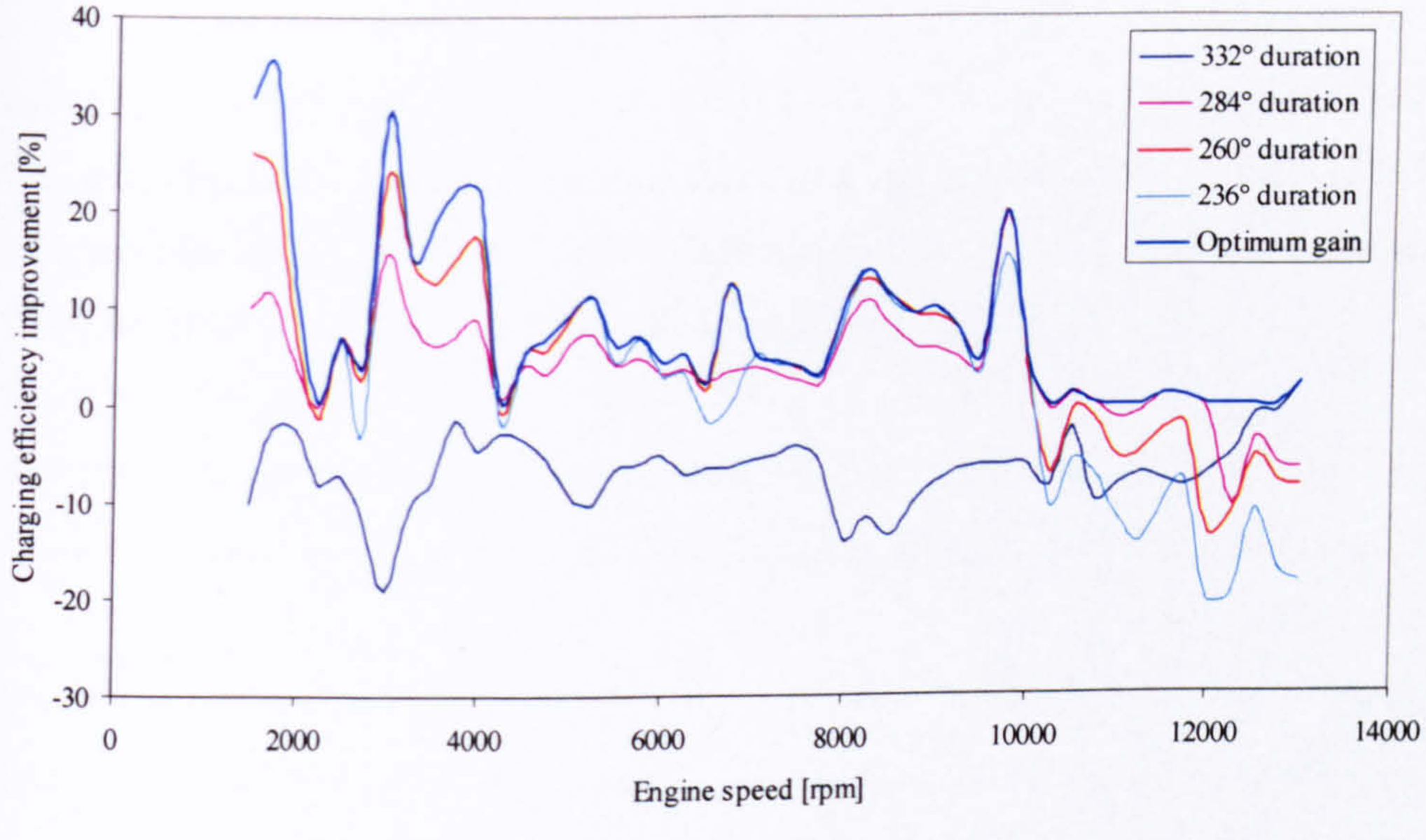

Figure 8.8: Possible improvement on charging efficiency from variation of valve event duration at different engine speeds

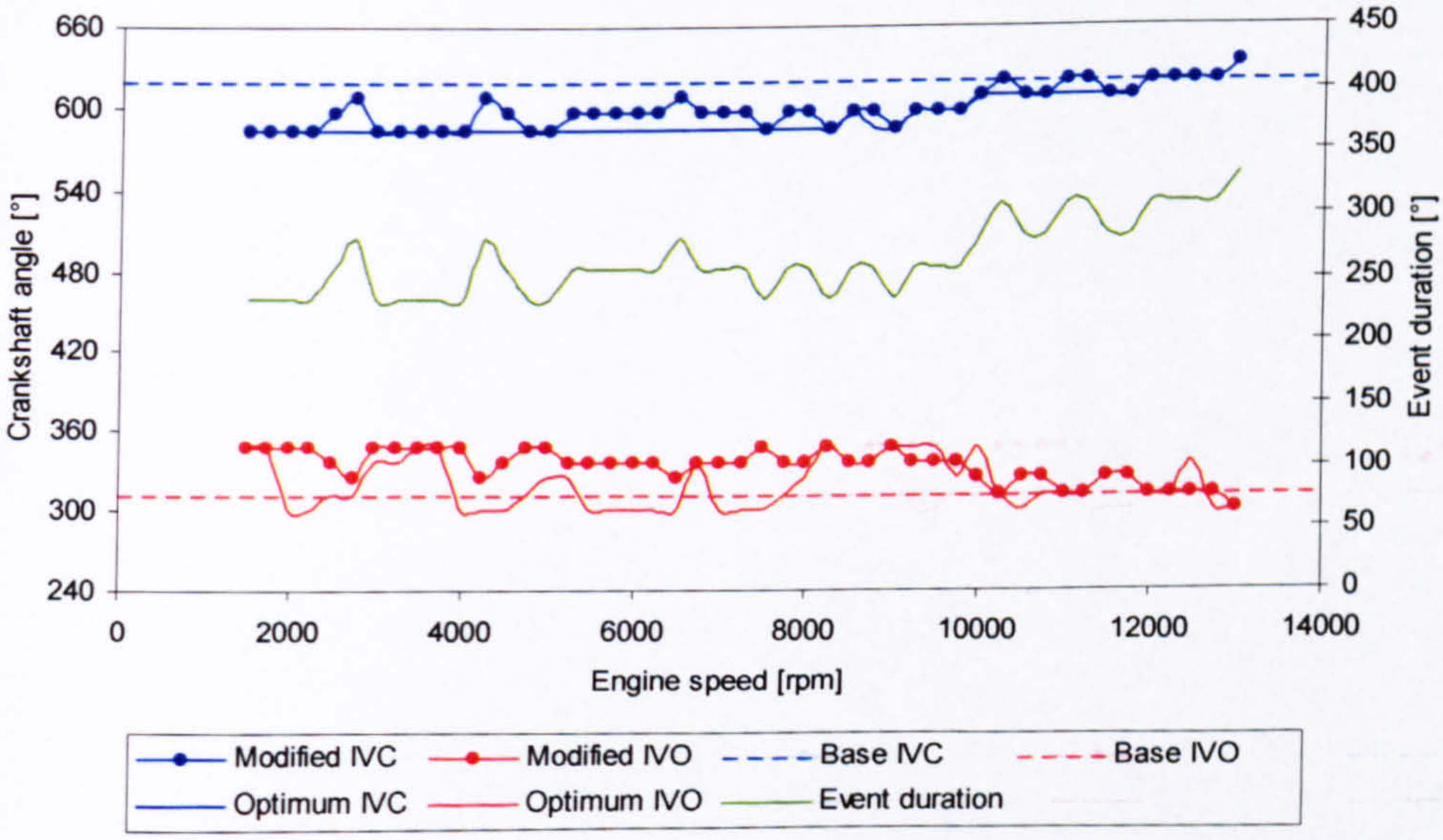

Figure 8.9: Control strategy with variable event duration at different engine speeds

The benefits are highest in the areas where the charging efficiency dips (e.g. 1750 rpm and 3750 rpm) and lower at the speeds where it peaks (e.g. 2750 rpm and 4250 rpm). This is because in these regions in order to achieve the optimal IVO and IVC the valve duration must be reduced, which is within the capabilities of this type of VVA system. At the speeds where peaks in the charging efficiency occur (e.g.2750 rpm and 4250 rpm) the gains are smaller as both optimum IVO and IVC require to be as early as possible. These are conflicting requirements, which this type of VVA system can not satisfy. A very small advantage is possible above 10000 rpm as expected.

The control strategy for this system is shown in Figure 8.9. At lower speeds shorter valve event durations are generally favoured. As speed increases above 9000 rpm longer durations are beneficial. This demonstrates the potential of simpler VVA systems, which are able to switch between valve lift profiles providing their high-speed operation capabilities are developed. According to previous research discussed in Chapter 1 there are additional benefits for engine performance from using smaller valve lift at low speeds possible with these systems.

Considering the same maximum lift is used the shortest valve event duration may result in excessively high closing velocities. The valvetrain must be able to tolerate them in speeds reaching 9000 rpm.

8.4.3 Combination of Non-constant velocity drive system and VCP system

This system can theoretically satisfy the optimum IVO and IVC timing. Figure 8.10 shows the control strategy for this type of system. Valve event duration changes in the range of 236° to 332° and the VCP system must work in a range of 36°. The same concerns regarding high closing velocities caused by the shortest valve event duration are valid. The valvetrain must be able to tolerate them in speeds reaching 9000 rpm.

The accuracy of this prediction is limited, as for the shortest valve event duration there is significant reduction of total valve flow area available. This combined with variation of other unexplored valve parameters such as MOP timing and valve closing velocity changes, may have an effect on the optimum valve events and the possible charging

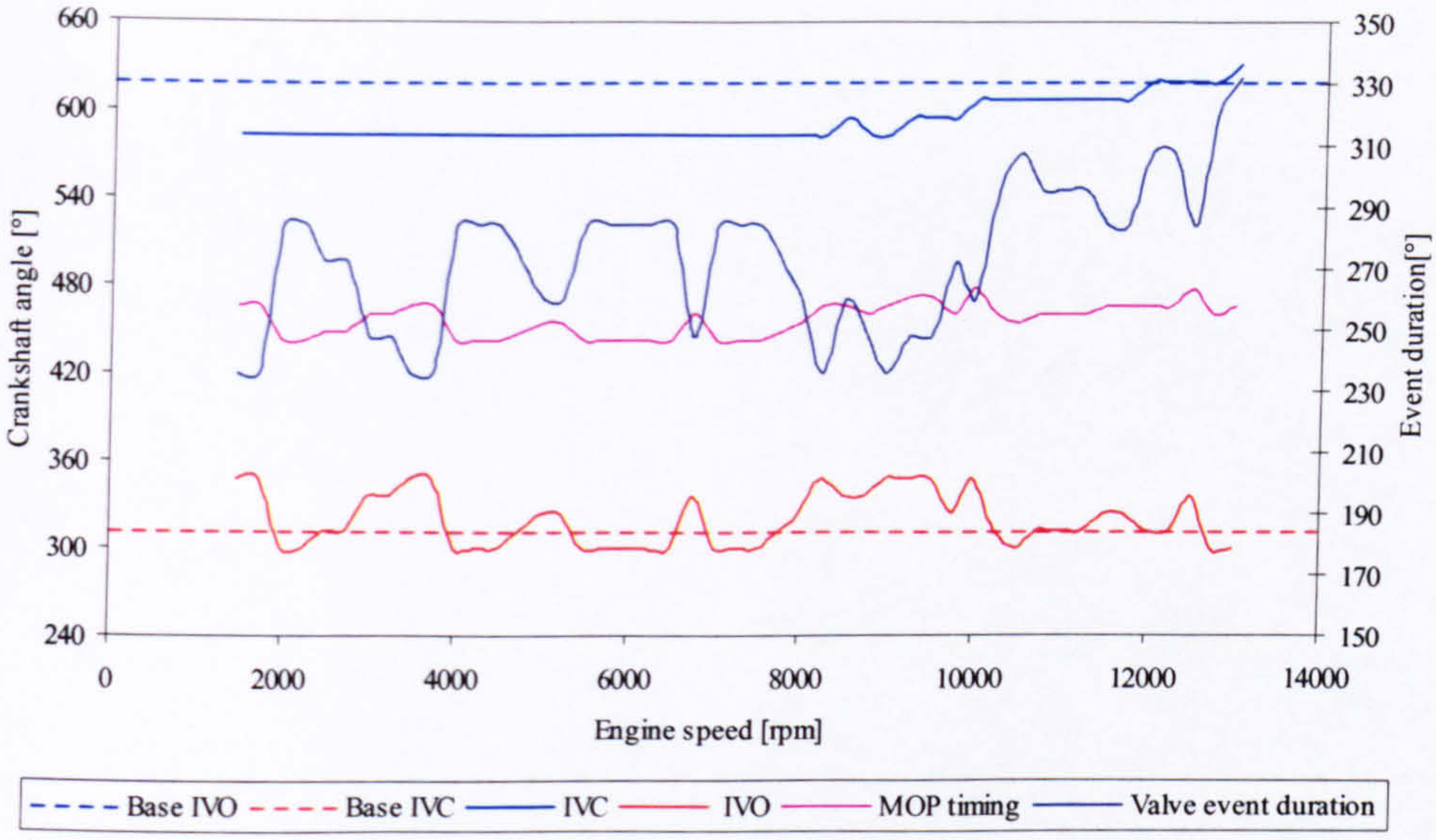

Figure 8.10: Control strategy for combined valve duration and MOP timing variation at different engine speeds

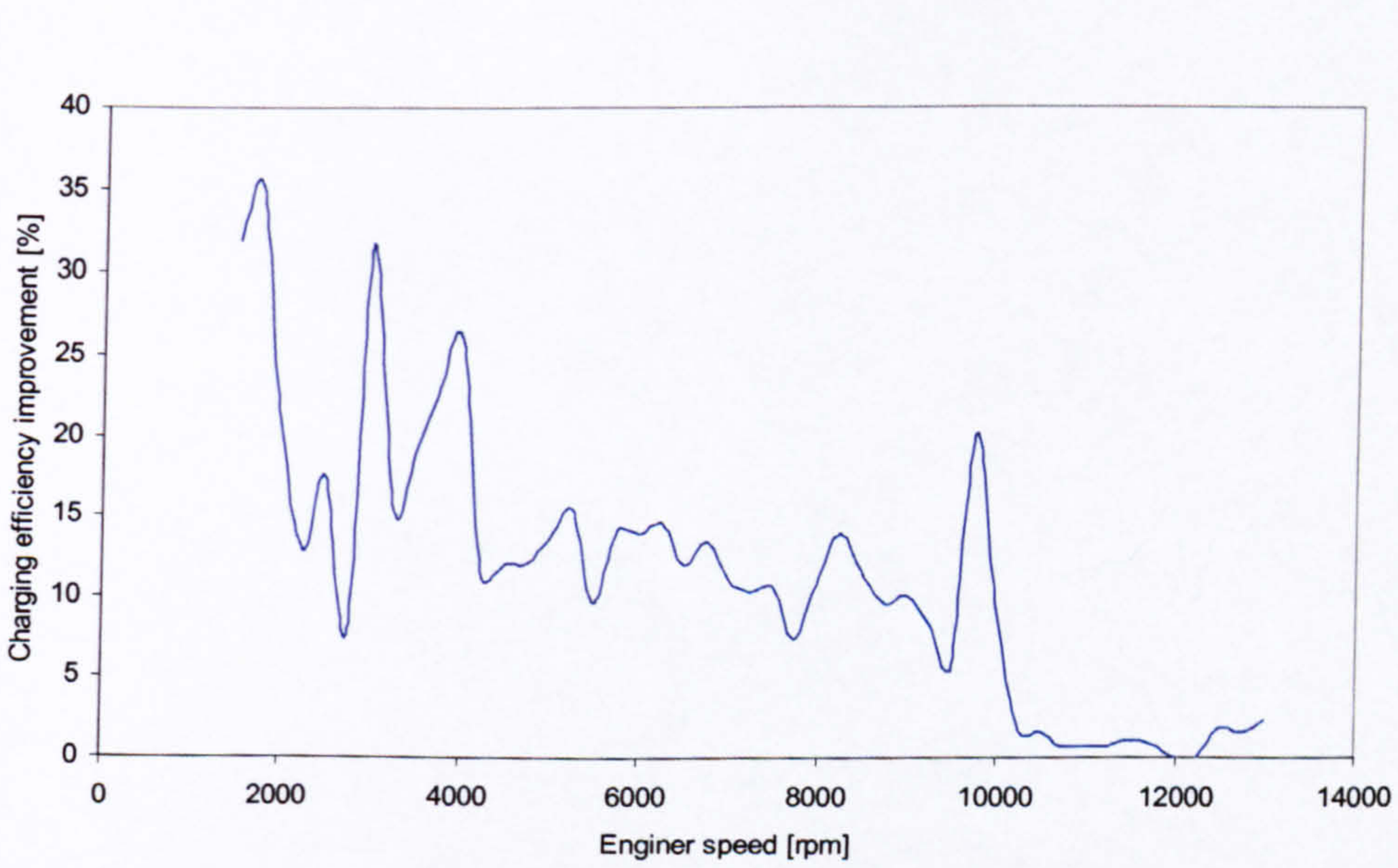

Figure 8.11: Possible improvement on charging efficiency from valve event duration and timing change at different engine speeds

efficiency improvements. Considering the gas exchange mechanisms involved the predicted trends should be realistic. This should allow a comparison between the potential of this and the other VVA systems to be made.

Figure 8.11. shows that significant gains up to 35% are possible in the speed range up to 10000 rpm. This is because the combination of systems can satisfy both optimum IVO and IVC requirements, which are often conflicting in terms of direction of shifting relative to TDC. A small improvement is also possible near the engines maximum speed, which may extend the maximum power range.

8.5 Sensitivity of charging efficiency to changes in IVO and IVC timing

In order to aid the selection of suitable VVA system it is important to understand the sensitivity of charging efficiency to changes in IVO and IVC timings. Both parameters were changed at 12° intervals and the effect on charging efficiency at different speeds is plotted in Figure 8.12 and Figure 8.13.

Figure 8.12 shows that the sensitivity of charging efficiency to changes of IVO is generally similar for all four steps at a fixed engine speed. The exceptions are at around 6750rpm and above 9750rpm. Generally 12° change in IVO results in a charging efficiency change no larger than 5% except around 1500 rpm, 3000 rpm, 6750 rpm, 9750 rpm and above 10500 rpm.

It is noticeable that the gradient of the sensitivity changes at different engine speeds. For example, at 1500rpm retarding IVO increases charging efficiency throughout the explored IVO range (Figure 8.13). Whilst at 5000rpm retarding IVO from 60° to 36° increases charging efficiency, but retarding it further has the opposite effect. The reason for this effect is because at certain engine speeds the optimal IVO value is within the explored IVO range and at other it is probably outside it.

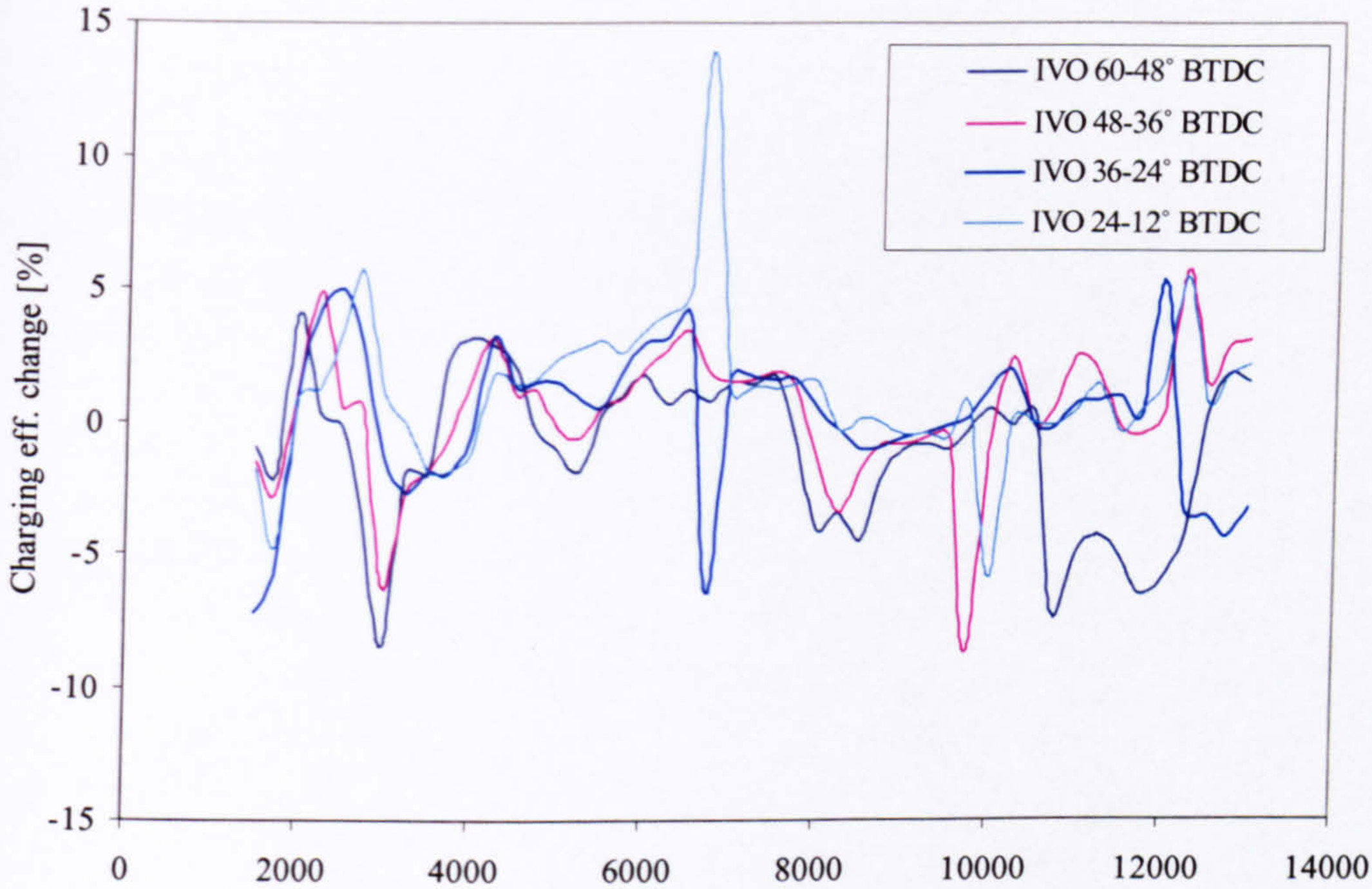

Figure 8.12: Sensitivity of charging efficiency to changes in IVO timing at different engine speeds

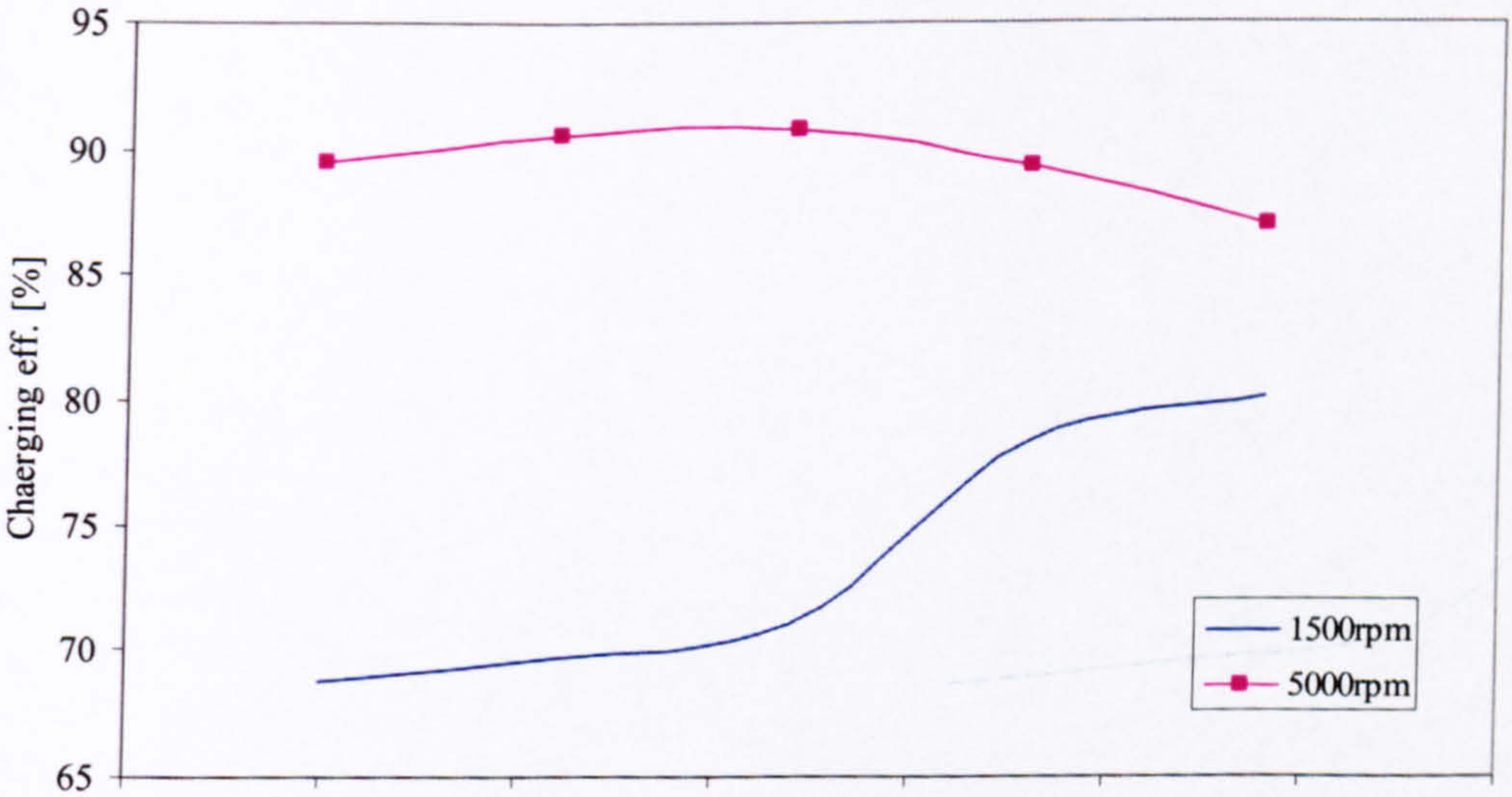

Figure 8.13: Charging efficiency for different IVO at several engine speeds (negative values indicate angle before TDC)

Figure 8.14 demonstrates that charging efficiency is more sensitive to changes in IVC than in IVO at most engine speeds. Different from IVO the sensitivity varies through the explored IVC range. Up to 8000rpm the sensitivity increases as IVC is retarded. For example at 5000rpm the sensitivity to changes from 44° to 56° is lower than the effect of variation from 80° to 92°. At higher engine speeds charging efficiency is more sensitive to changes in the earlier part of the explored region i.e. 44° to 56°.

The sign of the gradient of the sensitivity is constant up to 8000rpm e.g. retarding IVC at 5000 rpm reduces charging efficiency (Figure 8.15). At 11000rpm retarding IVC initially increases charging efficiency but then it reduces it. At maximum engine speed retarding IVC increases charging efficiency.

The differences in the sensitivity to IVO timing and IVC timing at different speeds indicates the potential difficulties of satisfying the optimal valve events with a simple cam phasing system.

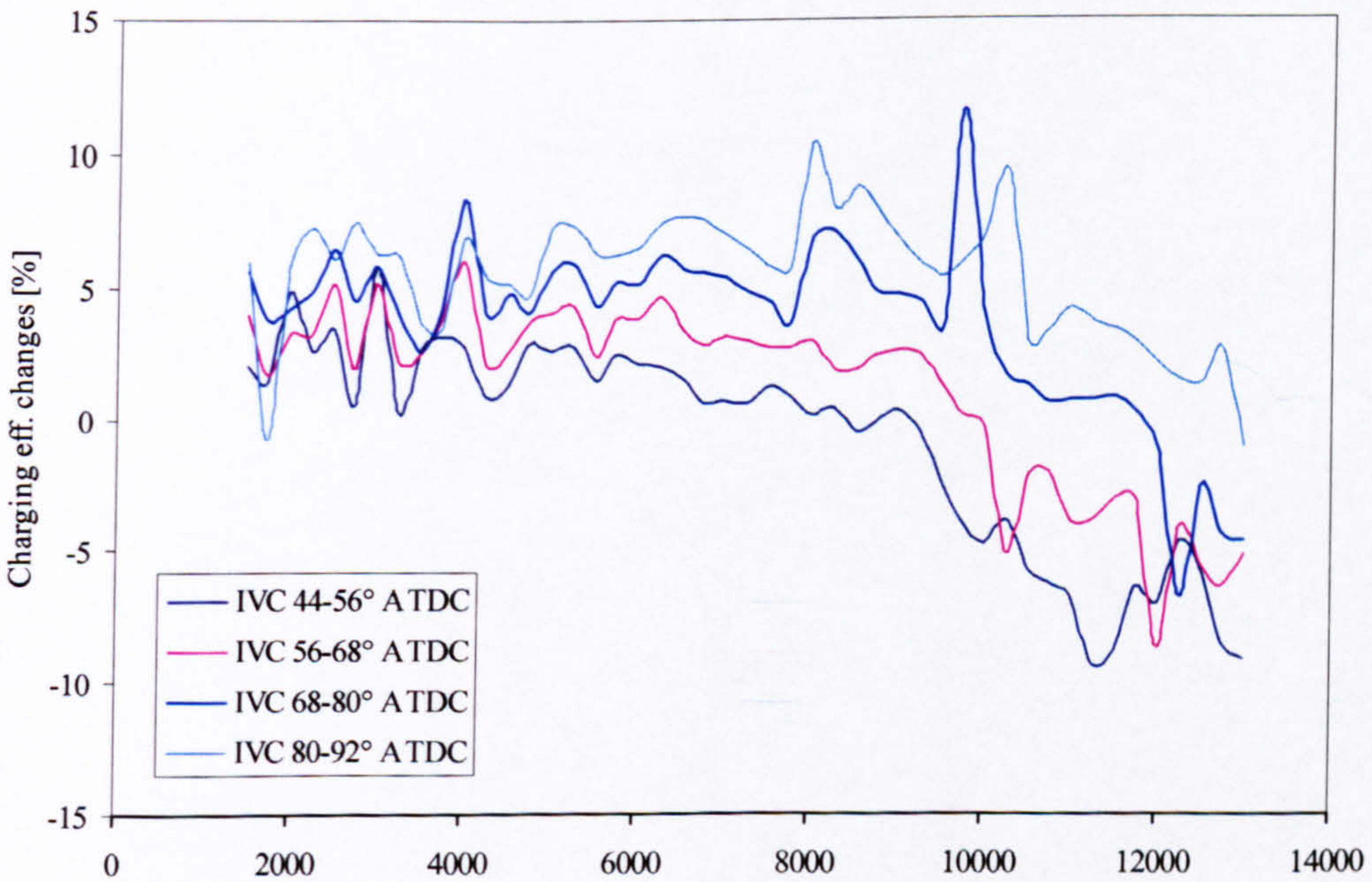

Figure 8.14: Sensitivity of charging efficiency to changes in IVC timing at different engine speeds

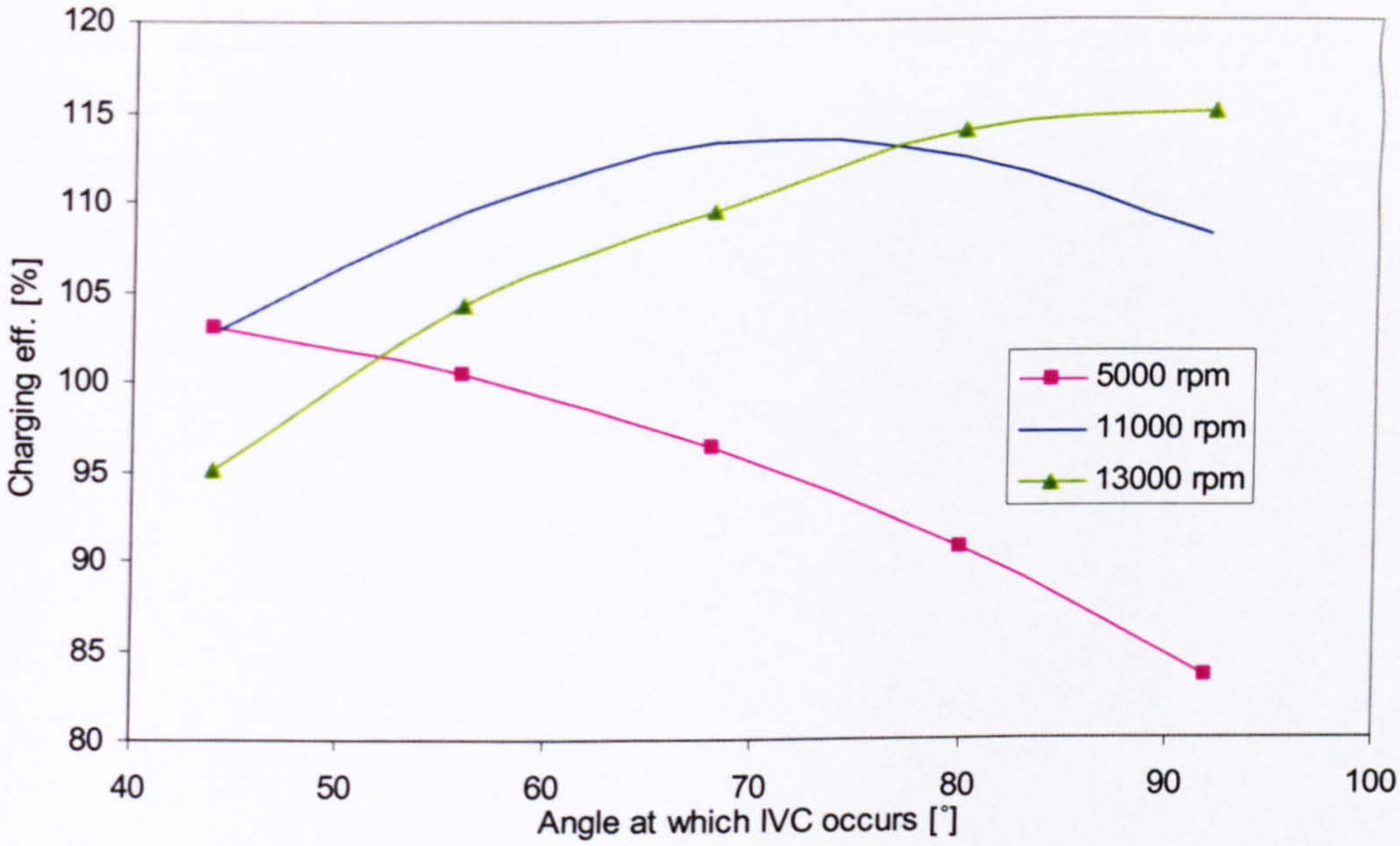

Figure 8.15: Charging efficiency for different IVC at several engine speeds (positive values indicate angle after BDC)

8.6 Potential improvements in Indicated Mean Effective Pressure (IMEP) and indicated power

If we further extend the assumption discussed in section 8.2 regarding the independence of the effect of IVO and IVC on charging efficiency we can plot the charging efficiency curve that could be achieved with optimised valve events as the sum of the potential improvements from individual event changes and the value of the base engine curve. Figure 8.16 shows comparison between the charging efficiency curve with optimised valve events and the base engine curve. It can be seen that as predicted in the previous sections of this chapter the improvements are mainly below 10000 rpm.

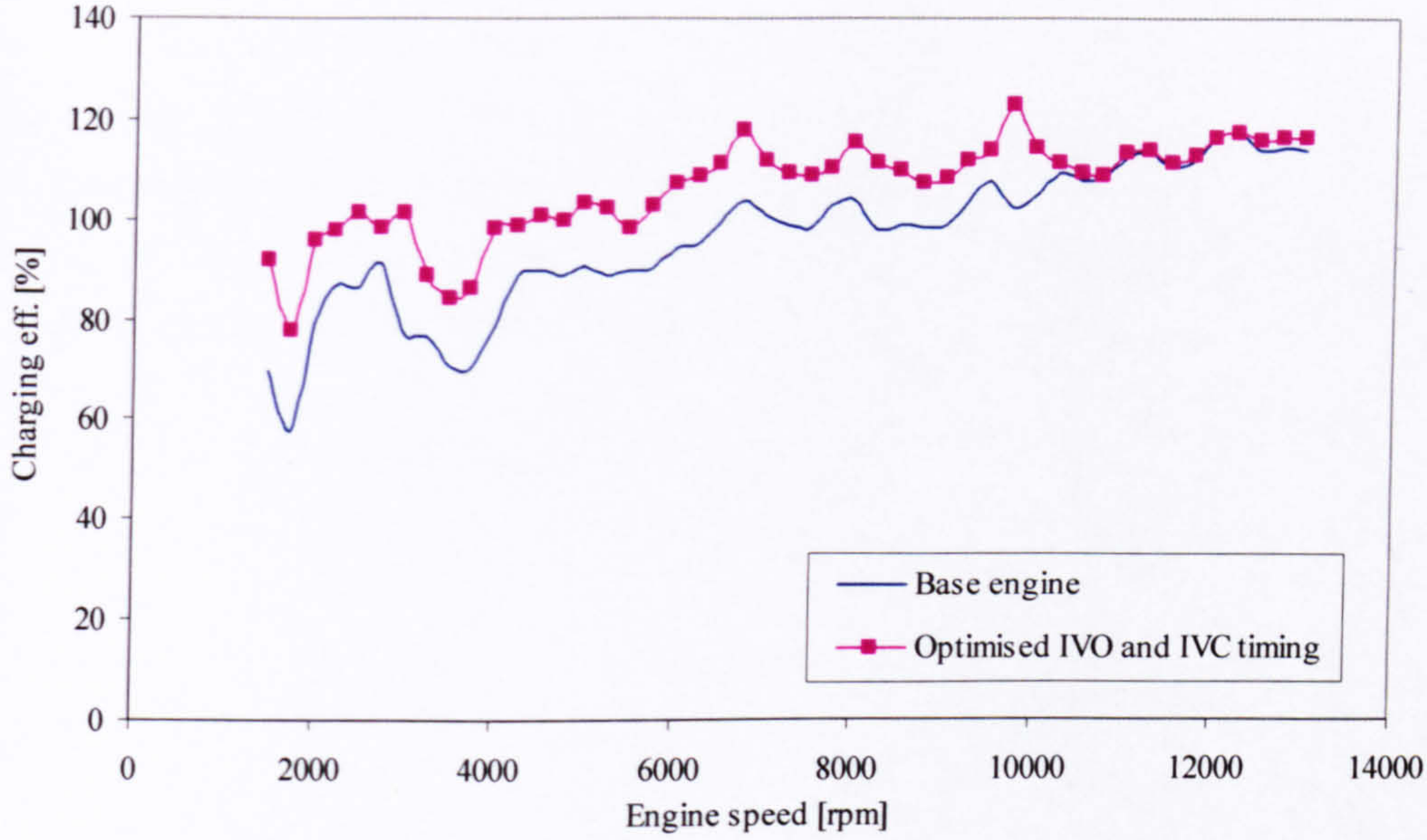

Figure 8.16: Calculated charging efficiency for base engine configuration and for the same engine with optimum valve events for different speeds

Whilst this research focuses on the effect of the valve events on charging efficiency it is important to visualise the potential improvement in other performance parameters such as IMEP and indicted power.

If assumption is made that changes of valve event timing have no effect on combustion efficiency and thermal efficiency then any improvements in IMEP and indicted power should be proportional to the improvements in charging efficiency. If we also apply the assumption discussed in section 8.2 regarding the independence of the effect of IVO and IVC on charging efficiency to IMEP and indicated power it is possible to plot the total effect of these parameters.

Figure 8.17 shows the comparison between the base engine IMEP and an engine with optimal valve events. It can be seen that as expected the improvements are in the same speed range where the possible improvements in charging efficiency are. As with the charging efficiency the main gains are at lower speeds up to 10000 rpm

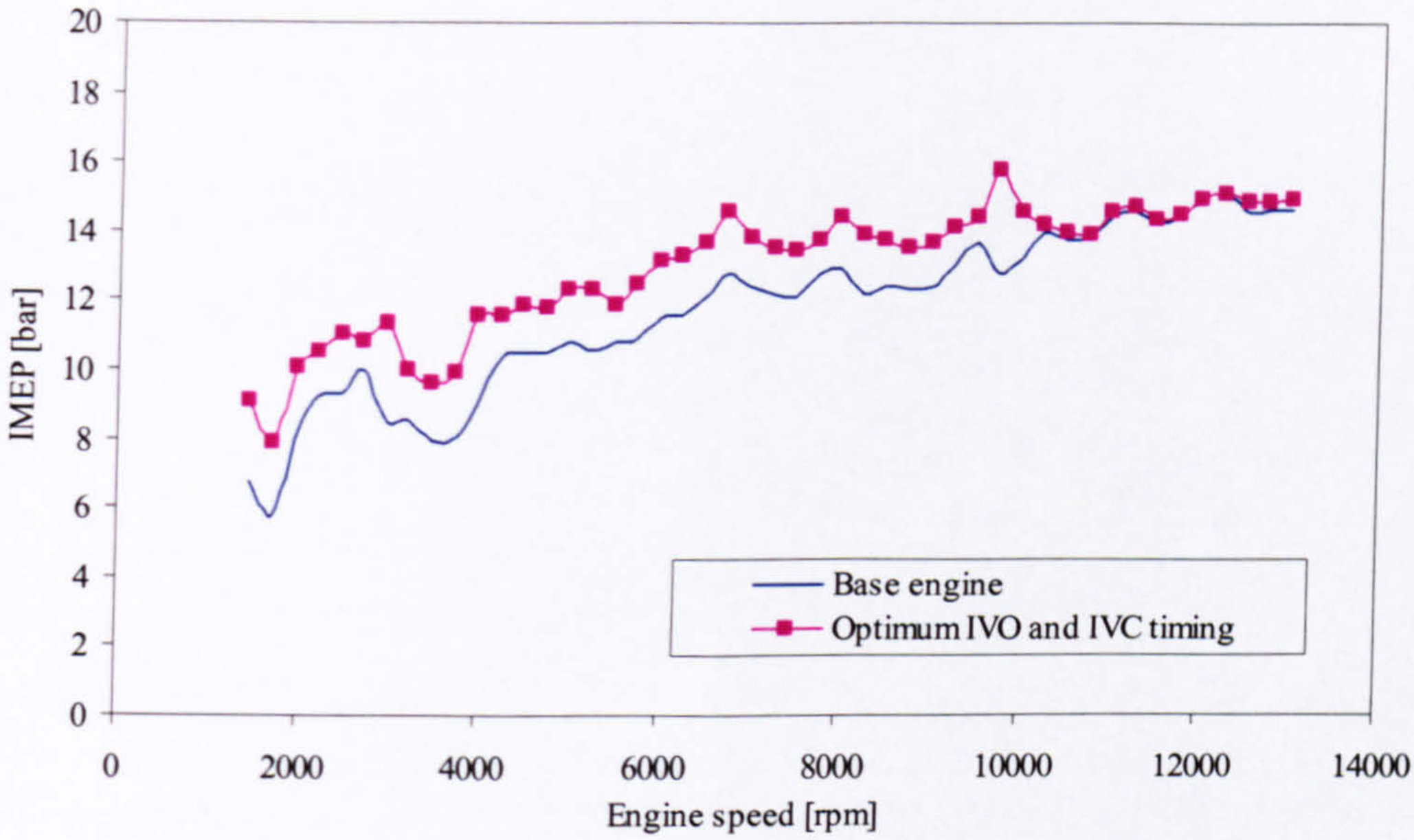

Figure 8.17: Calculated IMEP for base engine configuration and for the same engine with optimum valve events for different speeds

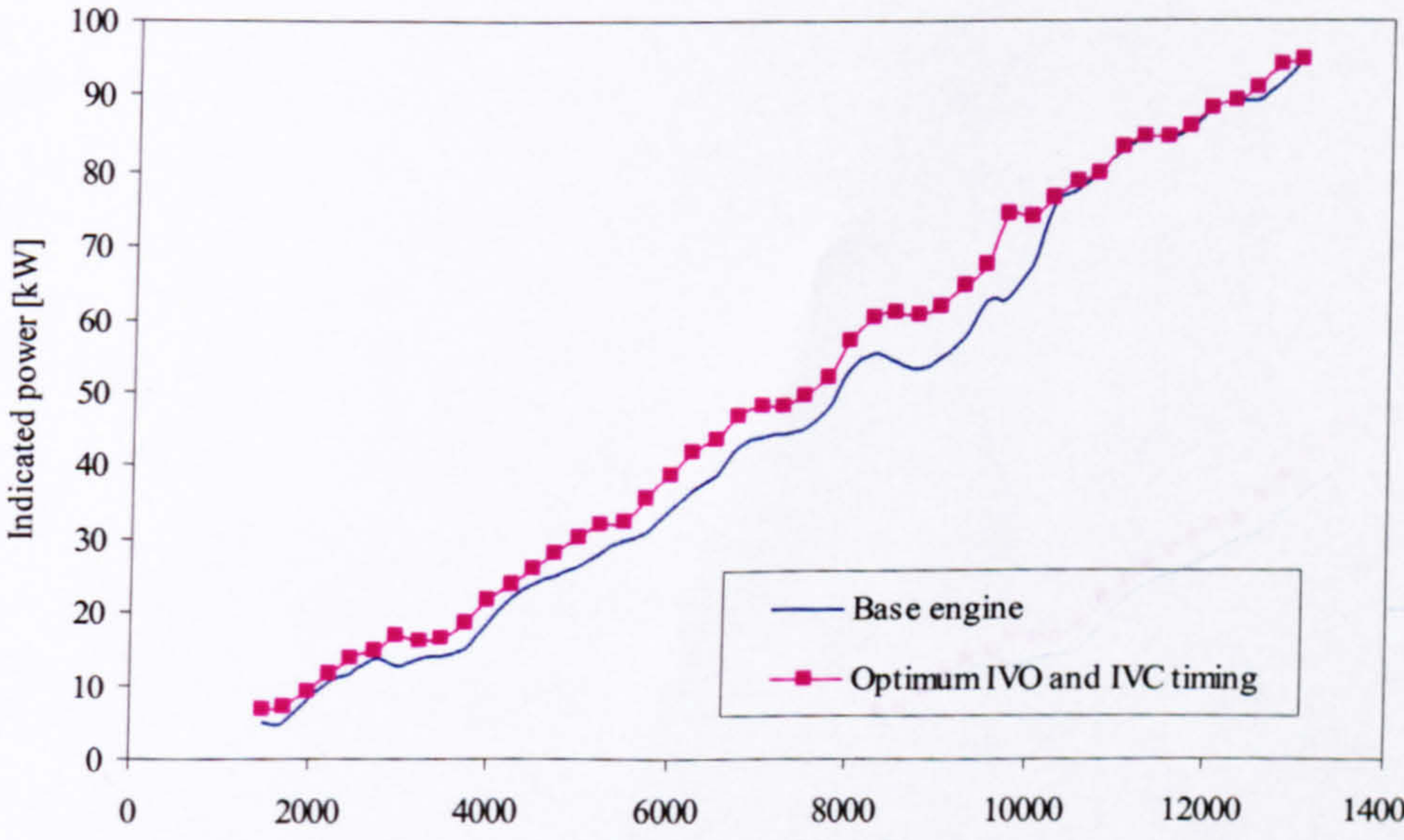

Figure 8.18: Calculated indicated power for base engine configuration and for the same engine with optimum valve events for different speeds

Figure 8.18 demonstrates the potential gains of optimal valve events on indicated power. It is noticeable that at higher speed similar improvements in IMEP result in higher absolute gains in indicated power. It is noticeable that there are very small improvements above 10000rpm. It should be noted that increase in IMEP would give rise to friction losses, which may reduce the improvement in break power.

8.7 Summary of conclusions

The relative independence of the mechanisms in which IVO and IVC affect charging efficiency allows the assumption that their effects can be combined. Hence a map of the ideal valve events can be generated allowing assessment of the ability of VVA systems. The way different systems can improve charging efficiency is shown in Figure 8.19.

The effect of the VCP system is generally confined to low engine speeds and maximum improvement of approximately 14% is possible at around 4000 rpm. No improvement is possible above 10500 rpm. Improvement in areas where charging efficiency dips are not always significant.

VVA system based on the Non-velocity drive principal allows valve event duration change that can significantly improve charging efficiency in some areas up to 10500 rpm. Around 1750 rpm a 35% gain is possible. In other areas such as 6000 rpm and 7000 rpm it performs worse than the VCP system. No significant gains are possible above 10500 rpm, however, a higher charging efficiency can be achieved at maximum engine speed, which may extend the maximum engine power range.

A combination of Non-constant velocity drive and VCP system results improvements above 10% in the engine speed range up to 8000 rpm. Significant gains are possible further up to 10000 rpm. As can be expected this system outperforms the individual systems but again no significant improvements are possible in the higher speed range.

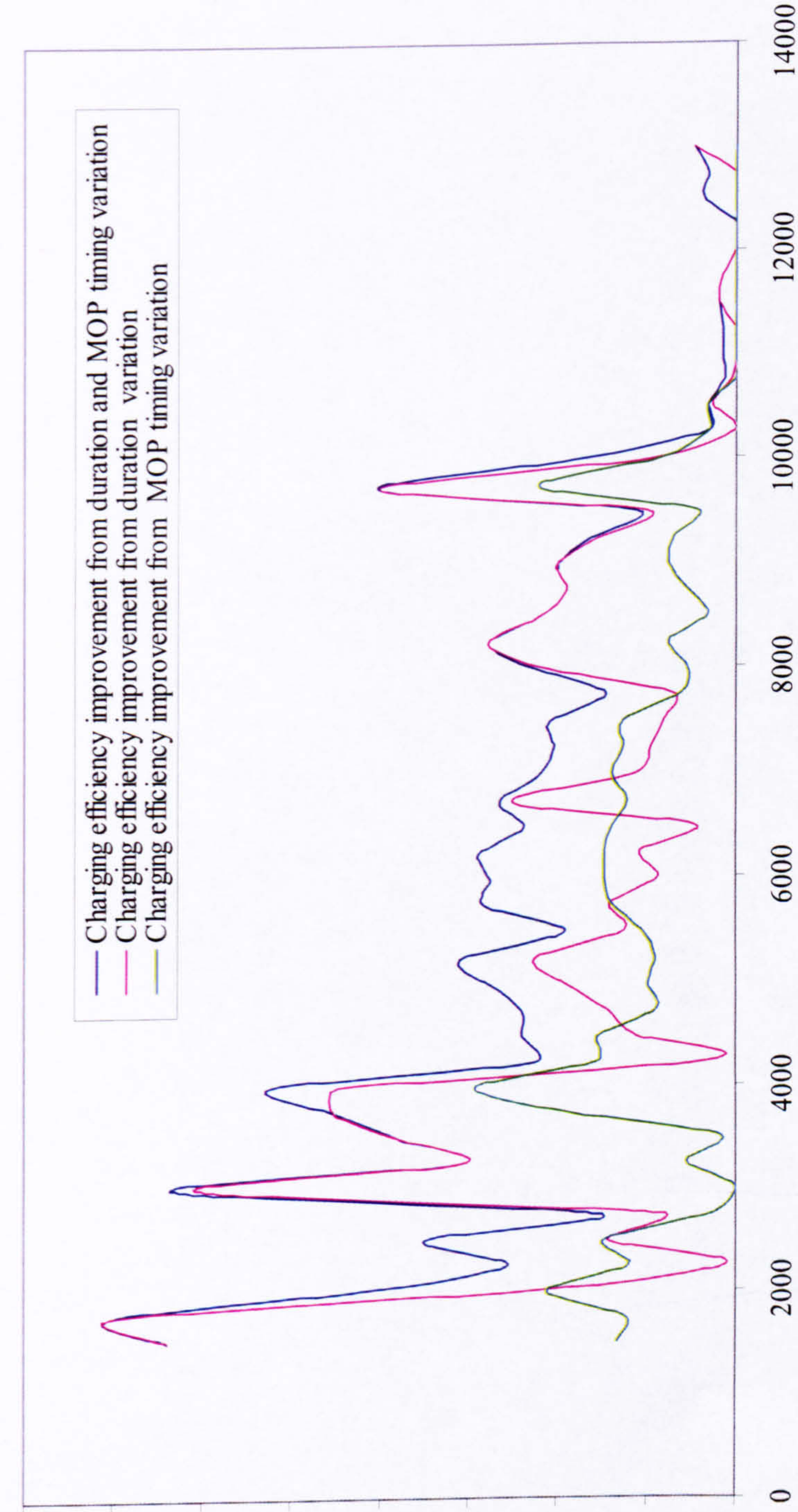

Figure 8.19 Comparison between the possible improvement in charging efficiency from the use of VCP system, Non-constant velocity system and their combination at different engine speeds

Chapter 9

Conclusions and Recommendations for Further Work

This investigation was motivated by the potential for the application of VVA technology in high-speed IC engines, the benefits of which have already been proven in medium speed automotive engines. The main aim of the research is to investigate the effect of the inlet valve events on the gas exchange mechanisms in such an engine and using this knowledge to assess the feasibility of VVA systems. To achieve this, three research objectives were formulated:

The first objective was to establish the high-speed operation feasibility of current VVA systems and identify mechanisms capable for such operation based on valvetrain and camdrive dynamic considerations.

The second objective of the research was to investigate the effect, which valve events have on breathing efficiency in high-speed IC engines. This was to explain the reason for these effects by looking at the gas exchange mechanisms involved and to establish the optimum valve events in terms of breathing efficiency.

The third objective was using this knowledge to assess the abilities of particular VVA systems and to suggest a strategy for best matching the optimum valve events.

9.1 Summary of the thesis and main findings

The following text provides a summary of the work completed to achieve these objectives and comments on the main findings.

Due to the large variety of VVA systems in existence, Chapter 2 only provided general information and an example of each major type. They vary greatly in their complexity and ability. Despite the large number of arrangements available it is only the Variable

Camshaft Phasing and Non-constant velocity drive mechanisms that do not have an impact on the valve and spring dynamics and were identified as suitable for high-speed operation. There are examples of other systems, which do not appear to be suitable for high-speed operation, that are used in engines running at 9000 rpm and even 12000 rpm as in the Honda Hyper VTEC. This is evidence that other mechanisms apart from the VCP system can be adapted to high-speed operation. This is why establishing the ideal valve events in terms of engine performance is important, not only to assess the abilities of the VCP system but also to give direction for future VVA technology development.

The main aspect of this investigation focused on the effect of inlet valve events on the gas exchange process of high-speed engines. Commercially available engine simulation software was employed to do this. Before using any simulation model it is essential to determine the assumptions made and the impact on the predicted results. The Lotus Engine Simulation software was discussed in Chapter 2 and an explanation was provided as to why it is a suitable tool for the investigation of gas exchange events in a high-speed engines. The theory of each submodel was briefly examined and the level of complexity used justified. In conclusion, a judgement was made that LES models the gas dynamic effects in a satisfactory way, allowing it to be used for the investigation of the effects of valve events on gas exchange processes.

In order to use the software as a tool for parametric investigation, accurate modelling of the gas dynamic process had to be experimentally proven. In order to do this a selection of parameters had to be validated with experimental data for the base engine configuration. This research concentrates itself on the gas dynamics in high-speed engines, therefore correlation of parameter characterising the gas flow is essential. It was considered that the most important gas dynamics parameter characterising the flow through the valves is instantaneous inlet and exhaust port pressure. The results presented demonstrate acceptable correlation between measured and predicted pressures from different parts of the engine. The phasing of the pressure pulsations was predicted accurately. However, some slight underdamping of their amplitudes was calculated by the model. Mean pressures along the length of the inlet and exhaust system were also

correlated. The mismatch at 11000 rpm and 13000 rpm was attributed to the same reason.

Whilst the gas dynamic behaviour in the inlet and exhaust is not the main subject of this research, it has an enormous impact on the effect of the individual valve events on engine breathing. This is why it was considered important to understand the different cylinder filling mechanisms before investigating the effect of valve events. This was done by examining this process in two single cylinder engine models, one with infinitely short exhaust duct and the other with infinitely short inlet duct. The use of such engine models allows the effects of the gas dynamics in the inlet pipe and exhaust pipes on the cylinder filling process to be investigated in isolation from each other. This effect is explained by examining the pressure gradient across the cylinder and the gas flow through the valve. The following conclusions were made:

- The gas dynamic behaviour in the inlet pipe in high-speed engines affects the charging efficiency by two mechanisms. The inlet port pressure has an effect on the pressure gradient across the cylinder during valve overlap and is partially responsible for the speeds where charging efficiency peaks and dips. The second mechanism relates to the inlet port pressure after BDC. A positive pressure gradient results in better cylinder filling and a negative one in backflow. Both filling effects are a function of pipe length, engine speed and gas temperature.

- The effect of the gas dynamic behaviour in the exhaust is confined to the valve overlap period. The arrival of a negative pressure wave is beneficial to charging efficiency.

After confirmation of the usefulness of the software tool and understanding the basic cylinder filling mechanisms the sensitivity of charging efficiency to variation of individual valve event parameters was investigated. The focus of Chapter 6 was the effect of Inlet Valve Opening timing on the gas exchange process, the mechanisms involved and the overall effect on charging efficiency. Five different IVO timings were explored with the use of engine simulation software. To explain the results, the inlet process was divided on three sectors and the effect of IVO timing on each of them was

studied. The overlap period was closely examined by comparing inlet and exhaust port pressures and mass flow through the inlet valve. The gas dynamic events taking part in the inlet and exhaust system were shown to be responsible for the effect of IVO on charging efficiency and the following important conclusions were made:

- The main effect of the IVO timing on charging efficiency is in the speed regions where peaks or troughs occur.

- Early IVO timing increases their amplitudes and later IVO reduces them. This is explained by the fact that IVO timing controls the length of the valve overlap and in this way governs the number of crankshaft degrees when the cylinder is exposed to the pressure gradient between the inlet and exhaust port.

- At engine speeds when positive pressure gradient is present across the cylinder during valve overlap an early IVO increases the charging efficiency peaks.

- Whenever negative pressure gradient occurs, IVO needs to be retarded to improve the dips in the charging efficiency curve.

- The above requirements result in the oscillatory shape of the optimum IVO timing for different engine speed.

- IVO timing has little effect on the mass flow into the cylinder after EVC except when significant exhaust backflow into the inlet during valve overlap has occurred. This has detrimental effect on cylinder filling after EVC.

After investigating the effect of IVO timing on the gas exchange mechanism the focus of the research became the effect of inlet valve closing. Again, five valve lift profiles with different IVC timings were generated in a similar way to that described in Chapter 6 and their effect on charging efficiency was explored by using engine simulation software. To explain the results the inlet process was again divided into three sectors as suggested in Chapter 5 and the effect of the gas flow to variations of IVC timing examined. The following findings were made:

- The main mechanism through which IVC timing affects charging efficiency is by controlling the net flow through the valve in the period BDC-IVC. This period was found most sensitive to IVC timing.

- At low speeds there is no pressure build up in the inlet after BDC due to the length of the primary inlet pipe. The effect on charging efficiency was found proportional to the ability to reduce the backflow after TDC caused by the gas dynamics in the inlet system.

- Early IVC reduces the backflow after BDC and yields higher charging efficiency. Potentially earlier IVC timing, which is outside of the range explored, can result in higher benefit.

- At higher engine speeds later IVC utilises the aftercharge effect and increases the amount of charge trapped in the cylinder.

- IVC timing variation can cause a phase shift of the pressure waves propagating in the inlet port at certain speeds. This may result in small changes in gas flow into the cylinder during the valve overlap period and hence the exhaust residuals. The effect on charging efficiency appears insignificant compared with the mechanism explained in the paragraph above.

One of the results from the parametric studies on the effect of IVO and IVC timing on charging efficiency is the determination of their optimum settings. This allowed an assessment of the ability of the VVA systems identified as dynamically suitable for high-speed operation to satisfy these ideal valve events. This is done by comparing their adjustment capabilities with the optimum IVO and IVC timing. The relative independence of the mechanisms in which IVO and IVC affect charging efficiency allows the assumption that their net effect can be combined. The VCP system and Non-constant velocity drive systems were assessed independently and when used in combination. The strategy involved was constrained by the requirement for generating the same or higher output than with fixed valve events. The results showed that:

- The effect of a VCP system is generally confined to low engine speeds and maximum improvement of approximately 14% is possible at around 4000 rpm, no improvement is possible above 10500 rpm. The improvements at some of the areas where the charging efficiency dips are not significant.

- VVA system based on the Non-constant velocity drive principal system allows valve event duration change that can significantly improve charging efficiency in some areas up to 10500 rpm. Around 1750 rpm a 35% gain is possible. In other areas it performs worse than the VCP system (e.g. the areas where charging efficiency peaks). No significant gains are possible above 10500 rpm. However, a higher charging efficiency can be achieved at maximum engine speed, which may extend the maximum engine power range.

- A combination of Non-constant velocity drive and VCP system results in improvements above 10% in the engine speed range up to 8000 rpm. Significant gains are possible further up to 10000 rpm. As can be expected this system outperforms the individual systems, but again no significant improvements are possible in the higher speed range.

- A profile switching system can perform in a similar way to the more complex Non-constant drive velocity system and it can bring other benefits related to reduction of effective valve flow area. This is why its high-speed development can be justified.

- The general conclusion is that none of the VVA systems are capable of significant improvement in the speed range where maximum power is developed because the valve events on the base engine are selected to achieve best output. However, the resulting compromise at low speeds can be significantly reduced by the use of VVA system. This is particularly valid for the Non-constant velocity system and the combinations of systems as they can fill the dips in the torque curve.

9.2 Main contributions of this thesis

The work presented in this thesis is considered to result in the following new contributions to the research field:

- The high-speed operational ability of current VVA systems was established based on valvetrain and camdrive dynamic considerations. Suitable systems were identified.

- The effect of the gas dynamic behaviour in the inlet and exhaust system on the gas exchange process in high-speed engines was established and the responsible cylinder filling mechanisms were identified.

- The effect of IVO and IVC timing on the charging efficiency of high-speed engine was explored and the responsible mechanisms examined.

- Based on the optimal IVO and IVC timing for each speed a control strategy for selected VVA systems was suggested. An assessment of the potential of these systems to improve the performance of high-speed engine was presented.

- One publication was produced from this research (Nouhov and Chen, 2002).

9.3 Recommendations for future research

- The validity of the assumption for relative independence of the effect of individual valve events can be proven by performing a combined parametric study. Alternatively lift profile curves with the suggested optimal IVO and IVC timings can be tested for the appropriate engine speeds.

- Due to the confidentiality surrounding the development of high-speed engines there is little data published regarding the gas exchange mechanism and effect of valve event on performance. This investigation proved that LES software is a useful tool for exploring this phenomenon. It will be useful to perform a similar investigation to the one discussed in this thesis for the exhaust valve events.

- Further work can study the effect of other valve event parameters such as opening and closing velocity and maximum lift of the inlet and exhaust valves.

- Natural progression of this research is to attempt to experimentally validate the findings of the effect of IVO and IVC on engine performance. This will include the effect that the valve events have on other factors affecting engine output. The validity of the assumption for perfect mixing for the cylinder scavenging model can also be proven. Further, camshaft profiles with different duration can be machined and tested to validate the predictions for the effect of Non-constant velocity drive system. Validating the effect of VCP can be achieved easily by testing the base camshaft profile with two different camshaft timings. The experimental setup can include inlet, exhaust and cylinder pressure transducer and an attempt can be made to calculate mass flow through the valves if cylinder pressure can be accurately referenced.

- Currently a commonly used way for establishing ideal valve events in industry is to machine a number of camshaft profiles and perform 'cam swings' to establish the optimum setting. However, this will cause variation of both IVO and IVC and may not allow the optimum timing for each event to be established. If the mass flow through the inlet valve can be calculated, bearing in mind the cylinder filling mechanisms described in this research the optimal IVO and IVC can be established.

References

1. Abthoff, J., Bruggemann, H., Bachschmid, R., and Willand, J., *A New 6-Litre 12-Cylinder Engine for the New Mercedes-Benz S-Class*, SAE, 911905

2. AFT Atlas Fahrzeugtechnik GmbH, www.aft-werdohl.de , 2004

3. Ahmad, T., and Theobald, M., A *Survey of Variable-Valve-Actuation Technology*, SAE, 891674

4. American Performance Engineering, www.aperaceparts.com , 2004

5. Anontaphan, T., *A Study of Mechanical Continuous Variable Rocker Arm*, SAE, 2003-01-0022

6. Asmus, T., *Valve Events and Engine Operation*, SAE, 820749

7. Auto Innovations Website, www.auto-innovations.com , 2004

8. AVL 670 Indimaster Operating Manual, AVL List GmbH, 2000

9. Becker, C., *Super Vario*, Christoporus 297, 2000

10. Benson, R., *The thermodynamics and gas dynamics of internal combustion engines (Volume 1)*, Clarendon Press, 1982

11. Berg, M., and Kachel, G., *Mechanical Fully-Flexible Valve Control with Delta-st*, SAE, 970251

12. Best Cars Website, www2.uol.com.br/bestcars , 2004

13. BMW AG Website, www.bmw.com , 2004

14. Ingenieurbüro Bockhmann and Hannibal, www.palivalenti.de , 2004

15. Boretti, A., and Villa, F., *Design of the Fiat Auto Corse ITC 96 Racing Engine-Part 1: Valve Lift Profiles and Timings*, SAE, 980124

16. Boretti, A. and Villa F., *Design of the Fiat Auto Corse ITC 96 Racing Engine-Part 2: Pipe Lengths and Diameters*, SAE, 980125, 1998

17. Boretti, A., Borghi, M., Cantore, G., and Mattarelli, E., *Numerical Optimisation of a Racing Engine with Variable Intake and Exhaust Geometry and Valve Actuation*, SAE, 962542

18. Borreti, A., and Cantore, G., *Comparison of V10 and V12 F1 Engines*, SAE, 983035

19. Bozza, F., Gimelli, A., Senatore, A., and Caraceni, A., *A theoretical Comparison of Various VVA Systems for Performance and Emission Improvements of SI-Engines*, SAE; 2001-01-0670

20. Brustle, C., and Schwarzenthal, D., *The 'Two in One'-Porsche's Variable Valve System (VVS)*, SAE, 980766

21. Chang, W., Parlikar, T., Kassakian, J., and Keim, T., *An Electromechanical Valve Drive Incorporating a Nonlinear Mechanical Transformer*, SAE, 2003-01-0036

22. Cheng, C., Cheng, W., Heywood, J., Maroteaux, D., and Collings, N., *Intake Port Phenomena in a Spark Ignition Engine at Part Load*, SAE, 912401

23. CMG Website, www.cmgonline.com , 2004

24. Courant, R., Isaacson, E., and Rees, M., *On the solution of non-linear hyperbolic differential equations by finite differences*, Commun. Pure Appl. Math. 5, 243-249, 1952

25. Davis, M., *Honda VTEC: A Cam For All Reasons*, Hotrod magazine, 2004

26. Davis, S., *TVD finite difference schemes and artificial viscosity*, NASA CR 172373, 1984

27. Delphi Corporation, www.delphi.com , 2004

28. Douglas, R., McGinnity, F., and Blair, G., *A Study of Gas Temperature Effects on the Prediction of Unsteady Flow*, IMechE Conference on Internal Combustion Engine Research, Paper C433/036, pp.47-53.

29. Dresner, T., and Barkan, P., *A Review and Classification of Variable Timing Mechanisms*, SAE, 890674

30. Entzminger, W., *Variable Valve Actuation (VVA) Through Variable Ratio Rocker Arms*, SAE, 880730

31. FEV Website, www.fev-et.com , 2004

32. Federation Internationale de L'automobile (FIA) Website, www.fia.com , 2004

33. Freudenstein, F., *The Syntheses and Analysis of Variable Valve-timing Mechanisms for Internal Combustion Engines*, SAE, 880387

34. General Engine Management Systems Ltd Website, www.gems.co.uk , 2004

35. Gray, C., *A Review of Variable Valve Timing*, SAE, 880386

36. Grohn, M., *The New Camshaft Adjustment System by Mercedes-Benz - Design and Application in 4-Valve Engines*, SAE, 901727

37. Grohn, M., and Wolf, C., *Variable Valve Timing in the new Mercedes-Benz Four-Valve Engine*, SAE, 891990

38. Hannibal, W., and Bertsch, A., *VAST: A New Variable Valve Timing System for Vehicle Engines*, SAE, 980769

39. Hara, S., Kumagai, K., and Matsumoto, Y., *Application of a Valve Lift and Timing Control System to an Automotive Engine*, SAE, 890681

40. Hatamura, K., Morishita, K., Asanomi, K., and Shiraishi, H., *Mazda's New V-6 Gasoline Engine and Its Innovative Induction System*, SAE, 871977

41. Hatano, K., Iida, K., Higashi, H., and Murata, M., *Development of a New Multi-Mode Variable Valve Timing Engine*, SAE, 930878

42. Henry, R., *Single-Cylinder Engine Tests of a Motor-Driven, Variable-Valve Actuator*, SAE, 2001-01-0241

43. Henry, R., and Lequesne, B., *A Novel, Fully Flexible, Electro-Mechanical Engine Valve Actuation System*, SAE, 970249

44. Heywood, J., *Internal Combustion Engines Fundamentals*, McGraw-Hill, 1988

45. Hilite International Website, www.hydraulik-ring.com , 2004

46. Honda Motor Company Website, www.honda.com , 2004

47. Horie, K., Nishizawa, K., Ogawa, T., Akazaki, S., and Miura, K., *The Development of a High Fuel Economy and High Performance Four-Valve Lean Burn Engine*, SAE, 920455

48. Hosaka, T., and Hamazaki, M., *Development of the Variable Valve Timing and Lift (VTEC) Engine for the Honda NSX*, SAE, 910008

49. INA-Schaeffer KG, www.ina.com , 2004

50. Inoue, K., *A High Power, Wide Torque Range, Efficient Engine with a Newly Developed Variable-Valve-Lift and -Timing Mechanism*, SAE, 890675

51. Jacquelin, F., *Cam Phaser Actuation Rate Performance Impact on Fuel Consumption and NOx Emissions Over the FTP-75 Drive Cycle*, SAE, 2003-01-0023

52. Jain, D., *Electronic Control of a Variable Geometry Turbocharger*, SAE, 900889

53. Jarvi, L., *Variable Valve Timing Mechanism with Control Ramp*, SAE, 980768

54. Jarvi, L., *VAVACT - Variable Valve Timing Mechanism*, SAE, 2003-01-0025

55. Kim, D., Levin, M., Anderson, M., and Tsao, T., *Dynamic Model of a Springless Electrohydraulic Valvetrain*, SAE, 970248

56. Kishi, N., Kikuchi, S., Seki, Y., Kato, A., and Fujimori, K., *Development of High performance L4 Engine ULEV System*, SAE, 980415

57. Kodai, A., Mori, T., Inukai, T., *Applying Hard Thin Coatings to Tappets to Reduce Friction*; SAE, 2001-01-1886

58. Kreuter, P. and Heuser P., *The Meta VVH System-A Continuously Variable Valve Timing System,* SAE, 980765

59. Kreuter, P., Heuser, P., and Schebitz, M., *Strategies to Improve SI-Engine Performance by Means of Variable Intake Lift Timing and Duration*, SEA, 920449

60. Larsson, T. Bergstrom, K., Bengtsson, A., Petersson, J., and Denbratt, I., *The Volvo 5-Cylinder Engine with 4-Valve Technology - A New Member of Volvo's Modular Engine Family*, SAE, 911906

61. Lee, J., Lee, C., and Nitkiewica, J., *The Application of a Lost Motion VVT System to a DOHC SI Engine*, SAE, 950816

62. Lenz, H., Geringer, B., Smetana, G., and Dachs, A., *Initial Test Results of an Electro-Hydraulic Variable-Valve Actuation System on a Firing engine*, SAE, 890678

63. Lotus Engineering, *Lotus Engine Simulation v.5.03 User Manual*, Lotus Cars Ltd., 2002

64. Lyon, K., *The Chrysler/Lamborghini 3.5l Formula One Engine: Control System Development and Calibration Methodology*, SAE, 962544

65. Maekawa, K., Ohsawa, N., and Akasaka, A., *Development of a Valve Timing Control System*, SAE, 890680

66. Matsumoto, I., and Ohata, A., *Variable Induction Systems to Improve Volumetric Efficiency at Low and/or Medium Engine Speeds* , SAE, 860100

67. MGFcar Website, www.mgfcar.de , 2004

68. Milovanovic, N., and Chen, R., *A review of Experimental and Simulation Studies on Controlled Auto- Ignition Combustion*, SAE, 2001-01-2890

69. Nakamura, H., Nakashima, T., Aihara, H., and Ookubo, M., *Development of Gear Parts for VVT Unit*, SAE, 970337

70. Nakayama, Y., Maruya, T., Oikawa, T., Fujiwara, M., and Kawamata, M., *Reduction of HC Emission During Cold-Start Condition*, SAE, 940481

71. Nakayasu, T., Yamada, H., Suda, T., Iwase, N., and Takahashi, K., *Intake and Exhaust Systems Equipped with a Variable Valve Control Device for Enhancing of Engine Power*, SAE, 2001-01-0247

72. National Instruments Corporation Website, www.ni.com , 2004

73. Nishimura, S., Fukuhara, T., and Teramoto, M., *Nissan V6 3.0 Litre, 4-Cam 24-Valve High Performance Engine*, SAE, 870351

74. Nouhov, D. and Chen R., *A Simulation Study on the Effect of Inlet Valve Opening on Performance of High Speed Engines*, The 17th Internal Combustion Engine Symposium, Japan, 2002

75. Ohata, A., and Ishida, Y., *Dynamic Inlet Pressure and Volumetric Efficiency of Four Cycle Four Cylinder Engine*, SAE, 820407

76. Otto, E., Rubbert, S., Borrmeister, J., *Thermodynamics and charge exchange of the new BMW six-cylinder engine*, IMechE, 214, 2000

77. Parker, P., *The variable valve timing mechanism for the Rover K16 engine Part 1: selection of the mechanism and the basis of the design*, IMechE, 214, 2000

78. Parker, P., *The variable valve timing mechanism for the Rover K16 engine Part 2: application to the engine and the performance obtained*, IMechE, 214, 2000

79. Pearson, R., and Winterbone, D., *A Rapid Wave Action Simulation Technique for Intake Manifold Design*, SAE, 900676

80. Pierik, R,. and Gecim, B., *A Low-Fraction Variable-Valve-actuation Device, Part1: Mechanism Description and Friction Measurement*, SAE, 970338

81. Podnar, D., and Kubesh, J., *Characteristics of a Small Engine Equipped With An Electromagnetic Valve Actuation System*, 981908

82. Prosser, T., *Induction Ramming a Motored High-Speed Four-Stroke Reciprocating Engine - Influence of Inlet Port Pressure Waves on Volumetric Efficiency*, IMechE, Vol.188, 1974

83. Riley, M., McElwee, M., and Wakeman, R., *A Mechanical Valve System with Variable Lift, Duration, and Phase Using a Moving Pivot*, SAE, 970334

84. Roth, D., *Intake Valve Optimisation*, SAE, 981028

85. Schechter, M., and Levin, M., *Camless Engine*, SAE, 960581

86. Shikida, T., Nakamura, Y., Nakakubo, T., and Kawase, H., *Development of the High Speed 2ZZ-GE Engine*, SAE, 2000-01-0671

87. Siemens VDO Website, www.siemensmedia.com , 2002

88. Siewert, R., *How Individual Valve Timing Events Affect Exhaust Emissions*, SAE, 710609

89. Soltic, P., and Guzzella, L., *Optimum SI Engine Based Powertrain Systems for Lightweight Passenger Cars*, SAE, 2000-01-0827

90. Stein, R., Galietti, K., and Leone, T., *Dual Equal VCT-A Variable Camshaft Timing Strategy for Improved Fuel Economy and Emissions*, SAE, 950975

91. Steinberg, R., Lenz, I., Koehnlein, G. Scheidt, M., Saupe, T., and Buchinger, W., *Fully Variable Cam Timing Concept for Intake and Exhaust Phasing*, SAE, 980767

92. Stone, R., *Introduction to Internal Combustion Engines*, Macmillan Press, 1999

93. Stone, R., and Kwan, E., *Variable Valve Actuation Mechanisms and the Potential for Their Application*, SAE, 890673

94. Stone, R., Garden, T., and Podmore, I., *Analysis of the effect of inlet valve disablement on swirl, combustion and emissions in a spark ignition engine*, IMechE, 207, 1993

95. Sulzer Metco, www.sulzermetco.com , 2004

96. Sung, N., Choi, J., and Jeong, Y., A *Study on the Flow in The Engine Intake System*, SAE, 952067, 1995

97. Takizawa, M., Uno, T., Oue, T., and Yura, T., *A Study of Gas Exchange Process Simulation of an Automotive Multi-Cylinder Internal Combustion Engine*, SAE, 820410, 1982

98. Taylor, C., *The Internal Combustion Engine in Theory and Practice*, The M.I.T. Press, 1, 1985

99. Theobald, M., Lequesne, B., and Henry, R., *Control of Engine Load via Electromagnetic Valve Actuators*, SAE, 940816, 1994

100. Titolo, A., *The Variable Valve Timing System - Application on a V-8 Engine*, SAE, 910009

101. Tsukui, T., Ichimura, T., Tsutsumizaki, K., and Nakajima, M., *Development of the Directly Actuated Variable Valve Control System*, SAE, 1999-01-3319

102. University of Sheffield, www.shef.ac.uk , 2004

103. Vogel, O., Guzzella, L., Roussopoulos, K., and Czekaj, J., *Variable Valve Timing Implemented with a Secondary Valve on a Four Cylinder SI Engine*, SAE, 970335

104. Wallesten, J., Sandquist, H., Holmstrom-Enwald, K., and Stromberg, S., *Influence of Valve Overlap Strategy on Residual Gas Fraction and Combustion in a SI Engine at Idle*, SAE, 972936

105. Wiebe, I., *Habempirische Formel fur die Verbrennungsgeschrwindigkeit Verlag der Akademie der Wissenschaften der VdSSR*, 1956

106. Wilson, N., Watkins, A., and Dopson, C., *Asymmetric Valve Strategies and Their Effect on Combustion*, SAE, 930821

107. Winterbone, D., and Pearson, R., *Theory of Engine Manifold Design. Wave action methods for I.C. engines. Professional Engineering Publications*, 2000

108. Wolters, P., Salber, W., Geiger, J., Duesmann, M., and Dilthey, J., *Controlled Auto Ignition Combustion Process with an Electromechanical Valve Train*, SAE, 2003-01-0032

109. Wright, P., *Formula 1 Technology*, Society of Automotive Engineers, 2001

110. Yagi, S., Ishizuya, A., and Fujii, I., *Research and Development of High-Speed, High Performance, Small Displacement Honda Engines*, SAE, 700122

111. Yamabe, K., and Ueda, H., *Exhaust Control System for Motorcycle 4-Straoke Engines*, SAE, 880269